Université de Montréal

# Apport de nouvelles techniques dans l'évaluation de patients candidats à une chirurgie d'épilepsie : résonance magnétique à haut champ, spectroscopie proche infrarouge et magnétoencéphalographie

par

Dang Khoa Nguyen

Département de physiologie

Faculté de Médecine

Thèse présentée à la Faculté des études supérieures

En vue de l'obtention du grade de

Philosophiae Doctor (Ph.D.)

en sciences neurologiques

Mai 2013

Université de Montréal
Faculté des études supérieures et postdoctorales

Cette thèse intitulée :

**Apport de nouvelles techniques dans l'évaluation de patients candidats à une chirurgie d'épilepsie : résonance magnétique à haut champ, spectroscopie proche infrarouge et magnétoencéphalographie**

Présentée par :
Dang Khoa Nguyen

a été évaluée par un jury composé des personnes suivantes :

Allan Smith, représentant du doyen
Maryse Lassonde, directrice de recherche
Richard Wennberg, examinateur externe
Alexandre Prat, examinateur interne

## RÉSUMÉ EN FRANÇAIS

L'épilepsie constitue le désordre neurologique le plus fréquent après les maladies cérébrovasculaires. Bien que le contrôle des crises se fasse généralement au moyen d'anticonvulsivants, environ 30 % des patients y sont réfractaires. Pour ceux-ci, la chirurgie de l'épilepsie s'avère une option intéressante, surtout si l'imagerie par résonance magnétique (IRM) cérébrale révèle une lésion épileptogène bien délimitée. Malheureusement, près du quart des épilepsies partielles réfractaires sont dites « non lésionnelles ». Chez ces patients avec une IRM négative, la délimitation de la zone épileptogène doit alors reposer sur la mise en commun des données cliniques, électrophysiologiques (EEG de surface ou intracrânien) et fonctionnelles (tomographie à émission monophotonique ou de positrons). La faible résolution spatiale et/ou temporelle de ces outils de localisation se traduit par un taux de succès chirurgical décevant. Dans le cadre de cette thèse, nous avons exploré le potentiel de trois nouvelles techniques pouvant améliorer la localisation du foyer épileptique chez les patients avec épilepsie focale réfractaire considérés candidats potentiels à une chirurgie d'épilepsie : l'IRM à haut champ, la spectroscopie proche infrarouge (SPIR) et la magnétoencéphalographie (MEG).

Dans une première étude, nous avons évalué si l'IRM de haut champ à 3 Tesla (T), présentant théoriquement un rapport signal sur bruit plus élevé que l'IRM conventionnelle à 1,5 T, pouvait permettre la détection des lésions épileptogènes subtiles qui auraient été manquées par cette dernière. Malheureusement, l'IRM 3 T n'a permis de détecter qu'un faible nombre de lésions épileptogènes supplémentaires (5,6 %) d'où la nécessité d'explorer d'autres techniques.

Dans les seconde et troisième études, nous avons examiné le potentiel de la SPIR pour localiser le foyer épileptique en analysant le comportement hémodynamique au cours de crises temporales et frontales. Ces études ont montré que les crises sont associées à une augmentation significative de l'hémoglobine oxygénée (HbO) et l'hémoglobine totale au niveau de la région épileptique. Bien qu'une activation contralatérale en image miroir puisse être observée sur la majorité des crises, la latéralisation du foyer

était possible dans la plupart des cas. Une augmentation surprenante de l'hémoglobine désoxygénée a parfois pu être observée suggérant qu'une hypoxie puisse survenir même lors de courtes crises focales.

Dans la quatrième et dernière étude, nous avons évalué l'apport de la MEG dans l'évaluation des patients avec épilepsie focale réfractaire considérés candidats potentiels à une chirurgie. Il s'est avéré que les localisations de sources des pointes épileptiques intericталes par la MEG ont eu un impact majeur sur le plan de traitement chez plus des deux tiers des sujets ainsi que sur le devenir postchirurgical au niveau du contrôle des crises.

**Mots-clés** : Épilepsie, chirurgie d'épilepsie, imagerie par résonance magnétique 3 T, électroencéphalographie, spectroscopie proche infrarouge, magnétoencéphalographie.

## RÉSUMÉ EN ANGLAIS

Epilepsy is the most common chronic neurological disorder after stroke. The major form of treatment is long-term drug therapy to which approximately 30% of patients are unfortunately refractory to. Brain surgery is recommended when medication fails, especially if magnetic resonance imaging (MRI) can identify a well-defined epileptogenic lesion. Unfortunately, close to a quarter of patients have nonlesional refractory focal epilepsy. For these MRI-negative cases, identification of the epileptogenic zone rely heavily on remaining tools: clinical history, video-electroencephalography (EEG) monitoring, ictal single-photon emission computed tomography (SPECT), and a positron emission tomography (PET). Unfortunately, the limited spatial and/or temporal resolution of these localization techniques translates into poor surgical outcome rates.

In this thesis, we explore three relatively novel techniques to improve the localization of the epileptic focus for patients with drug-resistant focal epilepsy who are potential candidates for epilepsy surgery: high-field 3 Tesla (T) MRI, near-infrared spectroscopy (NIRS) and magnetoencephalography (MEG).

In the first study, we evaluated if high-field 3T MRI, providing a higher signal to noise ratio, could help detect subtle epileptogenic lesions missed by conventional 1.5T MRIs. Unfortunately, we show that the former was able to detect an epileptogenic lesion in only 5.6% of cases of 1.5T MRI-negative epileptic patients, emphasizing the need for additional techniques.

In the second and third studies, we evaluated the potential of NIRS in localizing the epileptic focus by analyzing the hemodynamic behavior of temporal and frontal lobe seizures respectively. We show that focal seizures are associated with significant increases in oxygenated haemoglobin (HbO) and total haemoglobin (HbT) over the epileptic area. While a contralateral mirror-like activation was seen in the majority of seizures, lateralization of the epileptic focus was possible most of the time. In

addition, an unexpected increase in deoxygenated haemoglobin (HbR) was noted in some seizures, suggesting possible hypoxia even during relatively brief focal seizures.

In the fourth and last study, the utility of MEG in the evaluation of nonlesional drug-refractory focal epileptic patients was studied. It was found that MEG source localization of interictal epileptic spikes had an impact both on patient management for over two thirds of patients and their surgical outcome.

**Key Word**: Epilepsy, epilepsy surgery, magnetic resonance imaging 3.0 T, electroencephalography, near-infrared spectroscopy, magnetoencephalography.

# TABLE DES MATIÈRES

# LISTE DES FIGURES

**INTRODUCTION :**



**POSITION DU PROBLÈME :**



**LES MÉTHODOLOGIES :**



**ARTICLE 1 :**



**ARTICLE 2 :**

**ARTICLE 3 :**

**AVENUES FUTURES DE RECHERCHE :**



**ANNEXE 2 :**



**ANNEXE 3 :**

**ANNEXE 4 :**

**ANNEXE 6 :**

## LISTE DES ABRÉVIATIONS

| | |
|---|---|
| **aCG** | anterior cingulate gyrus |
| **aINS** | anterior insula |
| **ASR** | Antennes de surface en réseau |
| **ATL** | Anterior temporal lobectomy |
| **BOLD** | Blood-Oxygen-Level-Dependent |
| **EEG** | Électroencéphalographie / electroencephalography |
| **EPI** | Echo planar imaging |
| **ETLE** | Extratemporal lobe epilepsy |
| **EZ** | Epileptogenic zone |
| **FG** | Frontal gyrus |
| **FLE** | Frontal lobe epilepsy |
| **fMRI** | Functional magnetic resonance imaging |
| **fNIRS** | Functional near-infrared spectroscopy |
| **HA** | Hippocampal atrophy |
| **HbO** | Hémoglobine oxygénée / oxygenated haemoglobin |
| **HbR** | Deoxygenated haemoglobin / hémoglobine désoxygénée |
| **HbT** | Hémoglobine totale / total haemoglobin |
| **HRF** | Hemodynamic response function / réponse hémodynamique |
| **ICE** | Intracranial electroencephalography |
| **IED** | Interictal epileptiform discharge |
| **IFG** | Inferior frontal gyrus |
| **IPL** | Inferior parietal lobule |
| **ITG** | Inferior temporal gyrus |
| **L** | Left |
| **MEG** | Magnétoencéphalographie / Magnetoencephalography |
| **MFG** | Middle frontal gyrus |
| **MRI** | Magnetic resonance imaging / imagerie par résonance magnétique |
| **MST** | Multiple subpial transection |
| **MTG** | Middle temporal gyrus |
| **MTLE** | Mesial temporal lobe epilepsy |
| **NIRS** | Near-infrared spectroscopy |

| | |
|---|---|
| **NTLE** | Neocortical lateral temporal lobe epilepsy |
| **OLE** | Occipital lobe epilepsy |
| **pINS** | posterior insula |
| **PLE** | Parietal lobe epilepsy |
| **R** | Right |
| **SAH** | Selective amygdalo-hippocampectomy |
| **SFG** | Superior frontal gyrus |
| **SM** | Sensorimotor area |
| **SMA** | Supplementary motor area; |
| **SPIR** | Spectroscopie proche infrarouge |
| **STG** | Superior temporal gyrus |
| **TE** | Echo Time |
| **TEMP** | Tomographie d'émission monophotonique |
| **TEP** | Tomographie par émission de positons |
| **TLE** | Temporal lobe epilepsy |
| **TR** | Repetition Time |
| **WMSA** | White matter signal abnormality |

## REMERCIEMENTS

J'aimerais en premier lieu remercier Dr Maryse Lassonde, ma directrice de thèse, qui a été d'un support indéfectible et m'a ouvert son laboratoire pour mener à bien ces travaux de recherche. Je n'aurais pas pu trouver meilleure directrice : sage, brillante, généreuse, cultivée, équilibrée. J'aimerais également remercier Frédéric Lesage pour sa collaboration incroyable. Des remerciements sont également de mise pour les Drs Patrick Cossette, Lionel Carmant, Jean-Marc Saint-Hilaire, Franco Lepore, Isabelle Rouleau et Mohamad Sawan qui m'ont beaucoup aidé au cours de la dernière décennie dans mes projets de recherche.

J'aimerais aussi remercier Jean-Maxime Leroux pour son aide et amitié ainsi que François Guilbert pour la réalisation de la première étude. J'ai une grande dette de reconnaissance envers Phetsamone Vannasing, Julie Tremblay et Philippe Pouliot pour leur aide précieuse et indispensable pour la réalisation des études sur la spectroscopie proche infrarouge. Un grand merci aussi à Ismail Mohamed dont l'expertise en magnétoencéphalographie a été cruciale pour la dernière étude.

Plusieurs autres personnes ont été impliquées à un moment ou un autre aux travaux de cette thèse et il est important de souligner leur contribution : Olivia Florea, Manon Robert, Nathalie Bouloute, Christophe Grova, Pierre Jolicoeur, Micheline Gravel, Alain Bouthillier, Arline Bérubé, Patrice Finet, Gilles Beaudoin.

Pour terminer, j'aimerais remercier ma famille. Merci à mes parents qui ont fait de nombreux sacrifices pour offrir à leurs enfants un meilleur avenir. Merci à mes enfants, Nicolas et Emmanuelle, pour leur amour inconditionnel. Ma plus grande reconnaissance revient à Tram, mon épouse. Sans son amour je n'aurais eu ni le temps, le désir, ou la motivation de poursuivre mes projets.

# INTRODUCTION GÉNÉRALE

## 1. L'ÉPILEPSIE

L'épilepsie est une condition chronique caractérisée par une prédisposition à faire des crises épileptiques récidivantes, habituellement spontanées [1]. Il s'agit du désordre neurologique le plus fréquent après les maladies cérébrovasculaires avec une prévalence approchant un pour cent dans les pays développés et une incidence cumulative entre 2 et 3 % [2, 3]. Traduit à l'échelle provinciale, il est estimé qu'environ 70,000 Québécois sont épileptiques. Les causes de l'épilepsie sont nombreuses incluant entre autres les tumeurs cérébrales, les traumatismes crâniens, les maladies cérébrovasculaires, les infections du système nerveux central, les insultes périnatales, les malformations du développement cérébral, et des anomalies génétiques. Il existe deux grandes catégories d'épilepsie soit l'épilepsie focale (*syn.* partielle, localisée) et l'épilepsie d'emblée généralisée. L'épilepsie focale implique que les crises proviennent d'une zone spécifique du cortex cérébral alors que l'épilepsie d'emblée généralisée se réfère à des crises impliquant les 2 hémisphères cérébraux dès le début [4]. Les manifestations cliniques observées lors de crises varient selon entre autres leur point de départ, leur propagation et leur durée [5]. Alors que les crises focales de courte durée (secondes) sans atteinte de la conscience ou de la vigilance sont appelées aura ou crise partielle simple, les crises plus longues (minutes) qui altèrent la conscience sont appelées partielles complexes ou dyscognitives. Cette altération de l'état de conscience peut perdurer plusieurs minutes après la fin de la crise dans la période « postictale ». Avec la propagation additionnelle de l'activité épileptique, une crise partielle complexe peut devenir secondairement généralisée (crise bilatérale convulsive). Le patient est dit en « état de mal épileptique » lorsqu'une crise perdure plus de 30 minutes ou lorsque des crises se succèdent sur plus de 30 minutes sans reprise de l'état de conscience entre les crises [6].

Le contrôle à long terme des crises épileptiques se fait généralement au moyen d'anticonvulsivants. Malheureusement, environ 30 % des patients y sont réfractaires (pharmacorésistance) [7]. La persistance de crises constitue non seulement un

handicap neurologique personnel significatif (risque accru de blessures et de mort subite, faible estime de soi, troubles d'apprentissage, conduite automobile interdite, faible socialisation, pauvre qualité de vie), mais également un handicap socio-économique important (absentéisme, chômage, invalidité, coûts sanitaires) [8]. Chez ces patients aux prises avec une épilepsie focale pharmacorésistante, une guérison des crises est parfois possible par la résection chirurgicale de la région du cerveau à l'origine des crises (c.-à-d. la zone épileptogène – Annexe 1) [9-11]. Le succès de cette intervention chirurgicale est évidemment tributaire de la fiabilité de la localisation de cette zone.

## 2. L'ÉVALUATION PRÉCHIRURGICALE DANS LA PRATIQUE CLINIQUE COURANTE

Dans l'optique de localiser cette zone épileptogène, les candidats potentiels à une chirurgie d'épilepsie sont soumis à une évaluation préchirurgicale approfondie [12]. L'évaluation débute par un questionnaire clinique pouvant fournir d'importants indices sur le site du foyer épileptique en identifiant la zone symptomatogène. Par exemple, des crises débutant par des phosphènes lumineux suggèrent un foyer occipital alors qu'une aura épigastrique ou un sentiment de déjà vu pointe plutôt vers un foyer temporal. L'évaluation se poursuit par un électroencéphalogramme (EEG) (Figure 1a), une technique utilisant des électrodes de surface pour enregistrer l'activité électrique spontanée du cerveau [13]. Chez les patients souffrant d'une épilepsie focale, les anomalies épileptiques peuvent être a) « interictales » (c.-à-d. entre les crises) consistant en de brefs (20-200ms) graphoéléments pointus se détachant nettement du rythme de fond et tout à fait asymptomatiques (Figure 1b); ou b) « ictales » (au moment d'une crise) sous forme d'une activité rythmique soudaine, évoluant en amplitude, fréquence et distribution spatiale sur plusieurs secondes à minutes, générant habituellement des manifestations cliniques et se terminant tout aussi subitement (Figure 2a) [14]. Comme il est rare de pouvoir capter des crises lors d'un EEG de routine de 30 minutes en raison de leur survenue aléatoire, une étude d'enregistrement vidéo-électroencéphalographie télémétrique prolongé (vidéo-EEG) (Figures 2b; 2c**)** à l'unité d'épilepsie sur une durée d'une à deux semaines est

habituellement nécessaire [15]. L'analyse des anomalies électroencéphalographiques interictales (Figure 1b) (définissant ainsi la « zone irritative ») et surtout ictales (Figure 2a) permet parfois de latéraliser ou régionaliser le foyer épileptique. Par exemple, des décharges épileptiques rythmiques maximales au niveau des électrodes temporales gauches au début d'une crise orientent vers un foyer épileptique temporal gauche. Durant leur séjour intrahospitalier à l'unité d'épilepsie, une tomographie d'émission monophotonique (TEMP) ictale (Figure 3) et une tomographie à émission de positons (TEP) (Figure 4) interictale sont obtenues [16]. La TEMP est une méthode d'imagerie en médecine nucléaire permettant d'obtenir un reflet de la perfusion cérébrale. Son utilité est basée sur le principe que le débit sanguin cérébral régional augmente lors de crises partielles, maximalement au site d'origine. La technique consiste à injecter au début d'une crise un radioélément couplé à un radiotraceur qui sera capté au niveau du tissu cérébral proportionnellement au débit sanguin cérébral [17]. Ainsi donc, une hyperperfusion du lobe temporal droit sera retrouvée si l'injection est réalisée au début d'une crise provenant de cette région. Dans la plupart des centres d'épilepsie, les images de la TEMP ictale sont soustraites à celles de la TEMP interictale pour souligner les différences entre les 2 états dynamiques et améliorer la fiabilité du test. La TEP, quant à elle, est une technique d'imagerie en médecine nucléaire permettant d'explorer de nombreux aspects du métabolisme cérébral [18]. L'apport en épilepsie de la TEP exploite le fait que la région épileptogène est hypométabolique en période interictale soit à cause d'une perte neuronale ou par déafférentation. C'est ce qu'on appelle la zone de déficit fonctionnel. Ainsi, un hypométabolisme temporal droit suggère un foyer temporal droit. L'évaluation ne saurait être complète sans une résonance magnétique cérébrale (IRM) anatomique pouvant détecter des anomalies morphologiques épileptogènes telles des angiomes caverneux, malformations artérioveineuses, néoplasies bénignes, scléroses hippocampiques, et malformations du développement cortical [19] (Figure 5). L'IRM joue un rôle central dans l'évaluation préchirurgicale puisque le site d'une lésion épileptogène correspond généralement à la zone épileptogène.

Idéalement, les arguments cliniques, électrographiques (EEG ictal et interictal), fonctionnels (TEP, TEMP) et morphologiques (IRM anatomique) sont concordants et pointent vers une zone corticale épileptique commune.

# Électroencéphalographie

Figure 1. a) Installation des électrodes par le technicien en électrophysiologie pour la réalisation d'un EEG; b) Tracé typique obtenu permettant la détection des anomalies épileptiques (ici pointes temporales gauches).

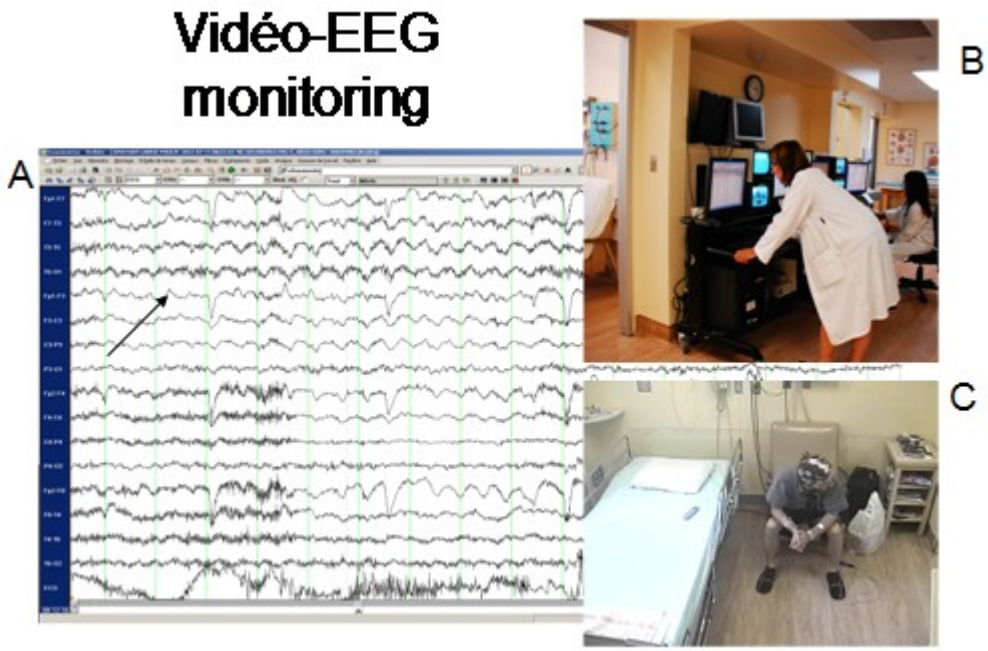


Figure 2. Activité thêta rythmique temporale gauche (a) au décours d'une crise chez un patient sous enregistrement simultané vidéo-électroencéphalographique (b) à l'unité d'épilepsie (c).

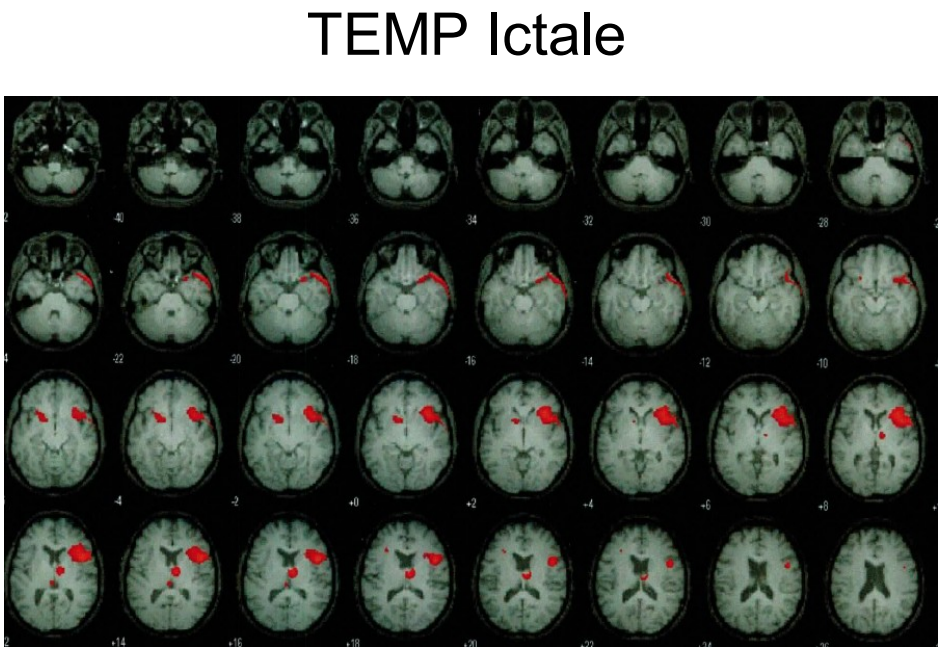


Figure 3. Zone d'hyperperfusion focale operculoinsulaire G démontrée par la tomographie par émission monophotonique (corégistration faite sur l'IRM du sujet).

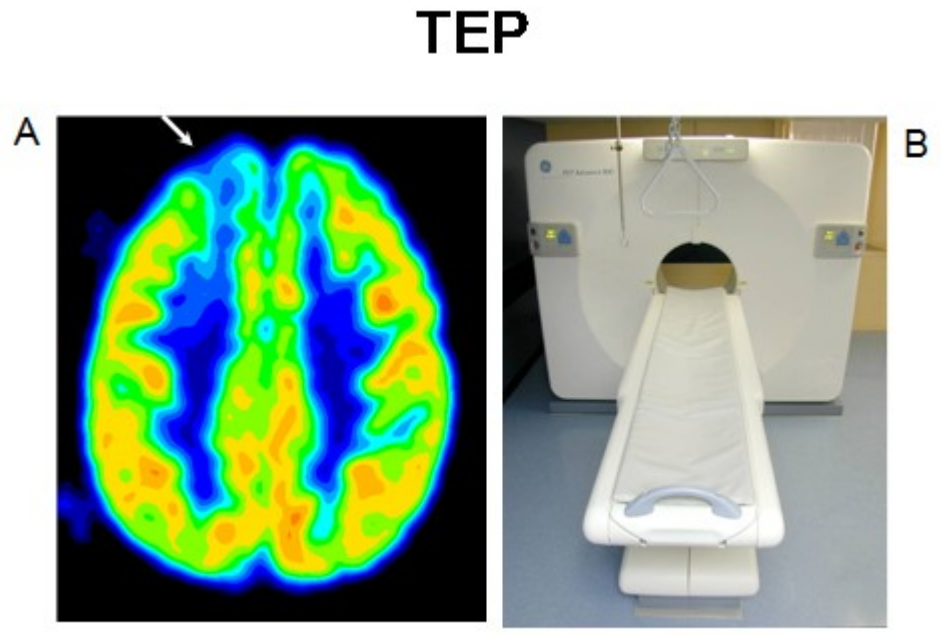


Figure 4. Détection d'une zone d'hypométabolisme frontale droite (a) à l'aide de la tomographie à émission de positon (b).

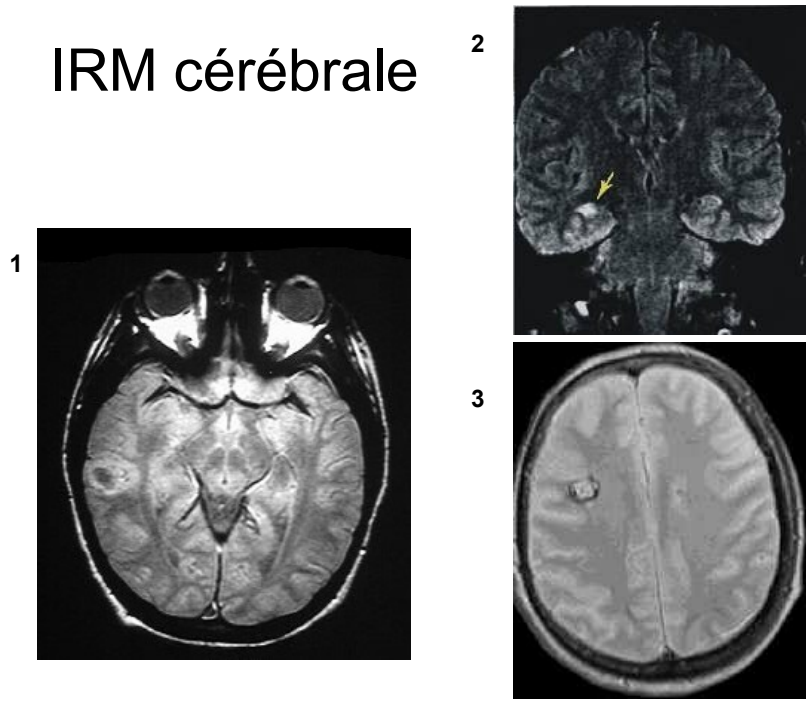


Figure 5. Images de résonance magnétique cérébrale mettant en évidence diverses lésions épileptogènes: 1- gliome 2- sclérose hippocampique 3- angiome caverneux.

## 3. POSITION DU PROBLÈME

Suite à cette évaluation préchirurgicale, les patients peuvent, de manière pratico-pratique, être catégorisés comme souffrant d'une épilepsie partielle pharmacorésistante a) lésionnelle versus non lésionnelle, et b) mésiotemporale versus néocorticale (c.-à-d. temporale latérale ou extratemporale). Alors que les taux de succès chirurgicaux oscillent autour de 60 à 75 % pour des procédures telles l'amygdalo-hippocampectomie sélective (pour les épilepsies mésiotemporales associées à une sclérose hippocampique) et les lésionectomies (pour les épilepsies néocorticales reliées à une lésion épileptogène bien délimitée tels un angiome caverneux ou une tumeur bénigne), le pronostic chirurgical demeure réservé pour les épilepsies néocorticales non lésionnelles. Ce dernier groupe de patients constitue actuellement un défi de taille alors que seulement 32 à 51 % d'entre eux seront exempts de crise après la chirurgie [20]. Or, on estime qu'environ le quart des patients avec une épilepsie partielle pharmacorésistante n'a pas de lésion épileptogène identifiable par IRM cérébrale [21-24] (voir Annexe 2). Chez ces patients, une origine génétique ou une lésion subtile sous-jacente mais indétectable par une IRM conventionnelle seraient responsables des crises [21, 23, 25-27]. En l'effet, l'absence de lésion radiologique ne préjuge pas de l'absence de lésion tissulaire, comme le confirment les examens anatomopathologiques postopératoires révélant souvent la présence sous-jacente de malformations subtiles du développement cortical (p. ex. microdysgénésie) ou une gliose. Par ailleurs, des études récentes ont confirmé la contribution importante de la génétique de certaines épilepsies partielles [28]. Les deux possibilités ne sont pas mutuellement exclusives puisque des défauts génétiques peuvent être responsables de malformations du développement cortical [29].

Face à une épilepsie partielle pharmacorésistante sans lésion identifiable par IRM conventionnelle, l'identification de la zone épileptogène repose essentiellement sur le questionnaire clinique et des examens paracliniques restants: la TEMP ictale, la TEP interictale, et l'EEG de surface interictale et ictale. Bien que performantes dans l'épilepsie mésiotemporale, ces techniques d'exploration réussissent rarement à bien délimiter la zone épileptogène en présence d'une épilepsie néocorticale de par leur

faible résolution spatiale ou temporelle [30]. Cliniquement, aucun syndrome d'épilepsie néocorticale bien défini n'est établi contrairement à l'épilepsie mésiotemporale. Les structures néocorticales sont larges et complexes, à l'origine de manifestations cliniques très variables et souvent non spécifiques de par la propagation rapide de l'activité épileptique. Ainsi, l'évaluation clinique réussit rarement à localiser fiablement la zone épileptogène. Bien que la TEMP ictale soit en mesure d'identifier correctement la zone épileptogène chez 90 % des épilepsies mésiotemporales, son exactitude diagnostique est nettement inférieure dans les épilepsies néocorticales. Dans une étude récente, la TEMP ictale n'a pu identifier le foyer que dans 33 % des cas d'épilepsies néocorticales [31, 32]. Ce faible rendement est en partie lié aux difficultés d'injection du radiotraceur lors de crises néocorticales souvent hypermotrices ainsi qu'à la dynamique des radiotraceurs mal adaptée pour des crises néorticales se propageant très vite et produisant des aires multiples d'hyperperfusion. De la même façon, la performance diagnostique de la TEP dans les épilepsies néocorticales est faible (~40 à 50 %), particulièrement dans les cas non lésionnels [33, 34]. Les données électroencéphalographiques intericales et ictales provenant de l'étude vidéo-EEG dans les cas d'épilepsies néocorticales sont souvent décevantes, tantôt parce les mouvements du patient pendant la crise entachent fortement l'EEG, tantôt parce que les crises provenant de structures profondes peuvent ne pas générer de signal mesurable en surface, tantôt parce que les anomalies sont diffuses en raison de la propagation rapide de l'activité épileptique [35-37]. Bref, bien que les techniques d'exploration actuelles du réseau épileptogène soient performantes pour l'épilepsie mésiotemporale, l'identification de la zone épileptogène chez les patients avec une épilepsie néocorticale non lésionnelle demeure, avec les outils actuels, laborieuse.

Lorsque la vidéo-EEG et les examens complémentaires non invasifs échouent dans la délimitation adéquate de la zone épileptogène, une étude électrophysiologique intracrânienne invasive est généralement nécessaire [38-40]. Une étude intracrânienne consiste en l'implantation d'électrodes intracérébrales via une craniotomie ou des trous de trépan sous anesthésie générale dans le but de mesurer directement l'activité corticale *in situ* (Figure 6). Suite à l'implantation, les patients sont transférés à l'unité d'épilepsie pour une télémétrie vidéo-EEG prolongée dans l'attente de crises

stéréotypées. Une fois la zone épileptogène délimitée par les nouvelles données ictales et intericales, le patient est reconduit en salle opératoire pour le retrait des électrodes et la résection (lorsque possible) de la zone identifiée. Les électrodes intracrâniennes remédient à la faible résolution spatiale des électrodes extracrâniennes (de surface) puisqu'elles sont plus proches des générateurs d'activité cérébrale. Toutefois, l'implantation chronique d'électrodes intracrâniennes comporte un risque d'infection et d'hémorragie et il est préférable de limiter dans la mesure du possible le nombre d'électrodes utilisées pour déterminer la zone épileptogène sans toutefois compromettre notre capacité à la détecter [41-43]. Parce que l'échantillonnage spatial est limité par le nombre d'électrodes pouvant être utilisées de manière sécuritaire, il est toujours possible qu'une étude intracrânienne échoue dans son objectif de localiser la zone épileptogène si les aires suspectes ne sont pas suffisamment couvertes.

Toutes les limites (énumérées ci-haut) des outils d'exploration actuels de l'épilepsie partielle non lésionnelle se traduisent par un pronostic chirurgical pauvre. Il est donc souhaitable de trouver d'autres méthodes permettant de déterminer le foyer épileptique dans l'optique d'éviter une étude intracrânienne ou du moins de mieux cibler les régions suspectes à investiguer au moyen d'électrodes intracrâniennes. Dans le cadre de cette thèse, nous allons explorer le potentiel de 3 de ces techniques : l'IRM à haut champ, la spectroscopie proche infrarouge (SPIR) et la magnétoencéphalographie (MEG). Ces trois techniques seront brièvement décrites dans la prochaine section.

Figure 6. Étude intracrânienne combinant grille sous-durale, bandelettes sous-durales et électrodes en profondeur.

## 4. LES MÉTHODOLOGIES

### *4.1. IRM à haut champ*

La grande majorité des investigations cliniques par IRM s'effectue à partir d'appareils de champs magnétiques de catégorie standard (1 à 2 Tesla). Malheureusement, les acquisitions ainsi obtenues ne permettent pas toujours la détection d'anomalies morphologiques. L'essor de nouvelles technologies en neuroimagerie offre le bénéfice potentiel d'améliorer la détection de lésions épileptogènes occultes.

Les systèmes à haut champ (≥3T) ont tout d'abord été utilisés dans le cadre de projet de recherche fondamentale. Les systèmes à 3 T gagnent progressivement les centres hospitaliers pour une utilisation clinique depuis leur approbation par la *Food and Drug Administration* (FDA) américaine pour une utilisation à des fins médicales. La valeur ajoutée de ces systèmes se traduit principalement par une augmentation substantielle du signal à partir duquel les images sont produites (Figure 7). Ce gain repousse les limites inhérentes à tout système d'imagerie en ce qui a trait au rapport signal sur bruit. Il augmente théoriquement la performance diagnostique de l'IRM [44]. Cette plus-value se manifeste soit par une capacité de résolution spatiale accrue permettant de détecter des anomalies corticales subtiles ou par un temps d'acquisition diminué [45]. Cette réduction du temps d'acquisition s'explique par le fait que pour un signal équivalent, la durée d'acquisition d'une séquence obtenue à champ standard (1,5 T) doit être portée au carré comparativement au temps d'acquisition nécessaire avec un champ magnétique de 3 T. Ce dernier élément joue un rôle important lorsqu'il est nécessaire de minimiser les artéfacts engendrés par les mouvements des patients lors de l'acquisition des séquences d'IRM, sachant que ces artéfacts dégradent la qualité de l'image. Ces mouvements deviennent inévitables lorsque la durée totale de l'examen éprouve la capacité des patients à conserver un état d'immobilité pour une longue période. Il s'agit malheureusement d'une situation courante lors des examens d'IRM servant à l'investigation de l'épilepsie à cause du grand nombre de séquences nécessaires pour compléter l'étude. L'équilibre entre la résolution spatiale et le temps d'acquisition qu'offre le niveau de signal à 1,5 T doit donc être pris en compte dans le

choix des séquences. Il en est de même pour l'imagerie à haut champ qui offre toutefois une plus grande latitude dans l'élaboration du schème d'investigation.

Le nombre d'études évaluant l'application clinique de l'IRM à haut champ est limité. De plus, la majorité de ces études portent principalement sur l'exploration des structures de la région mésiotemporale (hippocampe et corps amygdaloïde) dont la corrélation entre l'IRM à 1,5 T, la clinique et l'histopathologie est déjà bien connue [46]. Briellmann et al. (2001) conclurent à l'absence d'un avantage significatif de l'IRM à 3 T comparativement à l'IRM à 1,5 T pour la volumétrie de l'hippocampe chez huit sujets normaux et suggèrent que l'imagerie clinique actuelle à 1,5 T offre des images anatomiques satisfaisantes, car de haute qualité [47]. Sawaishi et al., rapportent le cas d'un garçon avec épilepsie temporale droite chez qui l'IRM à 3 T a permis de déceler une petite lésion hippocampique non visualisée avec l'IRM à 1,5 T [48]. Tchoyoson et al., rapportent également le cas d'un patient chez qui l'imagerie à 3 T aurait permis une caractérisation supérieure des détails anatomiques d'une schizencéphalie frontale avec polymicrogyrie et hétérotopie [49]. Enfin, Knake et al., mentionnent avoir détecté des lésions chez 15 patients à partir d'un échantillon de 23 patients (65 %) avec une IRM standard (1,5 T) négative [50]. Ces résultats préliminaires offrent un aperçu du potentiel de l'IRM à 3 T dans l'investigation des patients porteurs de lésions épileptogènes qualifiées à ce jour d'occultes

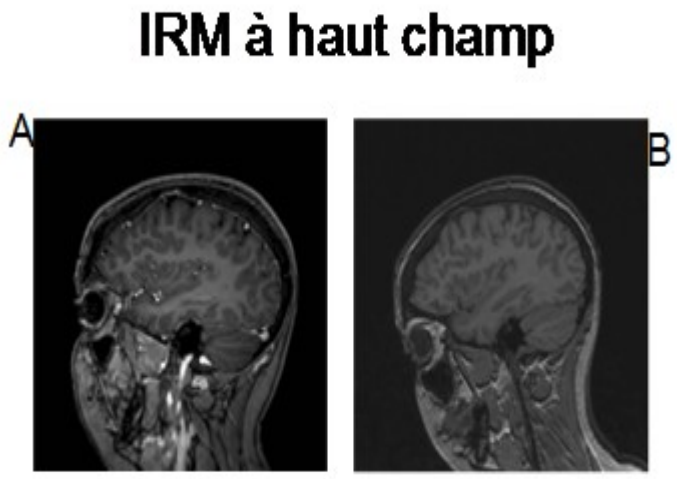


Figure 7. a) Image obtenue à partir d'une IRM 1,5T; b) Image obtenue à partir d'une IRM 3T.

### *4.2 Spectroscopie proche infrarouge (SPIR)*

La spectroscopie proche infrarouge cérébrale est une récente technique d'imagerie médicale d'un intérêt prometteur dans la localisation fonctionnelle du foyer épileptique. Cette technique non invasive consiste à utiliser la lumière dans les régions du spectre proches de l'infrarouge pour analyser le cerveau, les tissus humains étant relativement transparents à ces longueurs d'onde. Le principe de fonctionnement consiste en l'envoi d'un faisceau lumineux (de photons) perpendiculairement au crâne à l'aide d'émetteurs en plusieurs points du scalp (Figure 8). Les photons émis parcourent alors différents chemins optiques à travers les tissus cérébraux (cuir chevelu, crâne, méninges, liquide céphalorachidien, cerveau). Certains seront absorbés par les différentes couches cérébrales alors que d'autres seront dispersés et/ou réfléchis à l'extérieur du crâne. Les photons qui émergent sont collectés par des capteurs positionnés à quelques centimètres de distance en un autre point du scalp. L'intensité des signaux réfléchis dépend du chemin optique que chaque photon aura parcouru à l'intérieur des tissus cérébraux et variera selon le degré d'absorption, de réfraction, d'anisotropie et de réflexion. Comme les propriétés d'absorption du tissu cérébral sont largement déterminées par les chromophores sanguins [soit l'hémoglobine oxygénée/oxydée (HbO2) et désoxygénée/réduite (HbR)], les variations de l'intensité des signaux réfléchis peuvent être interprétées comme des changements dans les quantités relatives d'hémoglobine. Les deux types d'hémoglobine ayant des spectres d'absorption différents dans les régions proches de l'infrarouge, la SPIR peut mesurer les différentes concentrations d'HbO2, d'HbR, et d'HbT (hémoglobine totale = HbO2 + HbR). Les changements des quantités d'HbO2 et HbR reflètent les changements d'oxygénation des tissus cérébraux et les changements des quantités d'HbT reflètent les altérations du volume sanguin cérébral. Une cartographie quantitative des changements d'absorption nous informe sur les changements métaboliques et physiologiques du tissu cérébral et nous permet une visualisation de la distribution spatiale du débit sanguin cérébral régional (DSCr). L'utilisation des signaux SPIR, ayant des longueurs d'onde variant entre 600nm et 950nm, nous permet d'obtenir des mesures valables jusqu'à des profondeurs pouvant atteindre jusqu'à 3,5cm, lorsque la distance entre la source lumineuse et le capteur est maintenue à ~ 4cm [51, 52].

Une des applications cliniques prometteuses de la SPIR est l'étude de l'épilepsie. Les crises partielles (focales) suscitent une augmentation du DSCr. Cette augmentation du DSCr couplée à l'activité épileptique, exploitée par la TEMP ictale, peut également être mesurée par la SPIR (tel qu'expliqué ci-haut). L'avantage que la SPIR possède sur la TEMP ictale est sa haute résolution temporelle (<1 seconde) [53] . Alors que la TEMP ictale ne peut fournir qu'une mesure ponctuelle du DSCr, la SPIR est une méthode pouvant enregistrer de manière continue les changements rapides du flot cérébral avant, pendant et après les crises. À ce jour, relativement peu d'efforts ont été déployés pour déterminer le potentiel de la SPIR à localiser le foyer épileptique et évaluer sa place dans le bilan préopératoire des patients avec épilepsie partielle réfractaire considérés candidats à une chirurgie d'épilepsie. Les études initiales à l'aide de cette technique se sont essentiellement limitées à décrire les changements de l'oxygénation cérébrale lors de divers types de crises (spasmes infantiles, convulsions généralisées, crises partielles, absences) [54-57]. L'enregistrement se faisait alors au moyen d'un ou deux optodes seulement, généralement fixées sur le front. Bien qu'il était impossible de conclure sur leur valeur localisatrice, ces enregistrements initiaux confirmaient la possibilité de détecter des changements d'oxygénation cérébrale (et de DSCr) lors de la crise et même avant. Plus récemment, Watanabe et al., ont utilisé la technique SPIR pour enregistrer des crises induites par injection de bémégride chez 10 patients avec épilepsie temporale et 2 autres avec épilepsie pariétale implantés avec électrodes intracrâniennes. Les sondes SPIR étaient montées sur une coquille thermoplastique recouvrant la région suspecte. Huit canaux (4 de chaque côté) furent fixés chez 9 patients. Dans une aute étude, 24 canaux (12 de chaque côté) chez les 3 derniers patients étudiés [58]. Les enregistrements SPIR ont démontré une hyperperfusion au niveau de la zone épileptogène dans tous les cas, débutant 2-5 secondes après le début de la crise telle qu'enregistrée par les électrodes intracrâniennes. Une hyperperfusion dans les régions avoisinant la zone épileptogène fut notée chez 7 cas, aucune hyperperfusion dans 4 cas, et une hyperperfusion controlatérale dans un cas. Dans un article de revue scientifique, le même groupe rapporta des cas additionnels avec une base de données atteignant maintenant 28 patients incluant les 12 patients originaux (25 temporaux, 2 frontaux, 2 pariétaux) [59]. Une augmentation du DSCr ictal du côté du foyer épileptique fut enregistrée dans 96 % des cas. Ces données sont évidemment obtenues dans une population

hautement sélectionnée, au cours d'une étude intracrânienne (et donc en l'absence d'un volet osseux), et à l'aide d'optodes placées de manière biaisée sur les régions suspectes. Ces données préliminaires suggèrent toutefois que la SPIR pourrait s'avérer utile dans la localisation de la zone épileptogène.

Des raisons techniques peuvent expliquer en partie le nombre limité d'études sur la SPIR en épilepsie, notamment quant à sa valeur dans la localisation du foyer épileptique. En effet, les systèmes commerciaux actuels ne permettent généralement pas d'enregistrements continus sur une période prolongée. Or les crises épileptiques sont aléatoires et ne peuvent être provoquées sur demande lors des études SPIR conventionnelles. Par ailleurs, les appareils actuels sont trop gros et trop lourds pour des enregistrements prolongés dans les unités d'épilepsie avec des patients qui ne peuvent évidemment pas rester immobiles continuellement. De plus, les appareils commerciaux ne viennent pas avec des casques adaptés pour des sondes SPIR combinées à un enregistrement EEG continu. Finalement, le nombre d'optodes doit être suffisant pour couvrir toute la surface du crâne. Pour permettre un meilleur dépistage des signaux annonciateurs des crises épileptiques, le système idéal doit être en mesure de couvrir entièrement la tête du patient [60].

**Spectroscopie proche infrarouge combinée à l'EEG (EEG – SPIR)**

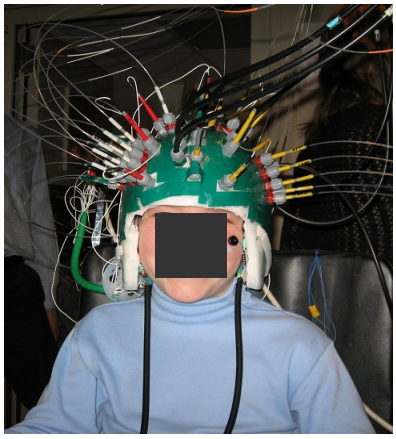

Figure 8. Appareil commercial de spectroscopie proche infrarouge modifié dans le laboratoire de Hôpital Ste-Justine pour permettre l'enregistrement simultané de l'électroencéphalogramme.

### *4.3. La magnétoencéphalographie (MEG)*

La MEG est une technique de localisation de l'activité cérébrale (qu'elle soit physiologique ou épileptique) via l'enregistrement de champs magnétiques induits par les courants électriques du cerveau [61-63]. En effet, les décharges épileptiformes donnent lieu à des courants ioniques générant des potentiels postsynaptiques excitateurs ou inhibiteurs le long de l'arborisation dendritique des neurones pyramidaux. Les flux de courant se produisant à l'intérieur des neurones pyramidaux sont nommés courants primaires. Ces courants intracellulaires produisent des courants extracellulaires compensateurs dans les tissus extracellulaires appelés courants secondaires. Or, tout courant induit un champ magnétique orthogonal (Loi de Maxwell). Parce que les courants secondaires sont distribués de manière symétrique autour du neurone, leurs champs magnétiques s'annulent à cause de la symétrie, laissant les courants primaires comme seule source du signal enregistré en MEG dans la plupart des circonstances. À l'inverse, les courants secondaires se propagent à travers le corps d'une manière déterminée par la conductivité de chaque tissu, générant des différences de potentiel à la surface du scalp observables lors d'un enregistrement EEG. Les courants dendritiques liés à la dépolarisation des neurones se propagent selon l'orientation des neurones pyramidaux et peuvent être représentés par un dipôle équivalent de courant [61]. Le cortex cérébral présentant de nombreuses circonvolutions avec plusieurs sillons et gyri, la source de courant dipolaire équivalente peut être soit tangentielle soit radiale (respectivement) par rapport à la surface corticale. Seuls les champs magnétiques générés par les sources de courant tangentielles au scalp sont détectables par les capteurs lorsque la population de neurones activés est suffisamment vaste. Avec la nouvelle possibilité d'avoir 275 capteurs placés tout autour de la tête, il est maintenant possible d'avoir un bon échantillonnage spatial de l'activité cérébrale (Figure 9a).

Le défi principal avec la magnétoencéphalographie est de déterminer la localisation de l'activité épileptiforme à l'intérieur du cerveau à partir des champs magnétiques captés à l'extérieur de la tête (communément appelée le problème inverse). Heureusement, des solutions adéquates peuvent être tirées en utilisant des modèles incorporant certaines connaissances acquises de l'activité cérébrale. Le modèle le plus

utilisé pour déterminer la source cérébrale de pointes intericales est celui du dipôle équivalent de courant (Figure 9b) [64].

Les avantages potentiels de la MEG par rapport à l'EEG sont basés sur les données physiques et les techniques d'enregistrement : a) La MEG utilise une haute densité de capteurs (275 capteurs pour l'appareil qui sera utilisé dans notre étude) difficile à obtenir avec l'EEG; b) les signaux MEG sont moins distordus par les interfaces entre la source et le capteur (par exemple les os du crâne) que les champs électriques; c) les sources d'activité électrique cérébrale sont plus faciles à localiser en MEG qu'en EEG (du moins pour les sources de courant tangentielles au scalp), car les estimations à partir de l'EEG nécessitent de construire un modèle multicompartimental (cerveau, liquide céphalorachidien, os, scalp) avec une bonne connaissance des conductivités de chacun des compartiments [65-67].

Des études comparatives ont pu confirmer sa grande sensibilité à détecter les pointes néocorticales dont les générateurs sont proches de la surface ainsi que la précision des sources localisées en MEG (que ce soit par rapport à la localisation établie par la position de diverses lésions épileptogènes ou par électrophysiologie invasive) [68, 69]. Les données suggèrent également que l'homogénéité de distribution spatiale des dipôles modélisés en MEG est corrélée à la qualité du résultat chirurgical [70-72]. Malheureusement, la majorité des sujets inclus dans ces études présentaient une épilepsie lésionnelle ou une épilepsie temporale (2 sous-populations pour lesquelles les outils diagnostiques actuels permettent généralement une bonne localisation du foyer). D'ailleurs, les études récentes semblent indiquer que la MEG n'apporterait des informations importantes complémentaires de celles des autres examens du bilan préchirurgical que chez un quart des patients [66, 73]. La valeur de la MEG n'a pas sérieusement été établie dans la sous-population difficile de sujets épileptiques potentiellement candidats à une chirurgie, soit ceux avec une épilepsie néocorticale non lésionnelle. Toutefois, les données obtenues jusqu'à maintenant sur des épilepsies lésionnelles ou sur un faible nombre d'épilepsies non lésionnelles sont fortement prometteuses [65, 74, 75].

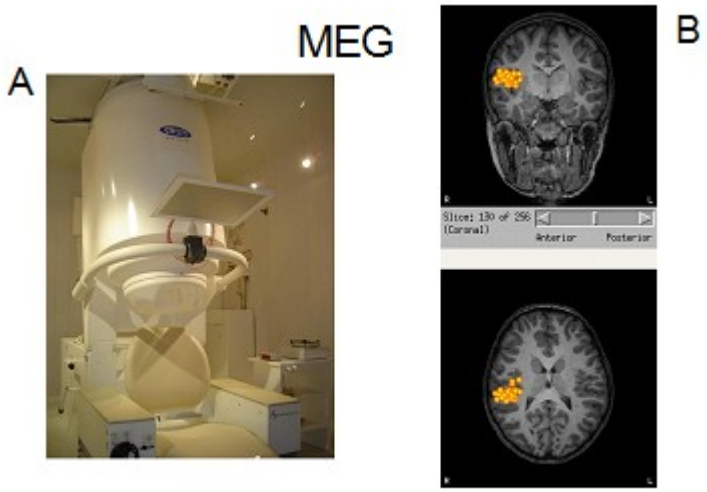


Figure 9. a) Appareil de magnétoencéphalographie installée dans une chambre blindée; b) localisation de sources des décharges épileptiques enregistrées déterminée par la méthode de dipôle équivalent de courant.

## 5. HYPOTHÈSE GÉNÉRALE

L'objectif général de cette thèse consiste à explorer le potentiel de nouvelles techniques pour localiser le foyer épileptique chez les patients souffrant d'une épilepsie partielle non lésionnelle considérés candidats à une chirurgie d'épilepsie. Plus spécifiquement, la thèse abordera le potentiel de a) l'IRM à haut champ (3T) pour la détection de lésions structurales épileptogènes; b) la (SPIR) pour la localisation fonctionnelle du foyer épileptique; c) la MEG dans la localisation neuromagnétique du foyer épileptique.

### *5.1. Première étude : étude sur la valeur de l'imagerie cérébrale à 3T dans l'épilepsie partielle réfractaire avec IRM 1,5T négative.*

L'objectif de cette première étude était de déterminer si l'IRM de haut champ à 3T pouvait détecter des lésions épileptogènes subtiles qui auraient été manquées sur une IRM conventionnelle à 1,5T chez une population de patients avec épilepsie focale réfractaire considérés candidats à une chirurgie d'épilepsie. Afin de répondre à cette question, les IRM 3T de 36 sujets épileptiques candidats à une chirurgie sans lésion détectable sur l'IRM 1,5T ont été révisées. Notre hypothèse de recherche principale stipulait que l'augmentation du rapport signal sur bruit que conférait une IRM 3T par rapport à l'IRM 1,5T nous permettrait de détecter une lésion conduisant potentiellement à un traitement chirurgical chez 17 à 29 % des patients (de 6 à 10/36 patients). Cette étude se voulait être un premier pas vers une étude prospective comparative évaluant la sensibilité et la spécificité propre à l'IRM 3T combinée ou non avec des antennes de surface matricielles chez des patients consécutifs avec épilepsie partielle pharmacorésistante pour qui aucune lésion n'est détectée à l'IRM 1,5T.

### *5.2. Deuxième étude : étude de crises temporales par SPIR*

La deuxième étude avait pour objectif d'étudier le potentiel de la SPIR dans la localisation du foyer épileptique chez un groupe de patients épileptiques avec un foyer temporal [76]. Comme expliqué plus haut, la SPIR permet d'enregistrer de manière continue les changements rapides du flot cérébral avant, pendant et après les crises. En théorie, la technique permettrait de discriminer entre la zone d'où provient la crise des aires de propagation de l'activité épileptique. Notre hypothèse était donc que la SPIR pouvait localiser adéquatement le foyer épileptique en détectant précocement l'augmentation du volume cérébral sanguin régional induit par la crise focale. Pour réaliser cet objectif, nous avons procédé à des enregistrements SPIR-EEG prolongés chez 9 patients avec épilepsie mésiotemporale pharmacorésistante. Cette étude constituait nos premiers pas dans l'évaluation du potentiel de la SPIR pour localiser le foyer épileptique chez des patients avec épilepsie focale en se concentrant d'abord sur les crises temporales.

### *5.3. Troisième étude : étude de crises frontales par SPIR*

La troisième étude avait pour objectif d'étudier le potentiel de la SPIR dans la localisation du foyer épileptique chez un groupe de patients épileptiques avec un foyer frontal. Les crises frontales se distinguent des crises temporales de nombreuses façons. Cliniquement, les crises frontales surviennent à une fréquence moyenne plus élevée, sont plus courtes, ont une tendance nocturne, incorporent souvent des comportements moteurs complexes et ont une période postictale relativement courte. Électrophysiologiquement, un dense réseau de connections permet une propagation très rapide de l'activité épileptique à des régions contiguës ou distantes rendant souvent difficile leur localisation voire leur latéralisation. Tout comme pour notre étude des crises temporales mentionnée ci-haut, notre hypothèse était que la SPIR pouvait localiser adéquatement le foyer épileptique en détectant précocement l'augmentation du volume cérébral sanguin régional induit par la crise focale. Pour réaliser notre objectif, nous avons procédé à des enregistrements SPIR-EEG prolongés chez 20 patients avec épilepsie partielle frontale non lésionnelle.

### *5.4. Quatrième étude : étude sur la valeur de la MEG dans l'évaluation préchirurgicale de patients avec épilepsie partielle réfractaire non lésionnelle.*

Cette quatrième et dernière étude visait à évaluer la valeur de la MEG dans l'évaluation préchirurgicale de patients avec épilepsie partielle réfractaire non lésionnelle. Comme mentionné précédemment, la plupart des études cliniques étudiant la MEG pour l'épilepsie ont inclus de manière indiscriminée des patients avec épilepsie lésionnelle (une sous-population pour laquelle la localisation du foyer épileptique peut être assumée de manière raisonnable de par le site de la lésion) et épilepsie non lésionnelle (généralement en faible nombre). Notre étude MEG contient la plus grande série de patients avec épilepsie focale réfractaire considérés candidats à une chirurgie rapportée jusqu'à maintenant.

# ARTICLES

**ARTICLE 1**

***Value of 3.0 T MR imaging in refractory partial epilepsy and negative 1.5 T MRI***

**Published by** :
2010 British Epilepsy Association. Published by Elsevier Ltd.
Seizure 19 (2010) 475–478

**Dang Khoa Nguyen[1], Émilie Rochette[1], Jean-Maxime Leroux[2], Gilles Beaudoin[2], Patrick Cossette[1], Maryse Lassonde[3, 4], François Guilbert[2].**

*[1] Service de Neurologie, Hôpital Notre-Dame du CHUM, Université de Montréal;*
*[2]Département de Radiologie, Hôpital Notre-Dame du CHUM, Université de Montréal;*
*[3]Centre de Recherche en Neuropsychologie et Cognition, Université de Montréal*
*[4]Centre de Recherche, Centre Hospitalier Universitaire Ste-Justine Université de Montréal, Montréal, QC, Canada;*

Running title: Impact of 3.0T MR imaging in nonlesional refractory partial epilepsy candidates for surgery.

Key words: Focal Epilepsy, Refractory Epilepsy, Magnetic Resonance Imaging, 3.0 Tesla vs 1.5 Tesla.

## ABSTRACT

*Background:* High-field 3.0 Tesla MR scanners provide an improved signal-to-noise ratio which can be translated in higher image resolution, possibly allowing critical detection of subtle epileptogenic lesions missed on standard-field 1.0-1.5T MRIs. In this study, the authors explore the potential value of re-imaging at 3.0T patients with refractory partial epilepsy and negative 1.5T MRI.

*Methods:* We retrospectively identified all patients with refractory partial epilepsy candidate for surgery who had undergone a 3.0T MR study after a negative 1.5T MR study. High-field 3.0T MRIs were reviewed qualitatively by neuroradiologists experienced in interpreting epilepsy studies with access to clinical information. Relevance and impact on clinical management was assessed by an epileptologist.
*Results.* Between November 2006 and August 2009, 36 patients with refractory partial epilepsy candidate for surgery underwent 3.0T MR study after a 1.5T MR study failed to disclose a relevant epileptogenic lesion. A potential lesion was found only in two patients (5.6%, 95% CI ; 1.5-18.1%). Both were found to have hippocampal atrophy congruent with other presurgical localization techniques which resulted in omission of an invasive EEG study and direct passage to surgery.

*Conclusions:* The frequency of detection of a new lesion by re-imaging at 3.0T patients with refractory partial epilepsy candidate for surgery was found to be low, but seems to offer the potential of a significant clinical impact for selected patients. This finding needs to be validated in a prospective controlled study.


## INTRODUCTION

Despite the regular introduction of new anticonvulsants on the market, many epileptic patients continue to have drug-resistant seizures. Their best option is often to consider surgery. In the context of epilepsy surgery, the main challenge is finding the precise location of the epileptogenic zone in the brain, in order to remove it and end the

seizures. In the presurgical evaluation, MRI (Magnetic resonance imaging) is particularly useful in that aspect as the location of a structural lesion is usually congruent with the epileptogenic zone. Several studies confirm that detection of an epileptogenic lesion on MRI substantially improves the outcome of an epilepsy surgery (Kuzniecky *et al*., 2002, Kral *et al*., 2003).

The strength of the magnetic field of an MRI scanner is measured in Tesla (T). Many refer to field strengths ≥ 3.0T as 'high-field', 1.0-2.0T as 'standard', and < 0.5T as 'low field'. The vast majority of epilepsy protocol MRI studies are currently performed on a 1.0-1.5T scanner and include (a) a volume acquisition T1-weighted data set acquired in an oblique coronal orientation and covering the whole brain in 0.9mm partitions; (b) an oblique coronal spin-echo sequence, with proton density, heavily T2-weighted and FLAIR acquisitions that are orientated perpendicular to the long axis of the hippocampus (Elger *et al*., 2004). Using these conventional acquisitions, abnormalities are detected in ≥80% of patients with refractory temporal lobe epilepsy but in only 50-60% of patients with refractory neocortical epilepsy (Wetjen *et al*., 2002). High-field 3T MRIs were approved recently by the *American Food and Drug Administration* (FDA) for clinical use and have been introduced progressively in academic centers over the last few years. High-field MRIs provide an improved signal-to-noise ratio which could theoretically result in higher image resolution, possibly allowing critical detection of subtle epileptogenic lesions missed on standard field MRIs (Griffiths *et al*., 2005). The question arises whether patients with refractory partial epilepsy and a previously negative 1.5T MRI should be re-imaged with a 3T MRI now that these are more popular. We address this issue in this retrospective study.

## METHODS

We retrospectively identified all refractory partial epilepsy patients candidate for epilepsy surgery in whom a 3.0T epilepsy protocol MRI was performed between November 2006 and August 2009 because a previous standard field MRI (1.0-1.5T) had failed to identify a relevant epileptogenic lesion. Patients were eligible if they had undergone a comprehensive presurgical evaluation including a clinical history and

examination, long-term video-EEG monitoring for recording of seizures, and at least one epilepsy protocol head-coil standard field (1.0-1.5T) MRI scan at our center or an affiliated academic center. All standard-field MRIs had been read previously by an unblinded experienced neuroradiologist. The study was approved by our institutional ethics committee with waiver of informed consent.

*MRI*

The initial 3.0T scans were performed at the CRIUGM, a research center affiliated with the University of Montreal on a Siemens Tim TRIO (Siemens AG, Berlin, Germany). The remaining 3.0T scans were performed at Notre-Dame Hospital when the Achieva Dual 3.0T system was installed in January 2008 (Philips Medical Systems, Best, Netherlands). All 3.0T studies included (a) a 3D T1-weighted gradient-echo acquisition of the whole brain (TR/TE, 24/6; flip angle, 25º; field of view, 256*256 mm; matrix, 256 x192); (b) axial T2-weighted (TR/TE, 24/6; flip angle, 25º; field of view, 256*256 mm; matrix, 256 x192) and FLAIR (TR/TE, 24/6; flip angle, 25º; field of view, 256*256 mm; matrix, 256 x192) acquisitions of the whole brain; (c) coronal T2-weighted and FLAIR acquisitions perpendicular to the longitudinal axis of the hippocampus. Intravenous contrast agents were given only if a mass lesion was demonstrated.

*Image review*

High-field MRIs were reviewed qualitatively by neuroradiologists experienced in interpreting epilepsy studies and with access to clinical information. If an abnormality was identified on the high-field MRI study, the finding was interpreted by an epileptologist to determine whether the abnormality was relevant to the patient's epileptic condition and if it resulted in a change in clinical management. The localization of each patient's epileptogenic zone was determined based on multimodal analysis of clinical, electrophysiological (scalp EEG, MEG) and functional (PET, SPECT, EEG-fMRI) data. Findings from intracerebral findings, pathological examination of the tissue resected and surgical outcome were also used when available.

## RESULTS

*Patients*

We identified 36 (20M; 16F; median age: ?) patients with refractory partial epilepsy candidate for epilepsy surgery whose 1.5T MRI failed to detect a relevant epileptogenic lesion and who underwent re-imaging at 3.0T between November 2006 and August 2009. Median interval between the two MRIs was 22.5 months (range 0day-13years). Localization of the epileptogenic zone was based on multimodal analysis of clinical, scalp EEG, functional (SPECT and PET) data for all patients. Magnetoencephalography was obtained in 26 subjects and EEG-fMRI in 24. Additional invasive EEG findings were available for ten patients. Sixteen had frontal lobe epilepsy, 15 had temporal lobe epilepsy, three had parietal lobe epilepsy and two had occipital lobe epilepsy.

*Standard-field MRI*

As determined by our inclusion criteria, standard-field MRI failed to reveal a congruent epileptogenic lesion in all patients. Twenty-five were performed at our institution using our epilepsy protocol. The remaining cases were scanned in other affiliated academic hospitals also benefiting from an epilepsy protocol. Ten patients had unspecific or unrelated brain abnormalities on their 1.5T MRI: Chiari type I malformation (1), arachnoid cyst (1), small white matter signal abnormalities (4), quadrigeminal plate lipoma (1), mild atrophy (2) or slight malrotation of hippocampus (1) but contralateral to the suspected epileptogenic zone.

*High-field MRI*

High-field MRIs were obtained using a 3.0T Siemens Tim TRIO (Siemens AG, Berlin, Germany) in 11 cases and a Philips Achieva Dual 3T (Philips Medical Systems, Best, Netherlands) in the other 25. High-field imaging identified an abnormality in two out of 36 patients (5.6%) (see table 1). A mild left hippocampal atrophy was discovered for case 6 whose electroclinical data suggested left mesial temporal lobe epilepsy. A mild right hippocampal atrophy was found for case 13 whose presurgical evaluation suggested right mesial temporal lobe epilepsy. Intervals between standard and high-field MRI studies for both patients were 32 and 10

months, respectively. In light of these findings, it was decided to omit the invasive EEG study in both cases. Patient 13 underwent a right anterior temporal lobectomy with Engel 1 outcome (31 months follow-up) while Patient 6 is waiting to be operated. Of the ten patients with unspecific or incongruent findings on their 1.5T MRI, 3.0T imaging provided no further information. One patient with negative 1.5T MRI was found to have a small white matter signal abnormality far from and contralateral to the suspected epileptogenic zone.

## DISCUSSION

Outcome of epilepsy surgery is intimately linked to accurate localization of the epileptogenic zone (Luders and Awad, 1992). Any technique enabling our capacity to detect an underlying pathological substrate is bound to increase our chance to delimit this epileptogenic zone. Introduction in the nineteen eighties of MRI for clinical use has revolutionized the evaluation of partial epilepsy, unveiling previously undetected lesions such as cortical developmental malformations and hippocampal atrophy. This in turn has led to better surgical outcome, reduced need for intracranial EEG studies as well as disclosing a new population of potential candidates for epilepsy surgery. Because numerous studies have shown such a strong correlation between seizure relief and resection of a visible structural lesion, finding evidence for such an epileptogenic lesion has assumed an important role in the presurgical work-up of patients with intractable partial epilepsy (Spencer *et al*., 1995).

Most hospitals are equipped with a commercial whole-body magnet operating at 1.0-1.5T. Several studies have already shown the benefit of dedicated MRI protocols interpreted by experienced neuroradiologists (McBride *et al*., 1998; von Oertzen *et al*., 2002). Technological advances have allowed the development of more powerful magnets and 3.0T MR scanners have been progressively installed worldwide for clinical use over the last few years. A greater magnetic field strength provides a higher signal-to-noise ratio which in turn allows faster imaging for a given resolution or higher resolution for a given imaging time. The obvious implication for epilepsy patients is that higher field MRI has the potential to detect subtle epileptogenic lesions that might have been missed by low-field or standard-field MRI. Formal comparison

is however required to confirm improvements in the detection of epileptogenic lesions by 3.0T scanners over current 1.5T clinical scanners as there are certain disadvantages of working at higher field. These include increased susceptibility artefact from magnetic field inhomogeneity in orbitofrontal and temporal brain regions nearing air-filled nasal cavities as well as poorer T1-weighted contrast by convergence of tissue T1 values which may negate the theoretical increase in signal to noise ratio over 1.5T images (Briellman *et al*., 2003; Knake *et al*., 2005).

Table 1. Summary of clinical and presurgical findings, intracranial EEG results, and surgical outcome.

| Patient | Epilepsy | MRI 1.5T; detected epileptogenic lesion | MRI 1.5T; non-specific abnormality | MRI 3T added findings | ICE | surgery | outcome (Engel) | F-U (mo) | pathology |
|---|---|---|---|---|---|---|---|---|---|
| 1 | R FLE | no | | no | no | no | | | |
| 2 | R FLE | no | small WMSA | no | no | no | | | |
| 3 | bi-MTLE | no | | no | no | no | | | |
| 4 | R FLE | no | | no | no | no | | | |
| 5 | R NTLE | slight malrotation of contra-lateral L hippocampus vs variant | | no | no | no | | | |
| 6 | L MTLE | no | | yes (mild L HA) | no | no | | | |
| 7 | bi-MTLE (L>>>R) | contralateral mild R HA | | no | yes | L ATL | I | 3 | CA1,3,4 cell loss, gliosis |
| 8 | R NTLE | no | Chiari type I | no | no | no | | | |
| 9 | R FLE | no | | no | yes | R F corticetomy | I | 2 | pending |
| 10 | L NTLE | no | | no | no | no | | | |
| 11 | L FLE | no | small lipoma, small WMSA | no | no | no | | | |
| 12 | L NTLE | no | | no | no | no | | | |
| 13 | R MTLE | no | | yes (mild R HA) | no | R ATL | I | 22 | CA1 cell loss, gliosis |
| 14 | R FLE | no | small WMSA | no | yes | R F corticetomy | I | 23 | normal |
| 15 | R PLE | no | | no | yes | R P corticectomy | I | 22 | cortical dysplasia |

| Patient | Epilepsy | MRI 1.5T; detected epileptogenic lesion | MRI 1.5T; non-specific abnormality | MRI 3T added findings | ICE | surgery | outcome (Engel) | F-U (mo) | pathology |
|---|---|---|---|---|---|---|---|---|---|
| 16 | R FLE | no | | no | yes | R F corticetomy | I | 23 | cortical dysplasia |
| 17 | L FLE | no | | no | no | no | | | |
| 18 | L NTLE | no | | no | no | no | | | |
| 19 | R MTLE | contralateral mild L HA | | no | yes | R SAH | I | 24 | not available |
| 20 | L NTLE | no | | no | no | no | | | |
| 21 | R FLE | no | | no | no | no | | | |
| 22 | L FLE | no | | no | yes | L F corticectomy | IV | 24 | microdysgenesis |
| 23 | R OLE | no | | no | yes | R O corticectomy | I | 12 | normal |
| 24 | R MTLE | no | | no | yes | R ATL | I | 4 | CA1, 3, 4 cell loss, gliosis |
| 25 | L NTLE | no | | no | no | no | | | |
| 26 | L PLE | no | | no | no | no | | | |
| 27 | bi-MTLE | no | small WMSA | no | no | no | | | |
| 28 | L NTLE | no | | no | no | no | | | |
| 29 | L FLE | no | | no | no | no | | | |
| 30 | R PLE | no | | no | no | no | | | |
| 31 | L FLE | no | | no (small WMSA) | no | no | | | |
| 32 | R FLE | no | discrete vermal atrophy | no | no | no | | | |
| 33 | R FLE | no | | no | no | no | | | |
| 34 | OLE | no | | no | no | no | | | |
| 35 | L FLE | no | | no | no | no | | | |
| 36 | R FLE | R HA but suspected EZ is R frontal | | no | yes | no | | | |

**LEGEND**

Abbreviations used: R= right; L= left; NTLE= neocortical temporal lobe epilepsy; MTLE= mesial temporal lobe epilepsy; FLE= frontal lobe epilepsy; PLE= parietal lobe epilepsy; OLE = occipital lobe epilepsy; ICE= intracranial electroencephalogram; HA= hippocampal atrophy; WMSA= white matter signal abnormality; ATL= anterior temporal lobectomy; SAH= selective amygdalo-hippocampectomy ; EZ= epileptogenic zone; Engel classification : I= free from imparing seizures; II= rare disabling seizures; III= worthwhile improvement; IV= no worthwhile improvement

Our study shows that re-imaging non-lesional focal epilepsy patients at 3.0 T provided clinical relevant findings in only two out of 36 patients (5.6%). This estimation is also associated with a substantial uncertainty (95% CI: 1,5%-18,1%) related to this small population. Despite this low detection rate, the abnormalities that were found did have an impact on clinical management. Both were found to have mild hippocampal atrophy congruent with other presurgical findings, obviating the need for invasive EEG monitoring. Higher-field imaging also disclosed an unrelated lesion (small white matter signal abnormality) in one case (false positive).

Limited studies have looked at the value of structural imaging at higher field for epilepsy. Volumetrically-derived volumes of amygdala and hippocampus from 1.5 and 3.0T images did not differ in eight healthy subjects (Briellman *et al*., 2001) and ten temporal lobe epilepsy patients (Scorzin *et al*., 2008). Griffiths *et al*., (2005) reported their initial experience of imaging 120 adults with localisation-related epilepsy using MR imaging at 3.0T (SENSE head coil) but provided no comparison with 1.5T imaging data. In the only prospective study available, Knake et al., (2005) reported that 3.0T MRI with a custom-made eight-channel flexible receive-only phased array coil resulted in the detection of a new lesion in 15 of 23 (65%) patients with medically intractable focal epilepsy and normal 1.5T MRI. Unfortunately, the authors were unable to separate the benefits of differences in expertise between radiologists, use of higher field strength, or use of the phased array head coil. Similar dramatic detection rates of new lesions have not been reported since. Phal *et al*., (2008) attempted a formal comparison of standard and high-field structural MRIs for epilepsy by retrospectively reviewing images from 25 patients who underwent both 1.5T (with transmit-receive single-channel head coil) and 3.0T (with six-channel SENSE head coil) scanning. MRI at 3.0T outperformed MRI at 1.5T for image quality parameters (distortion and artefact, lesion conspicuity, gray-white matter differentiation, and motion). Sub-analyses on the 19 patients with partial epilepsy revealed that lesions were detected in 74% of cases done on 1.5 T MRI compared to 88% at 3.0T. These findings are however not directly comparable to our series as the authors included patients regardless of the reason for repeating imaging (such as previously normal or equivocal results at 1.5T but also lesional follow-up and surgical planning). In fact, only 5 cases out of 19 partial epilepsy patients had a negative 1.5T

MRI. Strandberg *et al*. (2008) reported that 3.0T (4 channel head coil and parallel imaging) MRI provided new or additional information about structural grey matter abnormalities, compared to reports from 1.0-1.5T MRI, in five (out of 25) patients (20%). In one 1.5T MRI-negative patient, a malformation of cortical development was identified. In four other patients with unspecific findings (cortical atrophy, heterotopia, increased signal changes after subpial transection) on 1.0T or 1.5T MRI, malformations of cortical development were identified on 3.0T MRI. The higher detection rate compared to our findings could possibly be explained by the fact that two of their patients would have been excluded in our study. After removing the patient with heterotopia and the patient with increased signal changes after subpial transection detected at 1.5T, the detection rate drops to (8.7%). More recently, Zijlmans *et al*. (2009) scanned 37 epileptic patients considered ineligible for surgery based on available presurgical findings using a 1.5T MR (with an 8-channel phased array SENSE head coil) scanner and a 3.0T MR scanner (with a similar phased-array head coil). The first experienced neuroradiologist identified 22 lesions on both 1.5T and 3.0T studies while the second identified 28 lesions on the 1.5T MR study as opposed to 20 lesions on the 3.0T MR study. Hence, in total, fewer lesions were surprinsingly identified on 3.0T with phased-array coil than on 1.5T with phased-array coil. Sub-analyses suggested that 3.0T phased-array coil images might be more liable to detect dysplasias while 1.5T phased-array coil images were better to detect tissue loss. Although this study imaged a different population (i.e. patients ineligible for surgery and not necessarily nonlesional) than ours and used phased-array coils in both 1.5T and 3.0T scans (making it impossible to determine the benefit of going from 1.5T to 3.0T field strengths independent from the contribution of phased array coils), it provides argument that the gain provided by imaging at higher field is not necessarily obvious nor remarkable.

Hence, in response to our question whether re-imaging our nonlesional refractory patients was essential and what benefits it brought them, it would appear that the rate of detection of a new epileptogenic lesion by 3.0T structural imaging is low (5.6%) though the impact of identifying such a lesion on clinical management was significant. One could advocate that despite this low rate of detection, epilepsy surgery candidates with negative 1.5T MRI should still be re-imaged at 3.0T

considering it could prevent a costly invasive EEG study with potential risks of infection and haemorrhage as well as improve surgical outcome. However, there is little to support re-imaging at 3.0T patients with well-controlled partial epilepsy. The frequency of lesions not detected on standard-field MRI is expected to be even lower in this population as malformations of cortical development and hippocampal abnormalities are mostly encountered in refractory patients.

The retrospective nature of our study introduced certain limitations. As in other studies, some standard-field MRIs were performed in other centers where patients were previously followed prior to referral to our institution. Although these centers were affiliated academic centers using epilepsy protocols, small differences in MR systems and acquisitions parameters could result in variable image quality. Furthermore, there might be some differences between neuroradiologists in their expertise with epilepsy MR studies. Finally, an unblinded reader reproduces clinical practice but introduces a certain investigation bias in favor of the 3.0T. The delay between both 1.5 and 3.0T MRI was acceptable in our study to prevent introducing a bias that would be related to progressive tissue changes. In any case, a longer delay would have only created a bias in favor of 3.0T MRI.

With the increasing availability of 3.0T MR scanners for clinical purposes along with phased-array coil development, more robust data is clearly needed to provide recommendations. A prospective study addressing issues mentioned above is currently underway in our institution in which controls and patients with refractory partial epilepsy with negative 1.5T MRI will undergo three additional MR studies: 1.5T with phased-array coils, 3.0T and 3.0T with phased-array coils. Interpretation of images by two blinded experienced neuroradiologists on two separate occasions, correlation with other presurgical localization technique and intracerebral recordings or pathological examination when available, assessment of impact on clinical management will be performed.

**Acknowledgments**

The study was funded by the Fonds pour la Recherche en Santé du Québec. The authors would like to thank all patients and their treating neurologists.

## REFERENCES

**1**-Kuzniecky RI, Knowlton RC. Neuroimaging of epilepsy. Semin Neurol. 2002; 22: 279-288.

**2**-Kral T, Clusmann H, Blümcke I, Fimmers R, Ostertun B, Kurthen M, Schramm J. Outcome of epilepsy surgery in focal cortical dysplasia. J Neurol Neurosurg Psychiatry. 2003; 74: 183-188.

**3**-Elger CE, Von Oertzen J. MRI in presurgical evaluation of epilepsy. In: *The Treatment of Epilepsy,* 2nd edition; Shorvon S, Perucca E, Fish D, Dodson E, editors. Blackwell Publishing, 2004: 640-651.

**4**-Wetjen NM, Cohen-gadol AA, Maher CO, Marsh R, Meyer FB, Cascino GD. Frontal lobe epilepsy: diagnosis and surgical treatment. Neurosurg Rev 2002; 25:119-138.

**5**-Griffiths PD, Coley SC, Connolly DJA., Hodgson T, Romanowski CAJ, Widjaja E Darwent G, Wilkinson ID. MR imaging of patients with localization-related seizures: initial experience at 3.0T and relevance to the NICE guidelines. Clin Radiol. 2005; 60: 1090-1099.

**6**-Luders HO, Awad I. Conceptual considerations. In: Luders HO, ed. Epilepsy Surgery. New York: Raven Press, 1992; 51-62.

**7**-Spencer SS. MRI and epilepsy surgery. Neurology 1995; 45:1248-1250.

**8**-McBride MC, Bronstein KS, Bennett B, Erba G, Pilcher W, Berg MJ. Failure of standard magnetic resonance imaging in patients with refractory temporal lobe epilepsy. Arch Neurol 1998; 55: 346-348.

**9**-Von Oertzen J, Urbach H, Jungbluth S, Kurthen M, Reuber M, Fernández G, Elger CE. Standard Magnetic Resonance Imaging is Inadequate for Patients With Refractory Focal Epilepsy. J Neurol Neurosurg Psychiatry. 2002;73:643-647.

**10**-Briellman RS, Pell GS, Wellard RM, Mitchell LA, Abbott DF, Jackson GD. MR imaging of epilepsy: State of the art at 1.5 T and potential of 3 T. Epileptic Disord. 2003 ; 5(1):3-20.

**11**-Knake S, Triantafyllou C, Wald LL, Wiggins G, Kirk GP, Larsson PG, Stufflebeam SM, FoleyMT, Shiraishi H, Dale AM, Halgren E, Grant PE. 3T phased array MRI improves the presurgical evaluation in focal epilepsies: A prospective study. Neurology. 2005;65:1026-1031.

**12**-Briellman RS, Syngeniotis A, Jackson GD. Comparison of Hippocampal Volumetry at 1.5 Tesla and at 3 Tesla. Epilepsia. 2001; 42(8):1021-1024.

**13**-Scorzin JE, Kaaden S, Quesada CM, Müller CA, Fimmers R, Urbach H, Schramm J. Volume determination of amygdala and hippocampus at 1.5 and 3.0T MRI in temporal lobe epilepsy. Epilepsy Res. 2008;82:29-37.

**14**-Phal PM, Usmanov A, Nesbit G, Anderson JC, Spencer D, Wang P, Helwig JA, Roberts C, Hamilton BE. Qualitative Comparison of 3-T and 1.5-T MRI in the Evaluation of Epilepsy. AJR. 2008;191:890-895.

**15**-Strandberg M, Larsson EM, Backman S, Källén K. Pre-surgical Epilepsy Evaluation Using 3T MRI. Do Surface Coils Provide Additional Information? Epileptic Disord. 2008;10(2):83-92.

**16**-Zijlmans M, de Kort GAP, Witkamp TD, Huiskamp GM, Seppenwoolde JH, van Huffelen AC, Leijten FSS. 3T Versus 1.5T Phased-Array MRI in the Presurgical Work-up of Patients With Partial Epilepsy of Uncertain Focus. J Magn Reson Imaging. 2009; 30:256-262.

**17**-Sawaishi Y, Sasaki M, Yano T, Hirayama A, Akabane J, Takada G. A Hippocampal lesion detected by high-field 3 T Magnetic Resonance Imaging in a Patient with Temporal Lobe Epilepsy. Tohoku J Exp Med. 2005;205:287-291.

**18**-Marshall D, Hailey D, Menon D. Magnetic field strength issues in magnetic resonance imaging. Can Assoc Radiol. 1994; 45: 180-4.

**19**-Bachmann R, Reilmann R, Schwindt W, Kugel H, Heindel W, Krämer S. FLAIR imaging for multiple sclerosis: a comparative MR study at 1.5 and 3.0 T. Eur Radiol. 2006;16 : 915-921.

**20**- Goyal M, Bangert BA, Lewin JS, Cohen ML, Robinson S. High resolution MRI Enhances Identification of Lesions Amenable to Surgical Therapy in Children with Intractable Epilepsy. Epilepsia. 2004;45(8) : 954-959.

**21**-Grant PE. Structural MR Imaging. Epilepsia. 2004;45(Suppl.4): 4-16.

**ARTICLE 2**

***Non-invasive continuous EEG-fNIRS recording of temporal lobe seizures***

**Published by**:
Epilepsy Research, 2012; vol. 99 (1-2) pp.112-26.

**Dang Khoa Nguyen[1], Julie Tremblay[2], Philippe Pouliot[3], Phetsamone Vannasing[2], Olivia Florea[2], Lionel Carmant[2], Franco Lepore[4], Mohamad Sawan[3], Frédéric Lesage[3], Maryse Lassonde[2,4]**

*[1]Service de Neurologie, Centre Hospitalier Universitaire de Montréal (Hôpital Notre-Dame), Montréal, Canada*
*[2]Centre de Recherche de l'Hôpital Sainte-Justine, Montréal, Canada*
*[3]École Polytechnique, Université de Montréal, Montréal, Canada*
*[4]Centre de Recherche en Neuropsychologie et Cognition, Université de Montréal, Montréal, Canada*

Running title: Continuous near-infrared spectroscopy imaging of temporal lobe seizures

Key words: EEG-fNIRS, seizures, haemodynamic response, temporal lobe epilepsy

**SUMMARY**

*Purpose:* Functional near-infrared spectroscopy (fNIRS) is a technique that allows continuous non-invasive monitoring of tissue oxygenation and haemodynamics in the brain. By using com-bined EEG-fNIRS recordings, we sought to better understand the pathophysiology of temporal lobe seizures.

*Results:* Nine patients (5 males; mean age 35 years; range 11—56 years) with refractory mesial temporal lobe epilepsy underwent combined EEG-fNIRS recordings. Eight complex partial seizures from 3 patients were successfully recorded. All seizures were associated with significant local and remote haemodynamic changes which outlasted the duration of seizures. Over the epileptogenic temporal lobe, increased oxygenation [increase in cerebral blood volume (CBV) and oxyhaemoglobin (HbO), decrease in deoxyhaemoglobin (HbR)] was followed by a deoxy-genated state [increase in HbR]. A similar haemodynamic profile was seen over the contralateral temporal lobe (even without evidence of epileptic propagation) though variations generally had lower amplitudes. Heterogeneous haemodynamic changes in remote frontal and/or parietal areas were also noted early on when epileptic activity was limited to the temporal lobe.

*Conclusion:* EEG-fNIRS reveals complex local and remote oxygenation changes during temporal lobe seizures.

**INTRODUCTION**

Near-infrared spectroscopy [functional near-infrared spectroscopy (fNIRS)] is a light-based imaging technique which may be of great value in the study of epilepsy [1-3]. Near infrared light projected onto the scalp by optical fibres is transmitted into the intact skull, penetrating into the brain and diffusely propagating in the tissue. As it passes through the brain during these random scattering events, light is absorbed by pigmented compounds, mainly haemoglobin. Sensor probes placed at a certain distance from the transmitting probes receive the scattered light back from the brain

tissue. By using one wavelength more sensitive to deoxygenated haemoglobin (HbR) (here 690 nm) and another more sensitive to oxygenated haemoglobin (HbO) (here 830 nm), variations in amplitude of backscattered light can be used to infer on local changes in blood oxygenation. Furthermore, assuming a constant haematocrit, changes in total haemoglobin (HbT = HbO + HbR) can be used as an indicator of cerebral blood volume (CBV) variations. Intracranial propagation of near-infrared light is affected by multiple factors (e.g. age-dependent optical properties of the scalp, skull, cerebrospinal fluid and brain, distance between the transmitting and receiving probes). In the adult head, the fNIRS signal mainly reflects the absorption at a depth of one to two cm below the scalp when the inter-probe distance is set between three to five cm. By performing measurements with multiple sources and detectors distributed over the scalp, one obtains overlapping sensitivity profiles that allow the spatial localization of absorption changes within the superficial cortex. Because focal epileptic seizures elicit an increase in regional CBV in the seizure focus [4], continuous fNIRS monitoring could track regional haemodynamic and oxygenation changes before, during and after seizures without the limitations associated with single photon-emission computed tomography (SPECT) and combined electroencephalography-functional magnetic resonance imaging (EEG-fMRI). In ictal SPECT, a photon-emitting radiotracer is injected intravenously at the onset of a seizure, accumulates, and remains 'fixed' in different areas of the brain proportionally to the cerebral perfusion to these regions at the time of injection. Because it takes ~10-30 s to inject the radiotracer once one realizes a seizure has started, ~15-20 s for the tracer to reach the brain and tens of seconds for cerebral uptake proportional to blood flow and trapping into brain cells, the single ictal perfusion brain image cannot always discriminate between the seizure onset zone and areas receiving propagated activity [5]. EEG-fMRI relies on the blood oxygenation level-dependent (BOLD) contrast caused by an increase in oxygen delivery following epileptic discharges. However, EEG-fMRI studies of seizures are difficult to perform because seizures are unpredictable and rarely occur at the moment of scanning, and because patient movement can have a severe effect on data quality [6].

Until now, little effort has been made to evaluate the usefulness of fNIRS in the study of seizures in humans and even less its ability to localize the epileptogenic zone.

Previous observations using fNIRS during seizures were limited by the use of a single light source coupled with one or two detectors (i.e. optodes) usually affixed to the hairless skin overlying the frontal cortex (to avoid hair attenuation of light) but distant from the seizure focus, heterogeneity in seizure types, and/or lack of clear confirmation of the epileptogenic zone by intracranial recording or surgical outcome [7-12]. The best attempt to explore the potential of fNIRS-EEG in epilepsy was made by Watanabe et al. [13], who summarized in a symposium paper the ictal CBV changes which they observed during partial (mostly temporal lobe) seizures induced by bemegride injection. The higher number of optodes (8 to 24) allowed sampling of the prospective region and the contralateral homologous region. It was not enough, however, to sample surrounding regions and other distant areas. Furthermore, despite the high number of patients (n = 28), the authors surprisingly provided few details on the time course and behaviour of HbO and HbR.

Seizures are the result of abnormal and excessive neuronal discharges that may spread non-homogeneously across the cortex and subcortical systems, placing supranormal demands on the brain's autoregulatory mechanisms. Although it has been demonstrated that focal seizures are accompanied by an increase in local CBF, there are still many debated issues: (a) what is the timing of this local increase with regard to seizure onset [14]? (b) Is this local increase in CBF adequate to meet the metabolic demand throughout the ictus [15, 16]? (c) What is the haemodynamic behavior in surrounding and distant areas of the epileptogenic focus [17-19]? The present study will attempt to address some of these issues by reporting observations made during continuous simultaneous widespread EEG-fNIRS recordings of human mesial temporal lobe seizures.

## METHODS

### Patients

Nine patients (5 males; mean age, 35 years; range, 11 to 56 years) with refractory temporal lobe epilepsy who were candidates for epilepsy surgery were recruited for a session of simultaneous EEG-fNIRS recording at the Optical Imaging Laboratory of Sainte-Justine Hospital. Informed consents were obtained from all patients after

approval from the Sainte-Justine and Notre-Dame Hospitals' Ethics Committee. To increase the likelihood of recording a seizure, EEG-fNIRS studies were performed while patients were admitted for long-term continuous video-EEG monitoring as part of their presurgical evaluation since antiepileptic drug medications were then frequently tapered or dosages lowered. Scalp electrodes used for routine clinical video-EEG monitoring were removed to install the EEG-fNIRS helmet and reinstalled following the recording session to resume video-EEG monitoring. An epileptologist was present during the recording sessions to ensure patient safety. Following the non-invasive presurgical investigation, an intracranial study was performed when required prior to epilepsy surgery. Consensus on areas to cover was obtained during an epilepsy surgery conference after review of all available data. The final epileptogenic focus for each patient was determined by multimodal evaluation of clinical (history, physical examination, neuropsychological), structural (high-resolution MRI) and functional neuroimaging (ictal SPECT, PET, EEG-fMRI) and electrophysiological (scalp EEG, MEG, intracranial EEG) findings.

**Combined EEG-Near-infrared spectroscopy recording**

*Helmet trial and preparation*

Simultaneous EEG-fNIRS was accomplished using a rigid but light helmet drilled with holes to mount optic fibres, detectors and homemade EEG electrodes. Different helmet sizes were available and an initial visit to the EEG-fNIRS laboratory allowed for the selection of the helmet most adapted to the patient's head. Using the high-resolution anatomical MRI acquired as part of the presurgical evaluation, a 3D brain reconstructed image was obtained and co-registered to the patient's head using the program *Frameless 39* (Rogue research, Montreal, Canada). This stereotaxic system enabled us to visualize the position of a pointer in relation to the participant's head on the 3D brain reconstruction image, hence allowing us to draw regions of interest (i.e. bilateral anterior, middle and posterior temporal regions as well as frontopolar, frontocentral and dorsolateral frontal regions) accurately onto the helmet. As this procedure takes into account individual anatomic differences, it allowed us to obtain the best possible montage in terms of source-detector numbers, locations, and distances of the targeted regions for each participant.

*Simultaneous EEG-fNIRS recordings*

The EEG was recorded using a Neuroscan Synamps 2TM system (Compumedics, USA) by means of 19 homemade carbon fibre electrodes placed through holes in the helmet and fixed on the scalp according to the 10-20 system. EEG data were acquired using a sampling rate of 500 Hz and bandpass filtered between 0.1-100Hz with a 60 Hz notch filter. Simultaneously, fNIRS measurements were acquired with a multi-channel *Imagent* Tissue Oxymeter (ISS Inc., Champaign, Ill, USA) using up to 64 fibre sources and up to 16 fibre collectors mounted on the helmet for optimal coverage of bilateral temporal regions as well as frontal and parietal regions. The distance between the sources and the detectors was kept between three and five cm. Two wavelengths on either side of the 800 nm haemoglobin isosbestic point (i.e. the wavelength at which HbR and HbO absorb light equally) were chosen, one below (690 nm) more sensitive to HbR and one above (830 nm) more sensitive to HbO. The ISS Oxymeter uses a frequency-domain method which implies that light sources are intensity modulated over time at 110 MHz. The optical intensity (DC), modulation amplitude (AC) and phase changes in the collected light data were sampled at 19.5 Hz. Only the DC optical intensity was used for analysis.

The installation of the helmet took approximately one hour for each patient. Continuous simultaneous EEG-fNIRS monitoring was then carried out for one to two hours during which fNIRS was recorded in successive 15-minute blocks while EEG was recorded continuously. A camera mounted on a tripod filmed the whole session for offline review of ictal manifestations or artefact-generating movements. A pulse oxymeter was attached to a fingertip for visual monitoring of arterial blood oxygen saturation. During the recordings, patients did not perform any tasks; they sat on a chair as comfortably as possible. After the recording session, the location of every source, detector and fiducial point was digitized and recorded with the same stereotaxic system (Brainsight™ Frameless 39, Rogue Research, Canada) for co-registration with the anatomical MRI of each patient. The cortical surface was computed (Imagic, Neuronic, Havana); source and detector positions were co-registered on this surface by extrapolating the scalp positions in the normal direction from the surface (Matlab 7.04).

**Data analysis**

*Video and EEG data analysis*

After acquisition, the EEG data was reviewed offline by an epileptologist (DKN) using EEG Focus (BESA, Germany). Recordings were high-pass filtered at 0.3 Hz and low-pass filtered at 35 Hz. Seizure-onset and seizure-end times were respectively defined as the earliest and latest clinical or electrographic evidence of seizure activity.

*Optical data analysis*

After the acquisition, DC data from Boxy 8 (ISS Inc., Champaign, Ill, USA) was transferred to be analyzed with the HomER package (Photon Migration Imaging lab; Massachusetts General Hospital, Boston, USA) [20]. A modified Beer-Lambert law (MBLL) is used to relate light attenuation to changes in absorption $\Delta\mu_a$:

$$\Phi_\Delta(t,\lambda) = -\ln\left(\frac{I(t,\lambda)}{I_0(\lambda)}\right) = -\ln\left(\frac{\Phi(t,\lambda)}{\Phi_0(\lambda)}\right) = d \cdot DPF(\lambda) \cdot \Delta\mu_a(t,\lambda), \quad (1)$$

where $I(t,\lambda)$ describes the measured light intensity at wavelength $\lambda$ which, by using adequate boundary conditions, is related to $\Phi$, the fluence. Experimental factors related to illumination and detection efficacy and scalp-light coupling (all optodes are not equally efficient) cancel out in Eq. (1) by normalizing to a baseline measure, $I_0(\lambda)$. This baseline is measured on the same optode pair, but usually a few seconds prior to each activation event (here 5 s) or by a median value of the intensity signal over the whole experiment. The term "modified" arises from the inclusion of a differential pathlength factor, DPF($\lambda$). The DPF multiplies the source-detector distance $d$ to account for the additional path traveled by light due to scattering events in the diffusive medium [21]. This factor varies with wavelength and can be measured with either time or frequency domain instruments, or computed by using prior anatomical information and Monte-Carlo simulations. Using spectral extinction curves (Prahl SA. Tabulated molar extinction coefficient for hemoglobin in water; http://omlc.ogi.edu/spectra/hemoglobin/summary.html), the measured absorption (at two different wavelengths $\lambda_1$, $\lambda_2$) can be related to hemoglobin concentrations by

$$\begin{aligned}\Delta\mu_a(\lambda_1) &= \varepsilon_{HbO_2}^{\lambda_1}\Delta C_{HbO_2} + \varepsilon_{HbR}^{\lambda_1}\Delta C_{HbR} \\ \Delta\mu_a(\lambda_2) &= \varepsilon_{HbO_2}^{\lambda_2}\Delta C_{HbO_2} + \varepsilon_{HbR}^{\lambda_2}\Delta C_{HbR},\end{aligned} \quad (2)$$

where the extinction coefficients ε of hemoglobin species have been measured *in vitro* (Gratzer WB, Medical Research Council Labs, Holly Hill London and Kollias N, Wellman laboratories Harvard Medical School, Boston, MA; http://omlc.ogi.edu/spectra/hemoglobin/summary.html). The above linear system enables the estimation of the concentration of $HbO_2$ and HbR, as they vary in space and time. By estimating changes in absorption according to Eq. (1) at each wavelength then translating to concentrations using Eq. (2), one recovers measures of concentration changes in the region probed by the optodes.

Values reported here do not presume to indicate the exact concentrations in the brain, but rather reflect representative relative changes in the brain as we used a uniform partial volume factor of 1. Concentration curves are presented as a percentage of variation compared to typical steady state values of HbT 100uM, HbO 75uM and HbR 25uM [22]. HbT, the sum of HbR and HbO chromophores, was assumed equivalent to CBV under the standard hypothesis that the haematocrit remains constant. A low-pass frequency zero-phase digital filtering with a cut-off frequency of 0.5 Hz was performed on the data to eliminate cardiac artifacts. Channels with a raw DC intensity at the level of the equipment noise or with a standard deviation higher than 20 % were considered as artefactual and excluded from the analysis. The optical seizure onset time was marked when the first obvious haemodynamic changes occurred and was compared with the EEG seizure onset identified by the epileptologist. The selected channels (regions of interest) chosen to show the average temporal evolution of haemoglobin variations on both sides of the epileptic focus (ipsilaterally and contralaterally) in the figures below were close to T4-F8 and T3-F7 as measured with the 10-20 system.

*Topographic analysis*

A topographic view was created to display the evolution and the general propagation of HbO and HbR activations. The subject's MRI reconstruction was co-registered according to the fiducial points measured on the subject in order to produce a topographic view of the activation. A simple student T-test was performed to ensure that the amplitude of the activation was superior to the baseline noise using the following formula: T = X/SEM. Where, T is the uncorrected T-value, X is the

amplitude of the concentration during the seizure and SEM is the standard error for 5 s of baseline. To display the evolution and the general propagation of the activation, we mapped the T-value to a topographic view onto the skin segmentation. A home made-matlab code was developed to map the activation. By using the optodes' coordinates acquired on the skin, the activation was projected directly under the path between a source and a detector without interpolation. When two channels passed through the same position, the averaged value was mapped.

*Group analysis*

To assess overall variations of HbO and HbR, all seizures were aligned to seizure onset. For each seizure, a selected number (the same for each patient) of focal fNIRS channels was averaged, and the resulting times series was binned by averaging over windows of one second. Due to the upward skewness of the distribution, a Mann-Whitney test rather than a Student t test was performed on each such window of 8 data points, comparing its median to the median of a fixed baseline window taken 10 seconds prior to fNIRS onset (also 8 data points). No p-value adjustment was made to account for multiple tests.

*Laterality index*

To evaluate if fNIRS could adequately lateralize the epileptic focus, two laterality indexes were calculated. The Extent Laterality Index (ELI)compares the extent of HbO activation between both hemispheres and is calculated as follow: ELI (t) = [Number of Left vertices (t) – Number_Right vertices (t))/ (Number_Left vertices (t) + Number Right vertices (t)]. Only vertices bigger than 50% of the maximal T-value were used. The Peak Laterality Index (PLI) compares the peak T-value at every moment between both hemispheres and is calculated as follow: PLI (t) = [(Max_Peak Left (t) – Max_Peak Righ (t)/ (Max_Peak Left (t) + Max_Peak Right (t)].

**RESULTS**

Eight seizures were successfully recorded during EEG-fNIRS sessions from three out of the nine participants with refractory temporal lobe epilepsy. The other six participants had uneventful EEG-fNIRS sessions. Each recorded seizure was

accompanied by well-recognizable changes in the optical signal. We identified two distinct phases in the haemodynamic response. The first phase was characterized by increased oxygenation as HbO increased and HbR decreased. The second phase was characterized by decreased oxygenation during which HbR increased (while HbO continued to increase or even decreased). The peaks of each phase for each of the seizures are shown in Table 1 and detailed haemodynamic responses for each patient are described below.

Table 1 Details of haemodynamic changes of all recorded complex partial seizures: onset of fNIRS changes compared to first scalp EEG evidence of ictal activity; duration of EEG evidence of seizure activity; duration of haemodynamic changes for individual seizures; peak concentration variations recorded over the temporal region; phase 1 is defined by a decrease of HbR; phase 2 is defined by an increase of HbR; sz = seizure; P1, P2, P3: patients 1, 2 and 3 ; HbT = total haemoglobin; HbO = oxyhaemoglobin; HbR = deoxyhaemoglobin; SD = standard deviation Table 1 Details of haemodynamic changes of all recorded complex partial seizures: onset of fNIRS changes compared to first scalp EEG evidence of ictal activity; duration of EEG evidence of seizure activity; duration of haemodynamic changes for individual seizures; peak concentration variations recorded over the temporal region; phase 1 is defined by a decrease of HbR; phase 2 is defined by an increase of HbR; sz = seizure; P1, P2, P3: patients 1, 2 and 3 ; HbT = total haemoglobin; HbO = oxyhaemoglobin; HbR = deoxyhaemoglobin; SD = standard deviation

| | fNIRS onset (s) | EEG (s) duration | fNIRS (s) duration | Phase 1 peak | | | | | | Phase 2 peak | | | | | |
|---|---|---|---|---|---|---|---|---|---|---|---|---|---|---|---|
| | | | | HbT | Time | HbO | Time | HbR | Time | HbT | Time | HbO | Time | HbR | Time |
| P1-Sz1 | 0 | 93 | 200 | - | - | - | - | -4 | 21 | 15 | 68 | 15 | 71 | 25 | 88 |
| P1-Sz2 | 0 | 93 | > 80 | - | - | - | - | -9 | 27 | 13 | 58 | 14 | 58 | 17 | 77 |
| P1-Sz3 | 0 | 106 | 200 | - | - | - | - | -7 | 29 | 17 | 75 | 18 | 56 | 43 | 88 |
| P1-Sz4 | 0 | 77 | 200 | - | - | - | - | -8 | 26 | 11 | 53 | 10 | 56 | 16 | 53 |
| P1-Sz5 | 0 | 96 | 150 | - | - | - | - | -5 | 15 | 17 | 60 | 17 | 77 | 24 | 94 |
| **Mean** | **0** | **93** | **188** | | | | | **-7** | **24** | **15** | **63** | **15** | **64** | **25** | **80** |
| **SD** | **0** | **10** | **87** | | | | | **2** | **6** | **3** | **9** | **3** | **10** | **11** | **16** |
| | | | | | | | | | | | | | | | |
| P2-Sz1 | -37,4 | 70 | >150 | 1,3 | 17,6 | 4,1 | 40,0 | -8,6 | 43,9 | 4,7 | 90,1 | -8,4 | 125 | 42 | 131 |
| P2-Sz2 | -49 | 34 | 135 | 0,5 | 27,2 | 1,0 | 31,5 | -1,5 | 34,9 | -1,4 | 63,8 | -6 | 92 | 13 | 91 |
| **Mean** | **-43** | **52** | **135** | **1** | **22** | **3** | **36** | **-5** | **39** | **2** | **77** | **-7** | **109** | **28** | **111** |
| **SD** | **8** | **25** | **95** | **1** | **7** | **2** | **6** | **5** | **6** | **4** | **19** | **2** | **23** | **21** | **28** |
| P3-Sz1 | -32 | 49 | 275 | -3 | 39 | 9 | 62 | -14 | 36 | 10 | 65 | -14 | 156 | 48 | 142 |

*Case 1*

This 49 year-old man with prior meningitis at age 16 months started having seizures at age 34 years. Seizures were characterized by a foul odour or taste, altered consciousness and oroalimentary automatisms. During video-EEG monitoring, fourteen complex partial seizures were recorded, all associated with rhythmic theta activity evolving in amplitude and frequency over the left temporal region. In half of the seizures, late rhythmic theta and delta rhythmic slowing was noted in the contralateral temporal region after a mean of 48 s (range 27-68s) suggesting late contralateral propagation. Ictal SPECT showed mild left mesiotemporal activation, PET revealed left temporal hypometabolism and MRI disclosed discrete left hippocampal atrophy.

An EEG-fNIRS study was performed using 120 channels sampling bilateral frontal, temporal and parietal regions (figure 1A). Five complex partial seizures were recorded during the 82-minute session, clinically and electrographically identical to those recorded during the video-EEG monitoring study (figure 1B). Mean duration for EEG evidence of seizures was 93 s (range 77-106 s). Pulse oxymetry monitoring indicated no significant peripheral desaturation during seizures. Except for minor differences, cerebral haemodynamic responses as measured by fNIRS were relatively similar for all seizures. Figure 1C exemplifies changes in HbO and HbR over time as measured by selected optodes over the left (ipsilateral) and right (contralateral) temporal lobes during seizure 1. Electrographically, the onset was assumed to be where diffuse desynchronization occurred, several seconds prior to the obvious ictal rhythmic theta activity over the left temporal region (figure 1D). After ictal onset, an increase in HbT was observed, reaching 15 % and peaking at 68 s. This increase in HbT, most likely representing an increase in CBV, lasted ~ 25 s beyond the termination of the seizure. Similarly, HbO showed an increase and the maximal amplitude of this change was 15 % of baseline, peaking at 70 s. The HbR signal was biphasic with an initial decrease of 4 % at 21 s followed by an increase by 25 %, reaching a peak 88 s after seizure onset (and close to seizure offset). At seizure offset, both HbR and HbO gradually returned to baseline over ~ 100 s. Contralaterally, haemodynamic variations of HbO and HbR over the anterior temporal region closely paralleled those seen over the epileptogenic region from onset (despite any EEG

evidence of epileptic activity). The initial increase in HbO (and ultimate increase in HbR after the initial decrease) was more pronounced ipsilaterally (0.62 vs 0.35 % ) and started slightly earlier ipsilaterally at 5 s ipsilaterally versus 6 s contralaterally (figure 1E). In remote areas, a short-lasting decrease in HbO was found in frontal and parietal regions at seizure onset. Despite this initial decrease in HbO, a decrease in HbR was concomitantly noted in these remote areas. As the seizure went on, an increase in HbO and decrease in HbR occurred in adjacent middle and posterior temporal regions as well as inferior frontal and frontopolar regions starting ~6 s after onset. Further activation (increase in HbO and decrease in HbR) of contralateral homologous regions was also noted ~ 16 s after seizure onset. The later increase in HbR despite an increase in CBV occurred maximally over bitemporal regions (figure 1E).

Detailed haemodynamic responses for the remaining four seizures are available as supplementary data (supplementary figures S1-S4). The time course of haemodynamic responses averaged over all five seizures in the left temporal lobe is as follows: (a) an increase in HbT was observed which reached a peak of 15 ± 3 % at 63 ± 9 s (b) a concomitant increase in HbO which reached a peak of 15 ± 3 % at 64 ± 10 s after onset (27 ± 14 s before electrical offset) (c) an associated initial decrease in HbR of 7 ± 2 %, which reached a nadir at 24 ± 6 s, followed by an increase which reached a peak of 25 ± 11 % at 80 ± 16 s after onset (11 ± 10 s before electrical offset). The average length of EEG evidence of seizures was 93 s compared to 188 s for haemodynamic changes. Thus, the haemodynamic changes outlasted the duration of the seizure by 95 ± 30s. For this patient, the seizure phase that had the highest localization value was the period of initial HbO increase, as most seizures (4 out of 5) clearly displayed a faster increase on the ipsilateral side than on the contralateral side. This was not the case for seizure 3, the ‘strongest of them’, which was associated with symmetrical increases bilaterally (see supplementary figure S2)

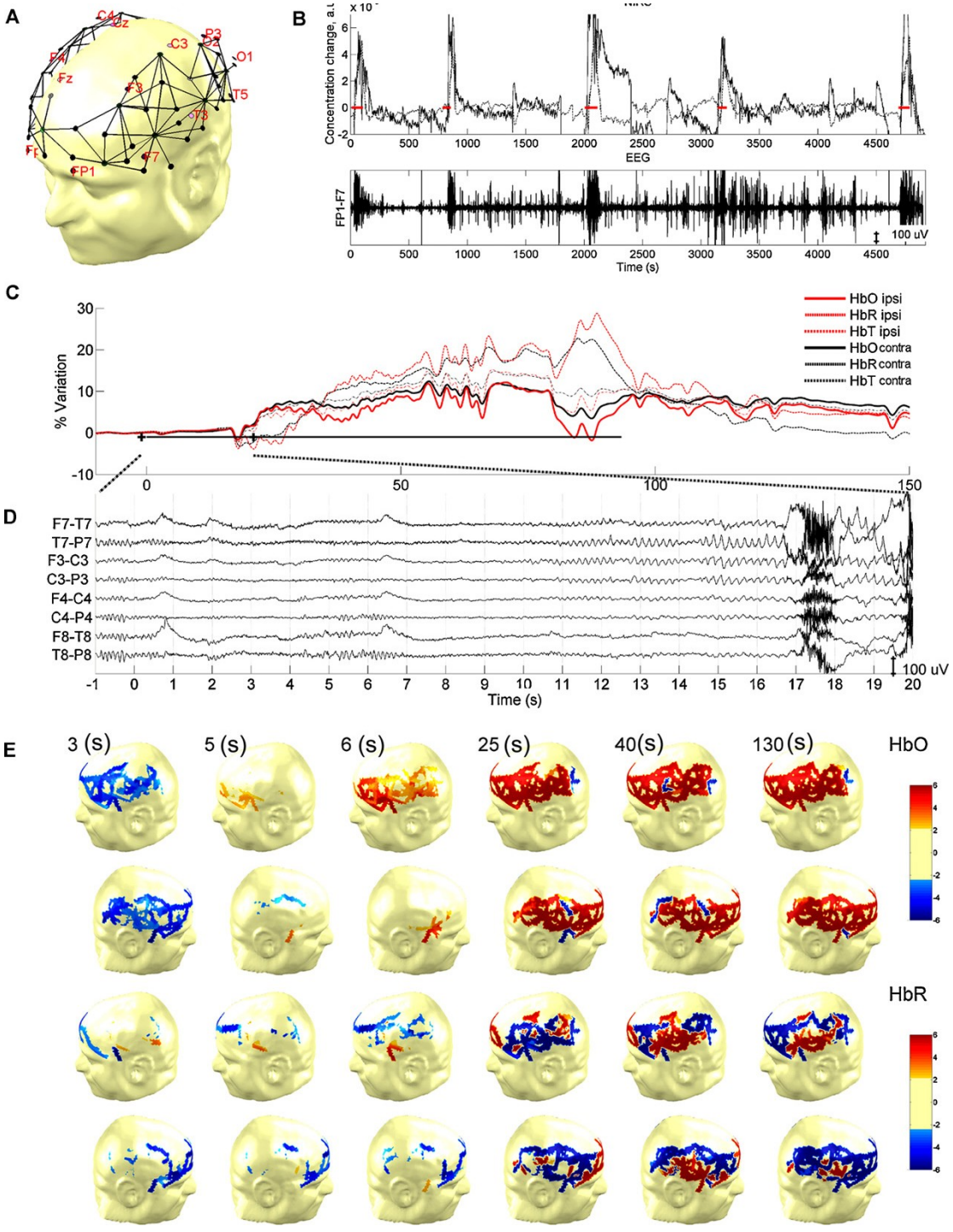


Figure 1. Case 1, seizure 1. (A) Channel configuration ($n$ = 120). (B) Haemodynamic variations (HbO line, HbR dotted) over the epileptogenic temporal lobe for the whole fNIRS recording, horizontal red lines indicate electrical seizure activity. Below, temporal EEG time course is shown. (C) Enlarged seizure 1 haemodynamic variations of ipsi- and contralateral region of interest. The black line indicates time of EEG evidence of seizure activity. (D) Blow-out of EEG showing early ictal changes. (E) Topographic uncorrected T-stats viewed at different time points during the course of the seizure. Region of the epileptic focus is indicated by a circle.

*Case 2*

This 47 year-old woman suffered from weekly seizures since age 15 years, characterized by an aura of déjà vu or an orgasmic sensation followed by altered consciousness. During video-EEG monitoring, some seizures were associated with left temporal rhythmic theta activity but many were non-localizing. High-resolution MRI was normal. An invasive EEG study revealed independent left and right mesiotemporal lobe seizures. Electrographically, seizures (n =11 ) were characterized by low-voltage fast activity evolving into rhythmic spiking starting in the hippocampus before spreading to the ipsilateral insula and ipsilateral lateral temporal contacts after a mean of 19 seconds (range 10-37 seconds) and ending after a mean of 71s (range 54-107s). No propagation to frontal subdural contacts was observed for all seizures. Electrodes were removed without resective surgery.

During the presurgical evaluation, a 38-minute EEG-fNIRS study (with 95 channels sampling bilateral temporal, inferior dorsolateral frontal, lateral parietal and occipital regions –figure 2A) captured two complex partial left temporal lobe seizures (figure 2B). Local cerebral haemodynamic responses observed over the ipsi- and contralateral temporal regions of interest during the first recorded seizure are shown in figure 2C along with ictal scalp EEG recordings (figure 2D). In the temporal region ipsilateral to the seizure focus, a mild increase in HbO was noted several seconds (~ 37.4 s) prior to first obvious ictal electrical changes identifiable on scalp electrodes but probably closer to true seizure onset as intracranial recordings demonstrated that spread from mesial to lateral temporal structures could take from 10 up to 37 seconds to occur (Figure 2E) This initial increase in HbO reached a peak at ~40 s (close to the scalp EEG changes); HbO then decreased until ~125s (18 s past seizure offset) prior to returning to baseline. HbR had a concomitant reversed pattern with an initial decrease followed by a significant increase. The latter increase in HbR continued well past seizure offset and was more pronounced over the ipsilateral temporal region. While the seizure lasted ~70s based on scalp EEG recordings, ictal haemodynamic changes were much longer, as HbO returned to baseline only after ~150 s. In the homologous contralateral temporal region, HbO and HbR showed a similar behaviour throughout the duration of the seizure, though variations were less marked throughout the entire course of the seizure. As the seizure went on, an increase in HbO was seen over a

wider area of the ipsilateral temporal region including the lateral middle and posterior temporal neocortices. In remote areas, a decrease in HbO was observed early on in frontal areas bilaterally without evidence of epileptic activity on frontal scalp electrodes. Despite this decrease in HbO in remote frontal regions, HbR did not increase (figure 2F). Although the second seizure was shorter (34s), a similar haemodynamic pattern was noted (see supplementary figure S5). Pulse oxymetry monitoring indicated no significant peripheral desaturation during either seizure.

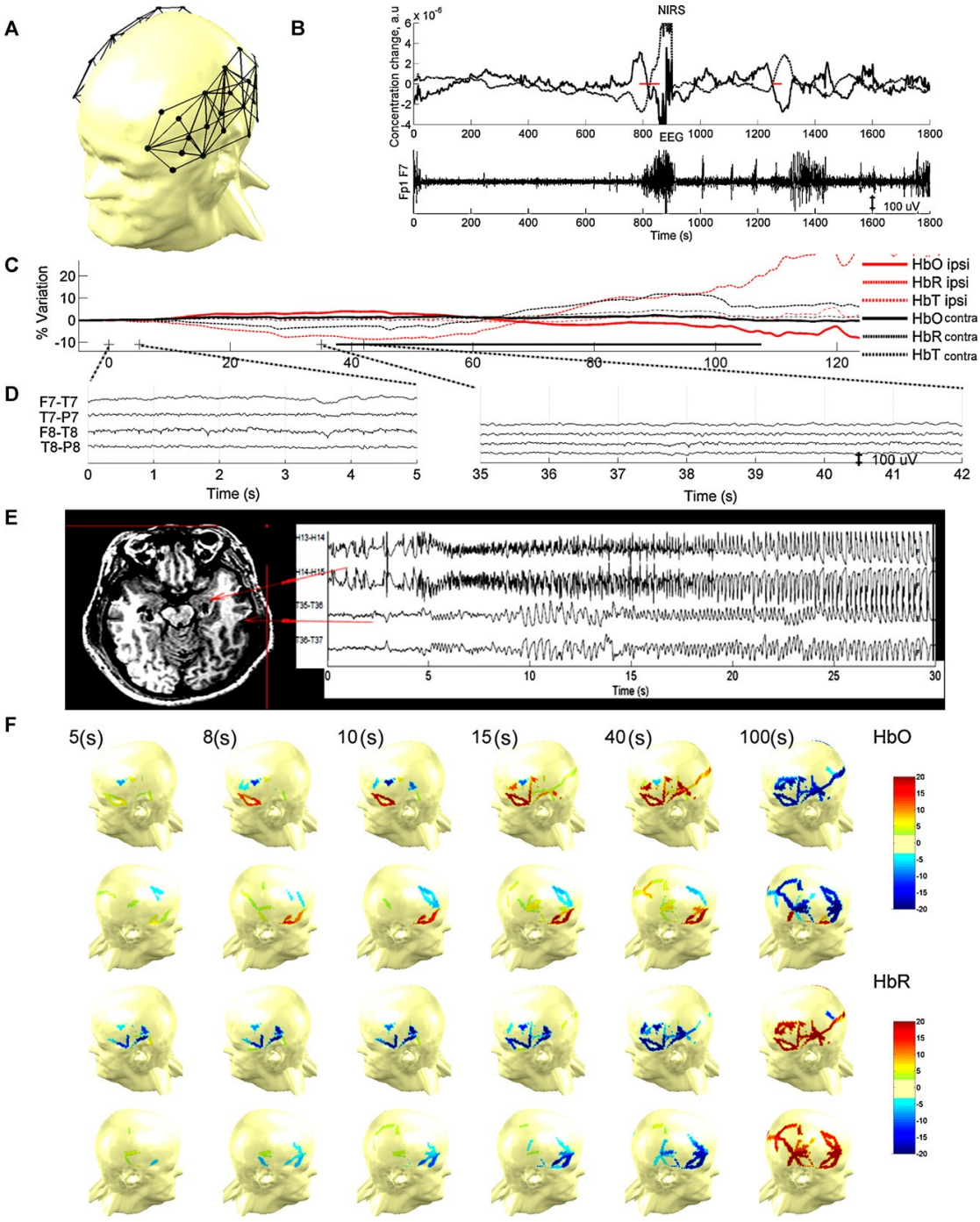


Figure 2. Case 2, seizure 1. (A) Channel configuration ($n$ = 95). (B—D) Same as Fig. 1. (E) Intracranial recording of a seizure starting which started over the left hippocampal depth contact and spread to the lateral temporal subdural contact after more than 20 s. (F) Topographic uncorrected T-stats viewed at different time points during the course of the seizure. Region of the epileptic focus is indicated by a circle.

*Case 3*

This 31 year-old man with onset of seizures at age 27 years underwent a comprehensive presurgical evaluation after failing ten antiepileptic drug trials. Spells consisted in initial light-headedness, altered consciousness and gestural automatisms. Seizures recorded during video-EEG monitoring were associated with rhythmic left temporal theta activity evolving in amplitude and frequency and late rhythmic theta and delta slowing over left parasagittal regions. Paradoxically, MRI revealed right temporal atrophy. An intracranial study confirmed a left mesiotemporal epileptogenic zone. Several electrical and simple partial seizures consisting of preictal spiking followed by low-voltage fast activity limited to left mesiotemporal structures were noted. Seven complex partial seizures started with an identical pattern but then evolved to rhythmic slowing and spiking over the lateral temporal contacts after a mean of 33s (range 6-55s). Limited spread of epileptic activity to contralateral mesiotemporal structures occurred after a mean of 34s (range 11-65s). No spread to the ipsilateral and contralateral frontal subdural strip electrodes was observed for all seizures. The patient underwent a left anterior temporal lobectomy with a resulting Engel 1 outcome (FU = 1 ½ year).

One complex partial seizure was captured during the 165-min EEG-fNIRS study using 114 channels (figure 3A). Electrographically, mild desynchronization followed by rhythmic theta activity over the left temporal region was noted, evolving in amplitude and frequency prior to termination after 49 s. The haemodynamic responses over the left temporal region of interest (ipsilateral to the seizure focus) and the contralateral homologous region along with ictal scalp EEG data are shown in figure 3C. Over the temporal region, a gradual increase in HbO and decrease in HbR was first noted 32 seconds prior to scalp electrical onset (but probably close to the actual seizure onset in the left mesiotemporal structures as intracranial recordings indicated a mean time of 33s for the epileptic activity to spread from mesial depth electrode contacts to lateral temporal subdural electrode contacts). The increase in HbO reached a peak at ~62 s (30s after EEG seizure onset and 19s before seizure offset) and gradually returned to baseline with a long undershoot (200 s) after offset. The initial decrease in HbR reached a nadir ~40 s after seizure onset before increasing dramatically to a peak ~150 s after onset (~70 s after seizure offset) and finally

decreasing towards baseline (~270 s after the first haemodynamic changes). Local haemodynamic responses over the right temporal region closely paralleled those seen from the left temporal region except for a higher increase in HbR ipsilaterally after the initial decrease noted after seizure onset (figure 3C). In remote areas, a progressive decrease in HbO is seen early on over the frontal and parietal regions bilaterally while HbR also decreases. However, as the seizure goes on, HbR increases diffusely in remote areas as well (figure 3F).

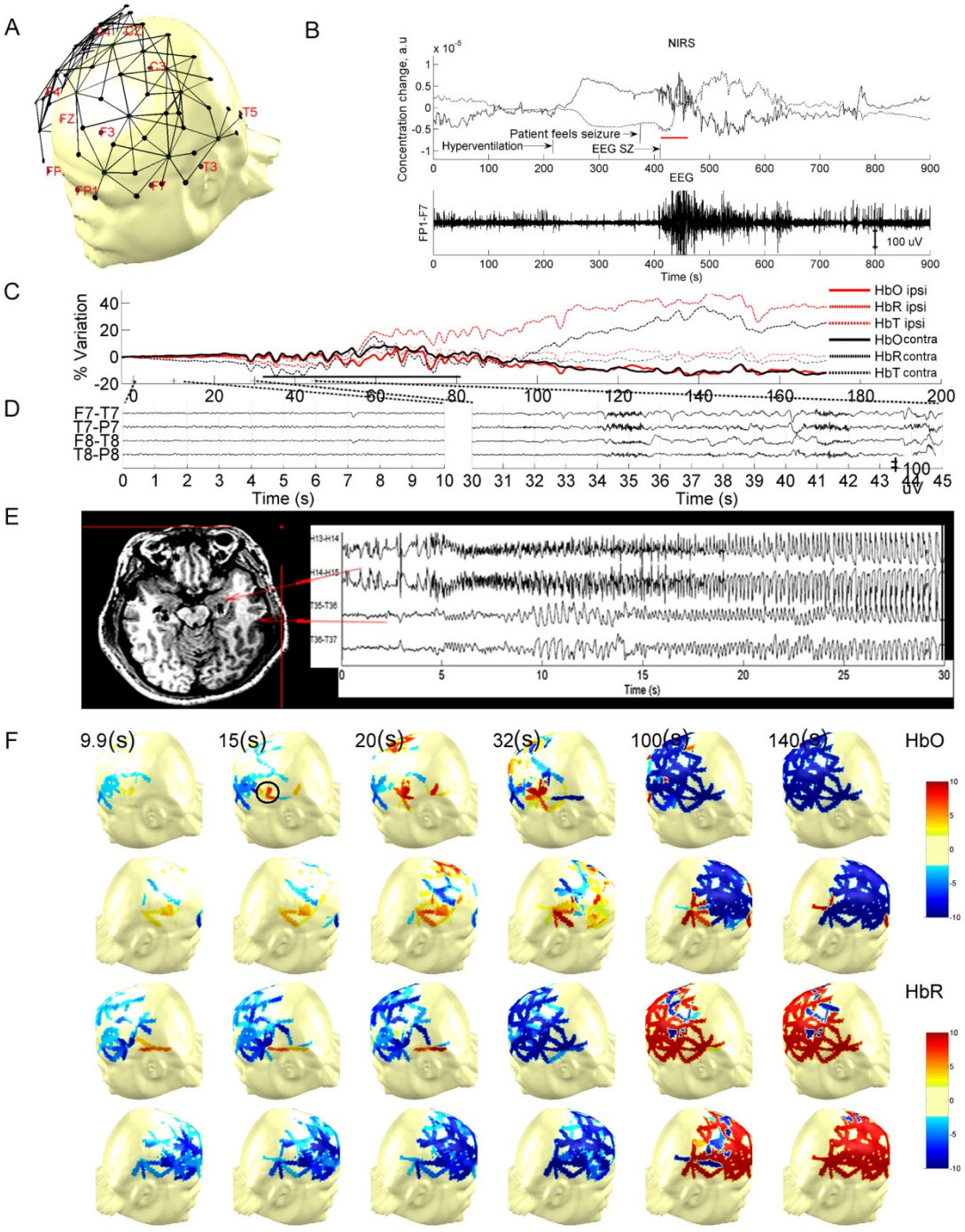


Figure 3. Case 3, seizure 1. A. Channel configuration (n = 114) B. to F. Same as figure 2.

*Group analysis*

All eight seizures recorded from the three patients presented above were aligned to seizure onset to assess overall variation of HbO and HbR (figure 4). For HbR, two phases are seen : (a) first, an initial decrease (significant for about 3 s), accompanied by an HbO increase; (b) followed subsequently by a phase of prolonged HbR elevation, indicating deoxygenation (significant from 53.3 s to 149.6s) during which HbO increased for patient 1 while HbO decreased for patients 2 and 3.)

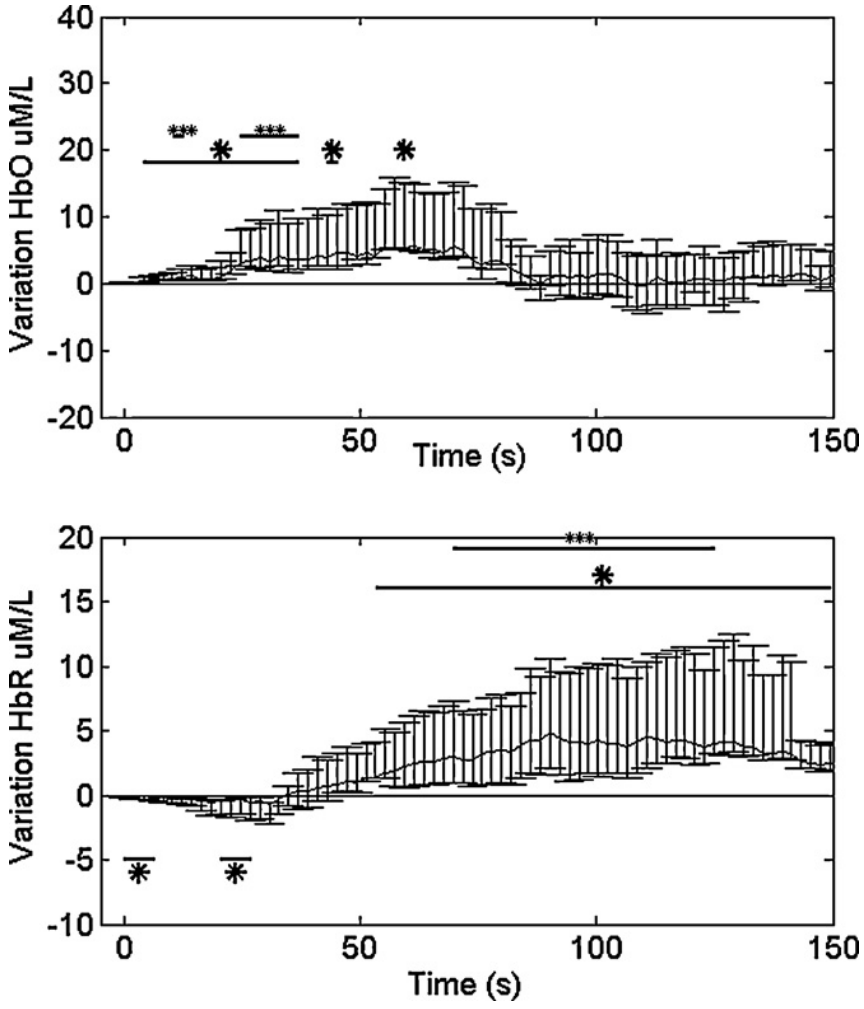


Figure 4. Median, 25th and 75th percentiles of eight seizures measured with NIRS from 3 patients, aligned to seizure onset at time = 0 (upper chart: variation of HbO during seizure (□M/L) lower chart: variation of HbR during seizure (□M/L). For HbR, two phases are seen : an initial decrease (significant for about 3 s), accompanied by an HbO increase, and a phase of prolonged HbR elevation, indicating hypoxia (significant from 53.3 s to 149.6, during which HbO increased for patient 1 while HbO decreased for patients 2 and 3.) Significance levels: $p<0.05$ (*), $p<0.001$ (***).

*Laterality index*

To evaluate if fNIRS could adequately lateralize the epileptic focus, two laterality indexes were calculated. The Extent Laterality Index compares the extent of HbO activation between both hemispheres while the Peak Laterality Index compares the peak T-value at every moment between both hemispheres. For patient 1, four out of five seizures showed a bigger and larger activation ipsilaterally during the initial phase of the seizure. For patient 2, the higher amplitude of activation ipsilaterally allowed adequate lateralization of the epileptogenic lobe for both seizures. For patient 3, lateralization was less certain as bilateral activation of equal intensity was observed during the only seizure recorded, possibly more so contralaterally. Figure 5 shows the mean Extent Laterality Index and Peak Laterality Index for all seizures recorded from each patient showing that both indexes were concordant with the side of seizure onset for patients 1 and 2 but discordant for the third.

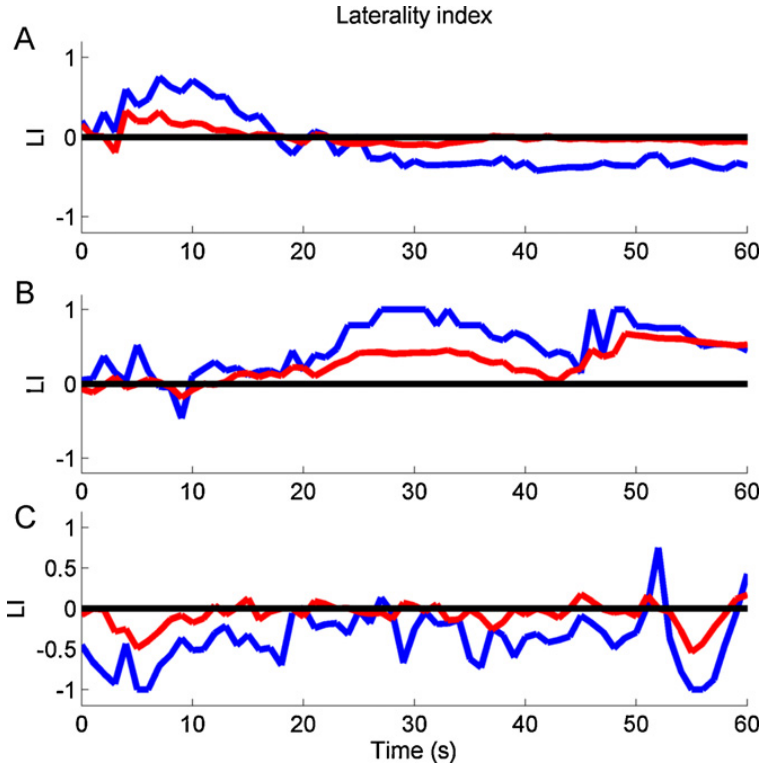


Figure 5. Laterality index of HbO variation in function of the time during the evolution of the seizure, in blue; Extent laterality index (ELI) using a half maximum T value threshold, in red; maximal peak laterality index (PLI). A) LMTLE Patient 1 (n=5 seizures), laterality index is concordant with the side of epileptic focus during the first 20 seconds. B) LMTLE Patient 2 (n=2 seizures), laterality index is concordant with the side of epileptic focus. C) LMTLE Patient 3 (n=1), laterality index is discordant with the side of epileptic focus.

## DISCUSSION

We have successfully used simultaneous EEG-fNIRS to record several seizures in three out of the nine tested patients. Our findings bring new evidence regarding the haemodynamic changes during temporal lobe seizures and the role of EEG-fNIRS in localizing the epileptogenic zone.

### FNIRS-EEG haemodynamic changes during temporal lobe seizures

*Detection of seizures* –In our analysis of eight complex partial seizures from three patients with refractory mesiotemporal lobe epilepsy using multichannel fNIRS-EEG, we have consistently been able to detect haemodynamic changes throughout the course of the ictus. All seizures were associated with significant alterations in cerebral haemodynamics with variations from baseline to the highest peak in the order of ~28% for HbR, ~13% for HbO and ~11% for HbT. These variations are 3 to 8 times more than what is seen during a physiological fluence paradigm [23]. It has been our experience with these and other not yet published cases that analyzing the fNIRS signal can guide a more careful review of a specific timeframe of the EEG signal to detect seizures with more subtle electrographic changes [unpublished data, 24]. The magnitude of these variations is in line with recent EEG-fMRI observations. In a patient with right temporo-parietal brief (~ 4 s) electrical seizures, Kobayashi et al. [17] also reported a large (6.1%) increase in BOLD signal compared to what is seen during interictal spikes or cognitive tasks (typically 0.5 to 1%).

*Timing of haemodynamic changes* –Onset of these fNIRS-detected haemodynamic changes occurred close in time with EEG-detected seizures. For patient 1, good approximation of true electrical onset was made possible by visualizing an early non-specific desynchronisation of baseline alpha rhythm prior to the more obvious evolving rhythmic theta activity over the epileptic temporal lobe on an artefact-free EEG recording. Haemodynamic changes were found to occur almost simultaneously to suspected electrical onset. For patients 2 and 3, no subtle clues on scalp recordings allowed for better approximation of true seizure onset time prior to the more obvious ictal rhythmic theta activity, but subsequent intracranial recordings showed that true

ictal onset likely occurred several seconds before (probably close to when haemodynamic changes were first noted) as spread of epileptic activity from mesiotemporal depth electrode contacts to lateral temporal subdural electrode contacts could take several seconds. Although Zhao et al. [14] recently suggested that haemodynamic changes precede true ictal electrical onset rather than follow it after a short latency as one would expect with normal neurovascular coupling [15], our setting does not allow for a more accurate assessment of the exact timing of haemodynamic changes with regard to true epileptic onset. Contrary to seizure onset, electrical seizure offset was more readily identifiable and there is no doubt that haemodynamic changes outlasted the duration of seizures. This is in line with previous SPECT, EEG-fMRI and optical imaging data [5, 14, 15, 25].

*Local haemodynamic changes* –Notwithstanding the exact timing of the haemodynamic response relative to ictal electrographic activity, there is possible evidence that cerebrovascular autoregulation is temporarily unable to meet the increased metabolic demands during temporal lobe complex partial seizures. Although seizures are associated with an expected increase in HbT and HbO as well as a decrease in HbR (congruent with a compensatory increase in local CBV to increase the oxygen supply to the epileptic tissue), we consistently show that this initial decrease in HbR over the epileptogenic region is followed by a longer increase in HbR which often outlasts the duration of the seizure. This suggests the brain may suffer from a temporary, intense increase in local oxygen metabolism responsible for the increase in HbR, which is not sufficiently compensated for by the reactive regional increase in cerebral blood supply to wash out HbR. In other words, the brain possibly suffers from hypoxia during complex partial seizures. The observed decrease in oxygenation cannot be ascribed to cardiorespiratory perturbations during seizures as no significant decrease in peripheral SaO2 was noted [26]. In addition, patients did not suffer from other co-morbidities which could have affected cerebral autoregulation such as cerebrovascular disease. Cerebral autoregulation may vary with age but no age-correlated changes were observed in our limited sample as the oldest patient (49 years-old) showed an increase in HbO in the second phase while the 2 other younger patients (47 and 31 years-old) both showed a decrease in HbO in the second phase.

Although the inadequacy of CBF to meet metabolic demand has been demonstrated in animal models of status epilepticus [28-30], there is growing evidence of inadequate oxygenation at the onset or throughout shorter duration ictal events as well. Zhao et al. [14] recorded spontaneous seizures (lasting less than 2 minutes but recurring every 5 minutes) related to a cavernous malformation using intraoperative optical recording of intrinsic signals (ORIS) combined with 4-contact grid electrode recordings. They reported a decrease in hemoglobin oxygenation and CBV within the epileptogenic zone starting 20 seconds before seizure onset followed by further decrease in hemoglobin oxygenation despite an increase in CBV throughout the seizure. These changes persisted for at least 1-2 minutes after the offset of the seizure. These findings appear to confirm that the increase in metabolic demand elicited by spontaneous focal human seizures is not adequately met by increases in CBF. Recent EEG-fMRI studies of motionless seizures have reported BOLD decreases in relation to the late ictal phase, suggesting a cerebral perfusion/mismatch and possible sustained tissue hypoxia [31, 32]. Further corroborating data comes from animal models of epilepsy. Zhao et al. [33] showed that ictal events elicited a transient decrease in pO2 (initial dip) in the 4-AP model despite a 50% increase in CBF, while Hoshi et al. [34] observed decreased oxygenation after seizures in the PTZ model. Kreisman et al. [35] reported increased cerebral oxygenation and oxidized cytochrome c oxidase early during the ictus but decreased oxygenation and reduced cytox later during and after the seizure.

*Haemodynamic changes in the contralateral temporal lobe* –A second significant finding is the surprisingly similar haemodynamic profile seen over the contralateral region, though variations have lower amplitude. These rapid haemodynamic changes in the opposite temporal region occurred in absence of obvious contralateral epileptic activity. Subsequent intracerebral recordings for the last two patients confirmed that propagation to the contralateral hippocampus and lateral temporal neocortex was not rapid but took several seconds, as is usually the case for hippocampal seizures [36]. Using four emitters and one detector over the right and left parietal areas, Wallois et al. [37] also observed a similar contralateral effect in a curarized, ventilated post-acute foetal distress neonate with a flat interictal EEG and subclinical temporal lobe seizures. The physiological basis of these contralateral changes is yet unclear. Prior SPECT studies of temporal lobe seizures had already demonstrated significant ictal

contralateral changes in regional CBF, usually symmetrical to the seizure onset zone (forming a mirror image) [38-40]. Because ictal SPECT provides a single snapshot of regional CBF based on the uptake over ~ 1-2 min by neurons of a radiotracer injected early after seizure onset, it was assumed that these contralateral changes represented patterns of seizure propagation [40, 41]. Our EEG-fNIRS findings indicate that contralateral activation is rapid and cannot solely be attributed to seizure propagation. In fact, our findings are reminiscent of recent observations made during EEG-fMRI studies of temporal interictal spikes showing BOLD responses occurring predominantly in the spiking temporal lobe but often also involving the contralateral homologous cortex as well as extra-temporal regions. This widespread effect of temporal epileptic spikes is hypothesized to be due to projected neuronal activity that is not sufficiently synchronized to be visible on the EEG [18, 42, 43].

*Haemodynamic changes in other remote areas* –While HbO increases over the temporal region for all subjects as the focal seizure starts, HbO decreases in frontal and/or parietal regions were also noted for patient 2 and 3 (and briefly for some seizures of patient 1). In a prior pilot fNIRS study of temporal lobe seizures using only two frontally-positioned optodes, Steinhoff et al. [8] had already noted a clear-cut decline in oxygen saturation in the ipsilateral frontal region in two patients and inconsistent findings contralaterally. Previous SPECT studies have shown significant ictal hypoperfusion of frontal, parietal and other remote areas (cerebellum, precuneus) during temporal lobe complex partial seizures [44-48] while secondarily generalized temporal lobe seizures (even with short injection times) were associated with multiple hyperperfusion areas in the frontal, temporal, and basal ganglia regions [49, 50]. In a recent study combining electrophysiological recordings, fMRI and laser-Doppler flowmetry, Englot et al. [51] found that electrically stimulated partial hippocampal seizures in rats were associated with ictal frontal neocortical slow activity, significant decreases in neuronal firing, haemodynamic measurements (BOLD, CBV, CBF), and cerebral metabolism (CMRO2), while secondarily generalized hippocampal seizures showed frontal fast polyspike seizure activity, significant elevations in electrophysiological responses (local field potentials and multiunit activity), haemodynamic measurements (BOLD, CBV, CBF), and CMRO2. Long-range depressive effects over the frontal lobe could explain why, HbR did not increase

initially but rather decreased as HbO decreased in our patients. Overall, these findings indicate that temporal lobe seizures have long-range effects, not only when they propagate to distant regions but even when they don't propagate to them. Among potential explanatory hypotheses, a 'vascular steal phenomenon' (shunting of blood towards the temporal at the expense of frontal and parietal regions) [44] is unlikely to explain such early, distant and bilateral changes [42, 47]. A more favoured theory has been that temporal lobe seizures functionally inactivate widespread regions of frontal and parietal cortices through long-range connections or disruption of normally active ascending projections of the medial thalamus and upper brainstem reticular formation [42, 47, 51]. However, as the seizure continues, areas of increased HbO as well as areas of increased HbR are eventually noted in frontal and parietal regions, probably reflecting the propagation of epileptic activity (and unmet metabolic demands) more than long-range effects (or both).

**Lateralization of the epileptogenic zone using EEG-fNIRS**

At present, the most commonly used imaging technologies for functional seizure localization are ictal SPECT and PET [52]. More recently, studies have shown that EEG-fMRI could also contribute further information on the non-invasive localization of the primary epileptogenic zone and reduce the number of non-invasive electrophysiological recordings [53, 54]. Although SPECT and PET give some information about functional processes, these methods are associated with radiation exposure to the patient and can only provide a single measure in time of CBF or neuronal metabolism respectively. EEG-fMRI is difficult to apply during seizures [55]. Some authors have suggested that EEG-fNIRS could be used to localize the epileptogenic zone. Watanabe et al. [56] analyzed the regional CBV changes in the early phase bemegride-induced seizures in 12 consecutive patients with medically intractable epilepsy (10 temporal, 2 parietal) using 8-12 channels (half over the prospective focus region and half on the other side). Ictal SPECT demonstrated hyperperfusion in the areas surrounding the seizure foci in seven cases while NIRS demonstrated regional CBV increase in the region of the focus in all twelve cases. The increase began within 2-5 s after the seizure onset and lasted for 45 + 12.3 s. The authors concluded that both methods could support each other in localizing the epileptogenic zone despite the biased coverage.

Our ictal recordings, with larger fNIRS coverage, indicate that the haemodynamic response, whether locally or at a distance, is more complex than initially thought. To our surprise, the increase in HbO observed at seizure onset was noted over the ipsilateral and contralateral temporal lobes, even before EEG evidence of contralateral spread. However, amplitude of HbO increase over the epileptogenic region and/or increase in HbO in surrounding channels as the seizure evolved ipsilaterally generally allowed localization of the epileptogenic lobe. In our study, lateralization to the correct side of the epileptic focus was possible for 6 out of 8 seizures using laterality indexes. In addition to HbO behaviour, analysis of HbR signal can help as it increased more significantly over the ipsilateral temporal region than contralaterally. Obviously, more work is necessary to determine if fNIRS-EEG data will one day have the potential to help in the localization of the epileptogenic region. In addition, further technical developments (e.g. device miniaturization) are necessary before one can envision using it in the video-EEG monitoring unit for comfortable long-term recordings.

**Limitations**

A particularly significant disadvantage of EEG-fNIRS when evaluating the recordings of mesial temporal lobe seizures is that only superficial neocortical haemodynamic changes can be assessed. Hence, several questions cannot be addressed such as: are there preictal haemodynamic changes prior to ictal onset, what are the haemodynamic changes in deep seated structures such as the epileptogenic hippocampus itself, the putamen or the thalamus. Some of these questions are currently being addressed using animal models [16, 33].

NIRS data acquisition could have been disturbed by movement during seizures. Fortunately, temporal lobe seizures are associated with little movement and consist mainly of subjective auras, behavioural arrest and occasional automatisms. Furthermore, we were careful to exclude channels exhibiting aberrant signals. Another potential point of criticism is the unknown influence of extracerebral tissue on cerebral fNIRS signal. Theoretically, the fNIRS signal is considered to originate from a banana-shaped volume starting from the superficial layers (skin and extracranial tissue) and extending to deeper cortical layers. Hence, contributions from

the superficial layers cannot be completely ruled out [57, 58. By using adjoining detectors located at short distance from the light source, subtraction methods could potentially correct for skin and bone haemoglobin oxygenation and account for variations in pathlength. For the purpose of this study however, using a configuration combining short and long source-detector separation channels would have meant sacrificing the large coverage necessary to determine the value of NIRS-EEG to localize the epileptogenic zone or to assess remote effects of focal seizures. We believe our results are still valid as regional variations are concordant with the site of the epileptic focus. Using the same fNIRS set-up, our group has also obtained language mapping results congruent with fMRI and the Wada test [23].

An additional limitation comes from the limited sample size. Despite having tested several patients with temporal lobe seizures, seizures were successfully recorded in only three. This is partly due to the fact that most patients became mildly uncomfortable after one to two hours of recording using such a highly loaded EEG-fNIRS helmet. Watanabe et al. [56] were more successful in recording seizures from temporal lobe epilepsy patients in a short span using bemegride but we felt that spontaneous seizures would better reflect reality. With further miniaturization of our instrumentation, long-term monitoring should be possible in upcoming years.

Finally, although there is evidence of inadequate oxygenation during temporal lobe complex partial seizures, there is no indication that any permanent tissue damage will occur during this brief period of time. Further studies are necessary to study the consequences of different partial seizures of varying duration, intensity and frequency, their contribution to cognitive changes seen in various epileptic syndromes, as well as the effect of some interventions (such as oxygen supplementation) during seizures. One could hypothesize that longer rather than shorter, repetitive rather than single, electroclinical rather than electrical seizures result in more significant tissue deoxygenation, but currently available data are unclear or even paradoxical [9, 10-13, 59, 60]. These studies will moreover benefit from additional improvements in our recording equipment to allow simultaneous pulse oximetry data recording and analysis (compared to visual monitoring with the initial cases reported in this study).

## CONCLUSION

EEG-fNIRS is a non-invasive technique of great potential for evaluation of epileptic seizures, whether to detect or monitor seizures, study haemodynamic changes associated with epileptic events and their impact, or lateralize the epileptogenic zone. In this study, observations made from the EEG-fNIRS recording of temporal lobe seizures reveal dynamic focal and remote haemodynamic changes. Tissue oxygenation appears to undergo a biphasic HbR response to ictal events with an initial decrease in HbR followed by a longer increase in HbR that often outlasts the duration of the seizure.

**Acknowledgments**

This work was supported by the Fonds de Recherche en Santé du Québec (FRSQ) grant 14385, the Canadian Institutes of Health Research (CIHR) Institute of Circulatory and Respiratory Health (ICRH) and the Heart and Stroke Foundation of Canada (HSFC) grant 62573, and the Savoy Foundation.

**Appendix A. Supplementary data** Supplementary data associated with this article can be found, in the online version.

## REFERENCES


1. Jöbsis F.F. Noninvasive, infrared monitoring of cerebral and myocardial oxygen sufficiency and circulatory parameters. Science 1977; 198(4323):1264-1267.
2. Irani F., Platek S.M., Bunce S., Ruocco A.C., Chute D. Functional near infrared spectroscopy (fNIRS): an emerging neuroimaging technology with important applications for the study of brain disorders. The Clinical Neuropsychologist; 2007; 21(1): 9-37.
3. Lloyd-Fox S., Blasi A., Elwell C.E. Illuminating the developing brain: The past, present and future of functional near infrared spectroscopy (review). Neuroscience and Biobehavioral Reviews 2010; 34: 269-284.
4. Penfield W., Jasper H. Epileptic mechanisms (cortical circulation) (Chapter VI) in Epilepsy and the functional anatomy of the human brain. 1954, Little, Brown and Company ed., Boston. pp. 246-264.
5. Goffin K., Dedeurwaerdere S., Laere K.V., Van Paescchen W. Neuronuclear assessment of patients with epilepsy. Semin Nucl Med 2008; 38:227-239.
6. Gotman J., Kobayashi E., Bagshaw A.P., Bénar C-G., Dubeau F. Combining EEG and fMRI: a multimodal tool for epilepsy research. J. Magn. Reson. Imaging 2006; 23:906-920.
7. Villringer A., Planck J., Stodieck S., Boetzel K., Schleinkofer L, Dirnagl U. Noninvasive assessment of cerebral haemodynamics and tissue oxygenation during activation of brain cell function in human adults using near infrared spectroscopy. Advances of Experimental Medicine and Biology 1994; 345: 559-565.
8. Steinhoff BJ., Herrendorf G., Kruth C. Ictal near infrared spectroscopy in temporal lobe epilepsy: a pilot study. Seizure 1996; 5:97-101.
9. Adelson PD., Nemoto E., Scheuer M., Painter M., Morgan J., Yonas H. Noninvasive continuous monitoring of cerebral oxygenation periictally using near-infrared spectroscopy: a preliminary report. Epilepsia 1999; 40(11): 1484-1489.
10. Sokol DK., Markand ON., Daly EC., Luerssen TG., Malkoff MD. Near infrared spectroscopy (NIRS) distinguishes seizure types. Seizure 2000; 9: 323-327.
11. Haginoya K., Munakata M., Kato R., Yokoyama H., Ishizuka M., Inuma K. Ictal cerebral haemodynamics of childhood epilepsy measured with near-infrared spectrophotometry. Brain 2002; 125: 1960-1971.
12. Shuhaiber H., Bolton S., Alfonso I. Cerebral regional oxygen fluctuations and decline during clinically silent focal electroencephalographic seizures in a neonate. J Child Neurol 2004; 19: 539-540.

13. Watanabe E., Nagahori Y., Mayanagi Y. Focus diagnosis of epilepsy using near-infrared spectroscopy. Epilepsia 2002; 43 (Suppl. 9): 50-55.
14. Zhao M., Suh M., Ma H., Perry C., Geneslaw A., Schwartz T.H. Focal increases in perfusion and decreases in hemoglobin oxygenation precede seizure onset in spontaneous human epilepsy. Epilepsia 2007; 48(11): 2059-2067.
15. Suh M., Ma H., Zhao M., Sharif S., Schwartz T.H. Neurovascular coupling and oximetry during epileptic events. Molecular Neurobiology 2006; 33: 181-197.
16. Bahar S., Suh M., Zhao M., Schwartz T.H. Intrinsic optical signal imaging of neocortical seizures: the 'epileptic dip'. Neuroreport 2006; 17(5): 499-503.
17. Kobayashi E., Hawco C.S., Grova C., Dubeau F., Gotman J. Widespread and intense BOLD changes during brief focal electrographic seizures. Neurology 2006; 66:1049-1055.
18. Kobayashi E., Bagshaw A.P., Benar C.G., Aghakhani Y., Andermann F., Dubeau F., Gotman J. Temporal and extratemporal BOLD responses to temporal lobe interictal spikes. Epilepsia 2006; 47(2): 343-354.
19. Englot D.J., Mishra A.M., Mansuripur P.K., Herman P., Hyder F., Blumenfeld H. Remote effects of focal hippocampal seizures on the rat neocortex. J. Neurosci. 2008; 28(36): 9066-9081.
20. Huppert T.J., Diamon S.G., Franceschini M.A., Boas D.A. HomER: a review of time-series analysis methods for near-infrared spectroscopy of the brain. Appl Opt. 2009; 48(10): D280-98.
21. Duncan, A., Meek, J. H., Clemence, M., Elwell, C. E., Fallon, P., Tyszczuk, L. & Delpy, D.T. Measurement of Cranial Optical Path Length as a Function of Age Using Phase Resolved Near Infrared Spectroscopy. *Pediatric Research*, 1996; *39*(5); 889-894.
22. Boas D.A.,Strangman G., Culver1 J.P., Hoge R.D., Jasdzewski G, Poldrack R. A., Rosen B. R. and Mandeville J. B. Can the cerebral metabolic rate of oxygen be estimated with near-infrared spectroscopy? Phys Med Biol 2003; 48; 2405-2418.
23. Gallagher A., Thériault M., Maclin E., Low K., Gratton G., Fabiani M., Gagnon L., Valois K., Rouleau I., Sauerwein H.C., Carmant L., Nguyen DK., Lortie A., Lepore F., Béland R., Lassonde M. Near-infrared spectroscopy (NIRS) as an alternative to the Wada test for language mapping in children, adults and special populations. Epileptic Disord 2007; 9(3): 241-255.
24. Gallagher A., Lassonde M., Bastien D., Vannasing P., Lesage F., Grova C., Bouthillier A., Carmant L., Lepore F., Béland R., Nguyen D.K. A non-invasive pre-

surgical investigation in a 10-year old epileptic boy using simultaneous NIRS-EEG: Seizure 2008; 17(6): 576-582.

25. Tyvaert L., LeVan P., Dubeau F., Gotman J. Noninvasive dynamic imaging of seizures in epileptic patients. Human Brain Mapping 2009; 30:3993-4011.
26. Bateman L.M., Chin-Shang L., Seyal M. Ictal hypoxemia in localization-related epilepsy: analysis of incidence, severity and risk factors. Brain 2008; 131:3239-3245.
27. Meldrum B.S., Horton R.W. Physiology of status epilepticus in primates. Arch Neurol 1973; 28(1): 1-9.
28. Meldrum B.S., Brierly J.B., Prolonged epileptic seizures in primates: ischemic cell change and its relation to ictal physiological events. Arch Neurol 1973; 128:10-7.
29. Kreisman N.R., Lamanna J.C., Rosenthal M., Sick T.J. Oxidative metabolic responses with recurrent seizures in rat cerebral cortex: role of systemic factors. Brain Res. 1981; 218(1-2): 175-188.
30. Kreisman N.R., Sick T.J., Rosenthal M. Concepts of brain oxygen sufficiency during seizures. Adv Exp Med Biol. 1984; 180:381-192.
31. Thornton R.C., Rodionov R., Laufs H., Vulliemoz S., Vaudano A., Carmichael D., Cannadathu S., Guye M., McEvoy A., Lhatoo S., Bartolomei F., Chauvel F., Chauvel P., Diehl B., De Martino F., Elwes R.D.C., Walker M.C., Duncan J.S., Lemieux L. Imaging haemodynamic changes related to seizures: comparison of EEG-based general linear model, independent component analysis of fMRI and intracranial EEG. Neuroimage 2010; 53: 196-205.
32. LeVan P., Tyvaert L., Moeller F., Gotman J. Independent component analysis reveals dynamic ictal BOLD responses in EEG-fMRI data from focal epilepsy patients. Neuroimage 2010; 49: 366-378.
33. Zhao M., Ma H., Suh M., Schwartz T.H. Spatiotemporal dynamics of perfusion and oximetry during ictal discharges in the rat neocortex. J. Neurosci. 2009; 29(9): 2814-2823.
34. Hoshi Y., Tamura M. Dynamic changes in cerebral oxygenation in chemically induced seizures in rats: study by near-infrared spectrophotometry. Brain Research; 1993:603:215-221.
35. Kreisman N.R., Sick T.J., Rosenthal M. Importance of vascular responses in determining cortical oxygenation during recurrent paroxysmal events of varying duration and frequency of repetition. J Cereb Blood Flow Metab. 1983; 3(3): 330-338.

36. Spencer S.S., Williamson P.D., Spencer D.D., Mattson R.H. Human hippocampal seizure spread studied by depth and subdural recording: the hippocampal commissure. Epilepsia 1987; 28:479-489.
37. Wallois F., Patil A., Kongolo G., Goudjil S., Grebe R. Haemodynamic changes during seizure-like activity in a neonate : A simultaneous AC EEG-SPIR and high-resolution DC EEG recording. Clinical Neurophysiology 2009; 39:217-227.
38. Lee H.W., Hong S.B., Tae W.S. Opposite ictal perfusion patterns of substracted SPECT. Hyperperfusion and hypoperfusion. Brain 2000; 123:2150-2159.
39. Tae W.S., Joo E.Y., Kim J.H., Han S.J., Suh Y-L., Kim B.T., Hong S.C., Hong S.B. Cerebral perfusion changes in mesial temporal lobe epilepsy: SPM analysis of ictal and interictal SPECT. Neuroimage 2005; 24: 101-110.
40. Huberfeld G., Habert M-O., Clemenceau S., Maksud P., Baulac M., Adam C. Ictal brain hyperperfusion contralateral to seizure onset: the SPECT mirror image. Epilepsia 2006; 47(1): 123-133.
41. Kaiboriboon K., Bertrand M.E., Osman M.M., Hogan E. Quantitative analysis of cerebral blood flow patterns in mesial temporal lobe epilepsy using composite SISCOM. J Nucl Med 2005; 46:38-43.
42. Gotman J. Epileptic networds studied with EEG-fMRI. Epilepsia 2008; 49 (Suppl. 3): 42-51.
43. Truccolo W., Donoghue J.A., Hochberg L.R., Eskandar E.N., Madsen J.R., Anderson W.S., Brown E.N., Halgren E., Cash S.S. Single-neuron dynamics in human focal epilepsy. Nat. Neurosci. 2011; 14(5): 635-641.
44. Rabinowicz A.L., Salas E., Beserra F., Leiguarda R.C., Vazquez S.E. Changes in regional cerebral blood flow beyond the temporal lobe in unilateral temporal lobe epilepsy. Epilepsia 1997; 38: 1011-1014.
45. Menzel C., Grunwald F., Klemm E., Ruhlmann J., Elger C.E., Biersack H.J. Inhibitory efects of mesial temporal partial seizures onto frontal neocortical structures. Acta Neurol Belg 1998; 98: 327-331.
46. Van Paesschen W., Dupont P., Van Driel G., Van Billoen H., Maes A. SPECT perfusion changes in patients with hippocampal sclerosis. Brain 2003; 126: 1103-1111.
47. Blumenfeld H., McNally K.A., Vanderhill S.D., Lebron Paige A., Chung R., Davis K., Norden A.D., Stokking R., Studholme C., Novotny Jr. E.J., Zubal G., Spencer S.S. Positive and negative network correlations in temporal lobe epilepsy. Cerebral Cortex 2004; 14: 892-902.

48. Dupont P., Zaknun J.J., Maes A., Supatporn T., Vasquez S., Bal C.S., Van Paesschen W., Carpintiero S., Locharernkul C., Dondi M. Dynamic perfusion patterns in temporal lobe epilepsy. Eur J Nucl Med Mol Imaging 2009; 36(5): 823-830.
49. Shin W.C., Hong S.B., Tae W.S., Kim S.E. Ictal hyperperfusion patterns according to the progression of temporal lobe seizures. Neurology 2002; 58(3): 373-580.
50. Chassagnon S., de Vasconcelos A.P., Ferrandon A., Koning E., Marescaux C., Nehlig A. Time course and mapping of cerebral perfusion during amygdala secondarily generalized seizures. Epilepsia 2005; 46(8): 1178-1187.
51. Englot D.J., Modi B., Mishra A.M., DeSalvo M., Hyder F., Blumenfeld H. Cortical deactivation induced by subcortical network dysfunction in limbic seizures. J Neurosci 2009; 29(41): 13006-13018.
52. la Fougère C., Rominger A., Forster S., Geisler J., Bartenstein P. PET and SPECT in epilepsy: a critical review. Epilepsy Behav 2009; 15(1): 50-55.
53. Zijlmans M., Huiskamp G., Hersevoort M., Seppenwoolde J-H., va Huffelen A.C., Leijten F.S.S. EEG-fMRI in the preoperative work-up for epilepsy surgery. Brain 2007; 130:2343-2353.
54. Moeller F., Tyvaert L., Nguyen D.K., LeVan P., Bouthillier A., Kobayashi E., Tampieri D., Dubeau F., Gotman J. EEG-fMRI: adding to standard evaluations of patients with nonlesional frontal lobe epilepsy. Neurology 2009; 73(23): 2023-2030.
55. Laufs H., Duncan J.S. Electroencephalography/functional MRI in human epilepsy: what it currently can and cannot do. Curr Opin Neurol 2007; 20:417-423.
56. Watanabe E., Maki A., Kawaguchi F., Yamashita Y., Koizumi H., Mayanagi Y. Journal of Biomedical Optics 2000; 5(3): 287-290.
57. Okada E., Delpy D.T. Near-infrared light propagation in an adult head model. I. Modeling of low-level scattering in the cerebrospinal fluid layer. Appl Opt. 2003; 42(16): 2906-2914.
58. Okada E., Delpy D.T. Near-infrared light propagation in an adult head model. II. Effect of superficial tissue thickness on the sensitivity of the near-infrared spectroscopy signal. Appl Opt. 2003; 42(16): 2915-2922.
59. Saito S., Yoshikawa D., Nishihara F., Morita T., Kitani Y., Amaya T., Fujita T. The cerebral haemodynamic response to electrically induced seizures in man. Brain Research 1995; 673: 93-100.
60. Munakata M., Haginoya K., Ishitobi M., Sakamoto O., Sato I., Kitamura T., Hirose M., Yokoyama H., Iinuma K. Dynamic cortical activity during spasms in three patients with West syndrome: a multichannel near-infrared spectroscopic topography study. Epilepsia 2004; 45(10): 1248-1257.

Supplementary figure S1

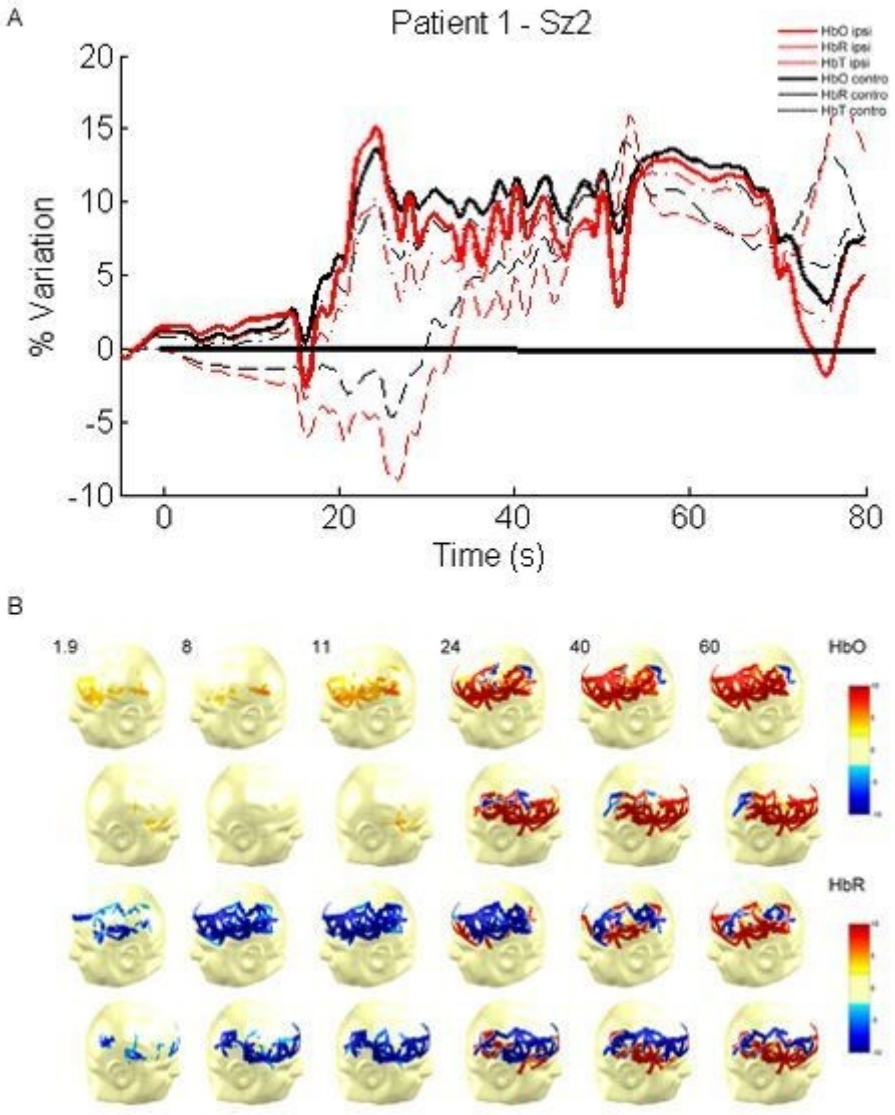


Case 1, seizure 2. A. Haemodynamic variations for the ipsilateral (epileptogenic) and contralateral temporal lobe. EEG evidence of seizure was visible above the black line. B. Topographic uncorrected Tstats during the time course of the seizure.

Supplementary figure S2

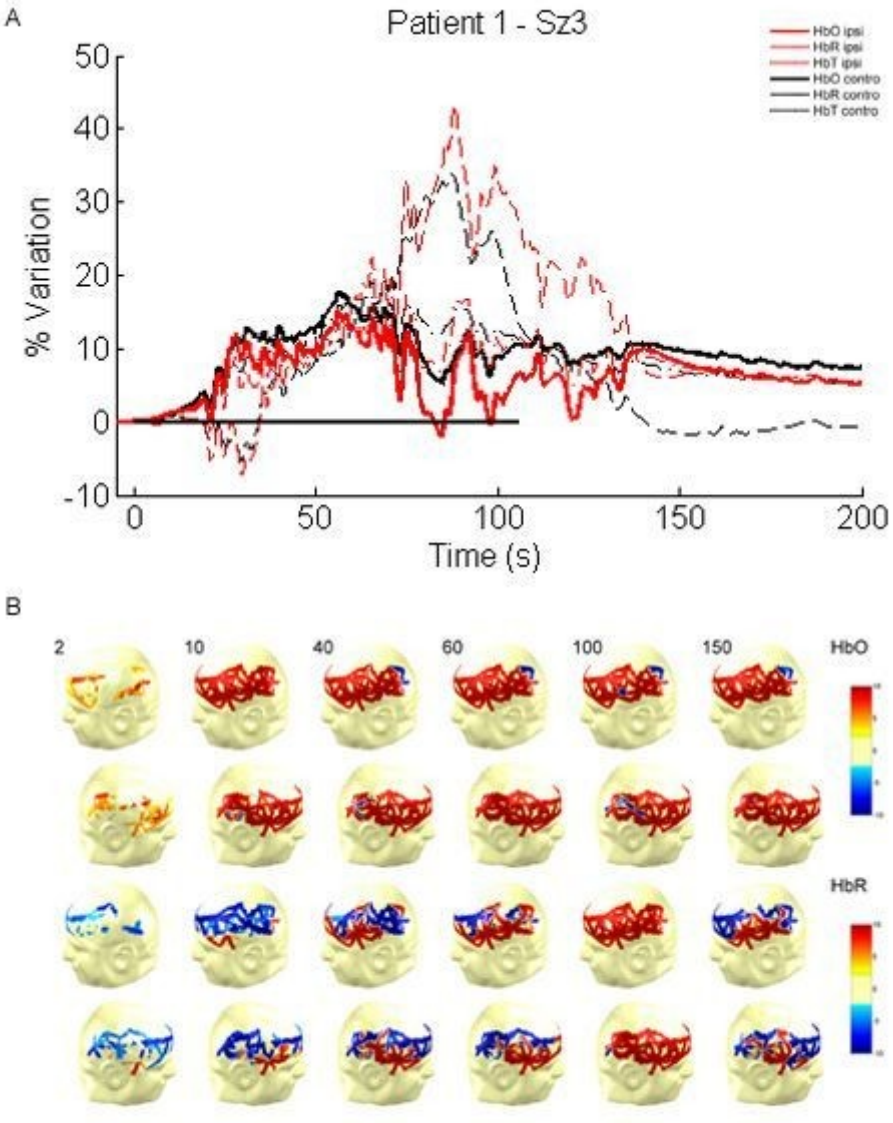


Case 1, seizure 3. A. Haemodynamic variations for the ipsilateral (epileptogenic) and contralateral temporal lobe. EEG evidence of seizure was visible above the black line. B. Topographic uncorrected Tstats during the time course of the seizure.

Supplementary figure S3

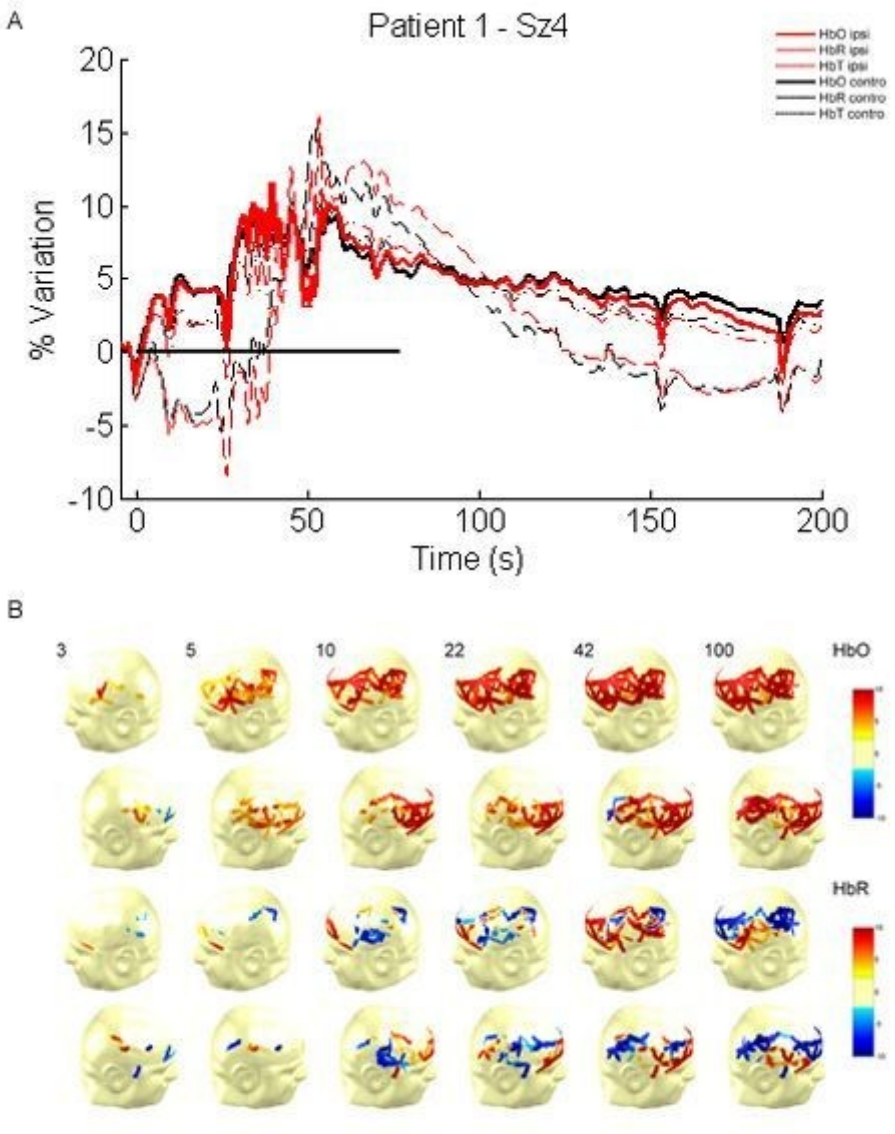


Case 1, seizure 4. A. Haemodynamic variations for the ipsilateral (epileptogenic) and contralateral temporal lobe. EEG evidence of seizure was visible above the black line. B. Topographic uncorrected Tstats during the time course of the seizure.

Supplementary figure S4

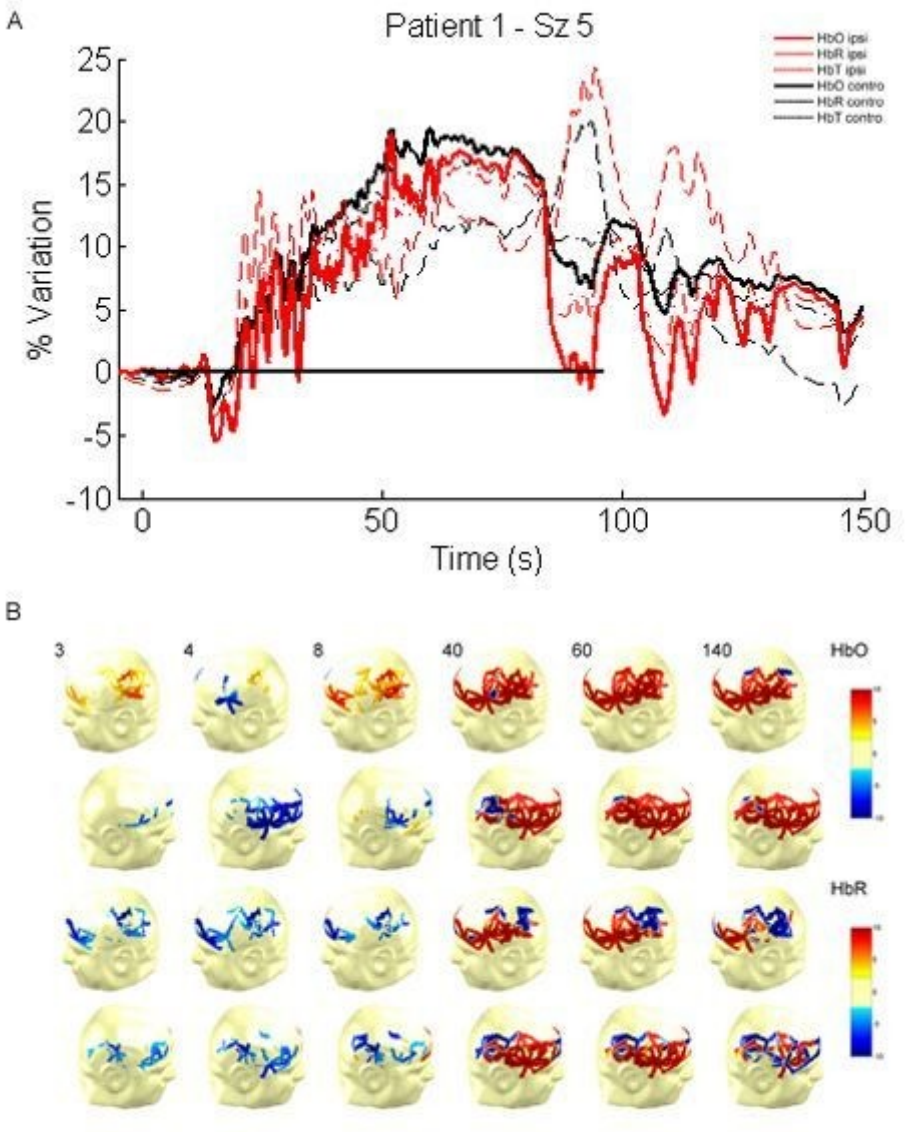


Case 1, Seizure 5. A. Haemodynamic variations for the ipsilateral (epileptogenic) and contralateral temporal lobe. EEG evidence of seizure was visible above the black line. B. Topographic uncorrected Tstats during the time course of the seizure.

Supplementary figure S5

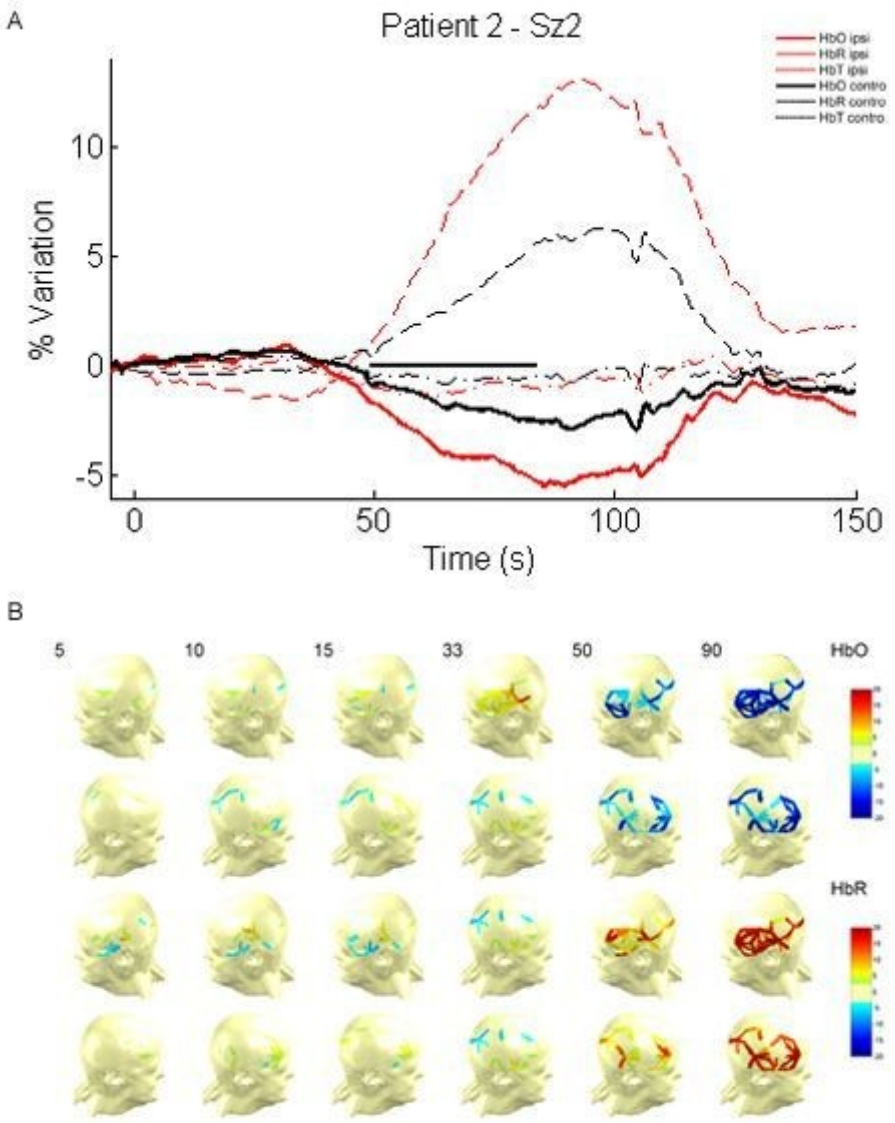


Case 2, seizure 2. A. Haemodynamic variations for the ipsilateral (epileptogenic) and contralateral temporal lobe. EEG evidence of seizure was visible above the black line. B. Topographic uncorrected Tstats during the time course of the seizure.

**ARTICLE 3**

***Noninvasive continuous functional near-infrared spectroscopy combined with electroencephalography recording of frontal lobe seizures***

**Published by**:
Epilepsia 2013 vol. 54(2) pp. 331-40

**Dang Khoa Nguyen[1], Julie Tremblay[2], Philippe Pouliot[3], Phetsamone Vannasing[2], Olivia Florea[2], Lionel Carmant[2], Franco Lepore[4], Mohamad Sawan[3], Frédéric Lesage[3], Maryse Lassonde[2,4]**

*[1]Service de neurologie, Centre hospitalier de l'Université de Montréal (CHUM) – Hôpital Notre-Dame, Montreal, Quebec, Canada*
*[2]Centre de recherche, Hôpital Sainte-Justine, Montreal, Quebec, Canada*
*[3]École polytechnique, Université de Montréal, Montreal, Quebec, Canada*
*[4]Centre de recherche en neuropsychologie et cognition, Université de Montréal, Montreal, Quebec, Canada*

Running title: fNIRS of FLE

Key words: EEG-fNIRS, seizures, haemodynamic response, frontal lobe epilepsy

**SUMMARY**

*Purpose:* To investigate spatial and metabolic changes associated with frontal lobe seizures.

*Methods:* Functional near-infrared spectroscopy combined with electroencephalography (EEG-fNIRS) recordings of patients with confirmed non-lesional refractory frontal lobe epilepsy (FLE).

*Key findings:* Eighteen seizures from 9 patients (7 males, mean age 27 years old, range 13-46) with drug-refractory FLE were captured during EEG-fNIRS recordings. All seizures were coupled with significant haemodynamic variations that were greater with electroclinical than with electrical seizures. fNIRS helped in the identification of seizures in 3 patients with more subtle ictal EEG abnormalities. Haemodynamic changes consisted of local increases in oxygenated (HbO) and total haemoglobin (HbT) but heterogeneous deoxygenated haemoglobin (HbR) behaviour. Furthermore, rapid haemodynamic alterations were observed in the homologous contralateral region, even in the absence of obvious propagated epileptic activity. The extent of HbO activation adequately lateralized the epileptogenic side in the majority of patients.

*Significance:* EEG-fNIRS reveals complex spatial and metabolic changes during focal frontal lobe seizures. Further characterization of these changes could improve seizure detection, localization and understand the impact of focal seizures.

## INTRODUCTION

Functional near-infrared spectroscopy (fNIRS) is an emerging neuroimaging technology for continuous, non-invasive monitoring of oxygenated (HbO), deoxygenated (HbR) and total haemoglobin (HbT = HbO + HbR). Assuming constant haematocrit, changes in HbT can serve as indicators of cerebral blood volume (CBV) variations (Lloyd-Fox et al., 2010). According to the implementation technique described below, photons from 2 wavelengths in the near-infrared range (one more sensitive to HbO, the other to HbR) shone by optic fibres penetrate the skull and superficial cortex, are absorbed (mainly by HbO and HbR) and scattered or reflected back to the surface where they can be measured by photodetectors. Changes in HbO or HbR concentrations in the superficial cortex will cause alterations in reflected light intensity (Jöbsis, 1977). When fNIRS is combined with continuous electroencephalography (EEG), the haemodynamic changes occurring before, during and after seizures can be investigated (Villringer et al., 1994; Steinhoff et al., 1996; Irani et al., 2007).

Combined EEG-fNIRS recently disclosed that temporal lobe seizures were associated with significant local and remote haemodynamic variations which outlasted seizure duration (Nguyen et al., 2011). Complex temporal lobe seizures were coupled with an initial increase in HbT and HbO as well as a decrease in HbR, congruent with a compensatory increment of local CBV to augment oxygen supply to the epileptic area. This initial phase was, however, consistently followed by an increase in HbR, indicating that ictal metabolic demands are then unmet during seizure progression.

Frontal lobe epilepsy (FLE) is distinct from temporal lobe epilepsy in many ways. Clinically, the seizures are frequent but short, have a nocturnal tendency, include frequent motor signs, and are followed by little or no post-ictal confusion (Fogarasi et al., 2001). The extensive network of subcortical connections in the frontal lobes permits rapid and distant spread of seizure activity. Here, we report the haemodynamic observations made during continuous EEG-fNIRS recording of frontal lobe seizures.

## METHODS

### Patients

Patients with non-lesional refractory FLE, candidates for potential epilepsy surgery, were recruited for a session of simultaneous EEG-fNIRS recording at the Optical Imaging Laboratory of Hôpital Sainte-Justine. The study was approved by the Université de Montréal Hôpital Sainte-Justine and Hôpital Notre-Dame Ethics Committees, and informed consent was obtained from all subjects. To increase the likelihood of recording seizures, EEG-fNIRS studies were undertaken when patients were admitted for video-EEG monitoring as part of their pre-surgical evaluation, since anticonvulsants were then frequently tapered off. Scalp electrodes for clinical video-EEG monitoring were removed to install an EEG-fNIRS helmet and re-installed after the recording session to resume video-EEG monitoring. An epileptologist was available at all times to ensure patient safety. After comprehensive, non-invasive, pre-surgical investigation, an intracranial study was performed to confirm epileptogenic zone localization.

### Combined EEG-fNIRS recording

Methodologies for simultaneous EEG-fNIRS recordings and data analysis have been detailed previously in Nguyen et al. (2011). Briefly, EEG was recorded with a Neuroscan Synamps 2TM system (Compumedics, Charlotte, NC, USA) via 19 home-made carbon fibre electrodes inserted through a perforated helmet and fixed on the scalp according to the 10-20 system (500-Hz sampling rate; 0.1-100-Hz band-pass filter; 60-Hz notch filter). fNIRS measurements were acquired with a multi-channel Imagent Tissue Oxymeter (ISS Inc., Champaign, IL, USA), using up to 64 fibre sources (operating at 690 nm and 830 nm, and modulated at a frequency of 110 MHz) and up to 16 photodetectors mounted on the helmet for optimal coverage of bilateral frontal regions as well as temporal and parietal regions. Later recordings had more channels than earlier ones as our technique improved over the years. The distance between the sources and detectors was kept between 3 to 5 cm. Except for patient 1, there were no overlapping channels. Optical intensity (DC), modulation amplitude and phase changes in collected light data were sampled at 19.5 Hz. Only DC was used for haemodynamic analysis. Continuous, simultaneous EEG-fNIRS monitoring was

carried out for 1 to 2 hours. A camera filmed the whole session for offline review of ictal manifestations or artefact-generating movements. A pulse oxymeter was attached to a fingertip for visual monitoring of arterial blood oxygen saturation. After the recording session, the location of every source, detector and fiducial point was digitized and traced (Brainsight Frameless 39, Rogue Research, Montreal, Qc, Canada) for co-registration (Matlab) with the cortical surface (Imagic, Neuronic, Havana, Cuba).

**Data analysis**

After acquisition, the EEG data were reviewed offline by an epileptologist (DKN). Seizure-onset and seizure end-times were respectively defined as the earliest and latest clinical or electrographic evidence of seizure activity. Raw light intensity was visually inspected to detect periods where movement artefacts caused discontinuity of the signal so they could be rejected. In addition, channels were completely rejected when the distance between them was lower than 2.5 cm, higher than 5 cm or if the standard deviation during baseline was higher than 20 %. Changes in HbO and HbR were calculated from DC variations according to the modified Beer-Lambert law. The values reported do not presume to indicate exact concentrations in the brain, but rather reflect representative relative changes in the brain, as we used a uniform partial volume factor of 1. Concentration curves are presented as percentages of variation compared to typical steady-state values of HbT 100 μM, HbO 75 μM, and HbR 25 μM (Boas et al., 2003). Low-pass frequency, zero-phase digital filtering of the data was performed with a cut-off frequency of 0.5 Hz, reducing the fast cardiac signal component. Channels with raw DC at the level of equipment noise or with a standard deviation higher than 20% were considered as artefactual and excluded from the analysis. Optical seizure onset time was marked when the first obvious haemodynamic changes occurred and was compared with EEG seizure onset identified by the epileptologist. To track the average temporal evolution of haemoglobin variations on both sides of the epileptic focus (ipsilaterally and contralaterally) in the figures below, channels were selected and averaged, based on the epileptogenic zone as determined by intracranial EEG.

*Topographic analysis*

A topographic view was created to display the temporal and spatial evolution of HbO and HbR activations. A student T-test was performed to ensure that the amplitude of the activation exceeded baseline noise using the following formula: T = X/SEM, where T is the uncorrected T-value, X is the amplitude of the concentration during the seizure and SEM is the standard error for 5 s of baseline. We mapped the T-value to a topographic view onto the skin segmentation using the patient's MRI. The activation was projected directly over the path between a source and a detector without interpolation using the optode coordinates acquired on the skin. When two channels passed through the same position, the maximal value was mapped.

*Laterality indices*

To evaluate if fNIRS could adequately lateralize the epileptic focus, 2 laterality indices were calculated. The extent laterality index (ELI), as a function of time, compares the extent of HbO activation between both hemispheres and is calculated as follows: ELI = (NL-NR)/(NL+NR), with NL = number of left channels and NR = number of right channels, keeping only channels exceeding 50% of the maximal T-value. The peak laterality index (PLI) compares the peak T-value at every moment between both hemispheres and is calculated as follows: PLI (t) = [(max peak left (t) – max peak right (t)]/[ (max peak left (t) + max peak right (t)].

**RESULTS**

Between June 2007 and July 2010, 20 patients with non-lesional, suspected refractory FLE underwent a continuous EEG-fNIRS study. Nine of these patients were excluded because they did not subsequently undergo an intracranial EEG study to confirm the location of the epileptogenic zone for the following reasons: pregnancy (1), evidence of multifocal seizures (1), drug abuse (1), psychosis (1), vagus nerve stimulation preferred to surgery (2), significant reduction in seizure frequency with additional drug changes (2), excessive bleeding upon skull opening due to a coagulation disorder (1). Of the remaining 11 patients who subsequently underwent an intracranial study, all were found to have a frontal epileptogenic focus as initially suspected. Of these 11 subjects, at least 1 clear electrical or electroclinical seizure was identified during pre-

surgical EEG-fNIRS recordings in 6 (Table 1, patients 1, 3, 5, 6, 7 and 8). In 3 others (Table 1, patients 2, 4 and 9), 'probable' seizures were identified after careful review of EEG segments, guided by evidence of optical signal deflectance in fNIRS data: patient 2 reported a brief seizure during a particular time-frame which coincided with a deflectance in the optical signal and associated with diffuse EEG de-synchronization; patients 4 and 9 had no ictal manifestations but the deflectance in the optical signal coincided with diffuse EEG de-synchronization with overlying low-voltage fast-activity followed by semi-rhythmic low-voltage slowing. Though less straight-forward than for the first 6 patients, these ictal scalp EEG patterns were, however, congruent with ictal patterns observed during intracranial EEG recordings. In the 2 other implanted patients, no seizures occurred during EEG-fNIRS. Based on intracranial recordings, the 9 identified patients (7 males, mean age 27 years old, range 13-46) who presented seizures on EEG-fNIRS had an epileptogenic zone localized to the fronto-polar cortex in 1, the mesial frontal region in 1, and the lateral frontal neocortex in the remainder (motor cortex in 1, dorso-lateral pre-motor cortex in 1, and intermediate dorso-lateral frontal region in 5).

Table 1. Demographic data, site of epileptogenic zone based on intracerebral recordings and date of EEG-fNIRS recordings with respective number of channels.

| Patient | Age (yrs) | Gender | EZ | Date of test | Number of fNIRS channels |
|---|---|---|---|---|---|
| | | | | | |
| 1 | 10 | M | R FP | 2007-03-25 | 44 |
| 2 | 13 | F | R MC | 2007-07-10 | 61 |
| 3 | 45 | M | R ILC (IFG)-Ins | 2008-10-16 | 96 |
| 4 | 39 | F | L ILC (IFG)-Ins-STG | 2008-11-05 | 68 |
| 5 | 21 | M | R ILC (IFG, MFG) | 2009-02-12 | 140 |
| 6 | 21 | M | L IMC (Medial FG, SFG), CC | 2009-09-10 | 100 |
| 7 | 46 | M | L DLPMC, ILC (SFG, MFG) | 2009-11-13 | 203 |
| 8 | 13 | M | R ILC (IFG) | 2010-01-19 | 140 |
| 9 | 35 | M | R ILC (IFG) | 2010-04-16 | 142 |
| Mean | 27 | | | | 110 |

**Local haemodynamic signal changes**

A total of 18 seizures were identified: 5 complex partial seizures, 5 simple partial seizures and 8 electrical seizures (Table 2). Pulse oxymetry monitoring indicated no significant peripheral desaturation during any seizure. Each ictal event was accompanied by changes in the NIRS optical signal over the epileptogenic zone. Ictal haemodynamic variations for each seizure are detailed in Figures 1-4 and Supplementary Figures S1-S9. On average, these changes occurred less than 2 s after the onset of EEG discharge (mean 1.39 ± 2.30 s). The optical signal alterations persisted after the end of EEG discharge in patients 1, 2, 7 and 8. In the remainder, the duration of optical variations was relatively close to the duration of ictal EEG changes.

Table 2.Details of haemodynamic changes in all recorded seizures: onset of fNIRS variations compared to first scalp EEG evidence of ictal activity, EEG evidence of seizure activity duration, duration of haemodynamic changes in individual seizures, peak concentration alterations recorded over the epileptogenic zone; HbT = total haemoglobin; HbO = oxyhaemoglobin; HbR = deoxyhaemoglobin; SD = standard deviation.

| Patient | Sz | Symptoms | Delay to fNIRS changes (s) | Sz duration EEG (s) | Sz duration fNIRS (s) | Peak | | | | | | Figure |
|---|---|---|---|---|---|---|---|---|---|---|---|---|
| | | | | | | HbT | Time | HbO | Time | HbR | Time | |
| 1 | 1 | SPS: sudden fear | 3 | 35 | 50 | 6.83 | 29 | 9.36 | 27 | -3.01 | 24 | |
| | 2 | SPS: sudden fear | 8 | 36 | 50 | 8.01 | 20 | 10.08 | 20 | 1.67 | 20 | see |
| | 3 | ES | 5 | 16 | 20 | 1.32 | 11 | 1.82 | 11 | -0.18 | 11 | Gallagher et |
| | 4 | ES | 3 | 6 | 10 | 0.80 | 5 | 1.06 | 5 | 0.01 | 5 | al., 2008 |
| 2 | 1 | SPS: shock in L arm | 0 | 3 | 7 | 1.47 | 3.2 | 2.08 | 3 | -0.47 | 3 | Figure S1 |
| 3 | 1 | ES | 0 | 13 | 16 | 1.14 | 11 | 1.42 | 11 | -0.28 | 8 | Figure 1 |
| | 2 | ES | 0 | 12 | 13 | 0.98 | 8 | 1.34 | 8 | -0.44 | 13 | Figure 1 |
| 4 | 1 | ES | 0 | 6 | 6 | 1.08 | 3.02 | 1.47 | 3 | -1.50 | 8 | Figure 2 |
| | 2 | ES | 1 | 12.26 | 15 | 0.51 | 6.83 | 0.94 | 7 | -0.81 | 7 | Figure S2 |
| 5 | 1 | CPS: gelastic sz | 0 | 62 | 62* | 3.73 | 11 | 6.41 | 12* | -6.09* | 13* | Figure S3 |
| 6 | 1 | CPS: arousal | 0 | 16 | 16* | 11.03 | 16 | 13.2 | 16 | 4.5 | 16 | Figure S4 |
| | 2 | CPS: arousal | 4 | 14 | 15* | 7.68 | 14 | 8.90 | 14 | 4.02 | 14 | Figure S5 |
| 7 | 1 | SPS: jaw + arm jerks | 0 | 20 | 30 | 5.12 | 15 | 4.69 | 15 | 7.02 | 15 | Figure 3 |
| | 2 | SPS: subtle hand jerks | 1 | 4 | 10 | 1.31 | 4 | 1.18 | 4 | 1.72 | 4 | Figure S6 |
| 8 | 1 | CPS: fixed gaze | 0 | 24 | 35 | 7.36 | 14 | 10.8 | 15 | -11.65 | 29 | Figure 4 |
| | 2 | CPS: fixed gaze | 0 | 38 | 38* | 4.32 | 21 | 6.87 | 21 | -10.39* | 26* | Figure S7 |
| 9 | 1 | ES | 0 | 4.81 | 5 | 0.65 | 2.94 | 0.75 | 3 | 0.43 | 3 | Figure S8 |
| | 2 | ES | 0 | 4.82 | 5 | 0.60 | 3.44 | 0.75 | 3 | 0.19 | 5 | Figure S9 |
| Mean total | | | 1.39 | 18.23 | 19.50 | 3.35 | | 4.34 | | -0.98 | | |
| SD total | | | 2.30 | 15.64 | 16.30 | 3.33 | | 4.21 | | 5.26 | | |
| Electrical seizures vs clinical seizures | | | | | | | | | | | | |
| Mean ES | | | | 9.42 | 11.25 | 0,88 | | 1.19 | | -0.32 | | |
| SD total | | | | 4.46 | 5.65 | 0,27 | | 0.38 | | 0.61 | | |
| Mean CS | | | | 25.28 | 31.30 | 5,68 | | 7.36 | | -1.36 | | |
| Total SD | | | | 17.96 | 18.99 | 3,07 | | 3.86 | | 6.37 | | |

Over the epileptogenic zone, HbO and HbT followed a bell-shaped curve with an initial rise from baseline to peak, followed by a gradual decline to a plateau or to initial baseline (see part B of Figures 1-4 and S1-S9). The mean maximal amplitude of HbT and HbO increase was 3.35 ± 3.33% and 4.34 ± 4.21% from baseline, respectively (Table 2). Electroclinical seizures led to higher increments of HbT and HbO (5.68 ± 3.07% and 7.36 ± 3.86%, respectively) compared to electrical seizures (0.88 ± 0.27 and 1.19 ± 0.38%, respectively). The peak amplitude of HbO increase was strongly correlated with seizure duration (r = 0.56). The behaviour of HbR changes was more heterogeneous (see part B of Figures 1-4 and S1-S9). While an inverted bell-curve (initial decrease to a nadir, followed by a progressive return to baseline or plateau) was noted in 4 (patients 1, 4, 5 and 8), an opposite response was observed in patients 6 and 7 with very little change in the remaining subjects. As with HbO, the nadir of HbR decrease correlated with seizure duration (r = -0.46).

**Remote haemodynamic changes**

In addition to the local haemodynamic alterations described above, significant changes were also noted in the homologous contralateral region (see part C of Figures 1-4 and S1-S9) where HbT, HbO and HbR behaviour closely mirrored that over the epileptogenic zone (see Figures 1-4 and S1-S9). No clear delay between the timing of ipsilateral versus contralateral changes was noted. The amplitude of HbO increase during the first seconds after seizure onset was slightly higher ipsilaterally in 8 (67%) of the 12 seizures and peaked slightly higher ipsilaterally in half of them. Of the 5 seizures (from patients 3, 4 and 6) associated with a decrease in HbR, the highest nadir was noted ipsilaterally in 2 (40%), contralaterally in 1 (20%), and bilaterally in the remainder.

**Lateralization**

To evaluate if fNIRS could adequately lateralize the epileptic focus, 2 laterality indices were calculated for 8 of the 9 patients (patient 1 did not have contralateral coverage) (Figure 5). At every time point, the ELI compares the extent of HbO activation between both hemispheres, while the PLI compares the peak T-value at every moment between both hemispheres. In the early phase of seizures, the ELI

adequately identified the epileptogenic hemisphere in 7 (88%) of 8 patients. The PLI adequately identified the epileptogenic hemisphere in only 50% of patients (table 3).

Table 3. Lateralization indexes: Time LI = time when index of laterality was highest. ELI = Extent laterality index; PLI = peak laterality index. A value between -1 and -0.1 indicates lateralization to the R hemisphere while a value between 0.1 and 1 indicates lateralization to the L hemisphere.

| Patient | Sz | Time LI | ELI | Concordant with side of focus | PLI | Concordant with side of focus |
|---|---|---|---|---|---|---|
| 2 | 1 | 3 | -0.34 | Yes | -0.30 | Yes |
| 3 | 1 | 6 | -0.35 | Yes | -0.12 | No |
| | 2 | 26 | -0.53 | | -0.04 | |
| 4 | 1 | 3,5 | 0.20 | Yes | -0.07 | No |
| | 2 | 4 | 1.00 | | 0.38 | |
| 5 | 1 | 3 | -1.00 | Yes | -0.33 | Yes |
| 6 | 1 | 7 | 1.00 | Yes | 0.41 | Yes |
| | 2 | 7 | 0.27 | | 0.18 | |
| 7 | 1 | 3 | 0.67 | Yes | 0.00 | No |
| | 2 | 5 | 0.55 | | 0.12 | |
| 8 | 1 | 5 | -1.00 | No | -0.46 | No |
| | 2 | 5 | 0.37 | | 0.28 | |
| 9 | 1 | 3 | -0.76 | Yes | -0.16 | Yes |
| | 2 | 3 | -0.22 | | -0.10 | |
| Percentage of patient adequately lateralised | | | | 88% | | 50% |

## DISCUSSION

In this study, we employed a non-invasive method to measure cortical haemodynamic and metabolic changes occurring throughout seizures, with high temporal resolution. We showed that focal frontal lobe seizures are associated with complex haemodynamic variations, i.e., a local, expected increase in HbO and HbT but heterogeneous HbR behaviour and, surprisingly, very early activation of the homologous region contralateral to the epileptogenic zone.

The observed ictal increments of HbT and HbO over the epileptogenic zone are congruent with the brain's attempt to perfuse active, epileptic neurons with

oxygenated haemoglobin by elevating local cerebral blood flow (CBF) and CBV (Suh et al., 2006). In our study, brief electrical seizures ( = 9.4 s) were associated with only small variations from baseline ( = 0.88% for HbT and 1.19% for HbO), but longer ( = 25.3 s) electroclinical seizures led to HbT and HbO increases as high as 11.0% and 13.2%, respectively ( = 5.68% for HbT and 7.36% for HbO). In a similar investigation of temporal lobe seizures (Nguyen et al., 2011), our group recently reported even higher changes from baseline ( = 11% for HbT and HbR), most likely due to their lengthier duration ( = 77.3 s). The longest temporal lobe complex partial seizure recorded (106 s) resulted in the highest HbT (17%) and HbO (18%) variations from baseline. These variations were 3 to 8 times larger than those observed during normal cognitive processing (Gallagher et al., 2007), indicating that seizures are an abnormal physiological state placing supranormal demands on the brain's autoregulatory mechanisms.

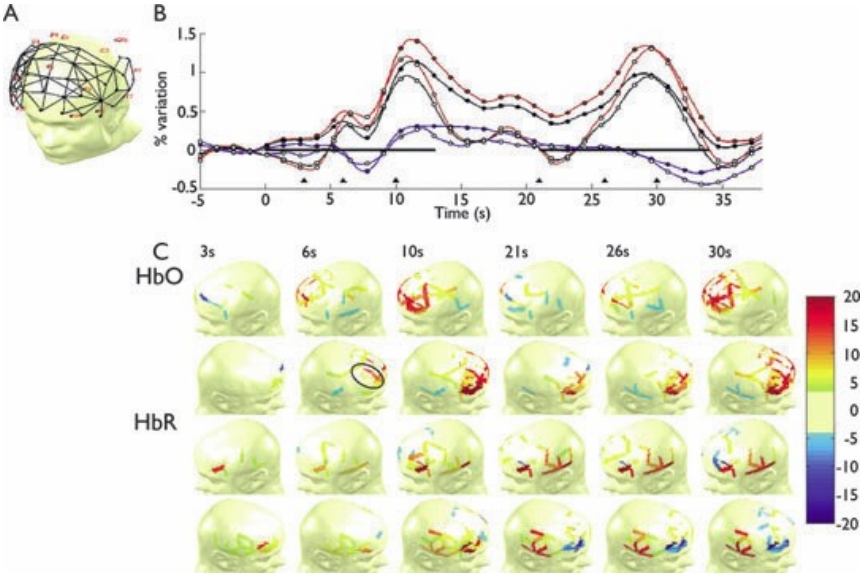


Figure 1.(A) Channel configuration. (B) Ictal hemodynamic variations (HbT, black; HbO, red; HbR, blue) over the epileptogenic zone (closed circles) and the contralateral homologous region (open circles). The black line indicates time of EEG evidence of seizure activity. (C) Topographic uncorrected T-stats viewed at different time points (black triangles) during the course of the seizure. The epileptogenic 14 zone is indicated by a circle. This 45-year-old man (Patient 3) with right frontoinsular epilepsy had two electrical seizures back to back during EEG-fNIRS recording associated each time with an increase in HbT and HbO over the epileptogenic zone and in the contralateral homologous region. Epilepsia ©ILAE

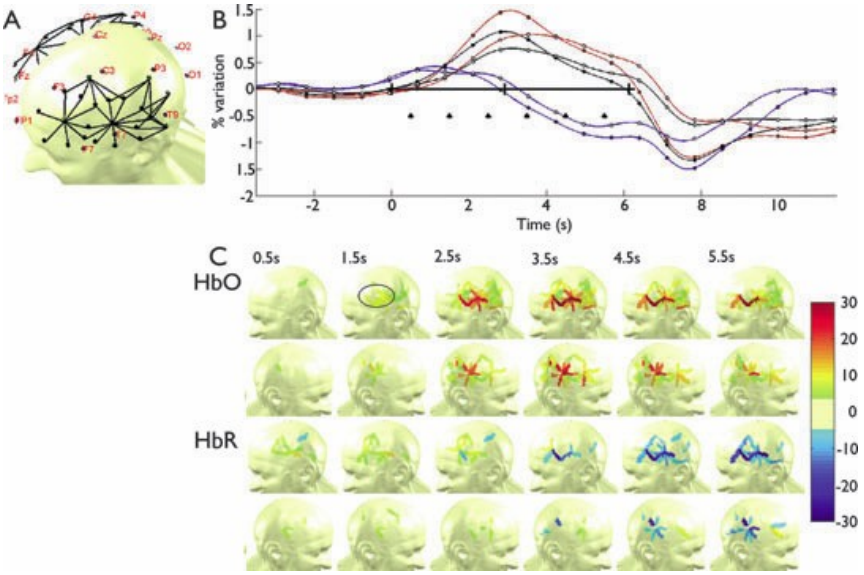


Figure 2. Same legend as in Fig. 1. This 39-year-old woman (Patient 4) with left perisylvian epilepsy did not experience any clinical seizures during EEG-fNIRS. A first look at the EEG failed to identify obvious electrical seizures. However, review of the fNIRS signal revealed HbO and HbT increases (and HbR decrease) at a certain time period. Closer attention to that particular EEG time-frame disclosed a previously missed electrical seizure characterized by EEG de- synchronization with overlying, low-voltage fast-activity followed by semi-rhythmic low-voltage slowing. Epilepsia ©ILAE

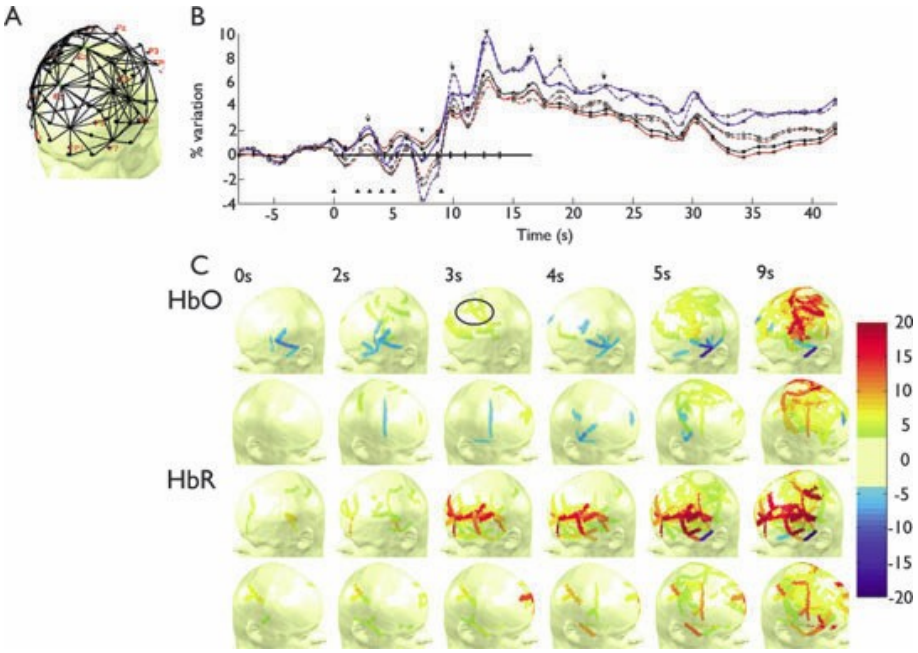


Figure 3. Same legend as in Fig. 1. This 46- year-old man (Patient 7), with a left premotor cortex focus, experienced clonic jerks of the right jaw and arm. Although each individual jerk generated a small artifact (arrow), the fNIRS signal in between jerks was of good quality. Note how this electroclinical seizure led to higher HbT, HbO, and HbR variations compared to electrical seizures shown in Figs 1 and 2. Also note the HbR increase despite the HbT and HbO increment during the ictus. Epilepsia ©ILAE

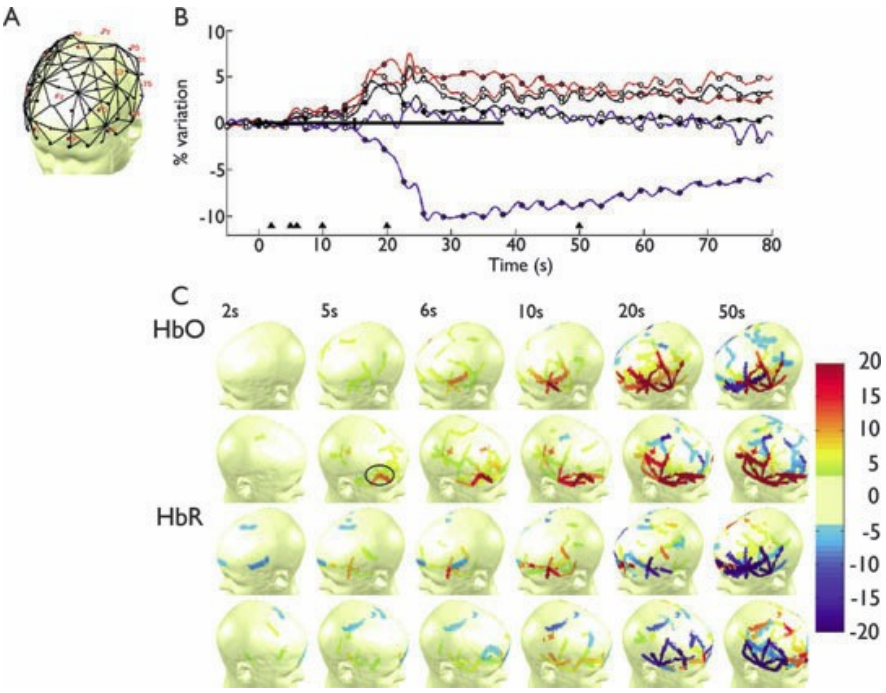


Figure 4. Same legend as in Fig. 1. This 13-year-old man (Patient 8) had seizures originating from the right inferior frontal gyrus. Contrary to the seizure shown in Fig. 3 (Patient 7), this seizure was associated with a significant HbR decrease during ictus. Epilepsia © ILAE

Some controversy remains in the literature as to whether local CBF and CBV increases are adequate to meet these supranormal demands throughout the ictus (Suh et al., 2006). Although the inadequacy of CBF in addressing metabolic demands has been demonstrated in animal models of status epilepticus (Meldrum & Horton, 1973; Meldrum & Brierly, 1973; Kreisman et al., 1984), there is growing evidence of inadequate oxygenation at the onset or throughout shorter-duration ictal events as well (Bahar et al., 2006; Zhao et al., 2007; Zhao et al., 2009). In our study of complex partial temporal lobe seizures (Nguyen et al., 2011), HbR (after an initial decrease) rose consistently as the seizure progressed, indicating that metabolic demands of the seizing tissue were not sufficiently compensated by the reactive regional increase in cerebral blood supply to wash out HbR. In this series of frontal lobe seizures, the ictal increments in CBF and CBV seemed sufficient for the majority of seizures since HbR showed little change (suggesting adequate HbO supply) or decreased (indicating HbO oversupply) for most of them. Although this could be ascribed to longer seizure duration in our temporal lobe epilepsy series compared to the present FLE series, other factors are probably in play, as exemplified by patient 6 who presented an increase in HbR (indicating an insufficient neurovascular response) for a 'mere' 20-s seizure. In rare EEG-fMRI analyses of fortuitous motionless seizures, significant generally positive BOLD changes (congruent with a decrease in HbR) have been reported in the seizure onset zone along with other remote smaller clusters of BOLD signal change (Kobayashi et al., 2006; Tyvaert et al., 2009; Donaire et al., 2009; Thornton et al., 2010; LeVan et al., 2010; Chaudhary et al., 2011). However, additional areas of BOLD signal decrease during seizures have been observed within the presumed seizure onset zone, in surrounding areas of BOLD signal increase, remotely from the seizure onset zone including on the opposite hemisphere. Although some have been ascribed to the default mode network, the significance of these BOLD signal decreases remains largely unknown. Further work is necessary to better ascertain the different potential factors underlying heterogeneity in the HbR response: seizure duration, location of seizure onset, volume of epileptogenic tissue involved during ictus, seizure frequency, underlying substrate of epileptogenicity, age, co-morbid medical conditions, etc. (Sokol et al., 2000; Haginoya et al., 2002; Shuhaiber et al., 2004).

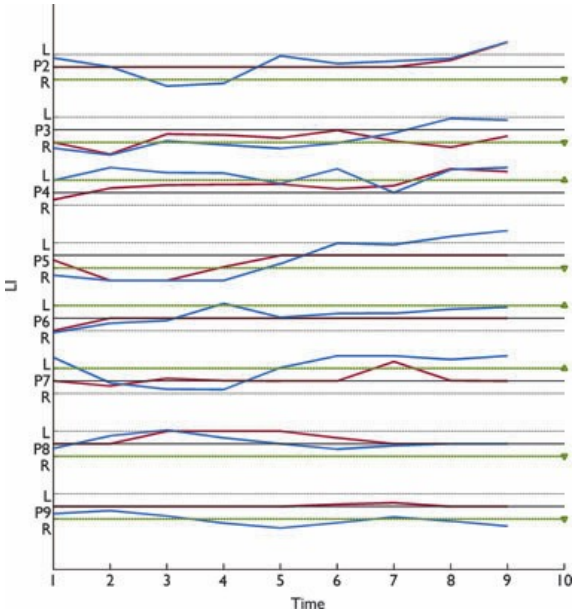


Figure 5. The laterality index of HbO variation in function of time during seizure(s) in each patient (except Patient 1, who did not have bilateral coverage). The data were averaged when there was more than one seizure per patient. Blue: Extent laterality index (ELI) with a half maximum T-value threshold. Red: Maximal 15 peak laterality index (PLI). The green line indicates the correct side of the epileptogenic zone for each patient. Epilepsia ©ILAE

In addition to haemodynamic changes over the epileptogenic zone described above, our study reveals significant modulations in contralateral homologous regions which almost mirrored those seen ipsilaterally. This is in line with some prior observations both on interictal spikes and focal seizures. Using intrinsic optical imaging, Schwartz and Bonhoeffer (2001) showed a clear increase in the optical signal in the contralateral hemisphere, homotopic to the acute bicuculline spiking foci in the ferret somatosensory cortex. Authors ascribed these contralateral changes to orthodromic effects of transcallosal projected neuronal activity (Schwartzkroin et al., 1975). In animal and human EEG-fMRI studies, widespread and distant (both positive and negative) BOLD signal changes are seen with focal interictal epileptic spikes or brief seizures (Kobayashi et al., 2006a; Englot et al., 2008; Truccolo et al., 2011). Using EEG spectral analysis, Yu et al. (2009) revealed significant contralateral EEG changes (predominating in lower frequencies) in 90% of contralateral BOLD activations triggered by spikes. These authors suggested that these spectral changes in areas corresponding to contralateral activations possibly reflected poorly synchronized but intense neuronal activity. It has been known for some time that frontal lobe seizure activity can spread rapidly through various pathways leading to widespread regional or multi-lobar interictal and ictal signal abnormalities both on scalp and intracranial

EEG (Quesney et al., 1992; Salanova et al., 1993). More recently however, it has been argued that rapid discharges at seizure onset observed over different brain sites were not necessarily due to propagation but instead to quasi-synchronous involvement of a network of neuronal populations distributed in distinct and distant brain structures (Bartolomei et al., 2008; Wendling et al., 2010). In our study, the limitations of scalp EEG (low signal to noise ratio, inability to detect early ictal rhythms emanating from deeper structures, attenuation or cancellation of signal by soft tissues and bone, signal artefacts etc.) and the limited number of seizures per patient prevent us from any clear conclusions on the pathophysiology of these contralateral and remote hemodynamic changes.

Prior studies have suggested that EEG-fNIRS could be used to localize the epileptogenic zone due to its high temporal resolution (Adelson et al., 1999; Watanabe et al., 2000, 2002; Schichiri et al., 2001; Gallagher et al., 2008), in contrast to ictal single photon computed tomography, for example, which can only provide a single snapshot of CBF several seconds after seizure onset when epileptic activity has already propagated to other regions (Goffin et al., 2008). These studies were, however, limited by the small number of optodes used. Benefiting from much larger spatial sampling, our demonstration of rapid and significant contralateral haemodynamic changes, even before evidence of seizure propagation, complicates the issue of lateralization/localization. In this preliminary work, the extent of HbO activation during the early phase of seizures was more indicative of the epileptogenic hemisphere than peak HbO activation. Additional work is required to establish the localization value of fNIRS. Can mirror activations be exploited to confirm the location of the focus (Huberfeld et al., 2006)? Can the presence of a mirror image facilitate the identification of the true epileptic focus in the presence of several areas of activation? Can the analysis of the preictal period be used for seizure localization (Zhao et al., 2007; Tyvaert et al., 2009)? Put aside its localization potential, fNIRS was found to be a robust tool for seizure detection in our study, as analyzing the optical signal was able to guide a more careful review of a specific time-frame of the EEG signal to detect seizures with subtle electrographic changes.

**Limitations**

One disadvantage of EEG-fNIRS is that only superficial neocortical haemodynamic changes can be assessed. Fortunately, the majority of our patients in this series had a neocortical frontal lobe focus. Because frontal lobe seizures are frequently associated with motor symptoms, fNIRS data acquisition could have been disturbed by movement during seizures. Fortunately, most recorded seizures generated no movements (electrical seizures) or only subtle or small movements (during electroclinical seizures). Furthermore, we were careful to exclude channels exhibiting aberrant signals. It should also be remembered that larger activation areas will also induce larger fNIRS responses due to partial volume effects. Untangling spatial effects from increased local demands remains difficult and will require tomographic approaches. Finally, the influence of extracerebral tissue (skin and bone haemoglobin) on cerebral fNIRS signals in our study is unknown (Okada & Delpy, 2003). Our setting, which favoured large spatial sampling, did not include short-source detector separation channels to allow subtraction of contamination from superficial layers.

## CONCLUSION

Non-invasive, continuous EEG-fNIRS recording of frontal lobe seizures with large spatial sampling reveals HbT and HbO increases but heterogeneous HbR responses, not only over the epileptogenic zone but also in the contralateral homologous region. Further work is necessary to elucidate the pathophysiology underlying these observations.

**Acknowledgments**

This work was supported by Fonds de la recherche en santé du Québec (FRSQ) Grant 14385, the Canadian Institutes of Health Research (CIHR) Institute of Circulatory and Respiratory Health (ICRH) and the Heart and Stroke Foundation of Canada (HSFC) Grant 62573, and the Savoy Foundation.

**Appendix A. Supplementary data**

Supplementary data associated with this article can be found, in the online version.

## REFERENCES


Adelson PD, Nemoto E, Scheuer M, Painter M, Morgan J, Yonas H. (1999) Noninvasive continuous monitoring of cerebral oxygenation periictally using near-infrared spectroscopy: a preliminary report. *Epilepsia.* 40: 1484-1489.

Bahar S, Suh M, Zhao M, Schwartz TH. (2006) Intrinsic optical signal imaging of neocortical seizures: the 'epileptic dip'. *Neuroreport.* 17: 499-503.

Bartolomei F, Chauvel P, Wendling F. (2008) Epileptogenicity of brain structures in human temporal lobe epilepsy: a quantified study from intracerebral EEG. *Brain*. 131: 1818-1830.

Boas DA, Strangman G, Culver JP, Hoge RD, Jasdzewski G, Poldrack RA, Rosen BR, Mandeville JB. (2003) Can the cerebral metabolic rate of oxygen be estimated with near-infrared spectroscopy? *Phys Med Biol*. 48: 2405-2418.

Chaudhary UJ, Duncan JS, Lemieux L. (2011) Mapping hemodynamic correlates of seizures using fMRI: a review. *Hum. Brain Mapp*. Nov 14. doi: 10.1002/hbm.21448

Donaire A, Bargallo N, Falcon C, Maestro I, Carreno M, Setoain J, Rumia J, Fernandez S, Pintor L, Boget T (2009). Identifying the structures involved in seizure generation using sequential analysis of ictal-fMRI data. *Neuroimage* 47; 173-183.

Englot DJ, Mishra AM, Mansuripur PK, Herman P, Hyder F, Blumenfeld H. (2008) Remote effects of focal hippocampal seizures on the rat neocortex. *J Neurosci*. 28: 9066-9081.

Fogarasi A, Janszky J, Faveret E, Pieper T, Tuxhorn I. (2001) A detailed analysis of frontal lobe seizure semiology in children younger than 7 years. *Epilepsia.* 42: 80-85.

Gallagher A, Lassonde M, Bastien D, Vannasing P, Lesage F, Grova C, Bouthillier A, Carmant L, Lepore F, Béland R, Nguyen DK. (2008) A non-invasive pre-surgical investigation in a 10-year-old epileptic boy using simultaneous NIRS-EEG. *Seizure*. 17: 576-582.

Gallagher A, Thériault M, Maclin E, Low K, Gratton G, Fabiani M, Gagnon L, Valois K, Rouleau I, Sauerwein HC, Carmant L, Nguyen DK, Lortie A, Lepore F, Béland R, Lassonde M. (2007) Near-infrared spectroscopy (NIRS) as an alternative to the Wada test for language mapping in children, adults and special populations. *Epileptic Disord*. 9: 241-255.

Goffin K, Dedeurwaerdere S, Laere KV, Van Paescchen W. (2008) Neuronuclear assessment of patients with epilepsy. *Semin Nucl Med.* 38: 227-239.

Haginoya K, Munakata M, Kato R, Yokoyama H, Ishizuka M, Inuma K. (2002) Ictal cerebral haemodynamics of childhood epilepsy measured with near-infrared spectrophotometry. *Brain*. 125: 1960-1971.

Huberfeld G, Habert MO, Clemenceau S, Maksud P, Baulac M, Adam C. (2006) Ictal brain hyperperfusion contralateral to seizure onset: the SPECT mirror image. *Epilepsia.* 47: 123-133.

Irani F, Platek SM, Bunce S, Ruocco AC, Chute D. (2007) Functional near infrared spectroscopy (fNIRS): an emerging neuroimaging technology with important applications for the study of brain disorders. *Clin Neuropsychol*. 21: 9-37.

Jöbsis FF. (1977) Noninvasive, infrared monitoring of cerebral and myocardial oxygen sufficiency and circulatory parameters. *Science*. 198: 1264-1267.

Kobayashi E, Bagshaw AP, Benar CG, Aghakhani Y, Andermann F, Dubeau F, Gotman J. (2006a) Temporal and extratemporal BOLD responses to temporal lobe interictal spikes. *Epilepsia.* 47(2): 343-354.

Kobayashi E, Hawco CS, Grova C, Dubeau F, Gotman J. (2006b) Widespread and intense BOLD changes during brief focal electrographic seizures. *Neurology*. 66:1049-1055.

Kreisman NR, Sick TJ, Rosenthal M. (1984) Concepts of brain oxygen sufficiency during seizures. *Adv Exp Med Biol*. 180: 381-392.

LeVan P, Tyvaert L, Moeller F, Gotman J. (2010) Independent component analysis reveals dynamic ictal BOLD responses in EEG-fMRI data from focal epilepsy patients. *Neuroimage* 49: 366-378.

Lloyd-Fox S, Blasi A, Elwell CE. (2010) Illuminating the developing brain: the past, present and future of functional near infrared spectroscopy (review). *Neurosci Biobehav Rev*. 34: 269-284.

Meldrum BS, Brierly JB. (1973) Prolonged epileptic seizures in primates: ischemic cell change and its relation to ictal physiological events. *Arch Neurol*. 28: 10-17.
Meldrum BS, Horton RW. (1973) Physiology of status epilepticus in primates. *Arch Neurol*. 28: 1-9.

Nguyen DK, Tremblay J, Pouliot P, Vannasing P, Florea O, Carmant L, Lepore F, Sawan M, Lesage F, Lassonde M. (2011) Non-invasive continuous EEG-fNIRS recording of temporal lobe seizures. *Epilepsy Res*. (Epub ahead of print).

Okada E, Delpy DT. (2003) Near-infrared light propagation in an adult head model. II. Effect of superficial tissue thickness on the sensitivity of the near-infrared spectroscopy signal. *Appl Opt.* 42: 2915-2922.

Quesney LF, Constain M, Rasmussen T, Olivier A, Palmini A (1992). Presurgical EEG investigation in frontal lobe epilepsy. *Epilepsy Res*. 5:55-69.

Salanova V, Morris III HH, Van Ness PC, Luders H, Dinner D, Wyllie E (1993). Comparison of scalp electroencephalogram with subdural electrocorticogram recordings and functional mapping in frontal lobe epilepsy. *Arch Neurol*. 50:294-299.

Schichiri M, Tanabe T, Hara K, Suzuki S, Wakamiya E, Tamai H. (2001) Usefulness of near-infrared spectroscopy for identification of epileptic foci in two localization-related epilepsy patients. *No To Hattatsu*. 33: 475-479.

Schwartz TH, Bonhoeffer T. (2001) In vivo optical mapping of epileptic foci and surround inhibition in ferret cerebral cortex. *Nat Med.* 7: 1063-1067.

Schwartzkroin PA, Futamachi KJ, Noebels JL, Prince DA. (1975) Transcallosal effects of a cortical epileptiform focus. *Brain Res*. 99: 59-68.

Shuhaiber H, Bolton S, Alfonso I. (2004) Cerebral regional oxygen fluctuations and decline during clinically silent focal electroencephalographic seizures in a neonate. *J Child Neurol*. 19: 539-540.

Sokol DK, Markand ON, Daly EC, Luerssen TG, Malkoff MD. (2000) Near infrared spectroscopy (NIRS) distinguishes seizure types. *Seizure.* 9: 323-327.

Steinhoff BJ, Herrendorf G, Kruth C. (1996) Ictal near infrared spectroscopy in temporal lobe epilepsy: a pilot study. *Seizure.* 5: 97-101.

Suh M, Ma H, Zhao M, Sharif S, Schwartz TH. (2006) Neurovascular coupling and oximetry during epileptic events. *Mol Neurobiol*. 33: 181-197.

Thornton RC, Rodionov R, Laufs H, Vulliemoz S, Vaudano A, Carmichael D, Cannadathu S, Guye M, McEvoy A, Lhatoo S, Bartolomei F, Chauvel F, Chauvel P, Diehl B, De Martino F, Elwes RDC, Walker MC, Duncan JS, Lemieux L. (2010) Imaging haemodynamic changes related to seizures: comparison of EEG-based general linear model, independent component analysis of fMRI and intracranial EEG. *Neuroimage* 53: 196-205.

Truccolo W, Donoghue JA, Hochberg LR, Eskandar EN, Madsen JR, Anderson WS, Brown EN, Halgren E, Cash SS. (2011) Single-neuron dynamics in human focal epilepsy. *Nat Neurosci*. 14: 635-641.

Tyvaert L, LeVan P, Dubeau F, Gotman J. (2009) Noninvasive dynamic imaging of seizures in epileptic patients. *Hum Brain Mapp.* 30: 3993-4011.

Villringer A, Planck J, Stodieck S, Boetzel K, Schleinkofer L, Dirnagl U. (1994) Noninvasive assessment of cerebral haemodynamics and tissue oxygenation during activation of brain cell function in human adults using near infrared spectroscopy. *Adv Exp Med Biol*. 345: 559-565.

Watanabe E, Maki A, Kawaguchi F, Mayanagi Y. (2000) Noninvasive cerebral blood volume measurement during seizures using multichannel near infrared spectroscopic topography. *J Biomed Opt*. 5: 287-290.

Watanabe E, Nagahori Y, Mayanagi Y. (2002) Focus diagnosis of epilepsy using near-infrared spectroscopy. *Epilepsia.* 43 (Suppl. 9): 50-55.

Wendling F, Chauvel P, Biraben A, Bartolomei F. (2010) From intracerebral EEG signals to brain connectivity: identification of epileptogenic networks in partial epilepsy. *Front. Syst. Neurosci.* 4:154. doi:10.3389/fnsys.2010.00154

Yu JM, Tyvaert L, Levan P, Zelmann R, Dubeau F, Gotman J, Kobayashi E. (2009) EEG spectral changes underlying BOLD responses contralateral to spikes in patients with focal epilepsy. *Epilepsia* 50: 1804-1809.

Zhao M, Ma H, Suh M, Schwartz TH. (2009) Spatiotemporal dynamics of perfusion and oximetry during ictal discharges in the rat neocortex. *J Neurosci*. 29: 2814-2823.

Zhao M, Suh M, Ma H, Perry C, Geneslaw A, Schwartz TH. (2007) Focal increases in perfusion and decreases in hemoglobin oxygenation precede seizure onset in spontaneous human epilepsy. *Epilepsia.* 48: 2059-2067.

Supplementary figure S1

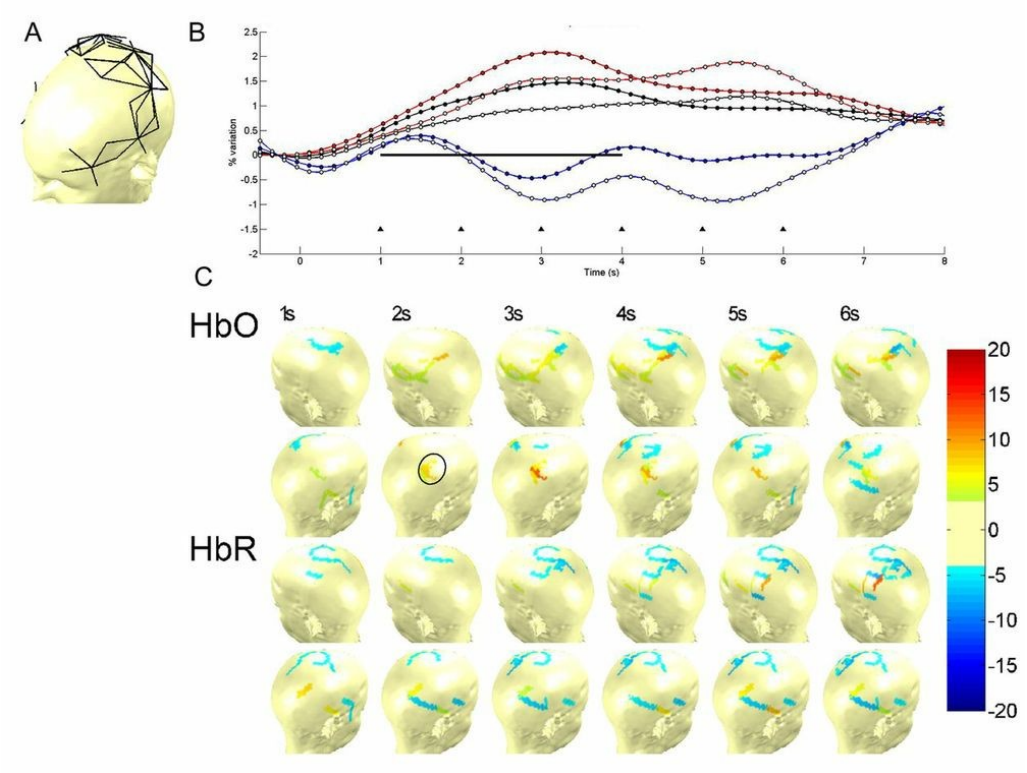


Figure S1. A) Channel configuration. B) Ictal haemodynamic variations (HbT –black, HbO –red, HbR –blue) over the epileptogenic zone (closed circles) and the contralateral homologous region (open circles). The black line indicates time of EEG evidence of seizure activity. C) Topographic uncorrected T-stats viewed at different time points (black triangles) during the course of the seizure. The epileptogenic zone is indicated by a circle.

This 13-year-old girl (patient 2) reported a brief sensation of electric shock in her left arm (typical of her seizures) during the EEG-fNIRS study. Review of the fNIRS signal showed HbO and HbT increases (and unstable HbR) during that time period. A closer look at EEG during that time-frame revealed sudden EEG de-synchronization, followed by semi-rhythmic slowing. Subsequent intracranial EEG confirmed that these brief electrical shock episodes were indeed seizures, associated with very low voltage fast-activity (underlying this sudden de-synchronization pattern on scalp EEG) from the right motor cortex.

Supplementary figure S2

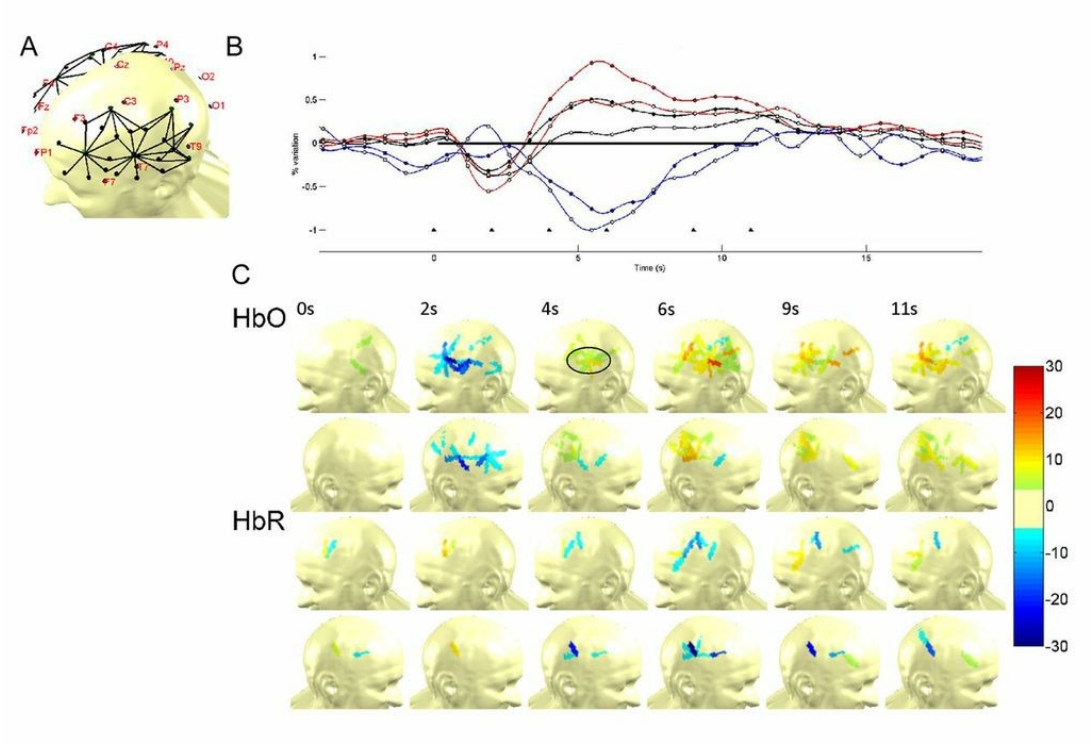


Figure S2. Second seizure identified during EEG-fNIRS recording of patient 4. Same legend as in Figure S1.

Supplementary figure S3

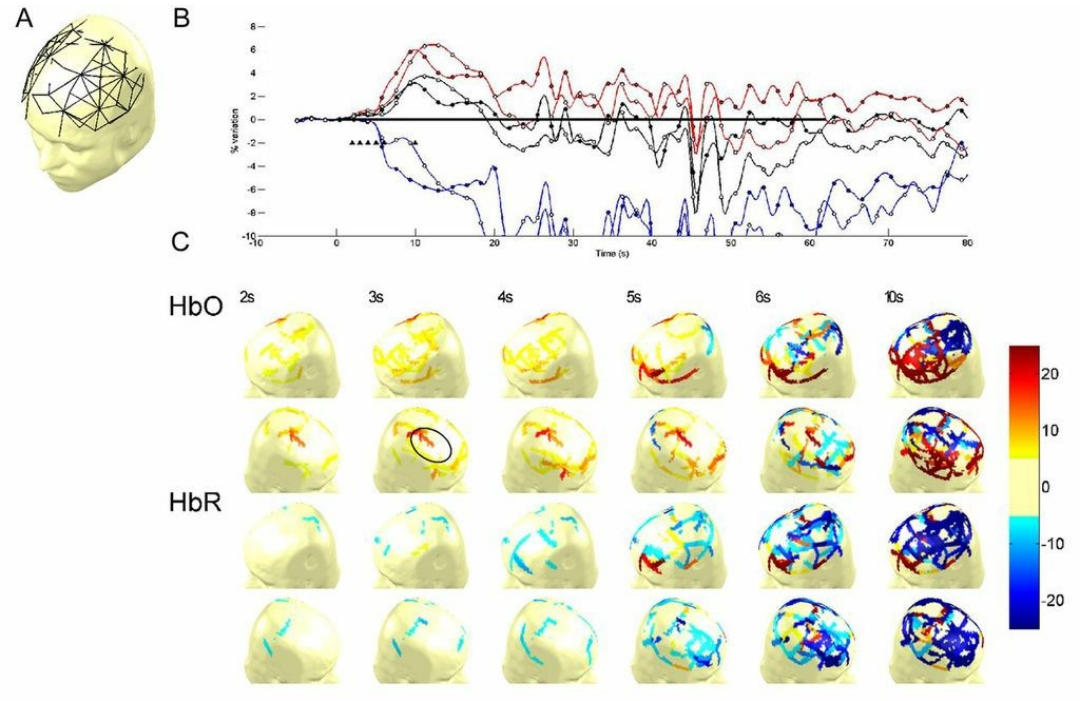


Figure S3. This 21-year-old male (patient 5), with a focus in the posterior portion of the right inferior/middle frontal gyri, experienced a gelastic seizure. Note the HbR decline during ictus. Movement artifacts can be seen on the fNIRS signal (and EEG) during seizure evolution. Same legend as in Figure S1.

Supplementary figure S4

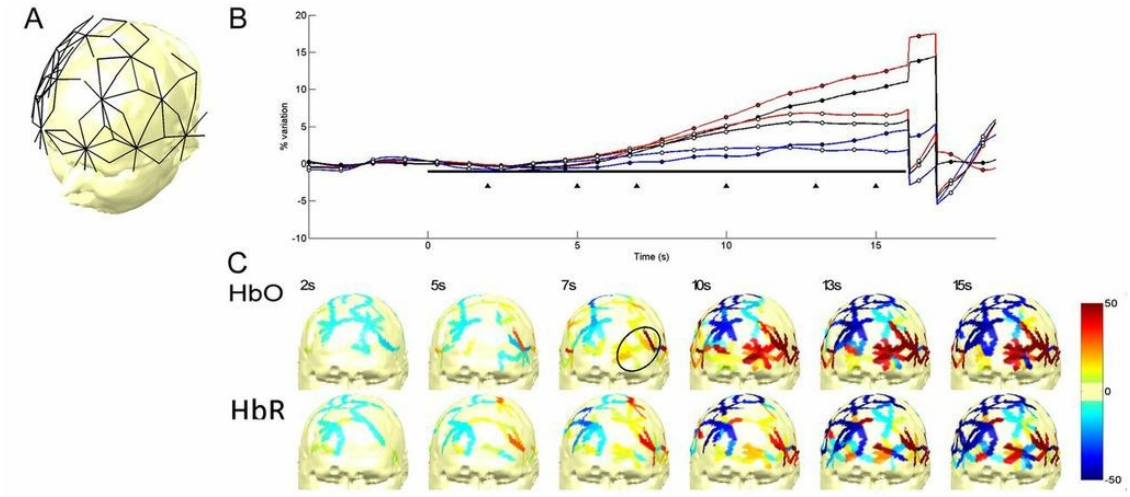


Figure S4. This 21-year-old male (patient 6) had a left medial frontal focus extending to the anterior portion of the superior frontal gyrus. Note the HbR increase despite the HbT and HbO increment during the ictus. The electrographic seizure led to an arousal responsible for the artefact at the end of recording. Same legend as in Figure S1.

Supplementary figure S5

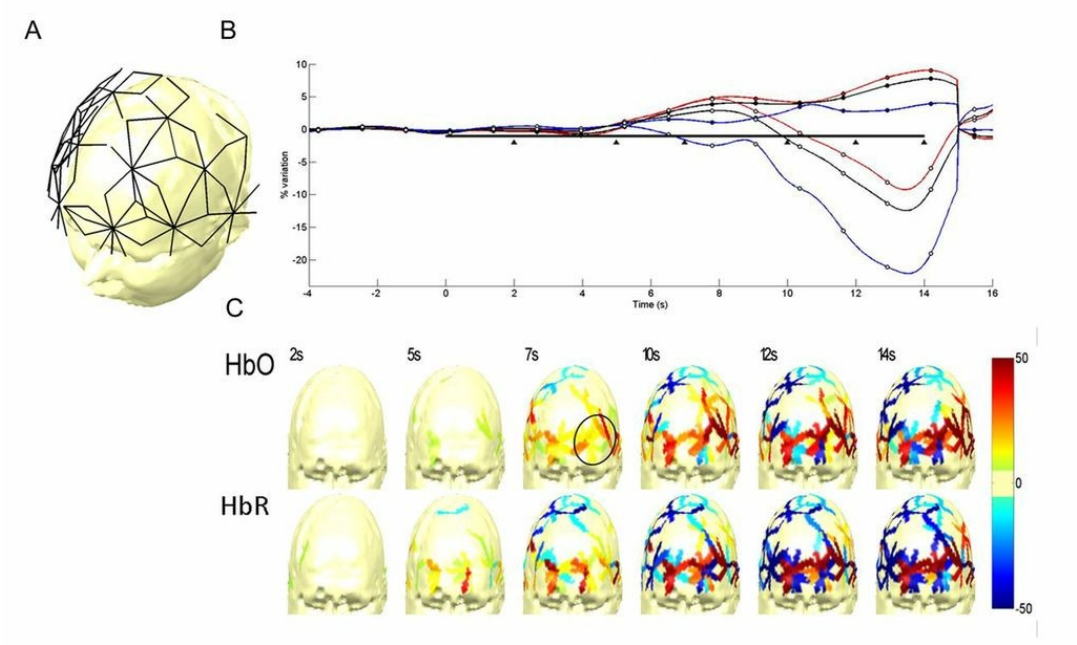


Figure S5. Second seizure recorded for patient 6. Same legend as in Figure S1.

Supplementary figure S6

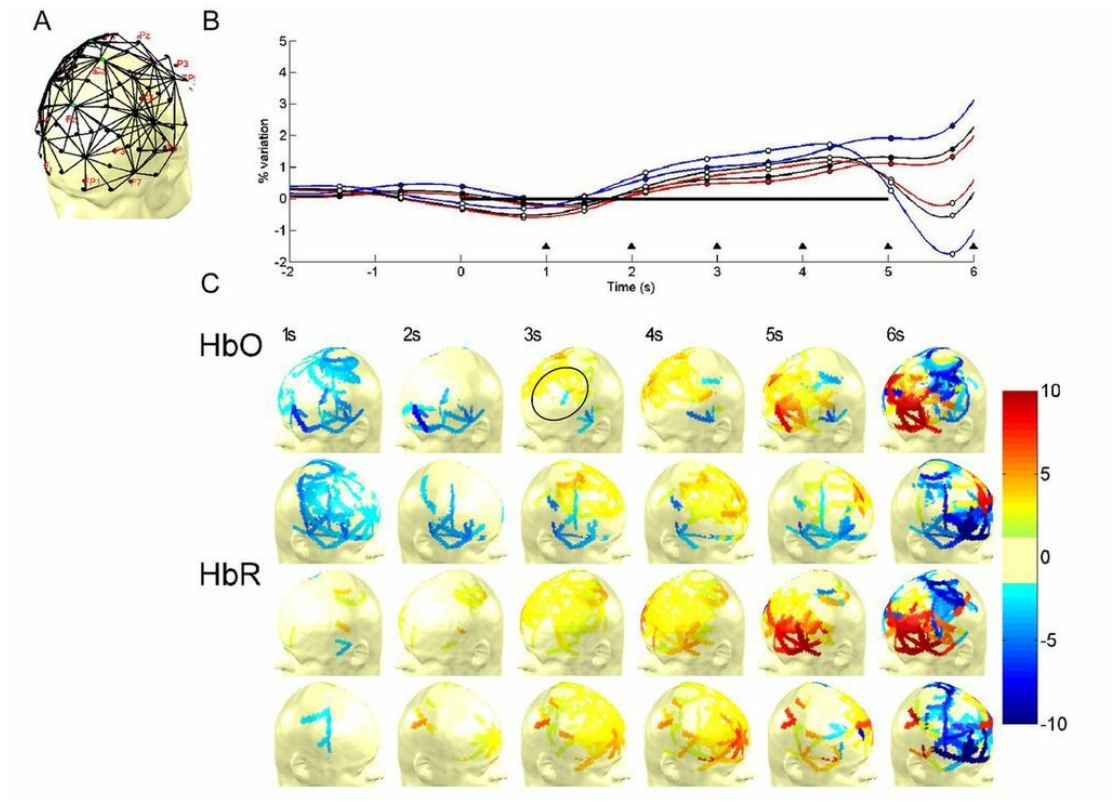


Figure S6. Second seizure recorded for patient 7. Same legend as in Figure S1.

Supplementary figure S7

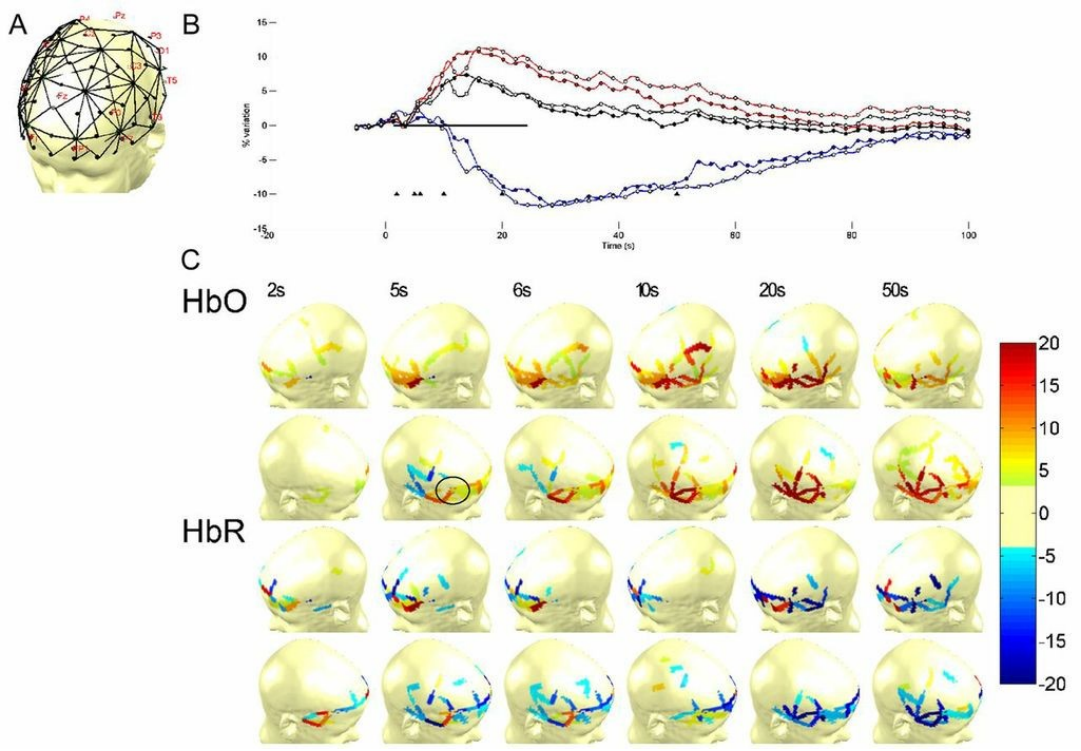


Figure S7. Second seizure recorded for patient 8. Same legend as in Figure S1.

Supplementary figure S8

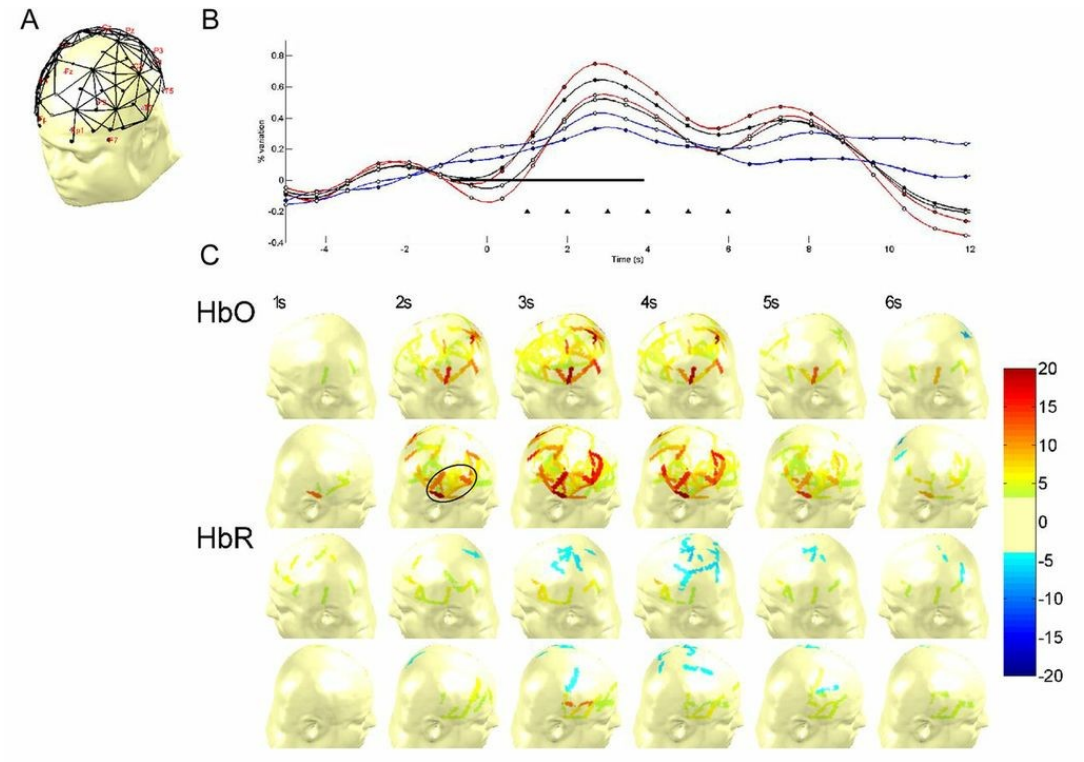


Figure S8**.** As in patient 4, this 35-year-old male (patient 9) was found to have an electrical seizure upon closer inspection of a certain EEG timeframe guided by the occurrence of fNIRS signal deflectance. Same legend as in Figure S1.

Supplementary figure S9

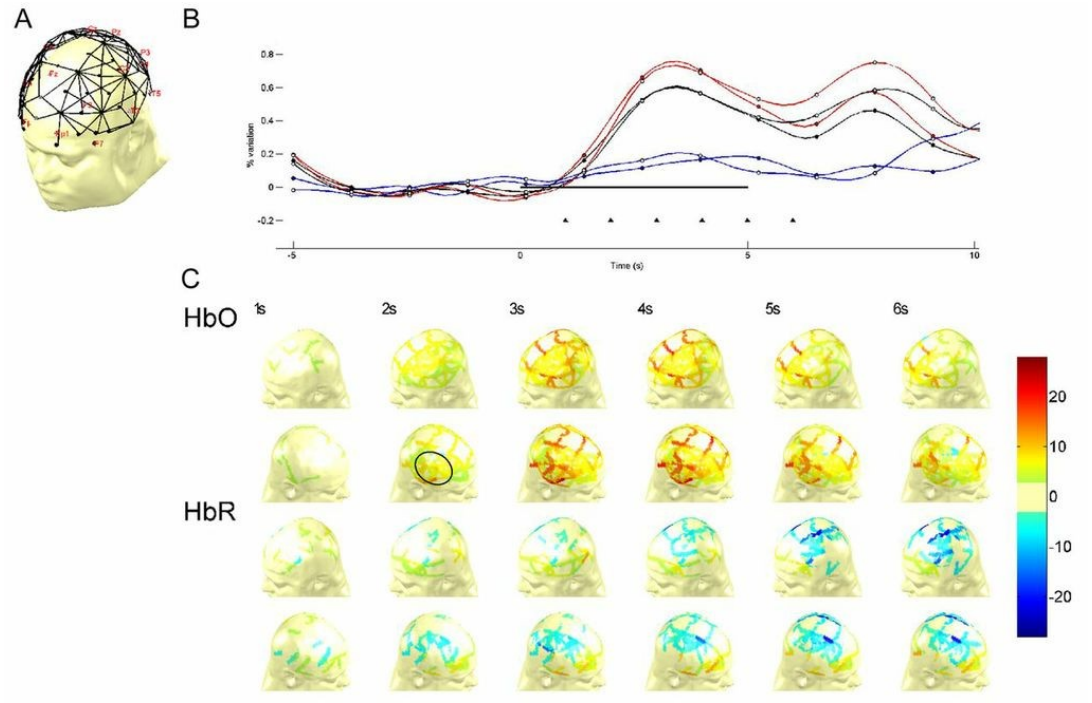


Figure S9. Second seizure recorded for patient 9. Same legend as in Figure S.

Supplementary table. Legend: Supplementary table: Results of other functional tests performed in the presurgical evaluation: single photon emission computed tomography (SPECT), positron emission tomography (PET) and neuropsychological evaluation.

| **Supplementary table** | | | |
|---|---|---|---|
| **Patient** | **Ictal SPECT** | **Interictal PET** | **Neuropsychological findings** |
| 1 | Frontopolar R>L | R Frontopolar | normal |
| 2 | R Temporo-insular | R Parietal (mild) | dyspraxic |
| 3 | R inferior frontal gyrus + multiple other sites | R Frontopolar | frontal profile |
| 4 | L Temporal | L Temporal | normal |
| 5 | R Frontal convexity | Normal | suboptical evaluation (unsustained effort) |
| 6 | Multiple sites | Normal | mild mental retardation, left profile |
| 7 | L Temporal + R orbitofrontal | Multifocal irregularities | L frontal and temporal profile |
| 8 | R inferior frontal gyrus | R Inferior frontal gyrus | frontal profile, attention deficit disorder |
| 9 | multiple sites | R Orbitofrontal (discrete) | normal |

**ARTICLE 4**

***Magnetic source imaging for presurgical evaluation of nonlesional refractory focal epilepsy***

**Submitted**:
Epilepsy Research

**Dang Khoa Nguyen[1], MD, Tania F. Tayah[1], MD, Alain Bouthillier[2], MD, Arline Bérubé[1], MD, Patrick Cossette[1], MD, PhD, Patrice Finet[1], MD, Jean-Marc Saint-Hilaire[1], MD, Manon Robert[3], MSc, Jean-Maxime Leroux[4], MSc, Christophe Grova[5,6], PhD, Maryse Lassonde[3], PhD, and Ismail S. Mohamed[7] , MD.**

[1] *Division of Neurology, Notre-Dame Hospital (CHUM), University of Montréal*
[2] *Division of Neurosurgery, Notre-Dame Hospital (CHUM), University of Montreal*
[3] *Neuropsychology and Cognition Research Center, Psychology Department, University of Montreal*
[4] *Radiology Department, Notre-Dame Hospital (CHUM), University of Montreal*
[5] *Montreal Neurological Institute, McGill University*
[6] *Biomedical Engineering Department, McGill University*
[7] *IIWK Health Center, Department of Pediatrics, Division of Neurology, Halifax*

Running title: MEG for nonlesional epilepsy

Key words: Epilepsy, Magnetoencephalography, Surgery, Nonlesional, Refractory

**ABSTRACT**

*Objective*: To report our experience with magnetoencephalography (MEG) in the presurgical evaluation of nonlesional refractory focal epilepsy (NLRFE).

*Design:* Observational case series

*Setting:* University hospital adult epilepsy center

*Participants*: 61 consecutive patients (mean age 34 years) with NLRFE (30% temporal; 70% extratemporal) underwent a MEG study.

*Results:* For the first 37 patients for whom MEG results were not included in the preoperative consensus for various reasons, MEG would have retrospectively changed the initial management in 24/37 (65%) had results been available such as reducing the number of intracranial electrodes, modifying their position, allowing for direct surgery, canceling the intracranial study or providing enough evidence to justify one. For the remaining 24 patients for whom MEG findings were available and presented during the epilepsy surgery conference after initial review of the standard presurgical work-up, MEG results modified the initial treatment plan in 15/24 (63%) cases. IcEEG recordings in 22/25 subjects showed interictal spikes and early ictal involvement at the location of MEG sources. In 19/21 (90%) subjects whose resection included the main MEG zone there was a good outcome, while 4/4 (100%) subjects whose main MEG zone was not resected had a poor outcome ($p = 0.001$).

*Conclusions:* MEG affects patient management, icEEG planning and surgical outcome in a significant percentage of patients with NLRFE.

## MANUSCRIPT

Brain surgery is recommended when medication fails and the seizures are confined to one area of the brain where tissue can be safely removed. 1 Detection of an epileptogenic lesion on a brain magnetic resonance study (MRI) substantially improves surgical outcome, since the location of the lesion is usually congruent with the epileptogenic zone (EZ). 2 Unfortunately, one-quarter of drug-resistant focal epilepsies have no identifiable lesions. 3 In these patients with nonlesional refractory focal epilepsy (NLRFE), identification of the EZ must rely heavily on the remaining available tools: scalp EEG, ictal single-photon emission computed tomography and positron emission tomography. 4 While generally useful in medial temporal lobe epilepsy, most of these tools lack adequate spatiotemporal resolution to accurately localize the EZ in neocortical epilepsy, and many will require invasive intracranial electrode studies. 5 Because chronic implantation of intracranial electrodes carries a risk of infection and hemorrhage, it is best to limit the number of electrodes without compromising the ability to localize the EZ adequately. The limitations listed above translate into a poor surgical outcome for NLRFE patients: ~51% for nonlesional temporal lobe epilepsy and ~36% for nonlesional extratemporal lobe epilepsy). 2

Magnetoencephalography (MEG) is being used with increasing frequency in the presurgical evaluation of patients with epilepsy. 6 Epileptiform discharges generate weak magnetic fields that can be recorded by using magnetic sensors in order to map the underlying neuronal generators. 7-9 In the present study, we report our experience with MEG in a large series of NLRFE patients being evaluated for epilepsy surgery.

## METHODS

### *Study context*

A MEG system was purchased and installed at our university in 2006 by a group of researchers on cognition. Benefiting from this platform, our group set up a research project to evaluate the value of MEG for patients with NLRFE. The study was approved by our institutional ethics committee, and all patients signed a consent form. For various reasons (limited funding, personnel recruitment and training, pipeline set-

up, exploration of different source analysis methods, learning curve for interpretation of results, etc.), MEG results were not included in the preoperative consensus decision until January 2010, as the acquired MEG data could not be analyzed in a timely fashion and/or were felt to still be experimental. This group of patients for whom MEG was not available for patient management will be referred to as group A. For all subsequent patients (group B), MEG findings were presented during the epilepsy surgery conference after the initial review of the standard presurgical work-up. The latter consisted in 3.0Tesla high-resolution cerebral magnetic resonance imaging, video-scalp EEG recording of seizures, ictal single photon emission computed tomography, and 18Fluroro-deoxy-glucose-positron emission tomography.

***Participants***

Between April 2006 and May 2012, 61 consecutive patients (mean age 34 years; range 8-68) with NLRFE investigated for potential epilepsy surgery were recruited for the study. Based on the standard presurgical evaluation, 18/61 (30%) were presumed to have nonlesional temporal lobe epilepsy and 43/61 (70%) nonlesional extratemporal lobe epilepsy. MR was negative in 52 subjects. Of the nine remaining subjects, three had an arachnoid cyst, two had non-specific white matter changes probably related to radiotherapy given in childhood for posterior fossa tumors, two had a non-specific millimetric T2 signal abnormality in the subinsular area, one had a prior normal MRI but now featured encephalomalacia related to a failed epilepsy surgery, and one had a Chiari type 1 malformation. None of these lesions were felt to be epileptogenic nor localizing at the time of the evaluation.

***Magnetic source imaging (MSI)***

MEG studies were generally performed while patients were admitted for long-term video-EEG monitoring as part of their presurgical evaluation. In that context, antiepileptic drugs had frequently been tapered off or dosages lowered. Furthermore, patients were in a state of mild sleep deprivation (4h) for the MEG study.

A CTF whole-head 275-sensor MEG system in a magnetically shielded room was used for the recordings (MISL, Coquitlam, BC, Canada). The total average recording time was 90 min, typically in multiple datasets, each 5 minutes in duration. EEG and MEG data were collected at a sampling rate of 600 Hz and band pass filtered at 5-

70Hz. The MEG was analyzed by an epileptologist (IM) who was experienced in MEG interpretation and only had access to a sample of the morphology of scalp-EEG recorded spikes. Interictal epileptiform discharges (IEDs) were identified by examining the MEG recordings and cross-referencing them with the simultaneous EEG recording. Source localizations of epileptic events were obtained using the single equivalent current dipole model (ECD) applied to the earliest peak of each IED with a multiple sphere conductor head model in which a single sphere was fit to the digitized head shape for each MEG sensor in each patient. IEDs were analyzed if they demonstrated a stable topography map over the rising phase of the spike and dipole fits were considered valid when the goodness of fit was >70% and with a dipole moment of 50 - 400 nAm. . ECDs were then superimposed on the co-registered patient's MRI (= MSI).

MEG datasets were classified into four categories (based on Fujimoto et al., and Funke et al.): 10-11 0) No or < 6 MEG spike sources; 1) Single cluster (≥ 6 spike sources ≤ 1 cm apart); 2) Multiple clusters; 3) Scatter (i.e. ≥ 6 spike sources > 1 cm apart).

***Assessment of MSI contribution to patient management***

To determine whether MSI influences patient management, anonymized results of the standard presurgical evaluation for all patients were presented randomly to a multidisciplinary epilepsy surgery team (blinded to MSI results). This team included three epileptologists (AB, PC, and JMSH) who had not previously been involved in the care of the patients discussed. For each patient, the presumed localization of the EZ (pTemporal, pExtratemporal) and the plan of action (A- focal resective surgery without icEEG, B- icEEG recordings, or C- rejected because considered poor surgical candidate except if new decisive information from MSI) was noted (based on De Tiège et al., 2012).37 When icEEG was planned, the electrode locations were anatomically determined and the total number of contacts calculated (for patients in group A, if there was a discrepancy between the number of icEEG contacts determined by this blinded process and the actual number of contacts used, the latter number was used). In a second step, MSI results were presented by a fourth epileptologist (DKN) who had not taken part in the decision-making process. Any changes in the initial patient plan management or changes in initial icEEG planning to

add or remove electrodes were noted. Clinical relevance of changes in patient management related to MSI findings were evaluated on a case-by-base basis for those with sufficient follow-up.

***Correlation between MSI, icEEG findings and outcome.***

We also compared MSI results in light of interictal and ictal icEEG findings on a case-by-case basis for the subset of patients who eventually underwent an icEEG study. MSI findings were considered concordant with interictal icEEG if interictal spikes were found in the same sublobar region. MSI findings were considered concordant with ictal icEEG if ictal onset electrodes were located in the same sublobar region. Surgical outcomes of patients for whom the resection included the predominance of spike dipole source estimates were compared to those for whom the resection did not use Fischer's exact test. An Engel I or II outcome was considered good, while an Engel III or IV outcome was deemed poor. 12

## RESULTS

### MSI findings

MEG showed spikes in 56/61 patients (92%) (Table 1). No MEG results were available for the five remaining patients due to a co-registration error (1), large artifacts due to dental filaments (1), or absence of spikes (3). Seven out of 56 (13%) had fewer than 6 MEG spike sources (MSI type 0), 34/56 (61%) had a single cluster (MSI type 1), 12/56 (21%) had two clusters, (MSI type 2) and 4 (7%) had scattered spike sources (MSI type 3).

***Influence of MSI results on patient management***

For group A (Table 1), MSI would have changed the initial management in 24/37 (65%) if results had been available at the time of decision-making by (a) reducing the number of icEEG contacts in 10/24 (42%); (b) increasing the number of icEEG contacts in 4/24 (17%); (c) keeping the same number of icEEG contacts but changing their position in 1/24 (4%); (d) allowing for direct surgery without prior icEEG study in 3/24 (13%); (e) providing enough evidence to justify an icEEG study in 3

previously rejected candidates (13%) or in 1 patient initially directed to surgery (4%); and (f) rejecting 2 cases previously destined for icEEG as the cluster overlaid an eloquent area (8%). For group B (Table 2), MEG results modified the initial treatment plan in 15/24 (63%) patients by (a) reducing the number of icEEG contacts in 7/15 (47%); (b) changing the position of icEEG contacts while keeping the same number of contacts as initially planned in 2/15 (13%); (c) allowing for direct surgery without prior icEEG study in 5/15 (33%); (d) providing enough evidence to justify an icEEG study in 1 previously rejected candidate (7%); and (e) rejecting a case previously destined for icEEG, as MEG showed evidence of a diffuse epileptogenic process with spikes arising from several cortical lobes.

***Clinical relevance of MSI-related changes***

For patients in group A, the actual clinical impact of not having MSI results at the time of the epilepsy surgery decision-making process was assessed in retrospect by analyzing the course of the 24 subjects mentioned above for whom MSI would have theoretically changed the team's management. For patients 3 and 11, insufficient coverage of the MEG zone led to a non-localizing icEEG study obviating any surgery. Both patients continue to have seizures despite having tried all available antiepileptic drugs and VNS therapy; unfortunately, both are reluctant to take part in a second icEEG study. For three patients (10, 36 and 37), lack of or insufficient coverage of the MEG cluster led to an unsuccessful resection misguided by a falsely localizing icEEG study. Two of these patients are reluctant to have a redo and the third is waiting for a second icEEG study. Patient 19 suffered an accidental laceration of the superior sagittal sinus during implantation of interhemispheric strips. Had MSI findings of a left posterior temporal cluster been available, this icEEG study would not have been done, as it overlaid an eloquent language area. Subject 35 presented dysphasia following implantation of electrodes, which resolved within a week. Had MSI findings been available, one wonders whether this complication would have occurred, since it would have changed our icEEG implantation scheme from 104 contacts to 80. For three more patients (5, 22 and 29) for whom MSI would have led us to reduce the number of icEEG contacts, no complications occurred from actually using a higher number of contacts. Finally, for two subjects (13 and 16) for whom direct surgery would have been decided upon if MSI results had been available at the time, no

complications occurred with the icEEG study. Of note, subject 22 still had a poor surgical outcome even though his icEEG study contained electrodes overlying the focus identified by MSI when it was eventually analyzed (Figure 1).

For group B patients, sufficient follow-up was available for 6/15 (40%) subjects for whom MSI led to a change in patient management in order to determine clinical relevance. For three subjects (1, 2 and 3), MSI findings were instrumental in guiding the insertion of depth electrodes and subdural contacts over the EZ. For three subjects (1, 2, and 20), MSI findings made it possible to reduce the number of icEEG inserted without a clear impact on outcome: the first two had an Engel I outcome and the third had no recurrence of preoperative seizures, although quality of life was not improved as he subsequently developed non-epileptic seizures. Finally, two patients who were sent directly to surgery after MSI findings pointed to a previously missed subtle cortical dysplasia also had excellent surgical outcomes. Similar to patient 22 from group A, patient 2 from group B with an adequate sampling of the epileptic focus showed widespread non-localizing icEEG changes (Figure 2).

***Correlation between MSI and icEEG findings***

Overall, 25 subjects had undergone an icEEG study at the time of manuscript submission. Correlation between MSI and icEEG findings could not be performed for 3 subjects: co-registration errors prevented MEG analysis for one subject, while the other two had no icEEG contacts overlying sources determined by MEG.

For the 22 remaining subjects, a review of the icEEG studies showed that interictal spikes were present at the location of sources identified by MEG in all subjects. However, the irritative zone defined by icEEG was generally more extended. In only two subjects were interictal spikes restricted to a few (≤ 3 contiguous contacts). For the rest, icEEG disclosed (a) larger irritative zone in the frontal (3), fronto-parietal (1), temporal (1), occipito-temporal (1) and perisylvian (1) areas; (b) a temporo-insular spiking network (4); (c) a widespread insula-inferior frontal gyrus-orbitofrontal-frontopolar-frontal medial gyrus spiking network (6); (d) bilateral synchronous supplementary motor area (SMA) spikes (found to originate from the right SMA after partial callosotomy) (1); and (e) a temporo-orbitofrontal spiking network (1).

Looking at ictal EEG patterns, electrode contacts sampling MEG-identified sources were always among those showing an early ictal pattern. As noted above, however, the ictal onset zone defined by icEEG was frequently more extended. Only nine patients had seizures associated with a focal ictal EEG pattern (≤ 3 contiguous contacts). Five patients had seizures involving several contiguous contacts at onset prompting a large resection, one patient had bilateral SMA seizure onsets that required a partial callosotomy to identify a right SMA focus, and seven patients had non-localizing (widespread) ictal onset EEG patterns despite having icEEG electrodes sampling the sources identified by MEG.

***Correlation between MSI and surgical outcome***

At the time of submission, surgery had been performed on 25 subjects (mean follow-up = 31mo): 19/21 (90%) subjects whose resection included the main MEG zone had a good outcome, while 4/4 (100%) subjects whose main MEG zone was not resected had a poor outcome ($p = 0.001$).

## COMMENTS

A number of studies have shown that MEG can contribute favorably to the localization of the epileptic focus in presurgical assessment of epilepsy surgery candidates. 8-11, 14-37 Most notably, a prospective and blinded study demonstrated that MEG provided non-redundant information that positively affected clinical decision-making and proved to be beneficial for the outcome in 33% of patients. 26 More recently, another prospective blinded study showed that MSI changed the initial management in 15/70 patients (21%). Most of these studies, however, have indiscriminately mixed patients with lesional (a subpopulation where the location of the EZ can already be fairly assumed) and nonlesional epilepsies, generally with a relatively low sample size of the latter (Table 3). Mixing lesional and nonlesional cases may result in underestimating the benefit of MEG. Our study shows, as expected, that MEG has a much higher impact in a population purely composed of NLRFE patients. In this particularly difficult set of patients, MSI would in retrospect have changed the initial management in 24/37 (65%) patients and modified it prospectively in 15/24 (63%) subjects.

Obviously, one of the most important modifications in patient management provided by MEG is the optimization of icEEG electrode placement. 44-45 No less important, however, is the way in which MEG can avoid or minimize procedural risks to patients, whether by allowing for direct surgery without prior icEEG study, reducing the number of icEEG contacts used, or excluding patients with a diffuse epileptogenic process or with an EZ in an inoperable area. In our group of patients, one of the most frequent modifications triggered by MSI was the decision that interhemispheric electrodes were no longer required. This by itself significantly reduces the duration and risk of the implantation procedure. Furthermore, the lower the number of contacts utilized, the lower the risk of edema and hemorrhage. 38

We also found that MSI can help interpret icEEG recordings. IcEEG is far from being a perfect gold standard for localization. 27, 39-41 False localization may occur even when electrodes are positioned in the proper epileptogenic lobe, because recording is generally limited to gyral regions. Furthermore, distributed or rapidly propagating epileptic activity may lead to numerous morphologically distinct epileptiform EEG discharges with maximal amplitude at variable electrode locations. This feature is even more prominent at seizure onsets when complex electrophysiological patterns can be found, often involving several distinct structures of a broad network. 5, 42-43 If more intracranial electrodes are positioned over one of these structures, it may produce a false electrographic picture with more emphasis on a small part of the network, to the detriment of the EZ farther away. This was exemplified in several cases in our series, revealing the limitations of icEEG.

It is increasingly accepted that MEG can provide clinicians with critical information regarding the location of the epileptic focus. 44 Unfortunately, clinical integration of the technique has been relatively slow. It is far from being accessible to all epilepsy centers and as yet is not reimbursed, at least in Canada. Our inability to provide reliable MSI results in a timely fashion for a number of initial subjects while our MEG program was being set up led to a set of unnecessary or complicated icEEG studies, surgical failures and redos. Taking this into consideration, it is possible that, in addition to improving surgical outcome, MEG may reduce the costs of epilepsy surgery evaluations.

In a significant number of patients with NLRFE, MSI improves the localization of the epileptic focus and affects patient management, surgical planning and outcome. We recommend that it be included in the routine presurgical work-up of such patients.

**Aknowledgments**

We confirm that we have read the Journal's position on issues involved in ethical publication and affirm that this report is consistent with these guidelines.

"Disclosure of conflicts of interest": none

## REFERENCES


1. Wiebe S, Jetté N. Epilepsy surgery utilization: who, when, where, and why? Curr Opin Neurol. 2012; 25(2): 187-93.
2. Téllez-Zenteno, JF, Hernandez Ronquillo L., Moein-Afshari F., Wiebe S. Surgical outcomes in lesional and non-lesional epilepsy: a systematic review and meta-analysis. Epilepsy Res. 2010; 89(2-3): 301-8.
3. Berg AT, Vickerey BG, Langfitt JT et al. The multicenter study of epilepsy surgery: recruitment and selection for surgery. Epilepsia. 2003; 44(11):1425-33.
4. Rosenow F, Luders H. Presurgical evaluation of epilepsy. Brain. 2001; 124:1683-1700.
5. Nguyen DK, Spencer SS. Chapter 53: Invasive EEG evaluation for epilepsy surgery. In: The Treatment of Epilepsy, 2nd edition; Shorvon S, Perucca E, Fish D, Dodson E, editors. Blackwell Publishing, 2004; 609-634.
6. Wheless JW, Castillo E, Maggio V, et al. Magnetoencephalography (MEG) and magnetic source imaging (MSI). The Neurologist 2004; 10: 138-153.
7. Papanicolaou AC. An introduction to magnetoencephalography with some applications. Brain and Cognition 1995; 27: 331-352.
8. Minassian BA, Otsubo H, Weiss S, Elliott I, Rutka JT, Carter Snead III O. Magnetoencephalographic localization in pediatric epilepsy surgery: comparison with invasive intracranial electroencephalography. Ann Neurol 1999; 46: 627-633.
9. Agirre-Arrizubieta Z, Huiskamp GJM, Ferrier CH, van Huffelen AC, Leijten FSS. Interictal magnetoencephalography and the irritative zone in the electrocorticogram. Brain 2009; 132: 3060-3071.
10. Fujimoto A, Ochi A, Imai K, et al. Magnetoencephalography using total intravenous anesthesia in pediatric patients with intractable epilepsy: lesional vs nonlesional epilepsy. Brain Dev. 2009; 31(1):34-41.
11. Funke ME, Moore K, Orrison WW Jr, Lewine JD. The role of magnetoencephalography in "nonlesional" epilepsy. Epilepsia. 2011; 52 Suppl 4:10-4.
12. Engel J Jr, Van Ness PC, Rasmussen TB, Ojemann LM. Outcome with respect to epileptic seizures. In Engel J Jr, ed. Surgical treatment of the epilepsies. New York: Raven Press, 1993: 609–21.
13. Moore KR, Funke ME, Constantino T, Katzman GL, Lewine JD. Magnetoencephalographically directed review of high-spatial-resolution surface-coil MR images improves lesion detection in patients with extratemporal epilepsy. Radiology. 2002; 225(3):880-7.

14. Stefan H, Hummel C, Scheler G, et al. Magnetic brain source imaging of focal epileptic activity: a synopsis of 455 cases. Brain. 2003; 126: 2396-405.
15. Toulouse P, Agulhon C, Taussig D, Napuri et al. Magnetoencephalographic studies of two cases of diffuse subcortical laminar heterotopia or so-called double cortex. Neuroimage. 2003; 19(4):1251-9.
16. Van 't Ent D, Manshanden I, Ossenblok P, et al. Spike cluster analysis in neocortical localization related epilepsy yields clinically significant equivalent source localization results in magnetoencephalogram (MEG). Clin Neurophysiol. 2003; 114(10):1948-62.
17. Assaf BA, Karkar KM, Laxer KD, et al. Magnetoencephalography source localization and surgical outcome in temporal lobe epilepsy. Clin Neurophysiol. 2004; 115(9):2066-76.
18. Bast T, Oezkan O, Rona S, et al. EEG and MEG source analysis of single and averaged interictal spikes reveals intrinsic epileptogenicity in focal cortical dysplasia. Epilepsia. 2004; 45(6):621-31.
19. Genow A, Hummel C, Scheler G, et al. Epilepsy surgery, resection volume and MSI localization in lesional frontal lobe epilepsy. Neuroimage. 2004; 21(1):444-9.
20. Shih JJ, Weisend MP, Lewine J, Sanders J, Dermon J, Lee R. Areas of interictal spiking are associated with metabolic dysfunction in MRI-negative temporal lobe epilepsy. Epilepsia. 2004; 45(3):223-9.
21. Pataraia E, Simos PG, Castillo EM, et al. Does magnetoencephalography add to scalp video-EEG as a diagnostic tool in epilepsy surgery? Neurology. 2004; 62(6):943-8.
22. Fischer MJ, Scheler G, Stefan H. Utilization of magnetoencephalography results to obtain favourable outcomes in epilepsy surgery. Brain. 2005; 128(Pt 1):153-7.
23. Knake S, Halgren E, Shiraishi H et al. The value of multichannel MEG and EEG in the presurgical evaluation of 70 epilepsy patients. Epilepsy Res. 2006; 69(1):80-6.
24. Ossenblok P, de Munck JC, Colon A, Drolsbach W, Boon P. Magnetoencephalography is more successful for screening and localizing frontal lobe epilepsy than electroencephalography. Epilepsia. 2007; 48(11):2139-49.
25. RamachandranNair R, Otsubo H, Shroff MM, et al. MEG predicts outcome following surgery for intractable epilepsy in children with normal or nonfocal MRI findings. Epilepsia. 2007; 48(1):149-57.
26. Sutherling WW, Mamelak AN, Thyerlei D, et al. Influence of magnetic source imaging for planning intracranial EEG in epilepsy. Neurology. 2008; 71(13):990-6.

27. Knowlton RC, Elgavish R, Howell J et al. Magnetic source imaging versus intracranial electroencephalogram in epilepsy surgery: a prospective study. Ann Neurol. 2006; 59(5):835-42.
28. Knowlton RC, Elgavish RA, Bartolucci A, et al. Functional imaging: II. Prediction of epilepsy surgery outcome. Ann Neurol. 2008; 64(1):35-41.
29. Knowlton RC, Elgavish RA, Limdi N, et al. Functional imaging: I. Relative predictive value of intracranial electroencephalography. Ann Neurol. 2008; 64(1):25-34.
30. Knowlton RC, Razdan SN, Limdi N, et al. Effect of epilepsy magnetic source imaging on intracranial electrode placement. Ann Neurol. 2009; 65(6):716-23.
31. Chang EF, Nagarajan SS, Mantle M, Barbaro NM, Kirsch HE. Magnetic source imaging for the surgical evaluation of electroencephalography-confirmed secondary bilateral synchrony in intractable epilepsy. J Neurosurg. 2009; 111(6):1248-56.
32. Tanaka N, Hamalainen MS, Ahlfors SP, et al. Propagation of epileptic spikes reconstructed from spatiotemporal magnetoencephalographic and electroencephalographic source analysis. Neuroimage 2010; 50: 217-222.
33. Shiraishi H, Ahlfors SP, Stufflebeam SM, et al. Comparison of three methods for localizing interictal epileptiform discharges with magnetoencephalography. J Clin Neurophysiol. 2011; 28(5):431-40.
34. Zhang R, Wu T, Wang Y, et al. Interictal magnetoencephalographic findings related with surgical outcomes in lesional and nonlesional neocortical epilepsy. Seizure. 2011; 20(9):692-700.
35. Stefan H, Wu X, Buchfelder M, et al. MEG in frontal lobe epilepsies: localization and postoperative outcome. Epilepsia. 2011;52(12):2233-8.
36. Wu X, Rampp S, Weigel D, Kasper B, Zhou D, Stefan H. The correlation between ictal semiology and magnetoencephalographic localization in frontal lobe epilepsy. Epilepsy Behav. 2011; 22(3):587-91.
37. De Tiège X, Carrette E, Legros B, et al. Clinical added value of magnetic source imaging in the presurgical evaluation of refractory focal epilepsy. J Neurol Neurosurg Psychiatry. 2012; 83(4):417-23.
38. Hamer HM, Morris HH, Mascha EJ, et al. Complications of invasive video-EEG monitoring with subdural grid electrodes. Neurology. 2002: 58(1):97-103.
39. Wennberg RA. Poor surgical outcome in patients with neocortical epilepsy is correlated with interictal epileptiform abnormalities outside the area of surgical resection. Epilepsia. 2000; 41(3):355-7.

40. Wennberg R. Is intracranial monitoring dispensable for neocortical epilepsy with normal magnetic resonance imaging? Ann Neurol. 2005; 58(5):814; author reply 814-5.
41. Wennberg R. Magnetic source imaging versus intracranial electroencephalogram: Neocortical versus temporolimbic epilepsy surgery. Ann Neurol. 2006; 60(2):271.
42. Bartolomei F, Chauvel P, Wendling F. Epileptogenicity of brain structures in human temporal lobe epilepsy: a quantified study from intracerebral EEG. Brain. 2008; 131(Pt 7):1818-30.
43. Jenssen S, Roberts CM, Gracely EJ, Dlugos DJ, Sperling MR. Focal seizure propagation in the intracranial EEG. Epilepsy Res. 2011; 93(1):25-32.
44. Bagic A, Funke ME, Ebersole J; ACMEGS Position Statement Committee. American Clinical MEG Society (ACMEGS) position statement: the value of magnetoencephalography (MEG)/magnetic source imaging (MSI) in noninvasive presurgical evaluation of patients with medically intractable localization-related epilepsy. J Clin Neurophysiol. 2009; 26(4):290-3.

Table 1. Theoretical influence of MSI if results had been available at the time of the epilepsy surgery process (group A).

**Group A: MSI results not available at time of decision on treatment plan**

| No | Age | Presumed focus | Plan (no MSI) | icEEG findings | | Surgery | Engel | MSI results | MSI type |
|---|---|---|---|---|---|---|---|---|---|
| | | | | interictal | ictal | | | | |
| 1 | 27 | TLE | B (78) | R lat T, R mesial T, R aINS | same | R ATL + aINS | I | One dipole R STG, one in R sylvian fissure | 0 |
| 2 | 49 | TLE | A (R ATL) | NA | | R ATL | I | R mesial T | 1 |
| 3 | 27 | ETLE | B (70) | R mesial T > R orbitoF, R mesial F | Non-localizing | No surgery | NA | R inferior and basal T | 1 |
| 4 | 48 | ETLE | B (140) | Extensive L mesial F and SFG | Non-localizing | L F (SFG, MFG, SMA, FMG) | IV | Co-registration errors | 0 |
| 5 | 13 | ETLE | B (104) | R PMA, M1, S1 | same | R F (PMA) + MST M1-S1) | I | Upper R SM strip | 1 |
| 6 | 15 | ETLE | B (96) | R precuneus-sup O/ R lingual-post parahip gyri | same | R O | I | R TO junction | 1 |
| 7 | 27 | ETLE | B (68) | Declined | | NA | NA | L SFG-MFG (pointed to a subtle CD after MR re-inspection) | 1 |

| | | | | | | | | | |
|---|---|---|---|---|---|---|---|---|---|
| 8 | 28 | TLE | B (106) | Declined | | NA | NA | L TP junction | 1 |
| 9 | 47 | biTLE L>R | B (92) | biTLE L>R + biO L>R | same | No surgery | NA | R mesial T | 1 |
| 10 | 45 | ETLE | B (112) | R Fpolar, R ant medial FG, R IFG, R SFG | Non-localizing, R Fpolar? | R Fpolar | III | R IFG cluster | 1 |
| 11 | 20 | ETLE | B (69) | R IFG > R MFG, R mesial T, R medial FG | Non-localizing | No surgery | NA | R PO junction | 1 |
| 12 | 42 | TLE | A (R ATL) | NA | | NA (moved) | NA | bilat neocortical T | 2 |
| 13 | 33 | TLE | B (84) | L mesial T > L aINS | L mesial T | L SAH | I | L medial T | 1 |
| 14 | 21 | ETLE | B (104) | Declined by patient; fear of hemianopia | | NA | NA | R O | 1 |
| 15 | 42 | ETLE | B (116) | L SFG, L MFG | Non-localizing | L F (SFG, MFG) | I | L SFG + MFG scatter | 3 |
| 16 | 19 | TLE | B (98) | R mesial T > R aINS, R lat T | R mesial T | R ATL | I | R medial T | 1 |
| 17 | 39 | TLE | B (122) | L lat T, L IFG, aINS | same | R aINS, T1, T2 | IV | lat T + PT junction scatter | 3 |
| 18 | 53 | ETLE | B (82) | SE while waiting for icEEG; then evolved to RE | | Biopsy | NA | L pINS cluster | 1 |
| 19 | 24 | ETLE | B (130) | Implantation interrupted by laceration of SSS | | Repair of laceration; no epilepsy surgery | NA | L PTO junction cluster | 1 |
| 20 | 32 | biTLE L>R | B (108) | L>R mesial T > bilat aINS, bilat lat T | L>R mesial T | L ATL | I | L mesial T > R mesial T | 2 |

| | | | | | | | | | |
|---|---|---|---|---|---|---|---|---|---|
| 21 | 32 | ETLE | B (94) | Postponed for personal reasons | | NA | NA | Very few spikes over L P | 0 |
| 22 | 21 | ETLE | B (130) | R Fpolar, R IFG, R orbitoF, R medial FG, R aCG | Non-localizing, max build-up max R Fpolar? | R Fpolar | IV | R IFG cluster | 1 |
| 23 | 27 | TLE | C | NA | | NA | NA | Bilat mesial T | 2 |
| 24 | 24 | ETLE | C | NA | | NA | NA | Few spikes, mirror foci over bil central regions | 0 |
| 25 | 50 | TLE | A | NA | | L ATL | I | L medial T | 1 |
| 26 | 38 | ETLE | C | NA | | NA | NA | No spikes | 0 |
| 27 | 56 | ETLE | B (184) | Cancelled for psychosis | | NA | NA | R MFG cluster | 1 |
| 28 | 24 | ETLE | B (160) | Cancelled (drug problems) | | NA | NA | R IFG cluster | 1 |
| 29 | 46 | ETLE | B (132) | R SFG, R MFG | same | L F (SFG, MFG) | I | L SFG, MGF | 1 |
| 30 | 56 | TLE | B (102) | Cancelled (re significant sz reduction with Rx) | | NA | NA | L post ITG and MTG | 1 |
| 31 | 30 | ETLE | B (118) | Unplanned pregnancy | | NA | NA | bilat mesial T, R INS cluster | 2 |

| | | | | | | | | | |
|---|---|---|---|---|---|---|---|---|---|
| 32 | 52 | biETLE | C | | NA | NA | NA | R MTG-ITG cluster, L T scatters | 2 |
| 33 | 68 | biTLE L>R | C | | NA | NA | NA | L T mesial and lat | 1 |
| 34 | 44 | ETLE | B (96) | L pINS | same | L pINS, GKS INS | I | L pINS cluster + L mesial T | 1 |
| 35 | 43 | ETLE | B (104) | L INS > L IFG, L orbitoF, L medial FG | L INS | GKS pINS | II | L pINS cluster | 1 |
| 36 | 50 | ETLE | B (122) | L Fpolar-orbitoF> L lat T, L mesial T | Non-localizing, max build-up in L lat T? | L T (T1, T2, T3) | IV | R Fpolar-orbitoF cluster, some mesioT and INS | 1 + 3 |
| 37 | 15 | ETLE | B (92) | Extensive L SFG, L medial FG | Non-localizing, max build-up in L SFG? | L F (F1, mFG, aCC) | IV | L mesioP | 2 |

MSI = magnetic source imaging; icEEG = intracranial electroencephalography; ECoG = intraoperative electrocorticography; MR = magnetic resonance imaging
TLE = temporal lobe epilepsy; ETLE = extratemporal lobe epilepsy
A = direct surgery without icEEG; B (x) = intracranial EEG (number of contacts planned); C = rejected (other drug trials or VNS)
ATL = anterior temporal lobectomy; MST = multiple subpial transection
F = frontal; T = temporal; P = parietal; O = occipital; aINS = anterior insula; pINS = posterior insula;
SFG = superior frontal gyrus; IFG = inferior frontal gyrus; MFG = middle frontal gyrus; medial FG = medial frontal gyrus;
SMA = supplementary motor area; SM = sensorimotor area; aCG = anterior cingulate gyrus
STG = superior temporal gyrus; MTG = middle temporal gyrus; ITG = inferior temporal gyrus; IPL = inferior parietal lobule
NA = not applicable
R = right; L = left; Max = maximum; Bilat = bilateral; MEG = Magnetoencephalography

**Table 1 Cont'd: Change in treatment plan if MSI results had been available**

| | | Clinical relevance |
|---|---|---|
| **Y/N** | **Description** | |
| N | NA | - |
| N | NA | - |
| Y | B (70) → B (80); (interhemispheric strips and 1 F dorsolateral strip removed; 4 T strips and 3 T depths added) | Insufficient coverage of neglected area led to unsuccessful icEEG study; no surgery |
| N | NA | - |
| Y | B (104) → B (76) | No complications from increased number of icEEG contacts used |
| N | NA | - |
| Y | B → A (ECoG) (direct surgery) | NA (surgery currently on hold due to unexpected pregnancy) |
| Y | B → C (eloquent cortex) | NA (thankfully, patient had declined icEEG and chosen VNS which led to sz-freedom) |

| | | |
|---|---|---|
| N | NA | - |
| Y | B (112) → B (80) (interhemispheric and L F strips removed; 2 INS depths added) | Insufficient coverage of MEG zone led to failed surgery |
| Y | B (69) → B (124) (medial and lateral P strips added) | No sampling of MEG zone led to unsuccessful icEEG study; no surgery |
| Y | A (R ATL) → B (80) | NA (moved) |
| Y | B → A | No complications from icEEG study |
| N | NA | - |
| N | NA | - |
| Y | B → A (R ATL) | No complications from icEEG study |
| N | NA | - |
| Y | B (82) → B (82) (change of grid position, 2 strips removed, 3 depths added) | NA (immunotherapy preferred) |
| Y | B → C (eloquent cortex) | IcEEG study led to hemorrhagic complications |
| N | NA | - |
| N | NA | - |

| | | |
|---|---|---|
| Y | B (130) → B (102) (interhemispheric and orbitoF strips removed; grid positioned lowered) | No complication from higher number of icEEG contacts; IcEEG not localizing despite adequate coverage; 1st epilepsy surgery failed; 2nd surgery successful with resection of MEG zone |
| Y | C → B (88) | NA (icEEG recently proposed, accepted and pending) |
| Y | C → B (96) | NA (icEEG declined; preferred VNS) |
| N | NA | - |
| N | NA | - |
| Y | B (184) → B (108) | NA (icEEG cancelled due to psychosis) |
| Y | B (160) → B (76) | NA (icEEG cancelled) |
| Y | B (132) → B (80) (F and T strips + INS depths removed) | No complications from higher number of icEEG contacts |
| Y | B (102) → B (68) (interhemispheric and orbitoF strips removed) | NA (icEEG cancelled) |
| Y | B (118) → B (148) (interhemispheric strips removed; 3 T depths and 6 T strips added | NA (icEEG postponed) |
| Y | C → B (80) | NA (icEEG declined) |

| | | |
|---|---|---|
| N | NA | - |
| Y | B (96) → B (94) (interhemispheric and P strips removed; 5 T strips added) | None |
| Y | B (104) → B (80) (interhemispheric contacts removed, change of grid position) | Transient dysphasia possibly due to higher number of icEEG contacts |
| Y | B (122) → B (144) | Insufficient coverage of MEG zone led to failed surgery |
| Y | B (92) → B (84) (removal of orbitoF strips; position of grid and interhemispheric strips changed) | Insufficient coverage of MEG zone led to failed surgery |

Table 2. Influence of MSI on patient surgical management in group B patients.

**Table 2: Group B: MSI results available at time of decision on treatment plan**

| No | Age | Presumed focus | Plan (no MSI) | MSI results | MSI type | Change in treatment plan post-MSI results | |
|---|---|---|---|---|---|---|---|
| | | | | | | Y/N | Description |
| 1 | 26 | ETLE | B (138) | R orbitoF operculum-hymen INS cluster | 1 | Y | B (138) → B (122) (interhemispheric strips and 2 dorsolat strips removed; 1 INS depth added; 1 orbitoF strip added; |
| 2 | 35 | ETLE | B (92) | R IFG-aINS cluster | 1 | Y | B (92) → B (84) (interhemispheric strips removed, 3 depths added, grid position changed) |
| 3 | 35 | ETLE | B (114) | R F operculum-aINS cluster | 1 | Y | B (114) → B (114) (helped to position depth electrodes in aINS) |
| 4 | 28 | ETLE | B (138) | R and L mesial T | 3 | Y | B (138) → B (118) (interhemispheric strips removed) |
| 5 | 19 | ETLE | B (112) | medial FG L>R | 2 | N | NA |
| 6 | 17 | ETLE | B (138) | No spikes | 0 | N | NA |

| | | | | | | | |
|---|---|---|---|---|---|---|---|
| 7 | 14 | ETLE | B (62) | R Fpolar cluster, R PO junction cluster + scatters (pINS, STG, IPL) | 2 + 3 | Y | B → C |
| 8 | 20 | TLE | C (biTLE with no predominance) | few spikes; L T neocortex | 0 | Y | C → B (126) |
| 9 | 31 | TLE | B (86) | L mesial and ant lateral T | 1 | Y | B → A (L ATL) |
| 10 | 54 | ETLE | B (104) | Uninterpretable (magnetic artefact) | 0 | N | NA |
| 11 | 20 | ETLE | B (106) | few spikes; R postcentral gyrus | 0 | Y | B (106) → B (88) |
| 12 | 20 | TLE | C (biTLE with no predominance) | L mesial T and R INS cluster | 2 | N | NA |
| 13 | 32 | TLE | C (biTLE with no predominance) | R and L mesial T | 2 | N | NA |
| 14 | 56 | ETLE | B (104) | L ITG-MTG cluster + few medial T | 1 | N | NA |
| 15 | 46 | TLE | A (L ATL) | few spikes; L mesial T | 0 | N | NA |
| 16 | 25 | ETLE | B (94) | few spikes; L orbitoF | 0 | Y | B (94) → B (78) (removal of interhemispheric contacts but additional coverage of orbitoF area) |
| 17 | 42 | ETLE | C (multifocal) | R MTG, INS, IFG, STG scatter | 3 | N | NA |

| | | | | | | | |
|---|---|---|---|---|---|---|---|
| 18 | 13 | ETLE | B (92) | R IFG cluster (pointed to a subtle CD after MR re-inspection) | 1 | Y | B → A |
| 19 | 34 | ETLE | B (100) | R central sulcus cluster (pointed to a subtle CD after MR re-inspection) | 1 | Y | B → A (ECoG) |
| 20 | 43 | ETLE | B (112) | L precentral gyrus cluster | 1 | Y | B (112) → B (104) (INS depths removed) |
| 21 | 11 | ETLE | B (102) | R Fpolar cluster (pointed to a subtle CD after MR re-inspection) | 1 | Y | B → A (ECoG) |
| 22 | 46 | ETLE | B (130) | L pINS-STG cluster + 2 dipoles in MTG | 2 | Y | B (130) → B (112) (removal of P strips) |
| 23 | 31 | ETLE | B (104) | No spikes | 0 | N | B (104) |
| 24 | 8 | ETLE | B (104) | R pINS (pointed to a subtle CD after MR re-inspection) | 1 | Y | B → A |

Same legend as Table 1

* free of habitual preop seizures but developed disabling nonepileptic seizures

Y = yes; N = no; CD = cortical dysplasia; ECoG = intraoperative electrocorticography

**Table 2 Cont'd: Group B: MSI results available at time of decision on treatment plan**

| icEEG | | Surgery | Engel | Clinical relevance |
|---|---|---|---|---|
| **interictal** | **Ictal** | | | |
| R orbitoF operculum-hymen INS junction | same | R F (orbitoF) + aINS | I | MSI reduced number of icEEG contacts and improved icEEG coverage |
| R IFG > R orbitoF, R medial FG/SMA | Non-localizing, max build-up IFG? | R F (IFG) + aINS | I | MSI reduced number of icEEG contacts and improved icEEG coverage |
| L F operculum-aINS> L IFG, L orbitoF, L medial FG | Non-localizing | L aINS | I | MSI improved icEEG coverage |
| Cancelled; significant sz reduction with Rx | | NA | NA | NA |
| bil medial FG; R medial FG (SMA) post-callosotomy | same | R F (SMA) | I | - |
| Cancelled; sz-free with change in Rx | | NA | NA | - |

| | | | | |
|---|---|---|---|---|
| | NA | Biopsy to r/o Rasmussen | NA | NA (immunotherapy preferred) |
| | Pending | NA | NA | NA |
| | Pending | NA | NA | NA (surgery pending) |
| | Pending | NA | NA | - |
| | Pending | NA | NA | NA (icEEG pending) |
| | NA | NA | NA | - |
| | NA | NA | NA | - |
| L medial T, basal T, IFG, T operculum | same | R ATL, IFG | I | - |
| | NA | Pending | NA | - |
| | Pending | NA | NA | NA (icEEG pending) |
| | NA | NA | NA | - |

| | | | | |
|---|---|---|---|---|
| | NA | RF (IFG) | I | Prevented an icEEG; allowed for direct surgery |
| | NA | Pending | NA | NA (surgery pending) |
| L PMC/M1, L IPL > L lat T | L PMC/M1 | L premotor corticectomy | IV* | MSI reduced the number of icEEG contacts |
| | NA | R frontopolar corticectomy | I | Prevented an icEEG; allowed for direct surgery |
| | Pending | NA | NA | NA (icEEG pending) |
| | Pending | NA | NA | NA (icEEG pending) |
| | NA | Pending | NA | NA (surgery pending) |

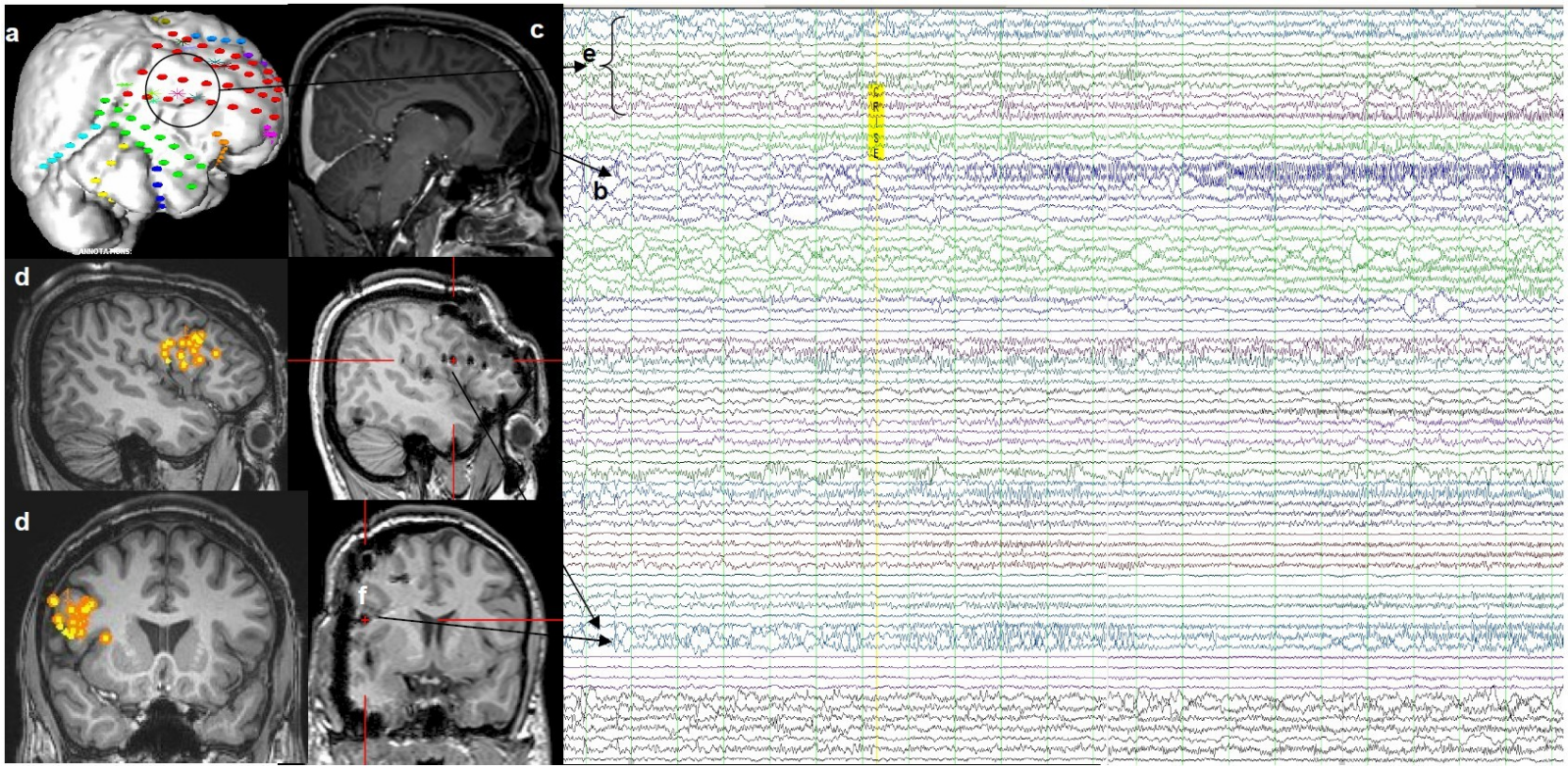


Figure 1.IcEEG study (a) showing ictal low-voltage fast activity (LVFA) over several contacts maximum over the R frontopolar region (b) which was resected (c) to no avail. MEG acquired preoperatively but only analyzed postoperatively show a cluster over the R inferior frontal gyrus (d), an area initially sampled (circle) by contacts revealed ictal LVFA but not necessarily earlier than other contacts or with higher amplitude or maximal buildup (e).

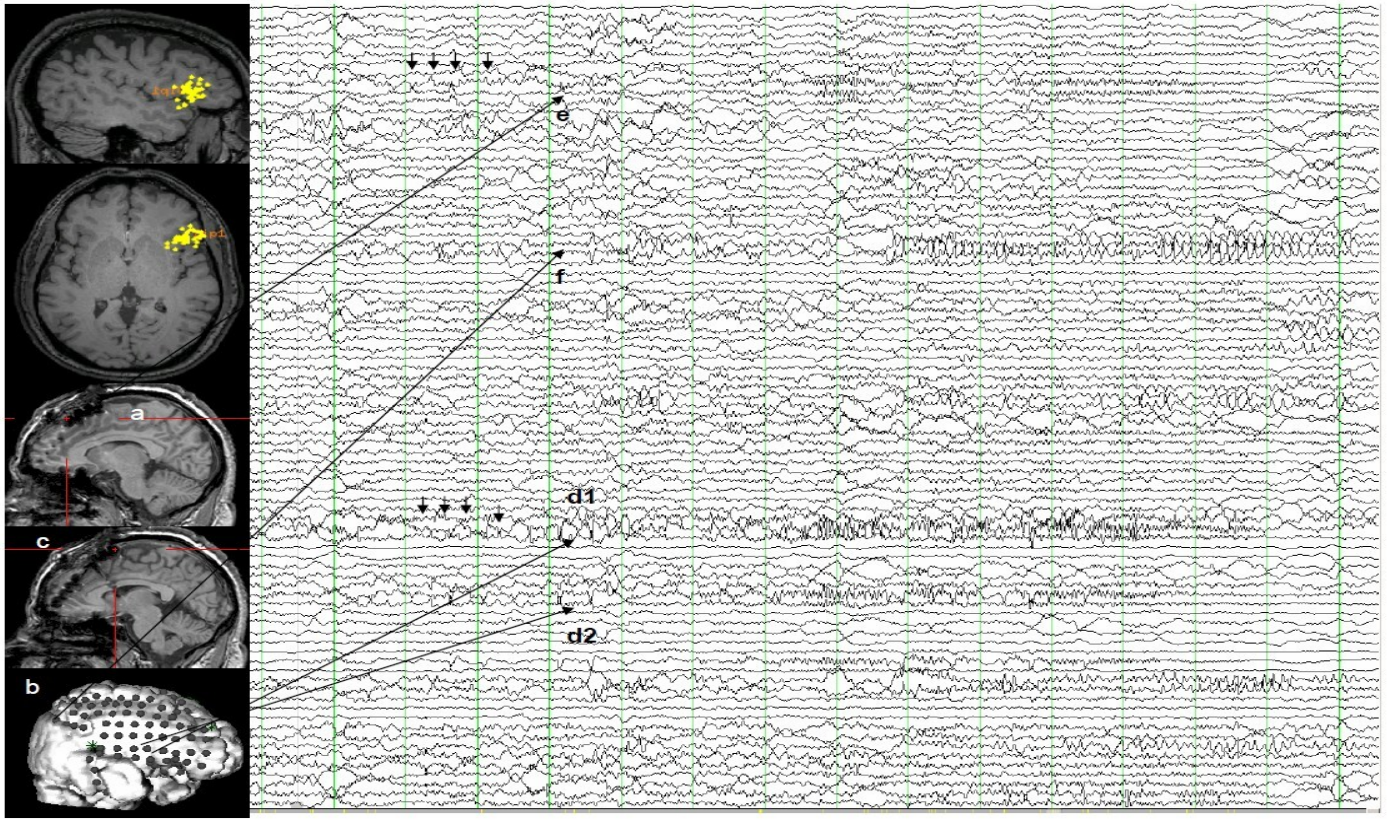


Figure 2. 35yo man with mild convexity atrophy (a) but discordant R inferior frontal gyrus (IFG) MEG cluster. Extensive IcEEG sampling (b) revealed interictal spikes noted concomitantly over the IFG and the supplementary motor area (SMA) (small arrows) and a poorly localizing ictal pattern with maximum buildup over the IFG (d1, d2), the SMA (e) and the superior parietal lobule (f). Resection of the MEG zone led to seizure freedom.

Table 3: Summary of nonlesional cases of refractory focal epilepsy analyzed by MEG reported in the literature.

| Reference | Design | Mean age (range) | Total | NL[1] | Subtle | NS | POESC | TLE/mTLE/nTLE/ ETLE[2] |
|---|---|---|---|---|---|---|---|---|
| Minassian et al., 1999 | Retrospective | 13 (5.5-16) | 11 | 9 | 0 | 1 | 1 | 0/0/0/10 |
| Moore et al., 2002 | Retrospective | 27.4 (10-45) | 20 | 8 | 0 | 1 | 0 | 1/0/1/8 |
| Stefan et al., 2003 | Retrospective | 34 (7-79) | 455 | NM | NM | NM | NM | NM |
| Toulouse et al., 2003 | Retrospective | 13.5 (7-20) | 2 | 0 | 0 | 0 | 0 | 0/0/0/0 |
| Van 't Ent et al., 2003 | Retrospective | 30.2 (21-39) | 4 | 1 | 0 | 0 | 0 | 0/0/0/1 |
| Assaf et al., 2004 | Prospective | NM | 26 | 2 | 0 | 0 | 0 | 2/0/2/2 |
| Bast et al., 2004 | Retrospective | 11.5 (3.5-15.9) | 9 | 0 | 0 | 0 | 0 | 0/0/0/0 |
| Genow et al., 2004 | Retrospective | 23.8 (19-32) | 4 | 0 | 0 | 0 | 0 | 0/0/0/0 |
| Shih et al., 2004 | Prospective | 30 (16-56) | 20 | 20 | 0 | 0 | 0 | 20/10/10/0 |
| Pataraia et al., 2004[3] | Retrospective | 25.3 (1.2-54) | 82 | NM[7] | NM | NM | NM | NM |
| Fischer et al., 2005 | Retrospective | 33.6 (18-60) | 33 | NM | NM | NM | NM | NM |
| Knake et al., 2006 | Prospective | 29.5 (9-56) | 70 | ≥12 | NM | NM | NM | ≥1/0/0/≥3 |
| Ossenblok et al., 2007 | Retrospective | 29 (7-59) | 24 | 1 | 0 | 0 | 0 | 0/0/0/1 |
| RamachandranNair et al., 2007 | Retrospective | 11.7 (4-18) | 24 | 14 | 8 | 2 | 0 | 0/0/0/22 |
| Sutherling et al., 2008 | Prospective | 38 (8-66) | 69 | NM | NM | NM | NM | NM |
| Knowlton et al., 2006; 2008a; 2008b; 2009[4] | Prospective | 27 (1-62) | 77 | ≥31[4] | ≥12[4] | NM[4] | NM[4] | ≥24/≥19/≥5/≥17[4] |
| Fujimoto et al., 2009 | Retrospective | 6.6 (3-14) | 28 | 10 | 0 | 0 | 0 | ≥1/?/?/≥3 |
| Chang et al., 2009 | Retrospective | 19.4 (3.5-45.1) | 16 | 7 | 0 | 0 | 0 | 1/0/1/6 |
| Agirre-Arrizubieta et al., 2009 | Retrospective | 30.2 (9-45) | 38 | 6 | 0 | 0 | 1 | 3/?/?/3 |
| Tanaka et al., 2010 | Retrospective | 14 (9-20) | 10 | 6 | 0 | 0 | 0 | 5/?/?/1 |
| Funke et al., 2011 | Retrospective | NM (3-54) | 40 | 17 | 0 | 0 | 8 | ?/0/nTLE+ETLE =17 |

| | | | | | | | | |
|---|---|---|---|---|---|---|---|---|
| Shiraishi et al., 2011 | Retrospective | 8.9 (3-15) | 14 | 5 | 0 | 0 | 0 | 0/0/0/5 |
| Zhang et al., 2011 | Retrospective | 19.9 (2-26) | 43 | 20 | 0 | 0 | 0 | 0/0/0/20 |
| Stefan et al., 2011 | Retrospective | 43.4 (37-54) | 39 | 5 | 0 | 0 | 0 | 0/0/0/5 |
| Wu et al., 2011 | Retrospective | 29.4 (20-43) | 7 | NM | NM | NM | NM | NM |
| De Tiège et al 2012 | Prospective | 31.5 (3-63) | 70 | 20 | 0 | 0 | 3 | 6/1/0/16 |
| Schneider et al., 2012 | Retrospective | 28.5 (6-54) | 18 | 18 | 0 | 0 | 0 | 6/4/2/12 |

Total = total number of subjects in the study; NL = nonlesional; Subtle = subtle MR changes indicative of possible underlying epileptogenic lesion; NS = Non-specific (white matter changes, diffuse atrophy, periventricular malacia, lesions not expected to give epilepsy or probably unrelated to epileptic condition); POESC = postoperative epilepsy surgery changes (patients with macroscopic resection of initially identified epileptogenic lesion); TLE = temporal lobe epilepsy; mTLE = mesial temporal lobe epilepsy; nTLE = neocortical lateral temporal lobe epilepsy; ETLE = extratemporal lobe epilepsy

[1] includes patients now showing post-operative epilepsy surgery changes but who had no epileptogenic lesion prior to epilepsy surgery

[2] Tabulated as ETLE when unclear if TLE vs. ETLE

[3] In Pataraia et al., (2004), post-operative histopathology is given but not preoperative MR results

[4] Patient population composed of patients with negative MRI, large, multiple or questionable lesions and focal cortical dysplasia; group results available; results for the subgroup of MR-negative patients could not be extracted.

NM = not mentioned, not available, unable to determine based on published data

# DISCUSSION GÉNÉRALE

## 1. RAPPEL DES OBJECTIFS EXPÉRIMENTAUX, DES PRINCIPAUX RÉSULTATS ET DES RETOMBÉES CLINIQUES

L'objectif principal de cette thèse consistait à étudier le potentiel de nouvelles techniques d'investigation non invasives pour localiser le foyer épileptique chez des patients souffrant d'une épilepsie focale réfractaire non lésionnelle considérés candidats potentiels à une chirurgie d'épilepsie. Après une brève introduction sur l'épilepsie, une description des différents tests actuellement utilisés en clinique ainsi que leurs limitations est fournie afin d'établir les besoins tout particuliers de cette sous-population d'épileptiques réfractaires au traitement médical et sans lésion épileptogène évidente à l'imagerie structurale conventionnelle. S'enchaîne ensuite une série de quatre articles exposant nos observations sur le potentiel de trois techniques d'investigation récentes pour améliorer la localisation du foyer épileptique : l'IRM à haut champ à 3T, la SPIR et la MEG.

La première étude visait à déterminer le gain que pourrait conférer l'utilisation d'une IRM 3T dans la détection de possibles lésions épileptogènes subtiles chez les sujets épileptiques chez qui une IRM 1,5T n'avait rien révélé. Bien que l'augmentation de la puissance du champ magnétique de la machine signe une augmentation du rapport signal sur bruit, elle peut également entraîner des artéfacts de susceptibilité magnétique notamment dans les régions orbitofrontales et temporales [44, 77]. Il n'était donc pas clair qu'un tel rehaussement des appareils allait se trouver bénéfique. Notre étude, avec ses limitations (voir ci-bas), suggère que la plus-value d'un scanneur 3T est loin d'être remarquable en termes de détection de lésions épileptogènes occultes. En effet, le fait de réimager avec une IRM 3T 36 patients sans lésion évidente sur un scanneur n'a permis au neuroradiologue de détecter que deux lésions épileptogènes (5,6 %). D'autres techniques d'investigation sont donc nécessaires pour mieux localiser le foyer épileptique.

Les deux études suivantes visaient alors à étudier le potentiel de la SPIR à localiser le foyer épileptique. Dans la première étude SPIR, les sujets avaient un foyer épileptique

temporal. Dans la seconde étude SPIR, les sujets avaient un foyer frontal. Globalement, nos enregistrements ont démontré que notre technique était en mesure de détecter les changements hémodynamiques régionaux survenant au décours de crises focales. En effet, toutes les crises identifiées à l'EEG ont été associées à des changements hémodynamiques identifiables par la SPIR, en l'occurrence une augmentation significative de HbO et HbT au niveau de la région épileptique. Mieux encore, ces modifications ont parfois même permis de détecter rétrospectivement des crises avec changements électrographiques plus subtils à l'EEG. Ces crises, qui avaient été manquées par l'épileptologue après une première lecture, n'ont été identifiées qu'après une relecture guidée des segments de l'EEG où des changements de signaux optiques avaient été observés. Plus importants encore, nos enregistrements ont pu révéler que des crises partielles complexes de quelques minutes peuvent être associées à une augmentation de HbR, témoignant possiblement d'un manque d'oxygénation adéquate du tissu cérébral en état de crise. Ce phénomène a été observé sur toutes les crises partielles complexes temporales et sur certaines crises frontales. Bien que nous sachions depuis un certain temps qu'un état de mal convulsif puisse entraîner des dommages hypoxiques [78-80], une possible désoxygénation tissulaire lors de crises focales de courte durée (comme en présentent sur une base régulière nos patients épileptiques) était relativement inattendue. Cette observation soulève de nombreuses questions notamment quant aux facteurs déterminatifs de cette augmentation de HbR, les mécanismes sous-jacents, la contribution de cette désoxygénation par rapport à l'état postictal ainsi qu'aux troubles cognitifs et de développement accompagnant l'épilepsie. Quant à l'objectif initial d'utiliser la SPIR pour mieux localiser le foyer épileptique, les changements hémodynamiques observés précocement non seulement localement, mais également à distance du foyer rendent la tâche plus difficile que prévu. En effet, hormis l'augmentation de HbO et HbT au site du foyer épileptique, une activation symétrique (en image miroir) pouvait aussi être observée sur la région homologue contralatérale. Heureusement, l'amplitude de l'activation, le comportement du signal optique dans les canaux avoisinants et l'évolution temporelle des changements permettaient dans la majorité des cas une latéralisation adéquate du foyer épileptique. Lors des enregistrements SPIR de crises temporales et frontales, une latéralisation correcte a pu être établie sur 75 % et 88 % des crises respectivement. Bien que nos résultats soient encourageants, des

développements supplémentaires autant au niveau des techniques d'acquisition que de l'analyse du signal optique sont nécessaires pour améliorer la résolution spatiale de la SPIR avant qu'elle ne puisse contribuer significativement au bilan préchirurgical des patients souffrant d'une épilepsie non lésionnelle. Elle représente toutefois un outil fort prometteur pour la détection de crises et l'étude de l'impact hémodynamique des crises sur l'oxygénation cérébrale.

La dernière étude portait sur la MEG, une autre technique alternative non invasive dans la détermination de la région du cerveau à l'origine des crises. Bien que la technologie existe depuis de nombreuses décennies, la MEG a pu bénéficier de nombreux développements au cours des dernières années qui en font un outil d'investigation clinique prometteur, tout particulièrement pour la clientèle abordée dans cette thèse. D'une manière générale, les études réalisées à ce jour ont permis de montrer que l'analyse de dipôles modélisés en MEG est relativement précise dans la localisation des sources des pointes épileptiques intericales. Quelques études cliniques montrent d'ailleurs qu'elle est pertinente pour à peu près le tiers des sujets présentant une épilepsie focale pharmacorésistante candidats à une chirurgie d'épilepsie [73, 81, 82] . La majorité des patients dans ces études présentaient toutefois une épilepsie lésionnelle et il est probable que son impact soit encore plus important que soupçonné pour les patients avec épilepsies non lésionnelles. Dans notre étude, 61 patients consécutifs souffrant d'une épilepsie partielle non lésionnelle ayant bénéficié d'un bilan préchirurgical standard ont de surcroît eu un enregistrement MEG. L'impact de la MEG dans le bilan préchirurgical des épilepsies pharmacorésistantes non lésionnelles a d'abord été évalué. À cette fin, les données anonymisées du bilan préchirurgical de base pour tous les sujets recrutés ont d'abord été présentées à une équipe multidisciplinaire spécialisée dans le traitement chirurgical de l'épilepsie de manière aléatoire. Après que le plan de traitement consensuel eut été colligé, les résultats de la MEG ont alors été révélés et le changement dans le plan de traitement examiné. Il s'est avéré que la MEG modifiait le plan de traitement dans près des deux tiers des patients, soit parce que les résultats permettaient de réduire le nombre d'électrodes intracrâniennes nécessaires, soit en modifiant leur positionnement, soit en permettant une chirurgie d'emblée sans étude intracrânienne préalable, soit en rendant caduque une étude intracrânienne parce que

la zone épileptogène surplombait une zone éloquente inopérable, soit en fournissant des données rendant maintenant un patient candidat à une étude intracrânienne alors que les données du bilan usuel ne le permettait pas. Notre étude avait comme particularité intéressante que les 37 premiers sujets, bien qu'ayant passé une étude MEG, n'ont pas pu bénéficier des résultats MEG dans la pratique clinique et la prise en charge de leur condition épileptique. Ceci était en partie dû aux aléas de l'implantation et de la familiarisation à une nouvelle technique d'investigation nous empêchant de fournir un résultat à la fois fiable (auquel nous pouvions faire confiance dans la pratique clinique) et de manière diligente (afin de ne pas retarder indûment le traitement des patients aux prises avec une condition invalidante). Bien que déplorable à un certain niveau, cette situation particulière nous a permis d'observer l'impact (non plus théorique mais) réel de cette technique. En effet, certains patients ont été opérés au mauvais endroit (avec comme résultat un devenir postopératoire défavorable) en raison d'un échantillonnage spatial incomplet négligeant la vraie zone épileptogène. D'autres ont eu des complications opératoires en raison du nombre plus élevé de contacts intracrâniens utilisés.

Par ailleurs, les localisations des sources des pointes épileptiques intericales ont également été comparées aux données recueillies sur les patients ayant effectivement eu des enregistrements EEG intracrâniens. Cette analyse confirme à nouveau que les sources identifiées par la MEG sont effectivement le site de décharges épileptiques intericales. Elle révèle aussi les limites de la technique soit disant de référence qu'est l'EEG intracrânien alors que les décharges intericales et surtout ictales ont fréquemment été visualisées simultanément sur plusieurs structures corticales organisées en réseau compliquant sensiblement la localisation de la zone épileptogène. Enfin, nous avons observé que la résection de la zone MEG était associée à un bon pronostic chirurgical. En résumé, nos travaux montrent que la MEG est une technique de haut impact clinique dans l'évaluation préchirurgicale des patients avec épilepsie pharmacorésistante considérés candidats à une chirurgie pouvant :

a) améliorer la planification de l'étude intracrânienne et en réduire ses risques,

b) substituer parfois même une étude EEG invasive

c) permettre d'accroître le taux de succès de traitements chirurgicaux ou d'éviter certaines opérations non curatives.

En somme, le travail accompli montre que pour la population d'épileptiques candidats à une chirurgie ne présentant pas de lésion épileptogène évidente sur une IRM standard, l'IRM 3T n'apporte qu'une valeur ajoutée faible, que la SPIR-EEG a un potentiel de localisation intéressant qui nécessite encore toutefois des avancées méthodologiques avant de percer au niveau clinique, et que la MEG est l'outil ayant le plus gros impact actuellement sur le traitement de ces patients.

## 2. CRITIQUES ET LIMITES DES ÉTUDES

Les études composant cette thèse et les techniques qu'elles évaluent ne sont pas indemnes de limitations.

La première étude portant sur l'apport de l'IRM 3T était rétrospective. Les IRM n'ont pas toutes été acquises sur la même machine avec des paramètres identiques bien que toutes aient bénéficié des séquences propres à un protocole d'épilepsie. Les IRM n'ont pas toutes été lues par le même neuroradiologue alors qu'il est bien reconnu que les mesures de concordance intra et inter observateur ne sont jamais excellentes. De surcroît, les neuroradiologues avaient accès aux renseignements cliniques. Finalement, mentionnons le nombre relativement restreint de participants (n = 36).

Les études 2 et 3 portant sur le potentiel de la SPIR partagent les mêmes limitations. Il aura fallu de nombreux développements maison autant dans l'acquisition que dans le traitement des données pour aboutir aux résultats présentés. Mentionnons notamment la nécessité d'un casque rigide, mais léger pour augmenter le confort et permettre de longs enregistrements pour augmenter les chances de capturer une crise, la nécessité de procéder simultanément à l'enregistrement de l'EEG en plus des données SPIR pour permettre une corrélation électro-optique, l'acquisition simultanée de la vidéo pour une corrélation clinique autant pour les manifestations ictales que pour les mouvements générateurs d'artéfacts, le suivi de la saturométrie périphérique, etc. Malgré tout, d'autres développements sont nécessaires pour améliorer les

enregistrements. Un élément critique à améliorer sera d'évaluer la contribution des tissus mous extracérébraux au signal optique enregistré [83]. En effet, le signal SPIR est non seulement affecté par le comportement de l'hémoglobine au niveau du cortex superficiel entre les paires émetteur-récepteur, mais aussi par l'hémoglobine dans la peau et le tissu extracérébral [84]. Par ailleurs, bien que des précautions aient été prises pour ne pas incorporer dans l'analyse des signaux artificiels (artéfacts), on ne peut exclure une contamination des résultats. Hormis ces problèmes, il faut également être prudent dans l'analyse temporelle des changements hémodynamiques, car l'EEG de surface ne peut de manière précise identifier le début des crises, les électrodes installées sur le scalp n'étant pas au voisinage immédiat de la zone du début des crises au niveau intracérébral. Finalement, bien que de nombreux sujets aient été testés, il demeure que seulement un nombre relativement petit de sujets ont présenté des crises lors des enregistrements et chez qui la localisation du foyer a pu être clairement établie par d'autres modalités de référence.

Quant à l'étude 4 portant sur la MEG, d'autres types de limitations doivent être soulevés. Premièrement, bien que la modélisation dipolaire de pointes intercritiques constitue la méthode d'analyse la plus répandue et éprouvée, certains diront qu'elle pourrait s'avérer trop simpliste et ne reflétant pas la réalité. Le modèle dipolaire permet de déterminer le centre de gravité qui décrit le mieux, au plan statistique, la distribution spatiale d'une région corticale activée à un moment donné. En d'autres termes, ce modèle ne permet pas d'obtenir le volume cérébral où se distribuent les anomalies intercritiques. Or, on observe lors des enregistrements EEG que les décharges épileptiques impliquent parfois diverses régions étendues simultanément ou séquentiellement ne pouvant être expliquées par un dipôle unique. Pour tenir compte de ce concept plus complexe de réseau épileptique, certains suggèrent plutôt des modèles avec plusieurs dipôles s'activant de manière séquentielle ou simultanée dans le temps. Ces modèles dits de sources distribués reflèteraient plus fidèlement l'étendue du réseau épileptique [85]. Ces modèles ont toutefois leurs propres limites. Le nombre de dipôles pouvant expliquer les données doit être fixé *à priori* selon les connaissances physiopathologiques et les données cliniques chez un patient donné. Ces modèles multi-dipôlaire sont donc au moins partiellement intrinsèquement arbitraires et l'analyse des données implique généralement un choix de

l'expérimentateur [86-88]. Par ailleurs, une autre critique de notre étude concerne la partie portant sur la corrélation avec le résultat postopératoire puisque seulement un nombre relativement modeste de sujets avaient été opérés au moment de la soumission de l'article.

## 3. AVENUES FUTURES DE RECHERCHE

Il existe de nombreuses avenues de recherche prometteuses pour améliorer la localisation du foyer épileptique.

### *3.1. Antennes de surface en réseau (ASR)*

Le développement de l'IRM a également conduit à la mise au point d'antennes haute performance qui améliorent la réception du signal de radiofréquence servant à constituer les images. Ainsi, les antennes de surface matricielles constituent une avancée importante permettant d'augmenter le rapport signal sur bruit (RSB). Cette performance accrue est le résultat (1) d'une sommation du signal de plusieurs petits échantillons de volume tissulaire et (2) de la grande proximité du récepteur avec le tissu étudié puisque l'antenne est en contact direct avec la tête du sujet étudié. L'utilisation de telles antennes conduit ainsi à des performances accrues en termes de capacité de résolution de l'image et de rapidité d'acquisition des séquences (Figure 10). L'utilisation de cet équipement est quasi incontournable afin de potentialiser le bénéfice de l'IRM à haut champ. Wald et al., [89] ont démontré que comparativement aux antennes de tête utilisées dans l'investigation clinique habituelle, le RSB obtenu avec quatre antennes de surface était augmenté de six fois. Il existe déjà quelques études démontrant que l'utilisation de ce type d'antennes augmente la détection et la spécificité du diagnostic chez les patients porteurs d'une lésion cérébrale focale. À l'aide d'antennes de surface, Grant et al., ont réussi à détecter de nouvelles lésions chez 3/25 (12 %) patients avec épilepsies partielles réfractaires indétectables avec une IRM de1,5T, Bronen chez 1/22 patients (5 %), et Goyal et al., [90] chez 5/9 patients (56 %). Ces publications démontrent à tout le moins la reproductibilité des résultats concernant la valeur diagnostique des antennes de surface. Sur la base de ces résultats

encourageants et dans le but de s'attaquer à certaines des limitations de notre première étude, nous avons débuté en 2009 une étude prospective étalée sur 3 ans visant à recruter 35 patients avec épilepsie focale réfractaire sans lésion épileptogène identifiable sur notre IRM 1,5T pour les réimager avec une IRM 1,5T avec ASR, une IRM 3T et une dernière IRM 3T avec ASR. La taille de l'échantillon est principalement limitée par les capacités d'investigation électrophysiologique (vidéo-EEG) et d'implantation neurochirurgicale d'électrodes et de traitement chirurgical des patients porteurs d'une épilepsie néocorticale non lésionnelle référés au CHUM. La taille de cet échantillon permettra de conclure à des résultats statistiquement significatifs (selon un test de McNemar pour une erreur alpha de 0,05 et une puissance de 80 %) si au moins 6 (17 %) patients sont porteurs d'une lésion cérébrale démontrée par les examens effectués sur le système3T. Cette proportion est inférieure à notre hypothèse d'un niveau de détection lésionnel d'environ 30 % dans la population ciblée et qui a été estimé à partir des données de la littérature sur les antennes de surface. Les données obtenues en dehors du cadre normal de l'investigation seront évaluées de façon indépendante pour garder à l'aveugle l'équipe médicale traitante afin de minimiser le biais de vérification. Pour des raisons éthiques évidentes, un observateur épileptologue indépendant, qui n'est pas impliqué dans l'investigation ou le traitement invasif du patient, sera chargé de vérifier la congruité des nouvelles données d'investigation de recherche et d'aviser l'équipe traitante si celles-ci modifiaient le plan de traitement établi par le consensus multidisciplinaire. L'équipe multidisciplinaire se réunira de nouveau pour l'obtention d'un second consensus qui tiendra compte des nouvelles informations disponibles. L'imagerie avec antenne de surface obtenue sur les appareils 1,5T et 3T sera analysée séparément et à l'aveugle par trois neuroradiologues, ceci à deux reprises après un intervalle de 3 à 6 mois. Les spécimens pathologiques seront analysés par notre neuropathologiste.

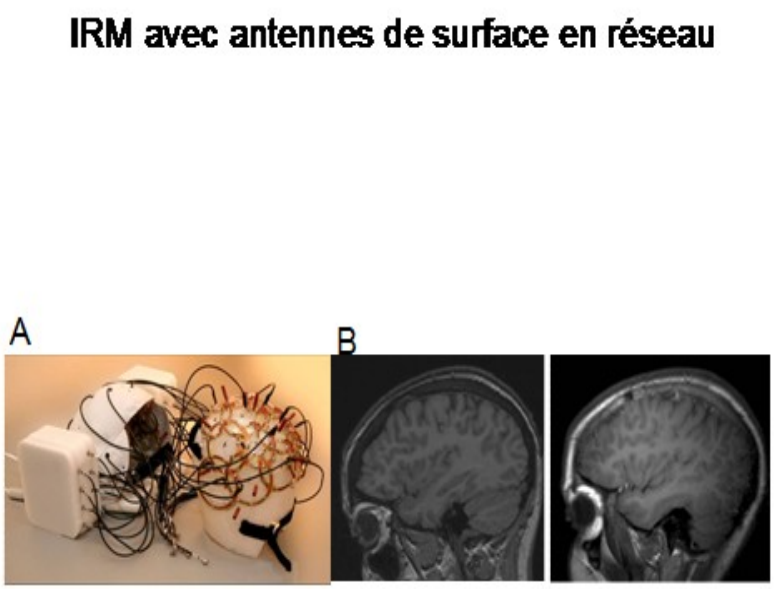


Figure 10. a) Antennes de surface en réseau pour la réalisation de l'IRM; b) Images de haute résolution obtenues par cette technique.

### *3.2. Analyse quantitative*

Les anomalies de malformations corticales sont reconnues comme une cause importante d'épilepsie focale pharmacorésistante. [71, 91, 92] Bien que l'IRM puisse déjà identifier des malformations corticales de développement chez plusieurs patients, certaines sont trop subtiles pour être identifiées par une analyse qualitative conventionnelle par le neuroradiologique. L'utilisation de techniques informatisées de traitement de l'image IRM peut améliorer la détection de ces lésions fugaces non aisément identifiables par l'analyse visuelle qualitative [93]. Des études sur un faible nombre de sujets montrent effectivement que des techniques informatisées telles la morphométrie axée sur les voxels, l'analyse des textures et l'analyse des formes peuvent faciliter la détection de ces lésions subtiles [94]. Ces techniques permettent d'étudier notamment l'épaisseur du manteau cortical, la morphologie du cortex et des sillons, la jonction substance blanche-substance grise, la présence de tissu gris en position ectopique [95] (Figure 11). Nous conduisons actuellement une étude prospective visant à évaluer la valeur de notre algorithme d'analyse quantitative sur

une série de sujets consécutifs avec épilepsie focale réfractaire considérés candidats à une chirurgie d'épilepsie.

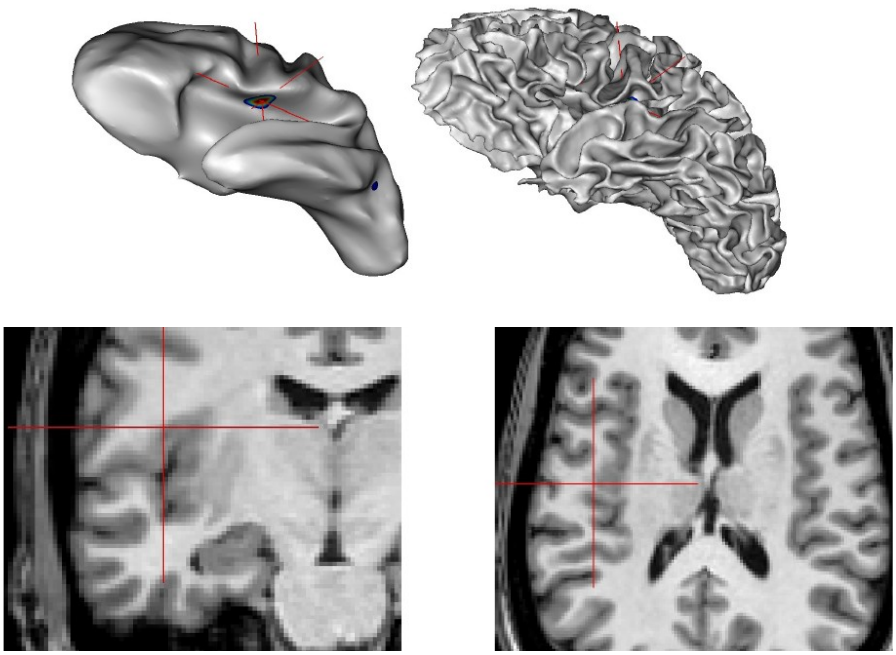

Figure 11. Analyse automatisée de l'épaisseur corticale permettant la détection d'une dysplasie corticale subtile dans la région insulaire droite initialement manquée lors de l'analyse visuelle par le neuroradiologue.

### *3.3. IRM avec nanoparticules magnétisées fonctionnalisées.*

L'utilisation de nanoparticules magnétisées fonctionnalisées est en théorie fortement prometteuse [96]. Le principe ici est d'utiliser des nanoparticules capables de traverser la barrière hémoencéphalique pour qu'ils se concentrent (d'une manière ou d'une autre) dans les tissus épileptogènes et les rendre visibles sur une IRM. Il s'agit en quelque sorte d'un agent de contraste fait de nanoparticules et fonctionnalisé pour illuminer le ou les tissus épileptiques. Une première étude de concept a ainsi été faite en attachant de l'alpha-méthyl-tryptophane à des magnétonanoparticules (l'utilisation de l'AMT ici reposait sur le fait que des études antérieures avec la TEP avaient noté une recapture préférentielle de l'AMT au niveau des tissus épileptogènes) [97]. Une fois injectées dans un modèle animal d'épilepsie, les zones identifiées par cette technique étaient congruentes avec les données électrophysiologiques subséquemment

obtenues. Nous travaillons actuellement sur une idée similaire. Ici, les magnétonanoparticules s'agrègeraient sous l'effet de champs magnétiques générés par les décharges épileptiques (intericales ou ictales). Il y a aurait alors de fortes chances que le site d'agrégation maximale des magnétonanoparticules identifiées à l'IRM consisterait à la zone épileptogène.

### *3.4. L'IRMf combinée à l'EEG*

Grâce à des développements techniques considérables, il est désormais possible d'enregistrer l'EEG dans l'enregistrement magnétique de l'IRM et de corriger les artéfacts générés sur l'EEG par cet environnement pour identifier les décharges épileptiques survenant lors de l'examen. Ceci permet alors de localiser les régions de modifications de perfusion cérébrale couplées à ces décharges selon un modèle de réponse hémodynamique [98]. Lors de décharges épileptiques, l'augmentation des besoins en oxygène des neurones épileptiques entraîne une augmentation locale du flux sanguin par vasodilatation apportant de l'hémoglobine oxygénée en excès des besoins réels et causant ainsi une diminution de la concentration en déoxyhémoglobine. Parce que la déoxyhémoglobine est paramagnétique (contrairement à la plupart des tissus biologiques), ce processus induit une modification de la susceptibilité magnétique et donc une augmentation du signal IRM BOLD (*Blood oxygenation level dependent*) détectable par des séquences IRM de type "*Echo Planar Imaging*" (EPI). Cette réponse hémodynamique, qui survient en général avec un délai approximatif entre 1 et 5 secondes et culmine autour de 4 à 5 secondes, peut être modélisée par la fonction de réponse hémodynamique (HRF) (Figures 12 et 13). Les études actuelles indiquent que l'IRMf-EEG est une technique pouvant aider à l'identification du foyer épileptique lors des évaluations préchirurgicales [99] . La majorité des études initiales ont porté sur les réponses associées aux pointes temporales [100]. Ont suivi par la suite des études, dont la nôtre (voir Annexe 3), suggérant aussi leur utilité dans le bilan préchirurgical de patients avec une épilepsie non lésionnelle extratemporale [101]. L'IRMf-EEG possède comme toutes techniques son lot de limitations : la nécessité d'avoir des pointes sans quoi aucune analyse ne peut être faite, l'importance d'être immobile pour limiter les

artéfacts de mouvement, l'interprétation parfois délicate en raison de la présence de plusieurs sites d'activation (et de désactivation) associée à des pointes en apparence focale (Annexe 4).

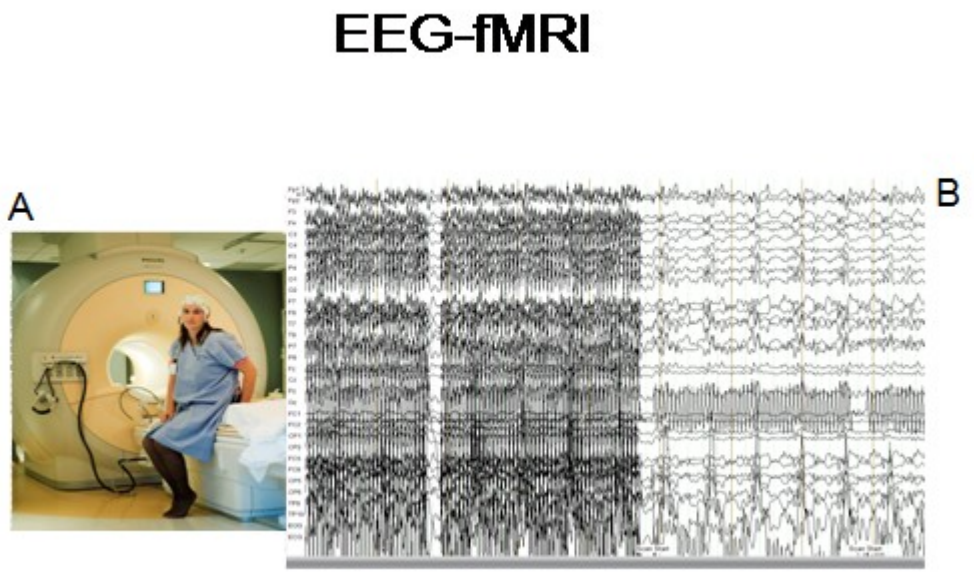


Figure 12. a) Casque EEG compatible avec l'IRM permettant l'obtention de l'activité cérébrale durant l'IRM; b) L'enregistrement EEG obtenu comportant de nombreux artéfacts qui doivent être éliminés par diverses techniques de filtrage.

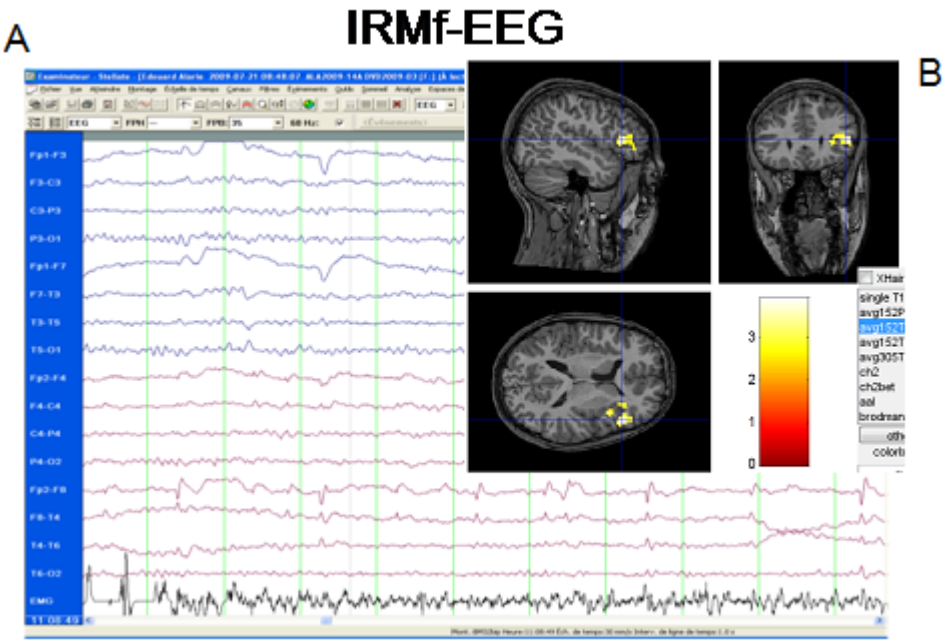


Figure 13. IRMf-EEG d'un jeune patient avec pointes frontales droites (a) mettant en évidence une activation du signal BOLD au niveau du gyrus frontal inférieur droit (b).

### *3.5. SPIR-EEG*

*Validation de la SPIR sur un grand nombre de sujets*

Le travail préliminaire accompli au cours des dernières années avec la SPIR-EEG et révélé ci-haut confirme le potentiel clinique du monitorage SPIR-EEG. Elle semble être un bon outil de détection des crises, a un certain potentiel dans la localisation des crises focales et finalement peut mesurer l'impact des crises sur l'oxygénation cérébrale [102]. Une validation plus approfondie est nécessaire sur un plus grand nombre de sujets avant d'envisager une implantation en milieu clinique et plusieurs observations préliminaires doivent être davantage investiguées. La SPIR peut-elle détecter avec fiabilité des crises ? Les changements initiaux détectés par la SPIR peuvent-ils localiser la région épileptogène de manière fiable ? Quels sont les facteurs sous-tendant la désoxygénation observée dans certaines crises focales ? Est-ce le type de crises, leur durée, leur fréquence, le substrat sous-tendant l'épileptogénicité, l'âge, des conditions comorbides ? Nous avons donc débuté un projet visant à étudier sur une période de 5 ans 116 sujets épileptiques, basé sur un calcul du nombre de sujets nécessaires pour atteindre nos objectifs.

*Développement d'un prototype de SPIR-EEG portable*

L'étude ou le monitorage des crises nécessitent des enregistrements de longue durée. Les montages traditionnels sont toutefois peu efficaces. L'équipe de Boas à Boston utilise des sources placées sur des bandes de velcro, mais celles-ci sont relativement peu résistantes au mouvement et se prêtent mal aux enregistrements EEG [103, 104]. La technique employée par Gratton au *Beckman Institute* consiste à utiliser un casque de moto, mais de nouveau, ce système est peu adapté à cause du poids qu'il exerce sur la tête du sujet. Le casque utilisé dans nos études est léger, opaque et résistant aux mouvements mais devient tout de même inconfortable après 5 à 6 heures d'enregistrements. Hormis l'incapacité d'enregistrer l'EEG simultanément avec les appareils commerciaux actuels, les autres problèmes auxquels nous avons eu à faire face lors de nos expériences ont été la nécessité de segmenter les enregistrements par manque de mémoire vive, la grosseur et la lourdeur de l'appareillage et l'insuffisance

du nombre d'optodes pour couvrir toute la surface du crâne. À cet effet, notre équipe travaille à la création d'un dispositif d'imagerie médicale fonctionnelle, portable et sans fil adapté pour l'enregistrement continu prolongé à l'aide d'un casque géodésique combinant électrodes de surface et optodes recouvrant entièrement la tête du patient pour un échantillonnage optimal. Ce dispositif aura l'allure d'une matrice d'optodes pouvant être portée continuellement sur la tête. L'instrument ne devra encombrer le patient que très peu, d'où l'avantage de sa petite taille et de l'absence de fils. De plus, l'électronique de contrôle pour la SPIR devra pouvoir être très rapidement activée et désactivée, ceci afin de multiplexer son opération avec un électroencéphalogramme portable. Ainsi, des données vidéo-EEG et SPIR pourront être prises en même temps sur la tête du sujet. Un prototype à 8 canaux a déjà été construit et des tests de validation doivent débuter sous peu (Figure 14) et (Annexe 5). Parallèlement, la construction d'un système à 32 canaux suit son cours. Ce projet bénéficiera aux sujets épileptiques dans la détection, la localisation et l'évaluation de l'impact des crises focales, mais on peut facilement envisager d'autres utilités dont le monitorage des patients avec état de mal épileptique nonconvulsif, le suivi de l'oxygénation et de l'activité cérébrale chez les patients aux soins intensifs neurologiques, les patients subissant une endartériectomie ou une chirurgie cardiaque, les patients à risque d'accidents vasculaires cérébraux par vasospasme ou embolies [105].

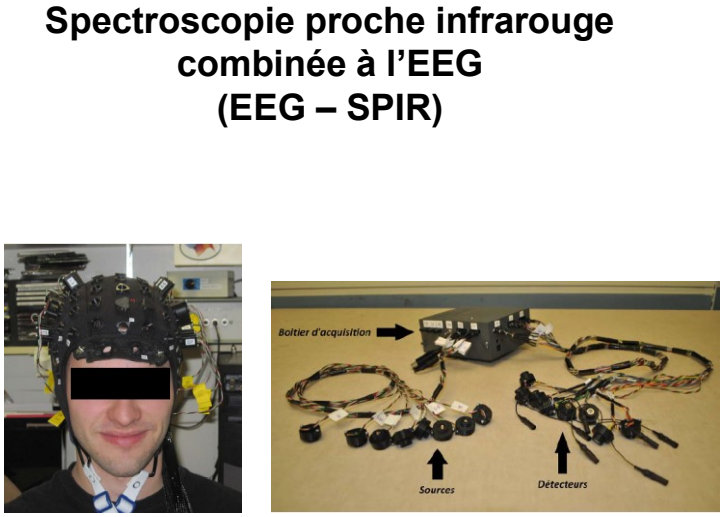


Figure 14. Prototype d'un système portable sans fil d'enregistrement simultané de l'électroencéphalographie et de la spectroscopie proche infrarouge.

### *3.6. Imagerie optique intrinsèque*

Les études SPIR de crises incluses dans cette thèse, comme pour la majorité des études de neuroimagerie chez l'humain, sont limités par de nombreux facteurs dont l'hétérogénéité des sujets (âge, foyer épileptique, comorbidités, fréquence des crises, durée des crises, etc.) [102, 106-108]. Afin de valider les observations faites lors de l'enregistrement de crises focales en SPIR, il est souhaitable d'utiliser un modèle animal d'épilepsie. C'est ce que nous tentons actuellement de faire en utilisant le 4-aminopyridine pour induire des pointes et crises épileptiques au niveau du cortex sensorimoteur de souris. Bénéficiant de la fenêtre de craniotomie, il est possible de procéder à des mesures de HbR, HbO et HbT avec l'imagerie optique intrinsèque et des enregistrements électrophysiologiques pour étudier la réponse hémodynamique au décours de pointes et crises. Avec une seconde fenêtre de craniotomie exposant le cortex sensorimoteur controlatéral, il est possible de valider s'il existe effectivement des changements en image miroir tel qu'observé dans les études SPIR et mieux comprendre les mécanismes sous-tendant ces changements (Annexe 6).

### *3.7. Magnétoencéphalographie*

Notre étude MEG a porté sur l'analyse des pointes épileptiques intericales. Les pointes intericales déterminent ce que l'on appelle la zone irritative. Or, bien que la majorité du temps, la zone épileptogène soit située au sein de la zone irritative, il arrive occasionnellement que la zone de début des crises soit située à distance de la zone irritative. Il existe donc un risque, bien que faible, que la résection de la zone irritative déterminée par la MEG ne résulte pas en une guérison des crises puisque la zone de début des crises n'a pas été réséquée.

Des études récentes utilisant l'EEG intracrânien acquis avec une fréquence d'échantillonnage élevée (1000-2000 Hz) ont permis de mettre en évidence des oscillations à haute fréquence d'intérêt pratique dans la détermination de la zone épileptogène [109]. Les OHF sont des activités >40 Hz incluant les oscillations gamma (30-80 Hz), haut gamma (60-120 Hz), "*ripples*" (100-250 Hz) et "*fast-ripples*" (250-500 Hz) (Figures 15 et 16). Présentes dans les périodes intericale,

préictale et ictale, elles seraient principalement localisées au sein de la zone de début des crises (et rarement dans les régions de propagation secondaire). Elles seraient aussi plus spécifiques au cortex épileptogène que les pointes intericales. Leurs résections seraient d'ailleurs associées à un bon résultat chirurgical. Il a été maintenant démontré que des OHF peuvent être détectées par la MEG et analysées par des techniques d'analyse du signal de type filtrage spatial ("*beamformer*") [110]. Il pourrait s'avérer que la source topographique de ces OHF soit supérieure à la modélisation dipolaire de pointes intericales pour identifier la zone épileptogène.

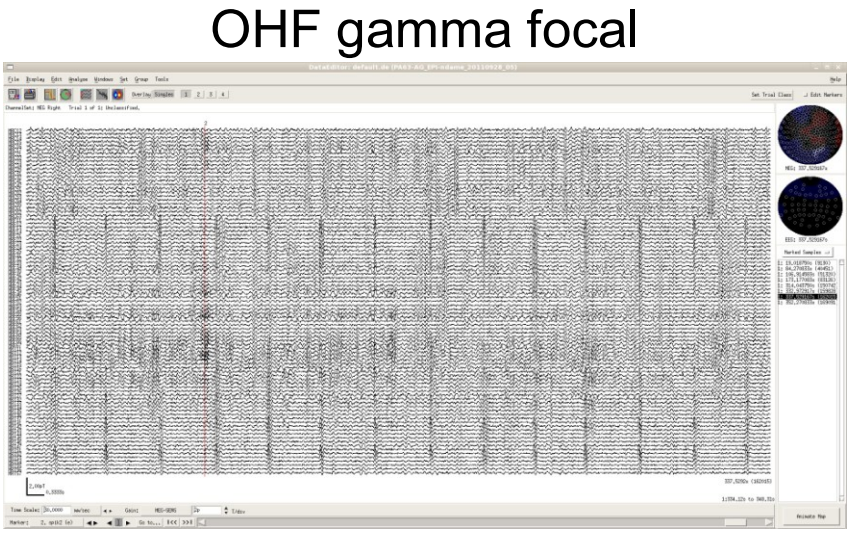


Figure 15. Enregistrement EEG obtenu durant l'étude MEG révélant la présence de pointes épileptiformes et d'oscillations rapide de haute fréquence (gamma) (ligne rouge)

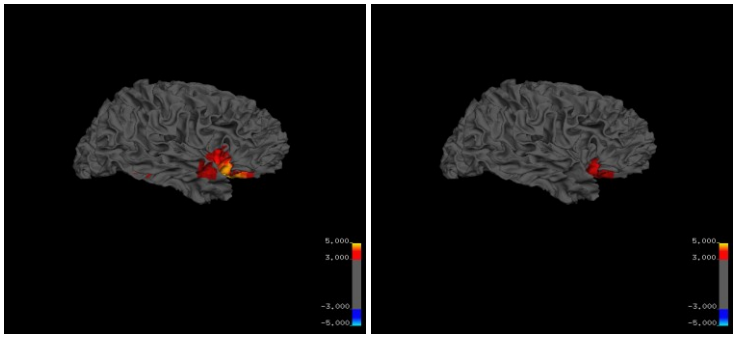

Figure 16. Localisation de source des oscillations rapides de haute fréquence par la méthode Beamformer

En somme, comme en font foi les travaux dans cette thèse, de nombreux développements en neuroimagerie/électrophysiologie au cours des dernières années nous permettent de mieux voir, analyser et surveiller l'activité épileptique. Bien qu'il reste encore beaucoup de travail de développement et de validation à faire, il est permis d'espérer que ces avancées résulteront en une meilleure compréhension de l'épilepsie et surtout en un meilleur contrôle des crises, favorisant ainsi un meilleur vécu des patients et de leurs proches.

## RÉFÉRENCES


1. Chang, B.S. and D.H. Lowenstein, *Epilepsy.* N Engl J Med, 2003. **349**(13): p. 1257-66.
2. Tellez-Zenteno, J.F., et al., *National and regional prevalence of self-reported epilepsy in Canada.* Epilepsia, 2004. **45**(12): p. 1623-9.
3. Leonardi, M. and T.B. Ustun, *The global burden of epilepsy.* Epilepsia, 2002. **43 Suppl 6**: p. 21-5.
4. Berg, A.T., et al., *Revised terminology and concepts for organization of seizures and epilepsies: report of the ILAE Commission on Classification and Terminology, 2005-2009.* Epilepsia, 2010. **51**(4): p. 676-85.
5. Loddenkemper, T. and P. Kotagal, *Lateralizing signs during seizures in focal epilepsy.* Epilepsy Behav, 2005. **7**(1): p. 1-17.
6. Brophy, G.M., et al., *Guidelines for the evaluation and management of status epilepticus.* Neurocrit Care, 2012. **17**(1): p. 3-23.
7. Kwan, P. and M.J. Brodie, *Early identification of refractory epilepsy.* N Engl J Med, 2000. **342**(5): p. 314-9.
8. Wiebe, S., et al., *Burden of epilepsy: the Ontario Health Survey.* Can J Neurol Sci, 1999. **26**(4): p. 263-70.
9. Engel, J., Jr., *Surgery for seizures.* N Engl J Med, 1996. **334**(10): p. 647-52.
10. Spencer, S.S., *Long-term outcome after epilepsy surgery.* Epilepsia, 1996. **37**(9): p. 807-13.
11. Siegel, A.M., *Presurgical evaluation and surgical treatment of medically refractory epilepsy.* Neurosurg Rev, 2004. **27**(1): p. 1-18; discussion 19-21.
12. Rosenow, F. and H. Luders, *Presurgical evaluation of epilepsy.* Brain, 2001. **124**(Pt 9): p. 1683-700.
13. Olejniczak, P., *Neurophysiologic basis of EEG.* J Clin Neurophysiol, 2006. **23**(3): p. 186-9.
14. Verma, A. and R. Radtke, *EEG of partial seizures.* J Clin Neurophysiol, 2006. **23**(4): p. 333-9.
15. Bartolomei, F., et al., *[EEG and video-EEG explorations in refractory partial epilepsy].* Rev Neurol (Paris), 2004. **160 Spec No 1**: p. 5S81-90.
16. Duncan, J.S., *Imaging in the surgical treatment of epilepsy.* Nat Rev Neurol, 2010. **6**(10): p. 537-50.
17. Goffin, K., et al., *Neuronuclear assessment of patients with epilepsy.* Semin Nucl Med, 2008. **38**(4): p. 227-39.

18. Mauguiere, F. and P. Ryvlin, *The role of PET in presurgical assessment of partial epilepsies.* Epileptic Disord, 2004. **6**(3): p. 193-215.
19. Cakirer, S., et al., *MR imaging in epilepsy that is refractory to medical therapy.* Eur Radiol, 2002. **12**(3): p. 549-58.
20. Tellez-Zenteno, J.F., et al., *Surgical outcomes in lesional and non-lesional epilepsy: a systematic review and meta-analysis.* Epilepsy Res, 2010. **89**(2-3): p. 310-8.
21. Berg, A.T., et al., *The multicenter study of epilepsy surgery: recruitment and selection for surgery.* Epilepsia, 2003. **44**(11): p. 1425-33.
22. Bien, C.G., et al., *Characteristics and surgical outcomes of patients with refractory magnetic resonance imaging-negative epilepsies.* Arch Neurol, 2009. **66**(12): p. 1491-9.
23. Scott, C.A., et al., *Presurgical evaluation of patients with epilepsy and normal MRI: role of scalp video-EEG telemetry.* J Neurol Neurosurg Psychiatry, 1999. **66**(1): p. 69-71.
24. Woermann, F.G. and C. Vollmar, *Clinical MRI in children and adults with focal epilepsy: a critical review.* Epilepsy Behav, 2009. **15**(1): p. 40-9.
25. Chapman, K., et al., *Seizure outcome after epilepsy surgery in patients with normal preoperative MRI.* J Neurol Neurosurg Psychiatry, 2005. **76**(5): p. 710-3.
26. Cohen-Gadol, A.A., et al., *Long-term outcome of epilepsy surgery among 399 patients with nonlesional seizure foci including mesial temporal lobe sclerosis.* J Neurosurg, 2006. **104**(4): p. 513-24.
27. Blumcke, I., *Neuropathology of focal epilepsies: a critical review.* Epilepsy Behav, 2009. **15**(1): p. 34-9.
28. Andermann, F., E. Kobayashi, and E. Andermann, *Genetic focal epilepsies: state of the art and paths to the future.* Epilepsia, 2005. **46 Suppl 10**: p. 61-7.
29. Crino, P.B., *Focal brain malformations: seizures, signaling, sequencing.* Epilepsia, 2009. **50 Suppl 9**: p. 3-8.
30. Burch, J., et al., *The clinical effectiveness and cost-effectiveness of technologies used to visualise the seizure focus in people with refractory epilepsy being considered for surgery: a systematic review and decision-analytical model.* Health Technol Assess, 2012. **16**(34): p. 1-157, iii-iv.
31. Spencer, S.S. and R.E. Bautista, *Functional neuroimaging in localization of the ictal onset zone.* Adv Neurol, 2000. **83**: p. 285-96.
32. Devous, M.D., Sr., et al., *SPECT brain imaging in epilepsy: a meta-analysis.* J Nucl Med, 1998. **39**(2): p. 285-93.

33. Kumar, A., et al., *Objective detection of epileptic foci by 18F-FDG PET in children undergoing epilepsy surgery.* J Nucl Med, 2010. **51**(12): p. 1901-7.
34. Engel, J., Jr., T.R. Henry, and B.E. Swartz, *Positron emission tomography in frontal lobe epilepsy.* Adv Neurol, 1995. **66**: p. 223-38; discussion 238-41.
35. Quesney, L.F., *Extratemporal epilepsy: clinical presentation, pre-operative EEG localization and surgical outcome.* Acta Neurol Scand Suppl, 1992. **140**: p. 81-94.
36. Salanova, V., et al., *Frontal lobe seizures: electroclinical syndromes.* Epilepsia, 1995. **36**(1): p. 16-24.
37. Lee, S.K., et al., *The clinical usefulness of ictal surface EEG in neocortical epilepsy.* Epilepsia, 2000. **41**(11): p. 1450-5.
38. Diehl, B. and H.O. Luders, *Temporal lobe epilepsy: when are invasive recordings needed?* Epilepsia, 2000. **41 Suppl 3**: p. S61-74.
39. Cossu, M., et al., *Stereoelectroencephalography in the presurgical evaluation of children with drug-resistant focal epilepsy.* J Neurosurg, 2005. **103**(4 Suppl): p. 333-43.
40. Pondal-Sordo, M., et al., *Usefulness of intracranial EEG in the decision process for epilepsy surgery.* Epilepsy Res, 2007. **74**(2-3): p. 176-82.
41. Wiggins, G.C., K. Elisevich, and B.J. Smith, *Morbidity and infection in combined subdural grid and strip electrode investigation for intractable epilepsy.* Epilepsy Res, 1999. **37**(1): p. 73-80.
42. Hamer, H.M., et al., *Complications of invasive video-EEG monitoring with subdural grid electrodes.* Neurology, 2002. **58**(1): p. 97-103.
43. Johnston, J.M., Jr., et al., *Complications of invasive subdural electrode monitoring at St. Louis Children's Hospital, 1994-2005.* J Neurosurg, 2006. **105**(5 Suppl): p. 343-7.
44. Phal, P.M., et al., *Qualitative comparison of 3-T and 1.5-T MRI in the evaluation of epilepsy.* AJR Am J Roentgenol, 2008. **191**(3): p. 890-5.
45. Griffiths, P.D., et al., *MR imaging of patients with localisation-related seizures: initial experience at 3.0T and relevance to the NICE guidelines.* Clin Radiol, 2005. **60**(10): p. 1090-9.
46. Andrade-Valenca, L.P., et al., *Clinical and neuroimaging features of good and poor seizure control patients with mesial temporal lobe epilepsy and hippocampal atrophy.* Epilepsia, 2003. **44**(6): p. 807-14.
47. Briellmann, R.S., A. Syngeniotis, and G.D. Jackson, *Comparison of hippocampal volumetry at 1.5 tesla and at 3 tesla.* Epilepsia, 2001. **42**(8): p. 1021-4.

48. Sawaishi, Y., et al., *A hippocampal lesion detected by high-field 3 tesla magnetic resonance imaging in a patient with temporal lobe epilepsy.* Tohoku J Exp Med, 2005. **205**(3): p. 287-91.

49. Lim, C.C., et al., *Malformations of cortical development: high-resolution MR and diffusion tensor imaging of fiber tracts at 3T.* AJNR Am J Neuroradiol, 2005. **26**(1): p. 61-4.

50. Knake, S., et al., *3T phased array MRI improves the presurgical evaluation in focal epilepsies: a prospective study.* Neurology, 2005. **65**(7): p. 1026-31.

51. Irani, F., et al., *Functional near infrared spectroscopy (fNIRS): an emerging neuroimaging technology with important applications for the study of brain disorders.* Clin Neuropsychol, 2007. **21**(1): p. 9-37.

52. Calderon-Arnulphi, M., A. Alaraj, and K.V. Slavin, *Near infrared technology in neuroscience: past, present and future.* Neurol Res, 2009. **31**(6): p. 605-14.

53. Knowlton, R.C., *The role of FDG-PET, ictal SPECT, and MEG in the epilepsy surgery evaluation.* Epilepsy Behav, 2006. **8**(1): p. 91-101.

54. Munakata, M., et al., *Dynamic cortical activity during spasms in three patients with West syndrome: a multichannel near-infrared spectroscopic topography study.* Epilepsia, 2004. **45**(10): p. 1248-57.

55. Sokol, D.K., et al., *Near infrared spectroscopy (NIRS) distinguishes seizure types.* Seizure, 2000. **9**(5): p. 323-7.

56. Buchheim, K., et al., *Decrease in haemoglobin oxygenation during absence seizures in adult humans.* Neurosci Lett, 2004. **354**(2): p. 119-22.

57. Adelson, P.D., et al., *Noninvasive continuous monitoring of cerebral oxygenation periictally using near-infrared spectroscopy: a preliminary report.* Epilepsia, 1999. **40**(11): p. 1484-9.

58. Watanabe, E., et al., *Noninvasive cerebral blood volume measurement during seizures using multichannel near infrared spectroscopic topography.* J Biomed Opt, 2000. **5**(3): p. 287-90.

59. Watanabe, E., Y. Nagahori, and Y. Mayanagi, *Focus diagnosis of epilepsy using near-infrared spectroscopy.* Epilepsia, 2002. **43 Suppl 9**: p. 50-5.

60. Hoshi, Y., *Towards the next generation of near-infrared spectroscopy.* Philos Transact A Math Phys Eng Sci, 2011. **369**(1955): p. 4425-39.

61. Papanicolaou, A.C., *An introduction to magnetoencephalography with some applications.* Brain Cogn, 1995. **27**(3): p. 331-52.

62. Colon, A.J., et al., *Use of routine MEG in the primary diagnostic process of epilepsy.* J Clin Neurophysiol, 2009. **26**(5): p. 326-32.

63. Ray, A. and S.M. Bowyer, *Clinical applications of magnetoencephalography in epilepsy.* Ann Indian Acad Neurol, 2010. **13**(1): p. 14-22.

64. Lau, M., D. Yam, and J.G. Burneo, *A systematic review on MEG and its use in the presurgical evaluation of localization-related epilepsy.* Epilepsy Res, 2008. **79**(2-3): p. 97-104.

65. Funke, M.E., et al., *The role of magnetoencephalography in "nonlesional" epilepsy.* Epilepsia, 2011. **52 Suppl 4**: p. 10-4.

66. Shiraishi, H., et al., *Comparison of three methods for localizing interictal epileptiform discharges with magnetoencephalography.* J Clin Neurophysiol, 2011. **28**(5): p. 431-40.

67. Barkley, G.L. and C. Baumgartner, *MEG and EEG in epilepsy.* J Clin Neurophysiol, 2003. **20**(3): p. 163-78.

68. Fuchs, M., M. Wagner, and J. Kastner, *Confidence limits of dipole source reconstruction results.* Clin Neurophysiol, 2004. **115**(6): p. 1442-51.

69. Knowlton, R.C., et al., *Effect of epilepsy magnetic source imaging on intracranial electrode placement.* Ann Neurol, 2009. **65**(6): p. 716-23.

70. Zhang, R., et al., *Interictal magnetoencephalographic findings related with surgical outcomes in lesional and nonlesional neocortical epilepsy.* Seizure, 2011. **20**(9): p. 692-700.

71. RamachandranNair, R., et al., *MEG predicts outcome following surgery for intractable epilepsy in children with normal or nonfocal MRI findings.* Epilepsia, 2007. **48**(1): p. 149-57.

72. Fischer, M.J., G. Scheler, and H. Stefan, *Utilization of magnetoencephalography results to obtain favourable outcomes in epilepsy surgery.* Brain, 2005. **128**(Pt 1): p. 153-7.

73. De Tiege, X., et al., *Clinical added value of magnetic source imaging in the presurgical evaluation of refractory focal epilepsy.* J Neurol Neurosurg Psychiatry, 2012. **83**(4): p. 417-23.

74. Schneider, F., et al., *Magnetic source imaging in non-lesional neocortical epilepsy: additional value and comparison with ICEEG.* Epilepsy Behav, 2012. **24**(2): p. 234-40.

75. Shorvon, S.D., E. Perucca, and J. Engel, *MEG in presurgical evaluation of Epilepsy*, in *The Treatment of Epilepsy*. 2009, Wiley-Blackwell: Chichester, UK ; Hoboken, NJ. p. 799-804.

76. Nguyen, D.K., et al., *Non-invasive continuous EEG-fNIRS recording of temporal lobe seizures.* Epilepsy Res, 2012. **99**(1-2): p. 112-26.

77. Nguyen, D.K., et al., *Value of 3.0 T MR imaging in refractory partial epilepsy and negative 1.5 T MRI.* Seizure, 2010. **19**(8): p. 475-8.

78. Meldrum, B.S. and J.B. Brierley, *Prolonged epileptic seizures in primates. Ischemic cell change and its relation to ictal physiological events.* Arch Neurol, 1973. **28**(1): p. 10-7.

79. Kreisman, N.R., T.J. Sick, and M. Rosenthal, *Concepts of brain oxygen sufficiency during seizures.* Adv Exp Med Biol, 1984. **180**: p. 381-92.

80. Kreisman, N.R., et al., *Oxidative metabolic responses with recurrent seizures in rat cerebral cortex: role of systemic factors.* Brain Res, 1981. **218**(1-2): p. 175-88.

81. Sutherling, W.W., et al., *Influence of magnetic source imaging for planning intracranial EEG in epilepsy.* Neurology, 2008. **71**(13): p. 990-6.

82. Bagic, A., et al., *American Clinical MEG Society (ACMEGS) position statement: the value of magnetoencephalography (MEG)/magnetic source imaging (MSI) in noninvasive presurgical evaluation of patients with medically intractable localization-related epilepsy.* J Clin Neurophysiol, 2009. **26**(4): p. 290-3.

83. Hoshi, Y., et al., *Reevaluation of near-infrared light propagation in the adult human head: implications for functional near-infrared spectroscopy.* J Biomed Opt, 2005. **10**(6): p. 064032.

84. Okada, E. and D.T. Delpy, *Near-infrared light propagation in an adult head model. II. Effect of superficial tissue thickness on the sensitivity of the near-infrared spectroscopy signal.* Appl Opt, 2003. **42**(16): p. 2915-22.

85. Wendel, K., et al., *EEG/MEG source imaging: methods, challenges, and open issues.* Comput Intell Neurosci, 2009: p. 656092.

86. Merlet, I., *Dipole modeling of interictal and ictal EEG and MEG paroxysms.* Epileptic Disord, 2001. **Special Issue**: p. 11-36.

87. Assaf, B.A., et al., *Magnetoencephalography source localization and surgical outcome in temporal lobe epilepsy.* Clin Neurophysiol, 2004. **115**(9): p. 2066-76.

88. Shorvon, S.D., E. Perucca, and J. Engel, *Experimental Neurophysiological techniques*, in *The treatment of Epilepsy*. 2009, Wiley-Blackwell: Chichester, UK ; Hoboken, NJ. p. 829-849.

89. Wald, L.L., et al., *Phased array detectors and an automated intensity-correction algorithm for high-resolution MR imaging of the human brain.* Magn Reson Med, 1995. **34**(3): p. 433-9.

90. Goyal, M., et al., *High-resolution MRI enhances identification of lesions amenable to surgical therapy in children with intractable epilepsy.* Epilepsia, 2004. **45**(8): p. 954-9.

91. Ansari, S.F., et al., *Surgery for extratemporal nonlesional epilepsy in adults: an outcome meta-analysis.* Acta Neurochir (Wien), 2010. **152**(8): p. 1299-305.
92. Jayakar, P., et al., *Epilepsy surgery in patients with normal or nonfocal MRI scans: integrative strategies offer long-term seizure relief.* Epilepsia, 2008. **49**(5): p. 758-64.
93. Bernasconi, A., *Quantitative MR imaging of the neocortex.* Neuroimaging Clin N Am, 2004. **14**(3): p. 425-36, viii.
94. Colliot, O., et al., *Individual voxel-based analysis of gray matter in focal cortical dysplasia.* Neuroimage, 2006. **29**(1): p. 162-71.
95. Thesen, T., et al., *Detection of epileptogenic cortical malformations with surface-based MRI morphometry.* PLoS One, 2011. **6**(2): p. e16430.
96. Stephen, Z.R., F.M. Kievit, and M. Zhang, *Magnetite Nanoparticles for Medical MR Imaging.* Mater Today (Kidlington), 2011. **14**(7-8): p. 330-338.
97. Akhtari, M., et al., *Functionalized magnetonanoparticles for MRI diagnosis and localization in epilepsy.* Epilepsia, 2008. **49**(8): p. 1419-30.
98. Gotman, J., et al., *Combining EEG and fMRI: a multimodal tool for epilepsy research.* J Magn Reson Imaging, 2006. **23**(6): p. 906-20.
99. Zijlmans, M., et al., *EEG-fMRI in the preoperative work-up for epilepsy surgery.* Brain, 2007. **130**(Pt 9): p. 2343-53.
100. Kobayashi, E., et al., *Temporal and extratemporal BOLD responses to temporal lobe interictal spikes.* Epilepsia, 2006. **47**(2): p. 343-54.
101. Moeller, F., et al., *EEG-fMRI: adding to standard evaluations of patients with nonlesional frontal lobe epilepsy.* Neurology, 2009. **73**(23): p. 2023-30.
102. Zhao, M., et al., *Focal increases in perfusion and decreases in hemoglobin oxygenation precede seizure onset in spontaneous human epilepsy.* Epilepsia, 2007. **48**(11): p. 2059-67.
103. Boas, D.A., et al., *Can the cerebral metabolic rate of oxygen be estimated with near-infrared spectroscopy?* Phys Med Biol, 2003. **48**(15): p. 2405-18.
104. Boas, D.A., et al., *The accuracy of near infrared spectroscopy and imaging during focal changes in cerebral hemodynamics.* Neuroimage, 2001. **13**(1): p. 76-90.
105. Lareau, E., et al., *Multichannel wearable system dedicated for simultaneous electroencephalographynear-infrared spectroscopy real-time data acquisitions.* J Biomed Opt, 2011. **16**(9): p. 096014.
106. Bahar, S., et al., *Intrinsic optical signal imaging of neocortical seizures: the 'epileptic dip'.* Neuroreport, 2006. **17**(5): p. 499-503.

107. Villringer, A., et al., *Noninvasive assessment of cerebral hemodynamics and tissue oxygenation during activation of brain cell function in human adults using near infrared spectroscopy.* Adv Exp Med Biol, 1994. **345**: p. 559-65.

108. Haginoya, K., et al., *Ictal cerebral haemodynamics of childhood epilepsy measured with near-infrared spectrophotometry.* Brain, 2002. **125**(Pt 9): p. 1960-71.

109. Levesque, M., et al., *High-frequency (80-500 Hz) oscillations and epileptogenesis in temporal lobe epilepsy.* Neurobiol Dis, 2011. **42**(3): p. 231-41.

110. Sampson, A.L., et al., *Beamforming approach to phase-amplitude modulation analysis of multi-channel EEG.* Conf Proc IEEE Eng Med Biol Soc, 2012. **2012**: p. 6731-4.

# ANNEXES

**ANNEXE 1**

***Description des zones et lésions corticales dans l'épilepsie focale (d'après Rosenow et Luders, 2001***

Zone épileptogène : Région corticale générant les crises épileptiques dont la résection est nécessaire et suffisante pour en guérir.

Zone irritative : Région corticale générant les décharges épileptiques intericales.

Zone du début des crises : Zone "pacemaker" au sein de la zone épileptogène dont l'activité paroxystique est à l'origine du déclenchement des crises.

Lésion épileptogène : lésion structurelle ayant un lien causal à l'épilepsie.

Zone symptomatogène ictale : Région corticale responsable des symptômes initiaux de la crise.

Zone de déficit fonctionnel : Région corticale qui est fonctionnellement anormale en période intericale.

Zone éloquente : Région corticale indispensable au maintien de fonctions définies.

L'épilepsie peut être causée (entre autres) par des lésions structurelles épileptogènes (généralement identifiables, mais pas toujours sur une IRM) perturbant l'excitabilité neuronale. Cette perturbation peut résulter en des dépolarisations massives paroxystiques se traduisant par des pointes épileptiques sur l'électroencéphalogramme. Ces pointes épileptiques intericales qui sont brèves (20-200ms) et asymptomatiques (sauf exception) définissent la zone irritative. Une crise épileptique est le résultat d'une décharge neuronale anormale, excessive et soutenue. La « zone du début de la crise » est la zone du cerveau où le seuil épileptogène est le plus bas et dont l'activité anormale déclenche la crise. Cette zone est généralement située au sein de la zone irritative et de plus petite taille. La crise s'accompagne en

général d'un changement comportemental quelconque (subjectif ou objectif, subtil ou évident). Toutefois, la zone symptomatogène peut parfois différer de la zone du début si la crise débute dans une zone cliniquement silencieuse avant de se propager plus loin vers une zone plus parlante. Le substrat à l'origine des crises ou les dommages induits par les crises peuvent également donner un déficit fonctionnel de base se reflétant par des déficits neurologiques ou neuropsychologiques, une dysfonction lente sur l'électroencéphalogramme ou un hypométabolisme sur la tomographie par émission de positons. Lorsqu'une zone de déficit fonctionnel est identifiable par la TEP, celle-ci est généralement plus étendue que la zone du début des crises en raison de la faible résolution spatiale de la technique et d'un phénomène de diaschisis.

Dans la majorité des cas, le site de la lésion épileptogène la zone irritative, la zone de début des crises et la zone de déficit fonctionnel coïncident. On reconnaît toutefois que la zone irritative est généralement plus étendue que ne l'est la zone de début des crises et qu'une guérison des crises peut survenir même si toute la zone irritative n'est pas réséquée. La zone épileptogène est définie par la région corticale générant les crises dont la résection est nécessaire et suffisante pour en guérir. Il s'agit d'une définition plutôt conceptuelle qui ne peut évidemment être validée qu'après la chirurgie.

Au fil des dernières années, le concept de « réseau épileptogène » s'est imposé puisque les crises focales semblent mettre en jeu plusieurs structures corticales soit à son début, soit au cours de son évolution temporelle de manière stéréotypée. Ainsi, la zone épileptogène serait plutôt organisée comme un réseau de structures cérébrales interconnectées interagissant de manière dynamique dans le temps. Une crise surviendrait lorsque la dynamique de ce réseau est suffisamment perturbée pour générer une crise.

Parfois même, les pointes épileptiques intericales peuvent se situer à une distance plus ou moins importante de la zone lésionnelle, voir même au niveau de l'hémisphère controlatéral.

**ANNEXE 2**

***Prevalence of Nonlesional Focal Epilepsy in an Adult Epilepsy Clinic***

**Published by** :
Can J of Neurol Sci 2013 vo. 40 (2). Pp. 198-202

**Dang Khoa Nguyen[1], Manuela Temgoua Mbacfou[2], Dong Bach Nguyen[1], Maryse Lassonde[3]**

*[1]Service de Neurologie, Hôpital Notre-Dame du CHUM,*
*[2]Département de Sciences Biologiques,*
*[3]Centre de Recherche de Neuropsychologie et Cognition, Université de Montréal, Montréal, QC, Canada.*

Running Title: Nonlesional partial epilepsy

**ABSTRACT:**

*Purpose:* To evaluate the prevalence of nonlesional focal epilepsy in an adult epilepsy clinic and its refractoriness to antiepileptic drug therapy.

*Background:* Focal epilepsy is frequently, but not always, associated with structural epileptogenic lesions identifiable on magnetic resonance imaging (MRI).

*Methods:* We analyzed the data from all patients evaluated at an adult epilepsy clinic from January 2002 to December 2011. Clinical and paraclinical findings were used to diagnose focal epilepsy. MRIs were reviewed and classified as normal, with an epileptogenic lesion, or with a lesion of unclear epileptogenicity. Epileptogenic lesions were further categorized as tumours, vascular malformations, gliosis (including hippocampal atrophy/sclerosis), and malformations of cortical development. Our study group included patients with no lesions on MRI. Pharmacoresistance of patients with nonlesional focal epilepsy was assessed using the ILAE and Perucca's criterias. Results: Out of 1521 patients evaluated (mean age 44 years; range 14-93 years), 843 had focal epilepsy. MRI data, available for 806 (96%) subjects, showed epileptogenic lesions in 65%, no obvious epileptogenic lesions in 31% and lesions of unclear epileptogenicity in 4%. MRI-identified lesions included gliosis due to an acquired insult (52% including 17% of hippocampal/sclerosis), tumours (29%), vascular malformations (16%) and malformations of cortical development (10%). Fifty-two percent of nonlesional focal epileptic patients were drug-refractory.

*Conclusion:* In a tertiary epilepsy clinic, close to a third of patients with focal epilepsy were found to be nonlesional, half of which were drug-resistant.

**Key Words:** Nonlesional focal Epilepsy, Magnetic Resonance Imaging, Prevalence, Refractory Epilepsy, Presurgical Evaluation

**RÉSUMÉ: Prévalence de l'épilepsie focale non reliée à une lésion dans une clinique d'épilepsie pour adultes.**

*Objectif :* Le but de l'étude était d'évaluer la prévalence de l'épilepsie focale non reliée à une lésion dans une clinique d'épilepsie pour adultes et sa résistance au traitement par la médication antiépileptique.

*Contexte :* L'épilepsie focale est souvent, mais pas toujours, associée à des lésions épileptogènes structurales identifiables à l'imagerie par résonance magnétique (IRM).

*Méthode :* Nous avons analysé les données des dossiers de tous les patients évalués à une clinique d'épilepsie pour adultes de janvier 2002 à décembre 2011. Les observations cliniques et paracliniques ont été utilisées pour poser un diagnostic d'épilepsie focale. Nous avons révisé les observations d'IRM et nous les avons classifiées comme étant normales, mettant en évidence une lésion épileptogène ou démontrant une lésion dont l'épileptogénicité n'était pas claire. Les lésions épileptogènes étaient ensuite catégorisées comme étant des tumeurs, des malformations vasculaires, de la gliose (dont de l'atrophie ou de la sclérose de l'hippocampe) et des malformations du développement cortical. Notre échantillon de patients comprenait des patients sans lésion à l'IRM. La pharmacorésistance des patients atteints d'une épilepsie focale sans lésion a été évaluée au moyen des critères de l'ILAE et de Perucca.

*Résultats :* Parmi les 1 521 patients évalués, qui étaient âgés de 14 à 93 ans et dont l'âge moyen était de 44 ans, 843 avaient une épilepsie focale. Les données d'IRM, qui étaient disponibles pour 806 patients (96 %), avaient démontré des lésions épileptogènes chez 65 %, pas de lésion épileptogène évidente chez 31 % et des lésions dont l'épileptogénicité était douteuse chez 4 %. Les lésions identifiées à l'IRM étaient de la gliose due à une lésion acquise (52 %, dont 17 % de lésions de l'hippocampe/sclérose), des tumeurs (29 %), des malformations vasculaires (16 %) et des malformations du développement cortical (10 %). Cinquante-deux pour cent des patients atteints d'une épilepsie focale non reliée à une lésion étaient résistants au traitement pharmacologique.

*Conclusion :* Dans une clinique de soins tertiaires de l'épilepsie, l'épilepsie n'était pas reliée à une lésion chez près du tiers des patients atteints d'une épilepsie focale et la moitié d'entre eux étaient pharmacorésistants.

**Mots-clés :** Épilepsie focale non lésionnelle, imagerie par résonance magnétique, prévalence, épilepsie focale réfractaire, évaluation préchirurgicale.

Epilepsy is a chronic condition characterized by recurrent seizures resulting from abnormal and excessive neuronal discharges[1]. It is the most common neurological disorder after stroke with a prevalence of 5-6 per 1,000 in Canada[2]. Each year an average of 15,500 Canadians learn that they have epilepsy. The major form of treatment is long-term drug therapy to which approximately 30% of patients are unfortunately refractory[3]. For these patients, other treatment alternatives include epilepsy surgery or neuromodulation. Seizures can be focal (activation of only part of one cerebral hemisphere) or generalized (more than minimal involvement of both cerebral hemispheres)[4]. Partial or focal epilepsy is the mostcommon form of epilepsy in adults and is frequently associated with an epileptogenic lesion[5]. Magnetic resonance imaging (MRI) is very useful in detecting structural abnormalities related to seizures such as tumours, gliosis/hippocampal sclerosis, malformations of cortical development or vascular malformations. It is not uncommon, however, that brain MRI fails to uncover such epileptogenic lesions. The prevalence of nonlesional epilepsy has been evaluated in some surgical series or during the presurgical evaluation phase but the prevalence of nonlesional focal epilepsy in the setting of an epilepsy clinic is unclear. In this study, we sought to determine the proportion of patients with nonlesional focal epilepsy in our adult epilepsy clinic. A secondary objective was to determine the degree of pharmacoresistance in patients with nonlesional focal epilepsy.

## PATIENTS AND METHODS

### *Patients*

Charts from all patients evaluated by a single epileptologist at an adult tertiary center epilepsy clinic between January 2002 and December 2011 were reviewed. The diagnosis of partial epilepsy was established based on review of all available clinical and paraclinical findings at the time of the study (clinical notes, electroencephalogram (EEG) and neuroimaging findings). The presence of focal spikes on standard EEG for the diagnosis of focal epilepsy as clinical evaluation (ictal semiology, neurological examination, age of onset etc.) and neuroimaging (type of lesion, location of lesion etc.) provided enough evidence to establish the diagnosis of focal epilepsy. Video-EEG was performed only in some subjects if clinically indicated (diagnostic dilemma

or presurgical evaluation). Patients with an unclear epilepsy diagnosis, a single seizure with normal EEG and neuroimaging, acute symptomatic seizures and idiopathic generalized epilepsy were excluded. Epileptic encephalopathies, a heterogenous group of epilepsy syndromes associated with severe cognitive, behavioral and epileptic disturbances in infancy or early childhood (e.g. Lennox-Gastaut syndrome), were excluded as well, even they could present focal seizures. These patients were generally investigated and diagnosed in a pediatric setting before being transferred to our adult epilepsy clinic for continued care. Magnetic resonance imaging was not generally performed or repeated due to lack of cooperation or clinical necessity.

***Magnetic Resonance Imaging***

Magnetic resonance imaging reports from all patients with focal epilepsy were reviewed. The MRIs were obtained using a 1.5T Avanto scanner (Siemens, Germany) or an Achieva Dual 3T system (Philips Medical Systems, Netherlands). All studies included (a) a 3-D T1-weighted gradient-echo acquisition of the whole brain; (b) an axial T2-weighted and fluid-attenuated inversion recovery (FLAIR) acquisitions of the whole brain; (c) coronal T2-weighted and FLAIR acquisitions perpendicular to the longitudinal axis of the hippocampus. Intravenous contrast agents were given only if a mass lesion was demonstrated. In our institution, all brain MRIs are reviewed by a group of four neuroradiologists experienced in interpreting epilepsy studies. Some clinical information was available on the MRI request form. Upon review of MRI interpretation, reported potentially epileptogenic lesions were classified into five categories: tumours (e.g. gliomas, gangliogliomas, dysembryoplastic neuroectodermal tumors), vascular malformations (e.g. cavernomas, arteriovenous malformations), gliosis from an acquired insult (including hippocampal atrophy and sclerosis), malformations of cortical development (e.g. cortical dysplasia, heterotopias, polymycrogyria) and others. Patients were considered to have nonlesional focal epilepsy if the MRI failed to disclose an epileptogenic lesion. Patients with MRI lesions not expected to give epilepsy (Chiari type 1, pineal cyst, septum pellucidum etc.) were included in this group. Diffuse cerebral or cerebellar atrophy, non-specific white matter changes, leukoaraiosis and arachnoid cysts were classified as lesions of unclear relationship to the patient's epileptic condition.

***Pharmacoresistance***

Response to medical treatment was assessed for all patients with nonlesional focal epilepsy. Patients were considered to be drug-resistant if they continued to have seizures despite two adequate antiepileptic drug (AED) trials whether used in monotherapy or in combination[6]. We also graded the degree of drug-resistance using the classification proposed by Perucca[7].

This study was approved by our institutional ethics committee.

**RESULTS**

***MRI of focal epilepsy patients***

Out of 1521 patients (mean age 44 years; range 14-93) evaluated at the epilepsy clinic between January 2002 and December 2011, 1051 (69%) had epilepsy. Among these patients, 843 (80%) were diagnosed with focal epilepsy, 130 (12%) with idiopathic generalized epilepsy, 61 (6%) with an epileptic encephalopathy and 17 (2%) with an unclear epileptic syndrome. While 37 subjects did not or could not undergo an MRI study, the majority of patients with focal epilepsy (806/843; 96%) did. In these 806 remaining patients with focal epilepsy, MRI disclosed a clear epileptogenic lesion in 520 (65%), no obvious epileptogenic lesion in 251 (31%), and lesions of unclear epileptogenicity in 35 (4%) (Figure1).

Among the 520 patients with an epileptogenic lesion, 153 (29%) had a tumour, 82 (16%) had a vascular malformation, 54 (10%) had a malformation of cortical development and 219 (42%) had gliosis due to an acquired insult. Included in this latter group were 86 (17%) patients with hippocampal atrophy/ sclerosis.

***Pharmacoresistance***

Out of 251 patients with nonlesional epilepsy, 131 (52%) were medically intractable according to the ILAE classification. Using Perucca's classification, 176 were drug-

resistant: 45 (26%) patients were refractory to one AED (grade I), 30 (17%) to two (grade II) and 101 (57%) to 3 or more (grade III).

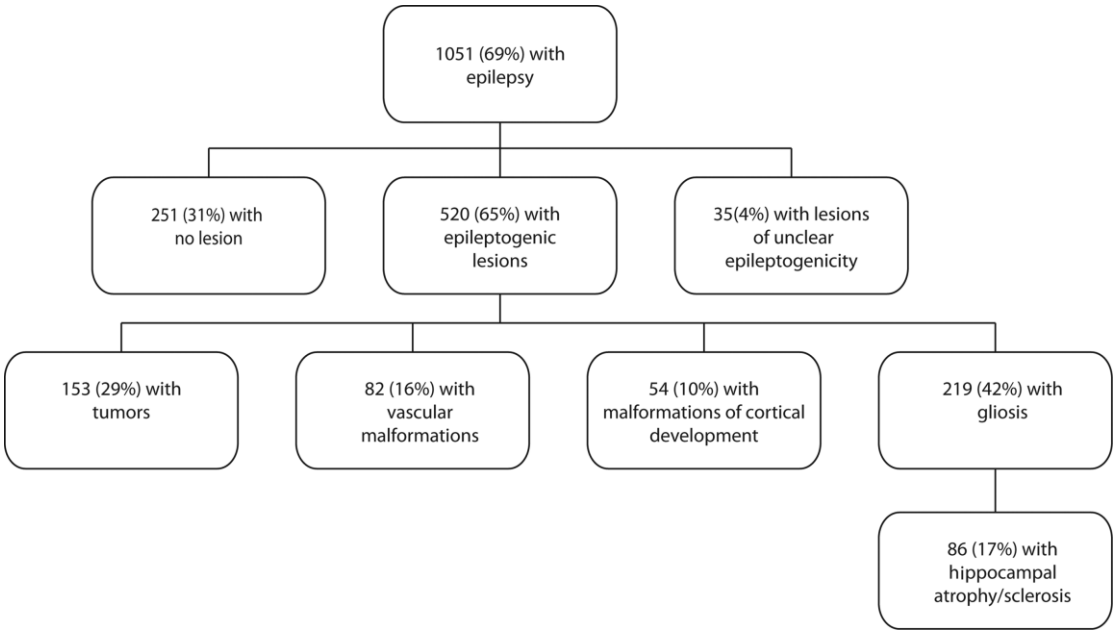


Figure 1. MRI findings in patients with focal epilepsy.

## DISCUSSION

Our study showed that, in nearly one third of patients with focal epilepsy in an adult epilepsy clinic, no clear epileptogenic lesions on MRI are seen. Many patients have some difficulty grasping the notion that focal epilepsy can occur without a structural lesion identifiable on MRI. One possible explanation for the lack of an apparent epileptogenic lesion is that an underlying lesion is present but is so subtle that it is undetected by standard MRI.

This is supported by histopathological studies of resected epileptogenic tissue in patients with normal standard MRIs which have revealed subtle cortical dysplasias or gliosis or hippocampal sclerosis[8-18]. Another potential explanation is that focal seizures are related to a genetic defect. This is supported by recent findings indicating that some partial epilepsies have a significant genetic component[19-24].

The prevalence of nonlesional focal epilepsy found in our epilepsy clinic is relatively in line with prior studies found in the literature. Prior series, using mostly standard

field MRIs, have mainly been dealt with three other slightly different subsets of populations: a) patients with refractory focal epilepsy being investigated for epilepsy surgery (presurgical investigation series); b) patients with refractory epilepsy who were operated (surgical series); and c) patients with refractory focal epilepsy who underwent an intracranial EEG study (invasive EEG series). In presurgical investigation series, the rate of nonlesional cases was lower (range from 15-23%) which is to be expected as not all focal epilepsy patients are drug-refractory and require further investigation for epilepsy surgery. For example, Scott et al (1999) reported that 40/222 (18%) of drug-resistant patients undergoing video-EEG for epilepsy surgery investigation had a normal MRI[25]. In another study by Berg et al (2003), 130/565 (23%) candidates for epilepsy surgery had normal MRI findings[26]. In Bien et al (2009), 190/1192 (16%) patients undergoing comprehensive presurgical assessment for intractable epilepsy had a negative MRI[14]. These nonlesional rates in presurgical investigation series are close to those reported in surgical series. Hence, in temporal lobe epilepsy surgery series, Berkovic et al (1995) reported that 24/135 (18%) patients undergoing an anterior temporal lobectomy had a normal MRI[27]. In a controlled randomized trial of surgery for temporal lobe epilepsy, Wiebe et al (2001) had 13/80 (16%) patients with normal MRI[28]. In Bell et al (2009), 44/272 (16%) patients with medically refractory temporal lobe epilepsy who had undergone an anterior temporal lobectomy were nonlesional[11]. Finally, in a study by Alarcon et al (2006), 21/136 (15%) operated patients had nonlesional epilepsy[29]. As for extratemporal lobe epilepsy series, an outcome meta-analysis of adult patients operated for nonlesional extratemporal lobe epilepsy found that 25/61 (19%) MRIs were normal[16]. These relatively comparable rates are, however, contrasted by the data collected by Berg et al (2003) in a multicenter study of epilepsy surgery in which 58/396 (45%) patients undergoing resective surgery had normal MRI findings[26]. Possible explanations include its prospective design, the academic setting (epilepsy surgery centers of reference) and earlier study years (1996-2001). Finally, when looking at invasive EEG series, one can observe with no surprise a very high rate of nonlesional focal epilepsy as implantation of intracranial electrodes are more often required in nonlesional than in lesional epilepsies. For example, Cukiert et al (2001) reported that 10/16 (62.5%) patients with refractory extratemporal epilepsy

investigated with subdural electrodes had normal MRI[30]. In a larger series of 100 patients undergoing stereoencephalography, 43 (43%) also had a normal MRI[31].

A normal MRI is not synonymous with self-limited or pharmacosensitive epilepsy. In our series, 52% of patients were drug-resistant according to the recent ILAE criteria, including 57% refractory to three or more antiepileptic drugs.

The limitations of our study are inherent to any retrospective design. Because MRI scans were not standardized in terms of magnet strength, one could argue that our rate of nonlesional focal epilepsy would have been lower had all patients benefited from a 3T MRI since high-field MR scanners provide an improved signal-to-noise ratio which can theoretically allow the detection of subtle lesions missed on standard 1.5T MRIs[32]. In a previous study however, we showed that re-imaging at 3T patients with refractory epilepsy and negative 1.5T MRIs only allowed the detection of 5.6% more lesions[33]. Of course, we also have to take into account the issue of radiologist intra and interater variability. Recent development of quantitative MRI postprocessing methods applied to digital data image may improve the detection of occult lesions not readily recognizable by visual analysis alone, in addition to reducing intra and interrater variability[34]. Finally, selecting patients from a specialized epilepsy clinic in a tertiary academic center may have biased the study into finding a higher rate of surgically challenging cases of nonlesional focal epilepsy cases or of lesions associated with intractable epilepsy. Hence, our numbers cannot necessarily be generalized outside the adult epilepsy clinic setting that typically deals with more complex and difficult to treat epilepsies than in general Neurology practices. Despite limitations mentioned above, our data helps to give a certain idea of the number of nonlesional cases encountered in the epilepsy clinic, not only for neurology and radiology colleagues or residents but, more importantly, for the patients themselves. Knowing that approximately a third of patients in the clinic are in the same situation is somewhat reassuring for them. In the near future, it may be interesting to test patients identified in this series for all mutations known to be associated with epilepsy and use advanced quantitative MRI postprocessing techniques to assess how many occult lesions might have been missed.

## CONCLUSIONS

In an adult epilepsy clinic setting, close to a third of patients with focal epilepsy have no obvious epileptogenic lesion on MRI, and more than half of these are drug-resistant.

## REFERENCES

1. Dichter MA. Overview: the neurobiology of epilepsy. In: Engel J, Pedley TA, editors. Epilepsy: a comprehensive textbook. 2nd ed. Philadelphia: Lippincott Williams and Wikins; 2008. p. 217-19.

2. Tellez-Zenteno JF, Pondal-Sordo M, Matijevic S, Wiebe S. National and regional prevalence of self-reported epilepsy in Canada. Epilepsia. 2004;45(12):1623-9.

3. Kwan P, Brodie MJ. Early identification of refractory epilepsy. N Engl J Med. 2000;342(5):314-19.

4. Berg AT, Berkovic SF, Brodie MJ, et al. Revised terminology and concepts for organization of seizures and epilepsies: report of the ILAE Commission on Classification and Terminology, 2005- 2009. Epilepsia. 2010;51(4):676-85.

5. Woermann FG, Vollmar C. Clinical MRI in children and adults with focal epilepsy: a critical review. Epilepsy Behav. 2009;15(1): 40-9.

6. Kwan P, Arzimanoglou A, Berg AT, et al. Definition of drug resistant epilepsy: consensus proposal by the ad hoc Task Force of the ILAE Commission on Therapeutic Strategies. Epilepsia. 2010;51(6):1069-77.

7. Perucca E. The management of refractory idiopathic epilepsies. Epilepsia. 2001;42(3):31-5.

8. Sylaja PN, Radhakrishnan K, Kesavadas C, Sarma PS. Seizure outcome after anterior temporal lobectomy and its predictors in patients with apparent temporal lobe epilepsy and normal MRI. Epilepsia. 2004;45(7):803-8.

9. Chapman K, Wyllie E, Najm I, et al. Seizure outcome after epilepsy surgery in patients with normal preoperative MRI. J Neurol Neurosurg Psychiatry. 2005;76(5):710-13.

10. Cohen-Gadol AA, Wilhelmi BG, Collignon F, et al. Long-term outcome of epilepsy surgery among 399 patients with nonlesional seizure foci including mesial temporal lobe sclerosis. J Neurosurg. 2006;104(4):513-24.

11. Bell ML, Rao S, So EL, et al. Epilepsy surgery outcomes in temporal lobe epilepsy with a normal MRI. Epilepsia. 2009;50 (9):2053-60.

12. RamachandranNair R, Otsubo H, Shroff MM, et al. MEG predicts outcome following surgery for intractable epilepsy in children with normal or nonfocal MRI findings. Epilepsia. 2007;48(1): 149-57.

13. Jayakar P, Dunoyer C, Dean P, et al. Epilepsy surgery in patients with normal or nonfocal MRI scans: integrative strategies offer long-term seizure relief. Epilepsia. 2008;49(5):758-64.

14. Bien CG, Szinay M, Wagner J, Clusmann H, Becker AJ, Urbach H.
Characteristics and surgical outcomes of patients with refractory magnetic resonance imaging-negative epilepsies. Arch Neurol. 2009;66(12):1491-9.

15. Wetjen NM, Marsh WR, Meyer FB, et al. Intracranial electroencephalography seizure onset patterns and surgical outcomes in nonlesional extratemporal epilepsy. J Neurosurg. 2009;110(6):1147-52.

16. Ansari SF, Tubbs RS, Terry CL, Cohen-Gadol AA. Surgery for extratemporal nonlesional epilepsy in adults: an outcome metaanalysis. Acta Neurochir. 2010;152(8):1299-305.

17. Funke ME, Moore K, Orrison WW, Jr., Lewine JD. The role of magnetoencephalography in "nonlesional" epilepsy. Epilepsia. 2011;52(4):10-14.

18. Smith AP, Sani S, Kanner AM, et al. Medically intractable temporal lobe epilepsy in patients with normal MRI: surgical outcome in twenty-one consecutive patients. Seizure. 2011;20(6):475-9.

19. Steinlein OK, Mulley JC, Propping P, et al. A missense mutation in the neuronal nicotinic acetylcholine receptor alpha 4 subunit is associated with autosomal dominant nocturnal frontal lobe epilepsy. Nat Genet. 1995;11(2):201-3.

20. Kalachikov S, Evgrafov O, Ross B, et al. Mutations in LGI1 cause autosomal-dominant partial epilepsy with auditory features. Nat Genet. 2002;30(3):335-41.

21. Scheffer IE, Phillips HA, O'Brien CE, et al. Familial partial epilepsy with variable foci: a new partial epilepsy syndrome with suggestion of linkage to chromosome 2. Ann Neurol. 1998; 44(6):890-9.

22. Xiong L, Labuda M, Li DS, et al. Mapping of a gene determining familial partial epilepsy with variable foci to chromosome 22q11-q12. Am J Hum Genet. 1999;65(6):1698-710.

23. Berkovic SF, Kennerson ML, Howell RA, Scheffer IE, Hwang PA, Nicholson GA. Phenotypic expression of benign familial neonatal convulsions linked to chromosome 20. Arch Neurol. 1994;51(11):1125-8.

24. Cendes F, Lopes-Cendes I, Andermann E, Andermann F. Familial temporal lobe epilepsy: a clinically heterogeneous syndrome. Neurology. 1998;50(2):554-7.

25. Scott CA, Fish DR, Smith SJ, et al. Presurgical evaluation of patients with epilepsy and normal MRI: role of scalp video-EEG telemetry. J Neurol Neurosurg Psychiatry. 1999;66(1):69-71.

26. Berg AT, Vickrey BG, Langfitt JT, et al. The multicenter study of epilepsy surgery: recruitment and selection for surgery. Epilepsia. 2003;44(11):1425-33.

27. Berkovic SF, McIntosh AM, Kalnins RM, et al. Preoperative MRI predicts outcome of temporal lobectomy: an actuarial analysis. Neurology. 1995;45(7):1358-63.

28. Wiebe S, Blume WT, Girvin JP, Eliasziw M. Effectiveness, Efficiency of Surgery for Temporal Lobe Epilepsy Study G. A randomized, controlled trial of surgery for temporal-lobe epilepsy. N Engl J Med. 2001;345(5):311-18.

29. Alarcon G, Valentin A, Watt C, et al. Is it worth pursuing surgery for epilepsy in patients with normal neuroimaging? J Neurol Neurosurg Psychiatry. 2006;77(4):474-80.

30. Cukiert A, Buratini JA, Machado E, et al. Results of surgery in patients with refractory extratemporal epilepsy with normal or nonlocalizing magnetic resonance findings investigated with subdural grids. Epilepsia. 2001;42(7):889-94.

31. McGonigal A, Bartolomei F, Regis J, et al. Stereoelectroencephalography in presurgical assessment of MRI-negative epilepsy. Brain. 2007;130(Pt 12):3169-83.

32. Phal PM, Usmanov A, Nesbit GM, et al. Qualitative comparison of 3-T and 1.5-T MRI in the evaluation of epilepsy. AJR Am J Roentgenol. 2008;191(3):890-5.

33. Nguyen DK, Rochette E, Leroux JM, et al. Value of 3.0 T MR imaging in refractory partial epilepsy and negative 1.5 T MRI. Seizure. 2010;19(8):475-8.

34. Bernasconi A, Bernasconi N, Bernhardt BC, Schrader D. Advances in MRI for 'cryptogenic' epilepsies. Nat Rev Neurol. 2011;7(2): 99-108.

**ANNEXE 3**

***EEG-fMRI Adding to standard evaluations of patients with nonlesional frontal lobe epilepsy***

**Published by**:
Neurology® 2009;73:2023–2030 by AAN Enterprises, Inc. 2023

**F. Moeller[1], L. Tyvaert[1], D.K. Nguyen[2], P. LeVan[1], A. Bouthillier[2], E. Kobayashi[1], D. Tampieri[1], F. Dubeau[1], J. Gotman[1].**

*[1]Montreal Neurological Institute and Hospital, McGill University;*
*[2]Hôpital Notre-Dame (CHUM), University of Montreal, Montreal, Canada.*

Running title: EEG-fMRI in non lesional frontal lobe epilepsy

Keywords: BOLD blood oxygen level dependent; FLE frontal lobe epilepsy; fMRI functional MRI; HFR hemodynamic response function; IED interictal epileptiform discharges; TE echo time; TR repetition time.

**ABSTRACT**

*Purpose:* In patients with non lesional frontal lobe epilepsy (FLE) the delineation of the epileptogenic zone is difficult. Therefore these patients are often not considered for surgery due to an unclear seizure focus. The aim of this study was to investigate whether EEG-fMRI can add useful information in the pre-operative evaluation of these patients.

*Methods:* Nine non lesional FLE patients were studied with EEG-fMRI using a 3T scanner. Spike related blood oxygen level dependent (BOLD) signal changes were compared to the topography of the spikes and to PET and SPECT results if available. The structural MRIs were reviewed for subtle abnormalities in areas that showed BOLD responses. For operated patients, post-operative resection and histology were compared to BOLD responses.

*Results:* Concordance between spike localisation and positive BOLD response was found in 8 patients. PET and SPECT investigations corresponded with BOLD signal changes in 4 of 5 investigations. In two cases, reviewing the structural MRI guided by EEG-fMRI data resulted in considering suspicious a deep sulcus that had not been noticed before. Two patients were operated. In one, the resected cortex corresponded with the suspicious sulcus and the fMRI results and histology showed cortical dysplasia. In another, histology revealed an extended microdysgenesis not visible on structural MRI. EEG-fMRI had shown activation just adjacent to the resected pathological area.

*Conclusions:* Our study provides different levels of support (topography, concordance with PET and SPECT, structural peculiarities, post-operative histology) that EEG-fMRI may help to delineate the epileptic focus in patients with non lesional FLE, a very challenging group in the pre-operative evaluation.

## INTRODUCTION

Approximately one third of all patients with epilepsy are pharmaco-resistant (Schuele and Luders 2008). In a selected subset of those patients, epilepsy surgery may lead to seizure freedom (Tellez-Zenteno et al. 2005). A condition precedent to surgery is the localisation and delineation of the epileptogenic zone. Especially in patients with frontal lobe epilepsy (FLE), this identification may be difficult: FLE is often characterized by a widespread epileptogenic zone, rapid spreading of ictal EEG changes, large areas inaccessible to scalp EEG and a variety of seizure semiologies. In addition, functional imaging techniques such as positron emission tomography (PET) and single photon emission computed tomography (SPECT) have their limitations in FLE. In extratemporal lobe epilepsy, normal PET scans are more frequently found than in mesial temporal lobe epilepsy (Ryvlin et al. 1998). If the MRI is normal, only 35-45 percent of the patients with FLE show abnormalities in PET investigations (Ryvlin et al. 1998, Kim et al. 2002). For ictal SPECT studies, an injection of the tracer within first 20 seconds is crucial (Lee et al. 2006). Even with a short injection time, the tracer lags behind seizure onset on EEG and may already represent spread pattern given the rapid propagation in FLE (Dupont et al. 2006). Furthermore, a SPECT investigation is impossible in many FLE patients due to very brief seizures. These limitations explain why surgical intervention for FLE are often less successful than for temporal lobe epilepsy, especially in non lesional cases (Jeha et al. 2007, Lee et al. 2008). The most important reason for this unfavourable outcome is the inherent complexity of identifying the epileptogenic zone. In this difficult situation, alternative approaches for evaluating patients with FLE are needed. Combined functional magnetic imaging (fMRI) and EEG recording is a non-invasive method that allows to map brain areas involved in interictal epileptiform discharges (IED) as well as in seizures (for review see Laufs and Duncan 2007, Gotman 2008). In the past years, EEG-fMRI studies have largely contributed to the understanding of pathophysiological mechanisms of epilepsy. However, the value for a clinical approach has scarcely been addressed. A recent study shows that EEG-fMRI may add useful information in the preoperative workup (Zijlmans et al. 2007). The aim of this study was to evaluate the yield of EEG-fMRI in non lesional FLE patients, a group that is often rejected for surgery due to an unclear seizure focus.

## METHODS

### Subjects

From April 2007 to November 2008 9 patients with non lesional FLE were recruited from the Montreal Neurological Hospital and the Service de Neurologie, Hôpital Notre-Dame du CHUM, Université de Montréal to participate in an EEG-fMRI study. The diagnosis of FLE was based on EEG findings and clinical semiology. Inclusion criteria were a normal MRI and frequent IED in previously recorded EEGs. Patients participated in the research study after giving their written informed consent, according to a protocol approved by the ethics committee of the Montreal neurological Institute and Hospital. All EEG-fMRI recordings were done following the same protocol. We did not try to induce seizures and no sleep deprivation or drug reduction was performed specifically for the test. During the investigation the patients were monitored by a video camera to detect clinical signs related to seizures.

**Standard protocol and approvals, registrations, and patient consent.** The study was approved by the institutional research ethics board. All patients gave their written informed consent.

### EEG acquisition

The EEG acquisition was always performed with 25 MR compatible electrodes (Ag/AgCl) placed on the scalp using the 10-20 (21 usual electrodes without Fpz and Oz) and 10-10 (F9, T9, P9, F10, T10 and P10) electrode placement systems. The reference electrode was at FCz. Two electrodes located on the back recorded the electrocardiogram (ECG). To minimize movement artifacts and for patient's comfort, the head was immobilized with a pillow filled with foam microspheres (Siemens, Germany). Data were transmitted from a BrainAmp amplifier (Brain Products, Munich, Germany, 5 kHz sampling rate) via an optic fiber cable to the EEG monitor located outside the scanner room.

**fMRI acquisition**

Functional images were acquired using a 3 T MR scanner (Siemens, Trio, Germany). A T1 weighted anatomical acquisition was first done (1 mm slice thickness, 256 x 256 matrix; for the 1.5 T: TE= 9.2 ms and TR= 22 ms; for the 3 T: TE= 7.4 ms and TR= 23 ms; flip angle 30°) and used for superpositon with the functional images. The functional data were acquired in series of 6-14 runs of 6 min each using a T2* weighted EPI sequence (voxel dimensions 5 x 5 x 5mm, 25 slices, 64 x 64 matrix; for the 1.5 T: TE= 50 ms and TR= 3 s; for the 3 T: TE= 30 ms and TR=1750 ms; flip angle 90°). The patients were at rest during the two hours of recording session. No sedation was given.

**EEG processing**

Brain Vision Analyser software (Brain Products, Munich, Germany) was used for off-line correction of the gradient artifact and filtering of the EEG signal. This software uses the method described by Allen et al. (2000). It is based on the subtraction of the average signal obtained during the interval of the scanner artifact. A 50 Hz low-pass filter was also applied to remove the remaining artifact. The ballistocardiogram (BCG) artifact was removed by independent component analysis (ICA) (Bénar et al., 2003).

A neurologist reviewed the entire EEG recording and selected the IED. Electrical events with clinical changes similar to those observed during typical clinical seizures were defined as ictal. The expert put markers corresponding to interictal and ictal events (timing and duration).

**fMRI processing**

The EPI images were motion corrected and smoothed (6 mm full width at half maximum) using the software package from the Brain Imaging Center of the Montreal Neurological Institute (http://www.bic.mni.mcgill.ca/software/). Temporal autocorrelations were accounted for by fitting an AR model of order 1 according to the methods of Worsley et al. (2002), and low frequency drifts in the signal were modeled with a third-order polynomial fitted to each run. A regressor for each type of interictal spike and a regressor for ictal events (ictal events were grouped if they were similar) were built using the timing and duration of each event and convolved with

four hemodynamic response functions (HFRs) with peaks at 3, 5, 7 and 9 s (Bagshaw et al., 2004). All these regressors were included in the same general linear model. A statistic t-map was obtained for each regressor using the other regressors as confounds (a study was performed for each type of interictal event and for the group of similar ictal discharges) in the fMRI analysis (fMRIstat, Worsley et al., 2002). At each voxel, the maximum t-value was taken from the four individual t-maps created with the four HRFs.

The EPI frames were realigned together using a linear 6-parameter rigid-body transformation (3 translations and 3 rotations) to correct for movement effects. The 6 parameters used for the realignment were also integrated in the analysis as confound regressors in the general linear model to account for residual movement artifacts.

**EEG-fMRI analysis**

To be significant, a response needed to have a minimum of five contiguous voxels with a t= 3.1, corresponding to $p<0.05$ corrected for the multiple comparisons resulting from the number of voxels in the brain and the use of four HRFs. The t-map results were represented using red-yellow scale corresponding to positive BOLD changes (activation) and blue-white scale to negative BOLD changes (deactivation).

**Evaluation of the BOLD signal changes *IED topography*:**

A BOLD response was considered to be within the EEG focus if it corresponded with the voltage map determined by BESA (Brain Electrical Source Analysis, Megis Software GmbH, Graefling, Germany) through voltage maps of the IEDs.

***PET and SPECT***: In patients where interictal FDG-PET, interictal and ictal $^{99m}$Tc-ECD SPECT investigations were performed, the BOLD signal changes were compared to the PET and SPECT results.

***Structural MRI***: The structural MRIs were re-reviewed by a neuroradiologist expert in epilepsy (D.T.) for subtle structural abnormalities in areas of BOLD signal changes. The structural MRIs based on an epilepsy protocol were acquired prior to the fMRI study and included T1, T2, T2*, flair and apparent diffusion coefficient sequences.

***Post-operative validation**:* In patients that were operated after the EEG-fMRI study the resected area and its histology were compared to the BOLD signal changes.

## RESULTS

### EEG recordings during fMRI

For every patient we recorded one type of IED; two patients (pts 2 and 4) additionally showed brief seizures during the same recording (table 2). The number of IED recorded during the fMRI session ranged from 9 to 744. Compared to the EEG recorded outside the scanner, the interictal events selected during scanning were similar for every patient (table 1 and 2).

Two patients had several ictal events. Patient 2 had 26 similar short seizures with movements of the legs. Patient 4 presented 15 similar events with a feeling of fear and the necessity to take a deep breath (visible on the online video).

Table 1. Characteristics of the patients: clinical and electrographic features recorded outside the MRI R: right, L: left, sz: seizure, GTCS: generalized tonic clonic seizure, AED: antiepileptic drug, LTG: Lamotrigine, CBZ: Carbamazepine, CBZ: Clobazam, VPA: Valproic acid, PHT: Phenytoin, TPM: Topiramate, LEV: Levetiracetam, PB: Phenobarbital

| *Patient* | *Age/onset (years)/sex* | *Seizure semiology* | *Video EEG monitoring* | *AED* |
|---|---|---|---|---|
| 1 | 24/4/F | **Nocturnal:** choking sensation, moaning, turning to L | **Interictal:** sw focus F3, less frequent F4<br>**Ictal:** seizure onset Fp1, F3 | LTG, CBZ, CLB |
| 2 | 20/5/M | **Nocturnal:** tonic sz, sometimes more predominant R,<br>**Daytime:** atypical absences | **Interictal:** sw focus frontal left with secondary generalization, less frequent frontal R<br>**Ictal:** atypical absences: bifrontal spike wave, nocturnal tonic seizure: polyspike without lateralisation | CLB, LTG, CBZ, VPA |
| 3 | 41/35/M | **Daytime:** Aura, flush in the face, rarely manual automatisms, secondary generalisation | **Interictal:** sw focus FL and FR<br>**Ictal:** sw frontotemporal R or bifrontal | PHT, TPM |
| 4 | 11/4/M | **Daytime:** Auras of fear, vocalisation, left ocular and head deviation | **Interictal:** R F spike-waves isolated or organized in short burst.<br>**Ictal:** Prolonged bursts of rhythmic bilateral F spike-waves with a clear R predominance | VPA, PHT |
| 5 | 31/?/M | **Nocturnal:** dystonic posturing and cloni of the left arm | **Interictal:** RF spikes<br>**Ictal:** generalized sharp wave, more predominat on FR | CBZ, CLB, LEV |
| 6 | 22/11/F | atypical absences, GTCS | **Interictal:** RF and LF spikes<br>**Ictal:** no lateralisation, posticta l: slowing and sw frontal L | CLB, CBZ, LTG |
| 7 | 30/6/F | **Nocturnal:** awakening, movement of limbs, raises her body | **Interictal:** LF spikes<br>**Ictal:** bilat frontocentral activity | CLB, CBZ |
| 8 | 18/17/F | **Nocturnal:** awakening: screams, dystonic posturing L arm | **Interictal:** RF spikes (frequent) LF spikes (infreuqent)<br>**Ictal:** sw frontocentral R | PB, CBZ, CLB |
| 9 | 16/0.5/M | Brief head deviation to the left with dystonic posturing of the right hand, left sided headache | **Interictal:** LF sharp slow wave with frequent generalisation<br>**Ictal:** no clear seizure onset<br>posticta l: slowing more on frontal L | LTG, TPM, LEV |

Table 2. fMRI results, PET and SPECT results, re-evaluation of structural MRI, operation, and histologysw: sharp wave, R: right, L: left.

| *Patient* | *events during fMRI (number)* | *fMRI activation* | *fMRI deactivation* | *PET / SPECT* | *Re-evaluation structural MRI* | *Operation / histology* |
|---|---|---|---|---|---|---|
| 1 | **Interictal**: sw Fp1, F3 (31) | L. middle frontal gyrus (max)<br>Left anterior cingulum, thalamus | Default mode | **PET:** no clear results | Suspicious deep left middle frontal sulcus | — |
| 2 | **Interictal:** Sw F3 (26)<br><br>**Ictal:** polyspike without lateralisation (25 seizures) duration 7.7 to58.6s | **Interictal:** L. superior and middle frontal gyrus (max)<br><br>**Ictal:** same as interictal but more extended including left cingulate gyrus and parietal left | **Interictal:** Thalamus<br><br>**Ictal**: Thalamus, occipital, frontobasal, parietal | **PET**: normal<br>**Interictal SPECT:** hypoperfusion frontal R and L<br>**Ictal SPECT:** hyperperfusion prefrontal L, paramedian L<br>**Subtraction SPECT:** Focus frontal L | Normal | L. frontoparamedial resection, histology: microdysgenesis |
| 3 | **Interictal:** sw Fp2, F8, T4 (19) | R. frontopolar and frontomesial (max) | Default mode | **SPECT:** no clear result | Normal | — |
| 4 | **Interical:** Sw F4, F8 (31)<br><br>**Ictal:** R F rhythmic spike and waves (15 seizures) duration 7.2 to 49.7 s | **Interictal and ictal:** R. frontopolar cortex | **Interical:** None<br><br>**Ictal:** orbitofrontal, posterior cingulate, | **PET:** hypometabolism frontal R<br>**Ictal SPECT**: hyperperfusion frontal R | Suspicious deep right middle frontal sulcus | Limited right frontal corticetomy , histology: dysplasia |
| 5 | **Interictal:** sw F4 F8 (27) | R. inferior frontal gyrus (max), bilat frontobasal | Default mode | No **PET** or **SPECT** | Normal | — |
| 6 | **Interictal:** sw F3, Fp1, Fp2 (45) | L. superior frontal gyrus (max) | Thalamus | No **PET** or **SPECT** | Normal | — |
| 7 | **Interictal:** sw F3, F7 (744) | Bilateral motorcortex | Precuneus | **PET**: no clear results<br>**Interictal SPECT:** hypoperfusion frontoparietal L<br>**Ictal SPECT**: hyperperfusion frontal L<br>**Subtraction SPECT:** Focus frontal L | Normal | — |
| 8 | **Interictal:** sw F8 (9) | R. anterior cing. (max), Thalamus | Caudate nuclei | No **PET** or **SPECT** | Normal | — |
| 9 | **Interictal:** sw F3, Fz (540) | L. frontomesial (max),<br>L frontolateral, bilateral parietal L>R | Default mode, caudate nuclei | **SPECT:** no results<br>**PET:** hypometabolism L frontal, parietal and temporal | Normal | — |

**BOLD responses**

**Interictal events:**

A BOLD response was observed in every study (figures 1-3 and supplementary figure). All patients showed positive BOLD responses. Negative BOLD signal changes were found in all studies except for patient 4 in whom negative BOLD responses were only observed for ictal but not for interictal events. The maximum of the BOLD activation corresponded well with the spike topography of the IED in all but one patient (pt 7, fig. 3). Less significant activations were found in the thalamus (pts 1, 8 and 9 in fig. 3 and suppl. fig.), and extended on frontolateral and bilateral parietal areas (pt 9, fig. 3). Negative BOLD signal changes were topographically not related to the IED and were seen in default mode areas (pts 1, 3, 5 and 9, fig. 3 and suppl. fig.), the caudate nuclei (pts 8 and 9, fig. 3 and suppl. fig) and the thalamus (pts 2, 6 and 7, fig 1, 3 and suppl. fig.).

**Ictal events**: In two patients (pt 2 and 4, fig 1 and 2) additionally to IED, seizures were recorded. Both positive and negative BOLD signal changes were found. The maximum of seizure related positive BOLD response corresponded well with the maximum of IED related activation. For patient 2 the ictal BOLD responses were more extended: while IED related BOLD signal increases were restricted to the left superior and middle frontal gyrus, ictal events additionally showed BOLD signal increases in the left cingulate gyrus and the left parietal cortex. Negative BOLD responses were also more widespread. Where IED had only shown some deactivation within the thalamus, ictal events were accompanied by occipital, frontobasal and parietal deactivation in addition to thalamic deactivation. For patient 4 the maximum of seizure related activation remained confined to the anterior cingulate gyrus as revealed by IED. Additional activation was found in the thalamus and adjacent to the ventricles. A negative response was observed in orbitofrontal areas, in the posterior cingulate, the superior parietal cortex, frontal areas and occipital regions.

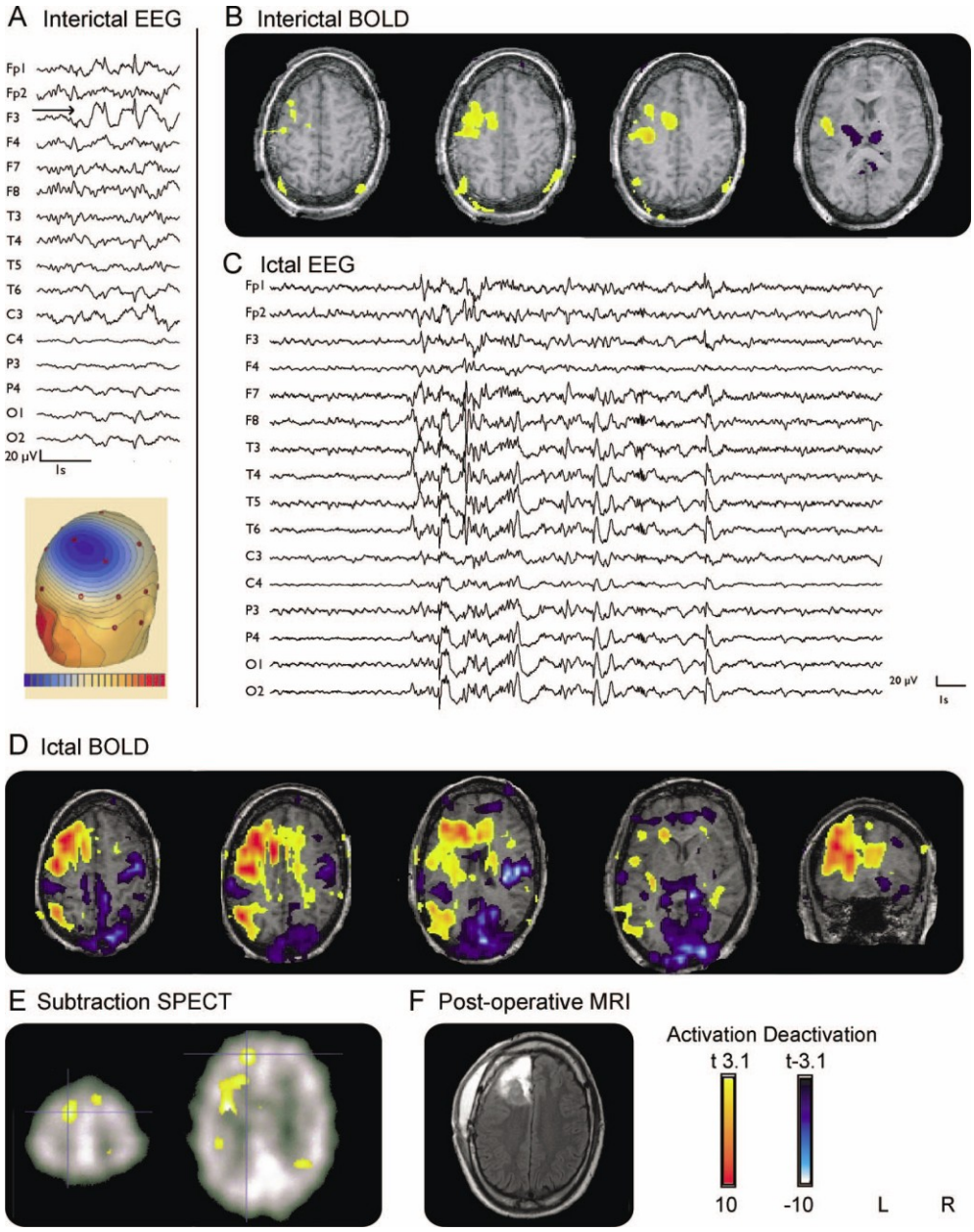


Figure 1 Patient 2.
(A) Interictal EEG (average montage): focus F3. (B) Interictal functional MRI (fMRI): positive blood oxygen level dependent BOLD) response: left superior and middle frontal gyri; negative BOLD response: thalamus. (C) Ictal EEG: polyspikes without lateralization. (D) Ictal fMRI: positive BOLD responses same as interictal but more extended including left cingulate gyrus nd left parietal; negative BOLD response: thalamus, occipital, frontobasal, parietal. (E) Subtraction of interictal and ictal SPECT showing a left frontal focus. (F) Postoperative MRI after frontoparamedian resection.

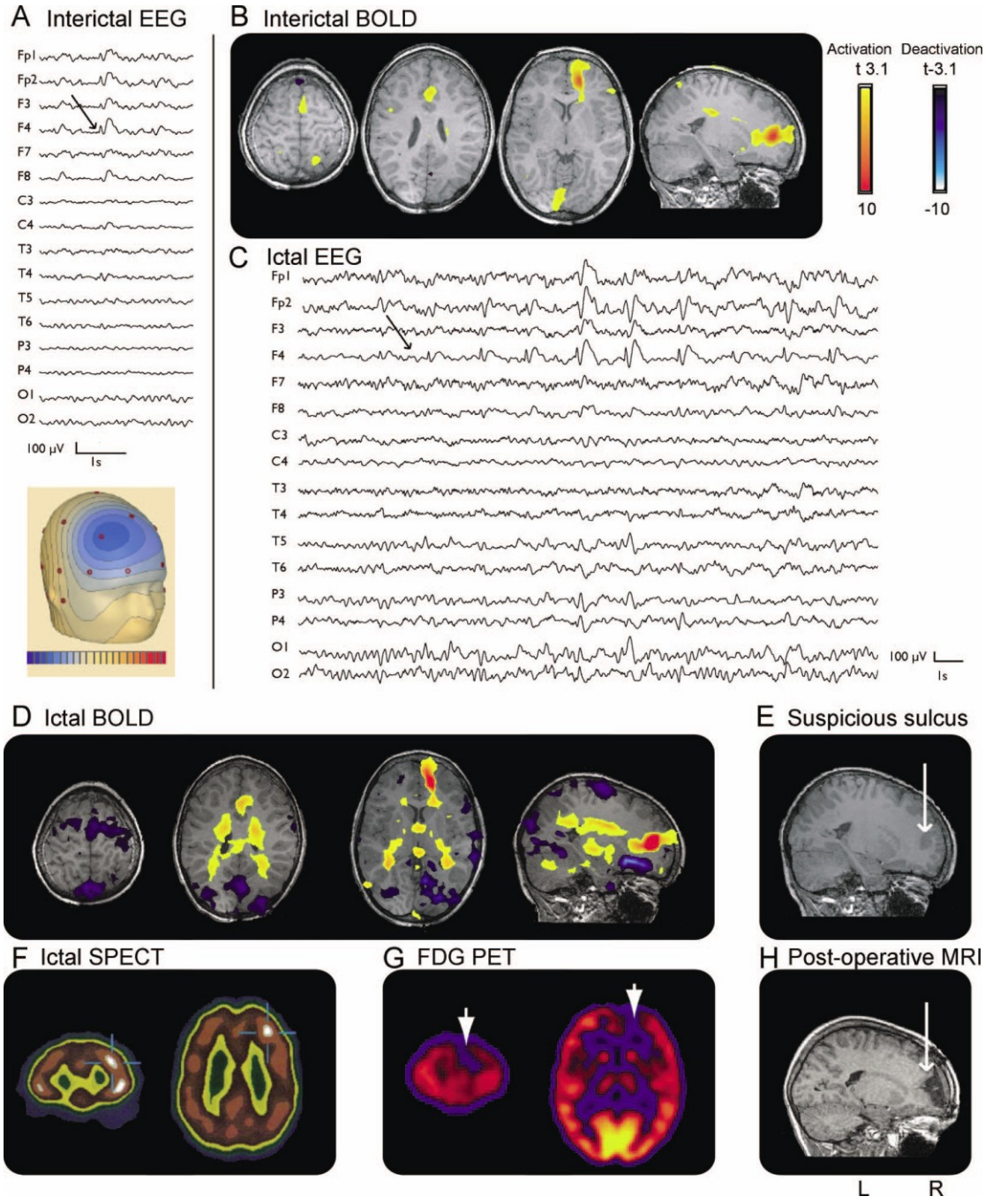


Figure 2 Patient 4
(A) Interictal EEG (average montage): focus F4. (B) Interictal functional MRI (fMRI): positive blood oxygen level dependent BOLD) response frontopolar; no negative BOLD response. (C) Ictal EEG: rhythmic spike and wave F4. (D) Ictal fMRI: positive OLD response: frontopolar; negative BOLD response: frontal and posterior cingulate. (E) MRI: suspicious deep right middle frontal sulcus. (F) Ictal SPECT: hyperperfusion frontal right. (G) FDG-PET hypometabolism frontal right.

**Concordance with PECT and SPECT**

FDG-PET studies were conducted in 5 patients but yielded results only in 2 patients (pt 4 and 9). In both patients the hypometabolism indicated by FDG-PET was in concordance with the maximum of BOLD signal increase: Patient 2 showed a right frontal hypometabolism matching with the fMRI activation in the right frontopolar cortex. FDG-PET in patient 9 revealed a hypometabolism of the left frontal lobe extending to the temporal and parietal lobes. The frontal hypometabolism concurred with the fMRI results which pointed to the left frontomesial cortex extending to frontolateral and frontopolar regions.

In 5 patients ictal $^{99m}$Tc-ECD SPECT studies were performed with a tracer injection within the first 10 seconds after seizure onset. Results were obtained for 3 patients. Interictal $^{99m}$Tc-ECD SPECT was obtained in two of these patients and allowed to perform a subtraction of interictal and ictal SPECT results (pts 2 and 7, fig. 1 and 3). In two patients the hyperperfusion in the SPECT showed a good correspondence to fMRI results: Patient 4 (fig. 2) showed an ictal right frontal hyperperfusion, matching with PET results as well as interictal and ictal fMRI. The ictal SPECT for patient 2 (fig. 1) revealed a hyperperfusion in left prefrontal and paramedian areas. Compared to the interictal BOLD increase, the SPECT hyperperfusion was located slightly more anteriorly. When comparing the more widespread ictal BOLD increase a good concordance between ictal SPECT and ictal fMRI was found. In patient 7 (fig 3) ictal hyperperfusion was frontolateral left. This was not consistent with the fMRI results which showed a bilateral activation of the motor cortex. This however was the only patient in which the positive BOLD response was topographically incongruent with the spike localisation.

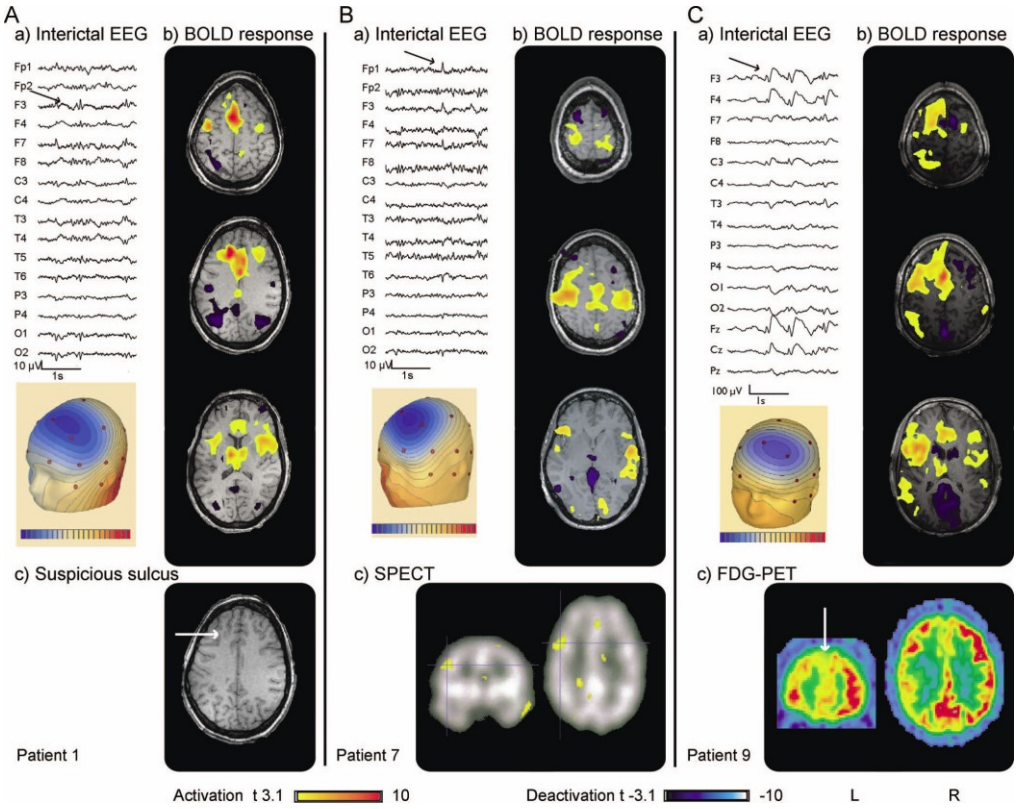


Figure 3 Patient 1: A) EEG (Average montage) focus F3, F7; B) maximum of positive BOLD response left middle frontal gyrus; negative BOLD response in default mode areas; C) MRI: suspicious deep left middle frontal sulcus: Patient 7: A) EEG (Average montage) focus F3, F7; B) positive BOLD response bilateral motor cortex, unrelated to spike topography; negative BOLD response: precuneus; C) Subtraction of interictal and ictal SPECT showing a focus frontolateral left; Patient 9: A) EEG (Average montage) focus F3, Fz, with frequent generalization; B) maximum of positive BOLD response left frontomesial, additionally frontolateral, bilateral parietal left more than right; negative BOLD response: default mode areas, caudate nuclei C) FDG-PET: hypometabolism left frontal cortex, extended to parietal and temporal

**Re-evaluation of structural MRIs**

When re-reviewing the structural MRIs guided by the fMRI results, no clear structural abnormalities in areas with maximal BOLD signal increase were detected. For two patients (pts 1 and 4, fig. 3 and 2) the maximum of BOLD signal increase pointed to a suspicious deep sulcus. Criteria for a cortical dysplasia were not fulfilled.

**Post-operative validation**

Two patients (pts 2 and 4, fig. 1 and 2) were operated. In patient 4 intraoperative electrocorticography (ECoG) revealed continuous spiking over the right frontal suspicious sulcus to which the EEG-fMRI had pointed. A limited right frontal corticectomy was performed. The histology of the resected cortex showed focal dysplasia. Two years after surgery the patient has remained seizure-free. For patient 2 invasive grid recording indicated a seizure focus at the anterior left cingulate and paramedian left areas. The patient underwent a left frontoparamedial resection and the histology of the resected cortex revealed an extended microdysgenesis, which had not been visible on structural MRI. Interictal positive BOLD signal changes had shown activation just adjacent to the resected pathological area, ictal positive BOLD signal changes which were more widespread included the resected area. The patient did not improve after surgery but continued having seizures.

**DISCUSSION**

Since the delineation of the epileptogenic zone is difficult in patients with non lesional FLE, these patients are often not considered for surgery. When operated, patients with non lesional FLE show a less favorable operative outcome compared to patients with lesional FLE (Jeha et al. 2007, Lee et al. 2008), probably as a result of an insufficient identification of the epileptogenic zone. The aim of this study was to investigate whether EEG-fMRI in patients with non lesional FLE can add useful information in the pre-operative evaluation. EEG-fMRI studies which investigated the relationship between IED related BOLD signal changes and intracranial recordings support the role of EEG-fMRI in the pre-operative evaluation:

Case reports within larger series (Bagshaw et al. 2004, Laufs et al. 2006, Tyvaert et al. 2008) and one study of five patients (Benar et al. 2006) showed a concordance between BOLD signal changes and the seizure onset zone revealed by intracranial recording. One study specifically addressed the role of EEG-fMRI in the preoperative work-up for epilepsy surgery and demonstrated that EEG-fMRI results may help to make decisions in complex cases (Zijlmans et al. 2007). However, when using EEG-fMRI in the presurgical evaluation in patients with epilepsy, one has to consider the characteristics and limitations of EEG-fMRI studies.

EEG-fMRI is a powerful and noninvasive method that localizes epileptic networks related to epileptic activity. It therefore does not only show BOLD signal changes related to the generator of the epileptic activity but also maps areas of propagation and areas influenced by the epileptic activity. Negative BOLD signal changes frequently occur in areas remote from the presumed epileptogenic focus (Kobayashi et al. 2006a, Laufs et al. 2007) but also positive BOLD signal changes in remote areas are observed (Kobayashi et al. 2006b). To avoid spurious results we applied a strict statistical threshold correcting for multiple comparisons based on random field theory (Friston et al. 1995) and focused on the global maximum of positive BOLD signal changes. In eight of nine patients a good concordance between EEG spike field distribution and maximal positive BOLD signal was found. These areas of positive BOLD signal presumably demonstrate the area of spike generation. Where available, PET and SPECT results supported these findings: In patients with concordance between EEG spike field distribution and maximal positive BOLD signal changes, PET and SPECT also showed correspondence.

Only in patient 7, in whom BOLD responses were unrelated to the spike topography, no concordance between BOLD changes and ictal SPECT results was found. When reviewing the structural MRI for subtle lesions in the areas of maximal BOLD signal changes, no clear abnormalities could be detected. Yet, the maximum of positive BOLD signal changes pointed to a suspicious deep sulcus in two patients (pts 1 and 4). The gold-standard to validate the observed BOLD responses is the comparison with post-operative resection and the pathology within the resected area. Until now only two patients (pts 2 and 4) underwent surgery. In patient 4 both interictal and ictal

BOLD signal changes had pointed to a suspicious deep right middle frontal sulcus. As described elsewhere (Gallagher et al. 2008) the patient underwent more diagnostic procedures including PET, SPECT, magnetoencephalography (MEG), near-infrared spectroscopy (NIRS) and ECoG, all in concordance with our fMRI results. After a limited right frontal corticectomy the patient remains seizure free for two years. The histopathology of the resected cortex revealed cortical dysplasia. In patient 2 the interictal fMRI results showed positive BOLD signal changes in the left superior and middle frontal gyrus, whereas ictal positive BOLD signal changes were more extended and additionally included the left anterior cingulate gyrus and left parietal cortex. Invasive grid recording indicated a seizure focus at the left anterior cingulate and paramedian area. The patient underwent a left frontoparamedian resection and the histology of the resected cortex revealed an extended microdysgenesis not visible on structural MRI. This is in keeping with previous studies in which a microdysgenesis was often missed even on high resolution MRI (Tassi et al. 2002, Widdes-Walsh et al. 2005). Since the extent of the epileptogenic tissue in those cases cannot be seen, adequate surgical treatment is difficult. This leads to less favourable outcome compared to well-circumscribed pathologies (Jeha et al. 2007). The fact that our patient did not improve after surgery but continued to have seizures indicates that the microdysgenesis probably extended beyond the resected area. One might speculate whether the interictal BOLD signal changes, which lay adjacent to the resected area, had pointed to a part of the microdysgenesis that was not resected.

Our study provides different levels of support (topography, concordance with PET and SPECT, structural peculiarities, post-operative histology) that EEG-fMRI may help to delineate the epileptic focus in patients with non lesional FLE. This group of patients is characterized by difficulties in identifying the epileptogenic zone (Kellinghaus and Luders 2004) and other non-invasive techniques have their limitations: a relatively low sensitivity for PET studies (Ryvlin et al. 1998, Kim et al. 2002) and the problem of differentiation of ictal onset zone and seizure propagation in SPECT studies (van Paesschen et al. 2007). Such alternative approaches are of great importance in this context. EEG-fMRI results may provide supporting evidence for a hypothesis regarding the localization of the epileptogenic zone and thereby contribute to decision making relating to intracranial EEG implantation.

## REFERENCES

Allen PJ, Josephs O, Turner R: A method for removing imaging artifact from continuous EEG recorded during functional MRI. Neuroimage 2000; 12: 230-39.

Bagshaw AP, Aghakhani Y, Bénar CG, Kobayashi E, Hawco C, Dubeau F et al. EEG-fMRI of focal epileptic spikes: analysis with multiple haemodynamic functions and comparison with gadolinium-enhanced MR angiograms. Hum Brain Mapp 2004; 22:179-92.

Bénar C, Aghakhani Y, Wang Y, Izenberg A, Al-Asmi A, Dubeau F, Gotman J. Quality of EEG in simultaneous EEG-fMRI for epilepsy. Clin Neurophysiol 2003; 114: 569-80.

Bénar CG, Grova C, Kobayashi E, Bagshaw AP, Aghakhani Y, Dubeau F, Gotman J.EEG-fMRI of epileptic spikes: concordance with EEG source localization and intracranial EEG. Neuroimage. 2006 ;30:1161-70.

Dupont P, Van Paesschen W, Palmini A, Ambayi R, Van Loon J, Goffin J, Weckhuysen S, Sunaert S, Thomas B, Demaerel P, Sciot R, Becker AJ, Vanbilloen H, Mortelmans L, Van Laere K. Ictal perfusion patterns associated with single MRI-visible focal dysplastic lesions: implications for the noninvasive delineation of the epileptogenic zone. Epilepsia. 2006;47:1550-7.

Friston KJ, Holmes AP, Worsley KP, Poline JB, Frith C, Frackowiak RSJ (1995) Statistical parametric maps in functional imaging: a general linear approach. Hum Brain Map 2: 189–210.

Gallagher A, Lassonde M, Bastien D, Vannasing P, Lesage F, Grova C, Bouthillier A, Carmant L, Lepore F, Béland R, Nguyen DK. Non-invasive pre-surgical investigation of a 10 year-old epileptic boy using simultaneous EEG-NIRS. Seizure. 2008;17:576-82.

Gotman J. Epileptic networks studied with EEG-fMRI. Epilepsia. 2008;49 Suppl 3:42-51. Review.

Jeha LE, Najm I, Bingaman W, Dinner D, Widdess-Walsh P, Lüders H. Surgical outcome and prognostic factors of frontal lobe epilepsy surgery. Brain. 2007;130:574-84.

Kellinghaus C, Lüders HO. Frontal lobe epilepsy. Epileptic Disord. 2004;6:223-39. Review.

Kim YK, Lee DS, Lee SK, Chung CK, Chung JK, Lee MC. (18)F-FDG PET in localization of frontal lobe epilepsy: comparison of visual and SPM analysis. J Nucl Med. 2002;43:1167-74.

Kobayashi E, Bagshaw AP, Grova C, Dubeau F, Gotman J. Negative BOLD responses to epileptic spikes. Hum Brain Mapp 2006a; 27: 488-97.

Kobayashi E, Bagshaw AP, Bénar CG, Aghakhani Y, Andermann F, Dubeau F, Gotman J. Temporal and extratemporal BOLD responses to temporal lobe interictal spikes. Epilepsia. 2006b;47:343-54.

Laufs H, Hamandi K, Walker MC, Scott C, Smith S, Duncan JS, Lemieux L. EEG-fMRI mapping of asymmetrical delta activity in a patient with refractory epilepsy is concordant with the epileptogenic region determined by intracranial EEG. Magn Reson Imaging. 2006 May;24(4):367-71.

Laufs H, Duncan JS. Electroencephalography/functional MRI in human epilepsy: what it currently can and cannot do. Curr Opin Neurol. 2007;20:417-23. Review.

Laufs H, Hamandi K, Salek-Haddadi A, Kleinschmidt AK, Duncan JS, Lemieux L. Temporal lobe interictal epileptic discharges affect cerebral activity in "default mode" brain regions. Hum Brain Mapp. 2007;28:1023-32.

Lee SK, Lee SY, Yun CH, Lee HY, Lee JS, Lee DS. Ictal SPECT in neocortical epilepsies: clinical usefulness and factors affecting the pattern of hyperperfusion. Neuroradiology. 2006;48:678-84.

Lee JJ, Lee SK, Lee SY, Park KI, Kim DW, Lee DS, Chung CK, Nam HW. Frontal lobe epilepsy: clinical characteristics, surgical outcomes and diagnostic modalities. Seizure. 2008;17:514-23.

Ryvlin P, Bouvard S, Le Bars D, De Lamérie G, Grégoire MC, Kahane P, Froment JC, Mauguière F. Clinical utility of flumazenil-PET versus [18F]fluorodeoxyglucose-PET and MRI in refractory partial epilepsy. A prospective study in 100 patients. Brain. 1998;121:2067-81.

Schuele SU, Lüders HO. Intractable epilepsy: management and therapeutic alternatives. Lancet Neurol. 2008;7:514-24. Review.

Tassi L, Colombo N, Garbelli R, Francione S, Lo Russo G, Mai R, Cardinale F, Cossu M, Ferrario A, Galli C, Bramerio M, Citterio A, Spreafico R. Focal cortical dysplasia: neuropathological subtypes, EEG, neuroimaging and surgical outcome. Brain. 2002;125:1719-32.

Téllez-Zenteno JF, Dhar R, Wiebe S. Long-term seizure outcomes following epilepsy surgery: a systematic review and meta-analysis. Brain. 2005;128:1188-98. Review.

Tyvaert L, Hawco C, Kobayashi E, LeVan P, Dubeau F, Gotman J. Different structures involved during ictal and interictal epileptic activity in malformations of cortical development: an EEG-fMRI study. Brain;131:2042-60.

Van Paesschen W, Dupont P, Sunaert S, Goffin K, Van Laere K. The use of SPECT and PET in routine clinical practice in epilepsy. Curr Opin Neurol. 2007;20:194-202. Review.

Widdess-Walsh P, Kellinghaus C, Jeha L, Kotagal P, Prayson R, Bingaman W, Najm IM. Electro-clinical and imaging characteristics of focal cortical dysplasia: correlation with pathological subtypes. Epilepsy Res. 2005;67:25-33.

Worsley KJ, Liao CH, Aston J, Petre V, Duncan GH, Morales F et al. A general statistical analysis for fMRI data. Neuroimage 2002; 15: 1-15.

Zijlmans M, Huiskamp G, Hersevoort M, Seppenwoolde JH, van Huffelen AC, Leijten FS. EEG-fMRI in the preoperative work-up for epilepsy surgery. Brain 2007; 130: 2343-53.

**Acknowledgment**

This work was supported by the Canadian Institutes of Health Research (CIHR) grant MOP-38079. Tyvaert L. was supported by the Rotary International and by the Savoy Foundation for epilepsy.

**Appendix A. Supplementary data** Supplementary data associated with this article can be found, in the online version.

Supplementary figure S1

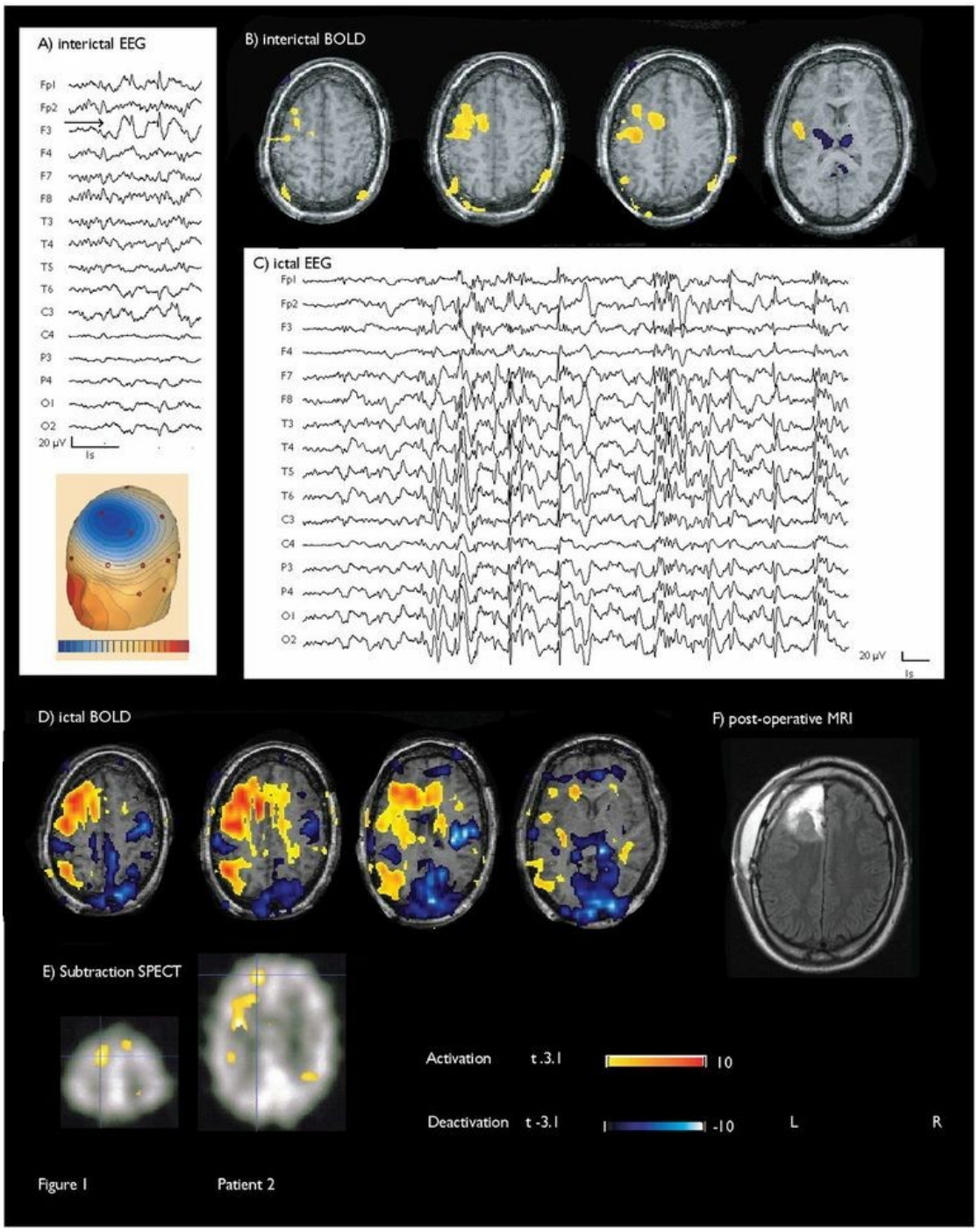


Figure S1. Patient 3: A) EEG (Average montage) focus Fp2, F8, T4; B) maximum of positive BOLD response right frontopolar and frontomesial; negative BOLD response in default mode areas

Supplementary figure S2.

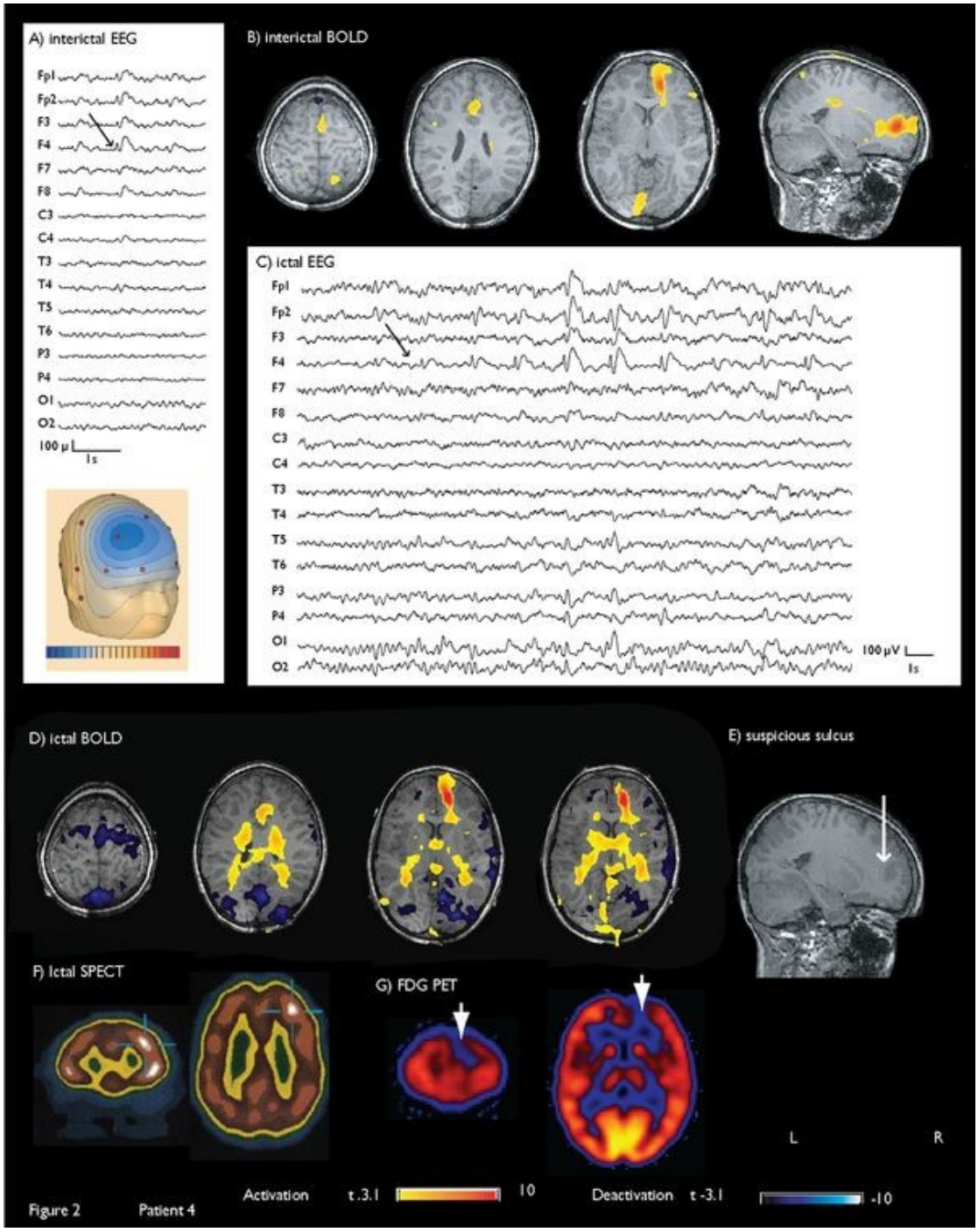


Figure S2. Patient 5: A) EEG (Average montage) focus F4, F8; B) maximum of positive BOLD response right inferior frontal gyrus; negative BOLD response in default mode areas

Supplementary figure S3.

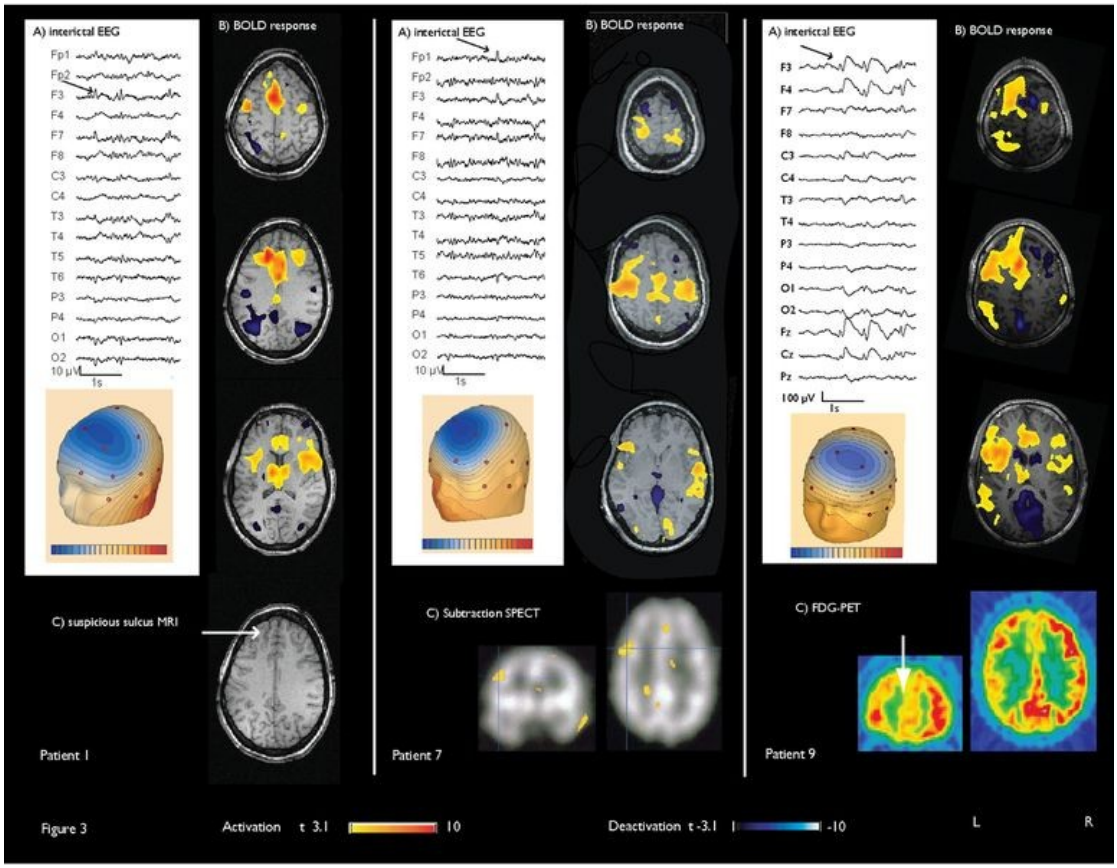


Figure S3. Patient 6: A) EEG (Average montage) focus Fp1, F3; B) maximum of positive BOLD response left superior frontal gyrus; negative BOLD response in default mode areas and the thalamus

Supplementary figure S4.

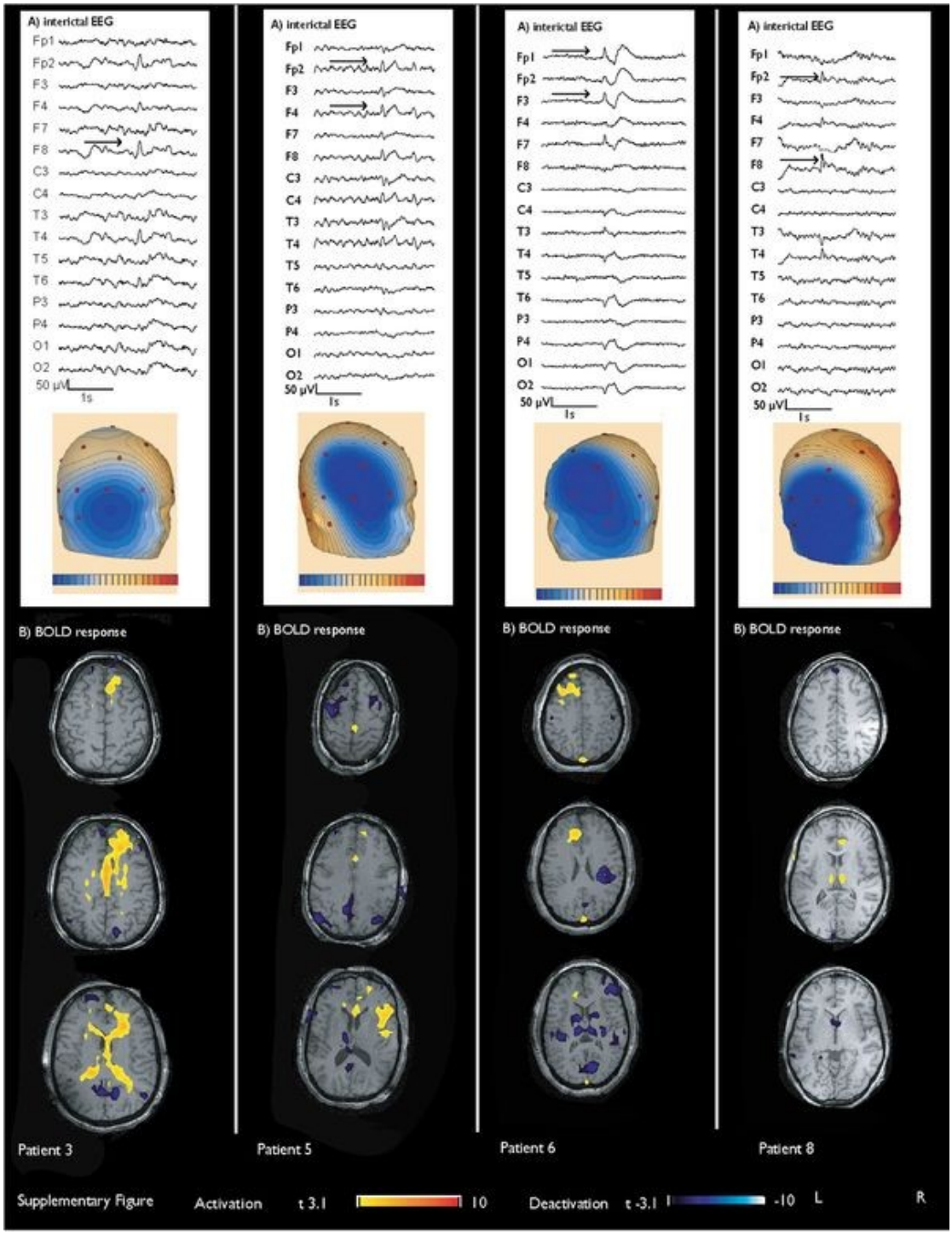


Figure S4. Patient 8: A) EEG (Average montage) focus F8; B): maximum of positive BOLD response: right anterior cingulum, additionally thalamus; negative BOLD response: caudate nuclei

**ANNEXE 4**

***Nonlinear hemodynamic responses in human epilepsy: A multimodal analysis with fNIRS-EEG and fMRI-EEG***

**Published by:**
Journal of Neuroscience Methods 204 (2012) Pp. 326-340

**Philippe Pouliot[a, e], Julie Tremblay[b], Manon Robert[c], Phetsamone Vannasing[b], Franco Lepore[c], Maryse Lassonde[c, b], Mohamad Sawan[a], Dang Khoa Nguyen[d], Frédéric Lesage[a, e]**

[a]*Département de génie électrique and Institut de génie biomédical, École Polytechnique de Montréal, C.P. 6079, Succ. Centre-ville, Montréal, Qc, Canada H3C 3A7*
[b]*Centre de recherche, Hôpital Sainte-Justine, 3175, Chemin de la côte-Sainte-Catherine, Montréal, Qc, Canada H3T 1C5*
[c]*Centre de recherche en neuropsychologie et cognition, Département de psychologie, Univ. de Montréal, Montréal, Qc, Canada H3C 3J7*
[d]*Service de neurologie, Hôpital Notre-Dame du CHUM, 1560, Rue Sherbrooke Est, Montréal, Qc, Canada H2L 4M1*
[e]*Institut de cardiologie de Montréal, Centre de recherche, 5000, Rue Bélanger Est, Montréal, Qc, Canada H1T 1C8*

Keywords: Nonlinear hemodynamic response, Volterra kernel expansion, fNIRS-EEG noninvasive human imaging, fMRI-EEG, Epileptic focus localization, Negative BOLD signal.

## ABSTRACT

Functional magnetic resonance imaging (fMRI) combined with electroencephalography (fMRI-EEG) is a neuroimaging technique based on the BOLD signal which has been shown to be useful in the study of epilepsy for the localization of the epileptogenic focus. Functional near-infrared spectroscopy (fNIRS) combined with EEG (fNIRS-EEG) is another imaging technique based on the measurement of both oxygenated and deoxygenated hemoglobin with complementary clinical potential in epilepsy, for continuous patient monitoring, language lateralization, and focus localization.

In this work fMRI-EEG and fNIRS-EEG are used to quantify nonlinear hemodynamic responses in three cases of human refractory focal epilepsy, by using the Volterra kernel expansion up to second order. Prior to analyzing real data, extensive simulations are carried out to show that nonlinearities are estimable. The Volterra methodology is then applied to multimodal data recorded from 3 epileptic patients selected for their frequent spiking activity. Care is taken to account for variability of hemodynamic responses due to other causes than Volterra nonlinearities. Statistically significant nonlinearities are observed for all patients and all modalities. Good concordance between fNIRS and fMRI is found for both the amplitude of the Volterra responses, and, with limitations, in the localization of the epileptic focus and regions of inverted responses (negative BOLD signals). In one patient, Volterra nonlinearities allowed epileptic focus identification with fMRI, while analyses without nonlinearities failed to see it. In simulations when nonlinearities were included, analysis without Volterra nonlinearities performed poorly. These two observations suggest routinely checking for nonlinearities in functional imaging of patients presenting with frequent spikes.

## 1. INTRODUCTION

In cognitive studies on normal subjects with functional Magnetic Resonance Imaging (fMRI), linearity of the Blood Oxygenation Level Dependent (BOLD) response to neuronal stimuli is well established (Boynton et al. 1996) for a range of conditions, both for temporal (Friston et al. 1998) and spatial linearity (Hansen, David, and Gallant 2004). However there is also evidence of the presence of nonlinearities when probing a wider range of conditions, such as stimulus duration, rate and amplitude (Toyoda et al. 2008; Soltysik et al. 2004). In pathological cases such as epilepsy, working under the simplifying assumption of linearity has been a successful strategy to put the high spatial resolution and non-invasiveness of fMRI to good use, despite inherent limitations reviewed in (Laufs and Duncan 2007). Using marked interictal spikes recorded with electroencephalography (EEG) to define an activation protocol, a number of results were obtained from epileptogenic zone localization (Krakow et al. 2001) to exploring effective connectivity networks involved in human epilepsy (Vaudano et al. 2009; Hamandi et al. 2008). However, various features in epilepsy have also been noted, which may be due to variability in the hemodynamic response or perhaps to more intrinsic nonlinearities. The group of Gotman at McGill has investigated several aspects of non-standard BOLD response in epileptic spikes and seizures (Jacobs et al. 2009; Kobayashi et al. 2006; Jacobs et al. 2008; CS Hawco et al. 2007) and observed significant variability between patients, in the timing, sign and extent of the response. Compared to the standard Hemodynamic Response Function (HRF, (Glover 1999)), the response in epilepsy may sometimes occur before the electrophysiological activity seen on scalp EEG, their amplitude can be much greater, with a slower return to baseline, and inverted responses are sometimes observed. Thus, it is a matter of debate whether the canonical HRF can be used for epileptics (LeVan et al. 2010; Grouiller et al. 2009).

Thanks to the measurement of both oxy- and deoxygenated (HbO and HbR) hemoglobin concentration changes, and to a higher temporal resolution than fMRI, another imaging technique that may help shed light on non-standard hemodynamic responses is functional near-infrared spectroscopy (fNIRS), combined with EEG. For a recent review of fNIRS, its use in epilepsy and an extensive list of references, see

(Desjardins, Pouliot, and Lesage 2011). As with other imaging modalities, the primary potential use of fNIRS-EEG in epilepsy is in patient assessment for eventual surgical removal of the epileptogenic focus (EF). A standard positive response with fNIRS in a controlled cognitive study shows a functional decrease in HbR with respect to baseline and a larger increase in HbO, resulting in a small increase of total hemoglobin (HbT) which is a proxy for regional cerebral blood volume (CBV). While a positive BOLD signal in fMRI is generally thought to correspond to a decrease in HbR, other scenarios are possible, since the BOLD signal is a function of both HbR and blood volume. Thus it is of interest to use fNIRS to unravel how much of a BOLD signal comes from HbR and blood volume changes and, indeed, various types of responses have been reported. Supporting results from fMRI-EEG, there are reports with fNIRS of inverted responses (HbO decrease and HbR increase) (Buchheim et al. 2004), responses prior to events on scalp EEG in an animal model of spikes (Osharina et al. 2010) (however this effect was not seen in Vanzetta et al. 2010) and a long time of return to baseline. Existence of these 3 phenomena was further confirmed recently in our group's patient data (Nguyen et al. submitted). In qualitative assessments of the time course of typical fNIRS time series in epilepsy at the initiation of seizures, one sees oscillatory behavior with increasing amplitude and delayed return to baseline, fitting well the intuition that epileptic seizures are runaway phenomena. This dynamic is well illustrated by the recent work of (Vanzetta et al. 2010) in an animal model of epilepsy, who observe nonlinearities consistent with Volterra-type nonlinearities when spiking rates exceed 0.2 Hz, although their focus was on the linearity of the response.

The accumulated evidence of patient-dependent hemodynamic response variability and potential nonlinearities in the BOLD signal of epileptic patients and in our fNIRS data underlines the importance of characterizing these effects quantitatively. However, understanding the detailed time-course of these nonlinear oscillations appears to be beyond current technology, at least due to a number of physiological confounds. Thus to make the study of nonlinearities tractable, this work will focus on studying one aspect of temporal nonlinearity to neuronal stimuli: The second order kernel in a perturbative expansion referred to as the Volterra expansion (Friston et al. 1998; Friston et al. 2000). There are two main advantages to the Volterra approach: few parameters and model independence. As it is maximally economical in the number of parameters (here there will be only one parameter measuring the degree of

nonlinearity), it is best suited to provide robust statistical evidence that this first-order nonlinearity (referred to as the second Volterra kernel later on) differs from zero in limited patient data. Another advantage is that this approach is model independent, up to a choice of the HRF. The main goal of this work is to develop a methodology to quantify nonlinear effects in epileptic patients using fNIRS. Two questions are to be answered: (1) Are nonlinear effects distinguishable from noise in fNIRS data from epileptic patients? If yes, (2) are they consistent with similar estimations performed in fMRI? In this work, the Volterra approach will be reviewed pedagogically and the nonlinear effects illustrated graphically. Extensive simulations will then be carried out on random protocols added over a background of realistic data using general linear model (GLM) methodology to show that nonlinearities are estimable from fNIRS measures. Finally, data from fMRI-EEG and fNIRS-EEG acquired in the same patients will be used to validate results across modalities and to calculate the statistical evidence for and amplitude of these nonlinear effects.

## 2. METHODS

### 2.1 Description of the Volterra approach for epileptic spikes

The Volterra expansion is a functional Taylor expansion (Friston et al. 2000) of the equation y = y(u) relating the time-dependent inputs u(t) (or "neuronal transients", here the epileptic spikes, which are a function of time t) to the output measures y, where the measures here are BOLD, HbO and HbR time series, at a given fMRI voxel or fNIRS channel. The expansion is in terms of derivatives of y with respect to u (the kernels), multiplied by the inputs and integrated over time:

$$y(t) = \int_0^\infty \kappa_1(\sigma)u(t-\sigma)d\sigma + \iint_0^\infty \kappa_2(\sigma,\tau)u(t-\sigma)u(t-\tau)d\sigma d\tau + \cdots$$

The first kernel, $\kappa_1(\sigma) = \frac{\partial y(t)}{\partial u(t-\sigma)}$, is associated with the driving efficacy of the inputs. It is assumed time-translation invariant, i.e. independent of the experiment time t. Convolution of the first kernel with the inputs u(t) gives the first term in the Volterra expansion. The second kernel, $\kappa_2(\sigma,\tau) = \frac{\partial^2 y(t)}{\partial u(t-\sigma)\partial u(t-\tau)}$, represents the modulatory influence of one input on another (also assumed independent of t). By convolving the second kernel with the inputs with respect to one time, and convolving

again the result with respect to the second time, one obtains the second term in the Volterra expansion.

It is then assumed that the kernels can be expanded with respect to a basis of functions, $B_i$: $\kappa_1 = \sum \beta_i B_i$ and $\kappa_2 = \sum \beta_{ij} B_i B_j$, where $\beta_i, \beta_{ij}$ are constants. The Volterra expansion is a model independent description of the hemodynamic response, up to the choice of basis functions used to describe the kernels. For completeness, calculations in this work were performed with different choices of HRF: The canonical HRF (one basis function, normalized to unit area), the canonical HRF with its time derivative and dispersion (3 basis functions), and the standard gamma function distributed with SPM8, $\mathbf{HRF}(t) = \frac{t^3 \exp(-t)}{\mathbf{6}}$, peaking at 3 seconds and also normalized to unit area. Mostly results for the canonical HRF will be shown, as it performed generally better on data from the 3 patients (but see Figs. 8 and S-12 for discussions of effect of HRF derivatives on patient data, and Figs. 1, 2 and S-6 for gamma HRF). Pursuing with HRF representing either the canonical or gamma HRF, the kernels take the explicit forms: $\kappa_1(\sigma) = \beta_1 \mathbf{HRF}(\sigma)$, while $\kappa_2(\sigma, \tau) = \beta_2 \mathbf{HRF}(\sigma) * \mathbf{HRF}(\tau)$, is a function of two times and is quadratic in the HRF with * denoting ordinary multiplication, and $\beta_{1,2}$ are constants ($\beta_2 = \beta_{11}$ in the earlier notation). For the GLMs, associated regressors in the design matrix are labeled $V_1$ and $V_2$, which are defined (up to an overall normalization factor $S$ described later) as $V_1(t) = \frac{\partial}{\partial \beta_1} \int_0^\infty \kappa_1(\sigma) u(t-\sigma) d\sigma = \int_0^\infty HRF(\sigma) u(t-\sigma) d\sigma$ and $V_2(t) = \frac{\partial}{\partial \beta_2} \iint_0^\infty \kappa_2(\sigma, \tau) u(t-\sigma) u(t-\tau) d\sigma d\tau = \left( \int_0^\infty HRF(\sigma) u(t-\sigma) d\sigma \right)^2$. The central purpose of the methodology used here to evaluate nonlinearities is to estimate from the data the proportionality coefficients $(\beta_1, \beta_2)$.

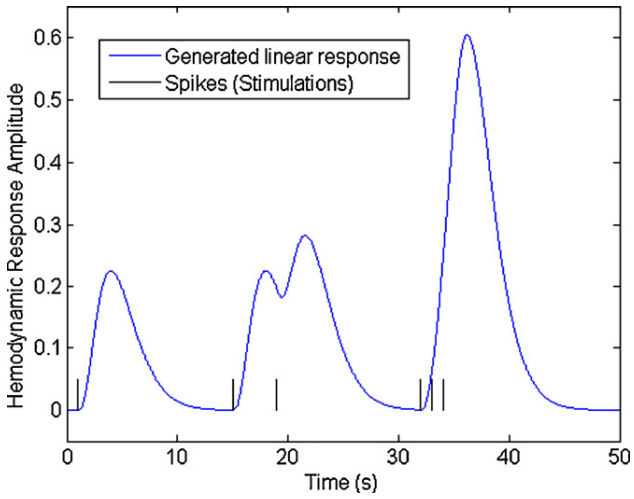


Figure 1. Linear hemodynamic response to 6 spikes occurring at times 1, 15, 19, 32, 33 and 34 s. Generated response to large enough number of spikes (or, more generally, stimulations) in rapid succession could be arbitrarily large in amplitude, for this linear model. Gamma HRF used.

## 2.2 Illustrations of nonlinear effects

### *2.2.1 Linear convolution of arbitrarily large amplitude*

To help develop an intuition for the Volterra nonlinearities, we have included three figures to illustrate the effects. In Fig. 1, 6 spikes (or more generally, stimulations, in a cognitive experiment) are shown occurring at times 1, 15, 19, 32, 33 and 34 seconds. The spikes are convolved with the standard gamma distribution in SPM8, which is more convenient to use for illustration than the canonical HRF because it has no negative component. Thus the convolution with the first spike at t = 1 in the window 1 to 15 seconds shows the gamma HRF, the convolution with the second and third spikes in the window 15 to 32 s shows the linear superposition of two spikes separated by 4 s, and finally for the last 3 spikes in the window 32 to 50 s the convolution of 3 spikes is shown. From this figure, one can directly infer that a linear hemodynamic response will be arbitrarily large if a large enough number of spikes occur in rapid succession. With spiking rates of 5 Hz sustained for more than 10 seconds (observed in patient data), a linear response, which would be more than 50 times larger than the response to 1 spike, is not physiologically plausible. Therefore this suggests that there are nonlinear corrections to linear convolution when a sufficiently large number of spikes occur in rapid succession. We would also expect the correction to amount to a reduction compared to the linear response, so that it may be characterized as inhibition. In this work, we will use the nouns/adjectives inhibition/inhibitory as generic terms to describe any response less than linear,

refraction/refractory for a more specific response that inverts due to very many spikes and saturation (no corresponding adjective) for a response that asymptotes to a maximum value as a function of the number of spikes; finally, excitation/excitatory will describe any response greater than linear in the number of spikes.

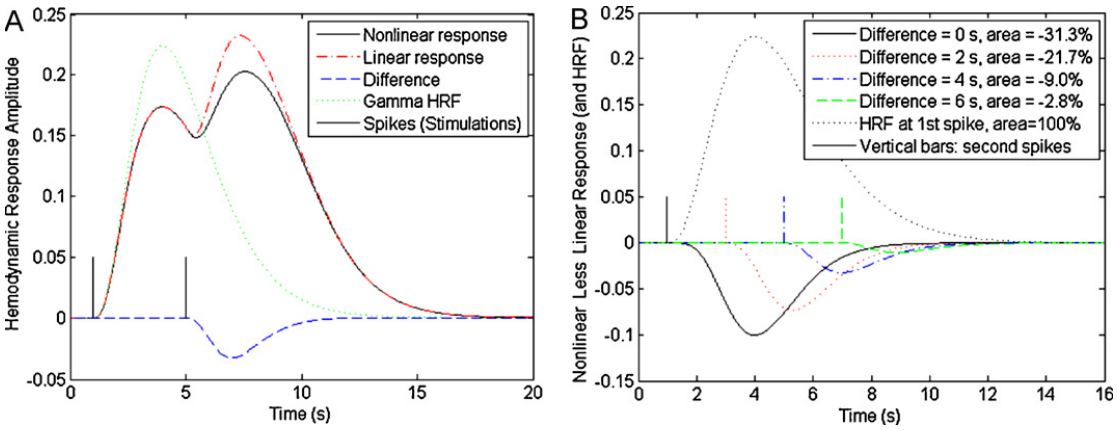


Figure 2. A. Linear and nonlinear hemodynamic responses to two spikes occurring at times 1 and 5 s, and their difference, for Volterra amplitudes (˘1, ˘2) = (1, −1). Linear response computed by adding the response of each spike computed separately, which is itself the sum of the first and second Volterra contributions for that spike. Nonlinear response to the two spikes calculated by adding the linear contribution from each of the two spikes, to the nonlinear Volterra contribution calculated from the two spikes together. Inhibitory effect observed, in that response of second spike is less for nonlinear than linear response. B. Size of inhibitory effect as function of time difference between two spikes. Signed area of response given in legend as function of time difference. Inhibition strongest for coincident spikes, decreasing in amplitude and area as function of this time difference. To illustrate effect size, underlying gamma distribution HRF is also shown in (A) and (B), normalized to unit area and convolved with first spike. (For interpretation of the references to color in this figure legend, the reader is referred to the web version of the article.)

### *2.2.2 Nonlinear response inhibition*

To illustrate graphically how the 2nd Volterra kernel can lead to this inhibition, we show the size and shape of a nonlinear effect in an idealized situation with just two spikes and no noise (Fig. 2). We use a ratio $\beta_2/\beta_1 = -1$, which is typical of the effect size that we will find in our patient data. Thus, with one spike at $t_1 = 1$ s and the other at $t_2 = 5$ s, of unit strength, we first plot the nonlinear (NL) hemodynamic response $y_{NL}(t)$ constructed as explained in section 2.1 (Fig. 2, solid black line). Explicitly, we use a discrete version of $y_{NL}(t) = \beta_1(H_1 + H_2) + \beta_2 (H_1 + H_2)^2$, with $H_1(t) = \frac{(t-1)^3 \exp(1-t)}{N}$, for $t > 1$ (and 0 otherwise) and $H_2(t) = (t-5)^3 \exp\frac{5-t}{N}$, for $t > 5$ (and 0 otherwise), where $N = 6$ is a normalization factor so that the response to one spike has unit area. Next, we compare

this nonlinear response to some suitable linear (L) response (Fig. 2, red hash-dotted line), which is: $y_L(t) = \beta_1(H_1 + H_2) + \beta_2\left(H_1^2 + H_2^2\right)$. The difference $y_{NL}(t) - y_L(t) = 2\beta_2(H_1 H_2)$ is an interference term. Note that the term $\beta_2\left(H_1^2 + H_2^2\right)$ is nonlinear in an uninteresting way for our purposes: It amounts to modifying the shape and the normalization of the HRF of a single spike by $\beta_2 H^2$ (a reduction of the amplitude of the response from the standard gamma HRF). The interference term, the nonlinear term proper, which is the difference between the nonlinear and the linear response, is $2\beta_2 H_1 H_2 = 2\beta_2(t-1)^3(t-5)^3 \exp(1-t)\exp(5-t)$ for $t > 5$ (and 0 otherwise), and it shows two exponential decays. Now generalizing the times $t_1 = 1$ and $t_1 = 5$ s to arbitrary times $t_1$ and $t_2$ for the two spikes, and rearranging the exponentials, we get $\exp(t_1 - t_2)\exp\left(2(t_2 - t)\right)$ for the behavior of the nonlinear term proper. We thus see that at fixed value of $t_2 - t$, the nonlinear effect falls off exponentially as the time between the two spikes increases, i.e. as a function of $t_2 - t_1$. In Fig. 2B, we show the size of this inhibitory effect as a function of $t_2 - t_1$. Inhibition is strongest for coincident spikes, decreasing exponentially in amplitude and area as a function of this time difference. To proportionally illustrate effect size, also shown is the underlying Gamma distribution HRF (Figs. 2A and 2B, dotted lines), normalized to unit area and convolved with the first spike. In summary, for a negative value of $\beta_1$, an inhibitory effect is seen, in that the response of the second spike is less for the nonlinear than the linear response, even after accounting for the trivial modification of the HRF due to $\beta_2 H^2$. Of course, a reverse, excitatory, effect would be seen if reversing the sign of $\beta_2$ (however we did not see this in patient data at a statistically significant level).

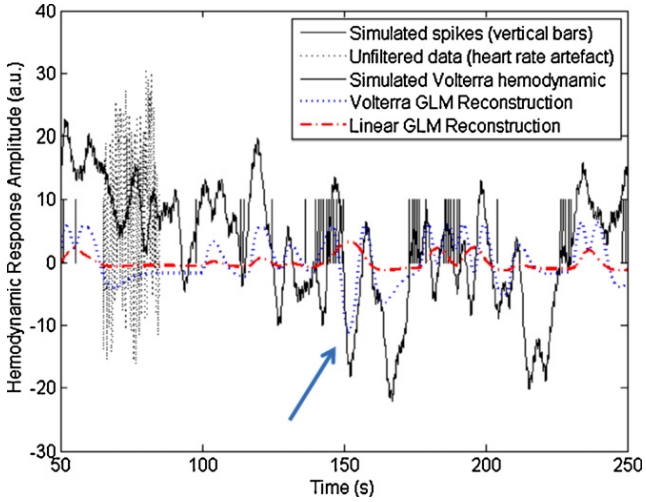


Figure 3. Simulated spikes and reconstructed hemodynamic linear and nonlinear (Volterra) responses over a 200 s window, using canonical HRF, after filtering. A 20 s sample of noisy unfiltered data is displayed from 65 to 85 s. Spikes represented as vertical bars. Nonlinear reconstruction is clearly better able to track the simu-lated hemodynamic response. In particular, considering large number of spikes in quick succession such as near time 150 s (arrow), the linear simulated response (not shown) ventures far above the figure upper boundary, while the simulated and estimated nonlinear Volterra responses are clearly inhibitive there, as both take negative values. Linear reconstruction is unable to explain such sustained negative responses.

### *2.2.3 Linear vs nonlinear GLM reconstructions*

We now illustrate Volterra nonlinearities on simulated data with many spikes, with the resulting GLM reconstructions (Fig. 3). For amplitude pair (2,-2), the 1$^{st}$ and 2$^{nd}$ Volterra contributions using the canonical HRF are added to a background of noisy NIRS patient data, which is then low and high pass filtered (See subsection 2.3.2 for details). A 20 s of unfiltered data within the 200 s window shows that only noise is apparent before filtering, mostly due to the cardiac artifact. The figure then shows the estimated response using GLMs with only the 1$^{st}$ Volterra regressor and a constant regressor (referred to as linear reconstruction), and the GLM containing 1$^{st}$ and 2$^{nd}$ Volterra regressors and a constant (referred to as nonlinear reconstruction). We note that the simulated nonlinear series of Fig. 3 takes negative values. In part, this is due to the so-called undershoot phase of the canonical HRF, but for the most part, the large negative values taken by the simulated series is due to an inhibitory effect caused by the nonlinearity. As this effect is pronounced, since the many spikes around 150 s caused an inversion of the response, by the terminology above, we will call it a refractory effect. This effect is also present in a simulation with a gamma function HRF that is always positive, and is not due to the canonical HRF having an undershoot. We note that the linear GLM reconstruction is unable to capture this refractory effect, as the estimated response is always positive for a gamma function

HRF and almost always positive for the canonical HRF. In contradistinction, the nonlinear GLM reconstruction is able to follow the simulated data during some of the periods where it turned negative. To summarize, this subsection provided an illustration of an effect that can be obtained using the Volterra nonlinearities. Simulation and patient results as shown below are estimated to be of the same order of magnitude.

## 2.3 Simulation methodology

### *2.3.1 Estimability of Volterra expansion amplitudes*

For general background on parameter identifiability and estimability, we refer the reader to (Jacquez and Greif 1985). First there is no issue here of parameter identifiability: The 1st and 2nd Volterra kernels are not exactly collinear, and therefore the response amplitude parameters $(\beta_1, \beta_2)$ are identifiable in principle. On the other hand, the Volterra kernels are highly correlated, so the pressing question to be explored is whether they are estimable in practice, on noisy data and for realistic time series of epileptic spikes. While fMRI data analysis is well established with standard reliable data processing and statistical analysis tools such as SPM (Friston et al. 2007) available, fNIRS is a relatively new imaging modality having a weaker signal-to-noise ratio (SNR). Therefore we will focus on demonstrating estimability of Volterra nonlinearities with fNIRS, and assume that analogous results would follow for fMRI. In (Machado et al. 2010) a study was done of the estimability of the hemodynamic response to epileptic spikes with fNIRS. Linearly in the canonical HRF, they showed that fNIRS epileptic data contained statistically significant information on epileptic spikes that is in concordance with clinical and fMRI observations, for one patient and in simulations. However with the poor SNR and various physiological confounds affecting real data from epileptic patients, it is not clear that the leading-order Volterra nonlinearities (2nd Volterra kernel) are also estimable. To test whether nonlinear effects are estimable with fNIRS, we extended their computer simulation approach to such nonlinear effects.

### *2.3.2 fNIRS preprocessing and GLM analysis*

Raw fNIRS data was first normalized to unit median and converted from recorded optical intensities to HbO and HbR concentrations using the modified Beer-Lambert

law (Delpy et al. 1988). The simulations were done on 10 HbO channels and 10 HbR channels from session 1 of epileptic Patient 1 (this is later referred to as the fNIRS data). The channels were individually selected to differ from each other in some way (position on head and relative to epileptic focus, length of channel, amount of drift). Channels chosen had no movement, the heart rate was clearly visible on HbO components, and the optical intensities were in an acceptable range. However, large drifts were still present on some channels, as is often the case with fNIRS data.

We generated a sufficiently large number (usually 100, but 1000 for Fig. S-4) of random protocols of spikes which we superimposed on the fNIRS data (See subsection 2.3.3 for details on protocol generation). To obtain the first and second Volterra contributions, the protocols were convolved with the canonical HRF (or gamma HRF for Fig. S-6) as explained in section 2.1, to obtain the 1st and 2nd Volterra regressors ($V_1$ and $V_2$). The targeted 1st and 2nd Volterra amplitude coefficients were given as a pair of amplitudes ($\beta_1$, $\beta_2$), specified as a percentage of the channel-wise standard deviation $S$ of the band-pass filtered data. The fNIRS filters (Huppert, Diamond, et al. 2009; Ye et al. 2009) used were a high-pass Butterworth infinite response filter of order 5 with cutoff at 0.004 Hz (unless using WMDL as in Fig. S-8) and the low-pass Gaussian filter of 0.67 Hz full-width at half-maximum of (Ye et al. 2009). The above definition of amplitudes was chosen to better control the results of the simulation, and was one significant methodological difference between our simulations and those in (Machado et al. 2010)). Thus, the contribution added to the unfiltered fNIRS data was $S(\beta_1 \mathbf{V_1} + \beta_2 \mathbf{V_2})$, and will be referred to as the convolved protocol. The SNR corresponding to an amplitude pair ($\beta_1$, $\beta_2$) was calculated for comparison with the same formula as in (Machado et al. 2010), except for our additional filtering of the convolved protocols and baselines: $\mathbf{SNR} = \mathbf{10}\log_{10}\left(\frac{\mathbf{P_p}}{\mathbf{P_b}}\right)$, where $\mathbf{P_p}$ is the filtered power of the protocol and $\mathbf{P_b}$ the power of the filtered baseline signal, with each power calculated relative to zero mean.

Once this convolved protocol contribution was added to the raw fNIRS HbO and HbR data, the resulting series were filtered with the same filters. The design matrix was constructed and the response was estimated with a general linear model (GLM) for each protocol, following the precoloring methodology of NIRS_SPM (Ye et al. 2009).

The design matrix of the protocol was constructed in the standard way: each spike as a neuronal impulse had a same amplitude of unity and a duration here equal to 1/10th (or 5 ms) of an fNIRS data point. As mentioned earlier, we used the canonical HRF from SPM8 (Friston et al. 2007). For the nonlinear reconstruction, the GLM design matrix consisted of either 3 regressors: $V_1$ and $V_2$ described above, and a constant. For the linear reconstruction, this was reduced to only $V_1$ and a constant. From the GLM results, we tested for true detection, for each channel and each generated spike train, and averaged over channels. Since the sign of the response simulated was known, this detection was done by applying a one-sided Student T-test (See subsection 2.3.4 for more details on statistical analysis). Thus we obtained a rate of true detection (sensitivity). We estimated the response again when no protocol had been added, to obtain the rate of false detections (=1-specificity). As there should be no response, the rate of false detections was estimated by a two-sided T-test. Note that the rates of true and false detections are functions of a number of factors, some that we controlled: the confidence threshold, the density and distribution of spikes in each protocol, the amplitude of each convolution kernel of the protocol; and others that we did not control: subject movement, presence of true epileptic events in the data unrelated to the simulated spikes, and differences in noise structure as a function of channel recording quality, mostly dependent on source-detector distance (Mayer waves and cardiac and respiratory amplitude and pace).

*2.3.3 Simulation of realistic epileptic spike time series*

Three patients were selected for their frequent spiking activity. Several measures of the distribution of spikes are presented in Table 1. The key features we wanted to model were bursts of frequent spikes in a background of infrequent spikes. As the distributions of time intervals between spikes were far from normally distributed, we aimed to match these distributional characteristics, using the measures in Table 1, that are arguably more intuitive than the third (skew), fourth (kurtosis) and higher moments of the distribution.

An algorithm described below was proposed to generate protocols that model realistically this type of epileptic data. We calibrated two sets of parameters for this algorithm (referred to as Type 1 and Type 2) until they matched patient data well on several distributional characteristics (Table 1). For calibration, an iterative procedure

was used, which was repeated about 10 times: With an initial set of parameters, 100 protocols were generated, statistics were computed and compared to patient data, and a new set of parameters was manually chosen. The steps were then repeated, until the final parameters given below were obtained, and resulting in the statistics of Table 1. As the spike time series are notoriously non stationary, with large between-session differences, there would be no reason to call for a closer match unless some more specific features of the spike time series needed to be investigated.

For the algorithm description below, parameters are listed as pairs (Type 1, Type 2). For each random protocol, the algorithm begins by generating one set of infrequent spikes, where the number of spikes in a set is drawn from a Poisson distribution with characteristic number of (2, 1), and with a time interval between spikes drawn from an exponential distribution with time scale of (10, 6). Next, a set of frequent spikes are generated, where the number of spikes in a set is drawn from a Poisson distribution with characteristic number of (4, 6), and with a time spacing drawn from a uniform distribution over an interval from 0.5 to 1 s (both types). The algorithm repeats and alternates between infrequent and frequent sets of spikes, until the desired total number of spikes is generated. The time series is finally rescaled by an overall factor so that it fits the data size (here 15 minutes). The total number of spikes per random protocol was (180, 400). Random seeds were tightly controlled, so that our first N protocols were always the same ones to better allow comparison of the different simulations.

*2.3.4 Note on the method of statistical analysis*

The statistical analysis performed in this article was standard. For both simulations and patient data, one question to be addressed was: since the input-convolved canonical HRF ($V_1$) and the convolved second-order Volterra HRF x HRF ($V_2$) were not orthogonal, but instead were strongly correlated, how could we ensure that an estimate for the response to $V_2$ was not as well captured by a slightly different estimate for the response to $V_1$? This was provided by estimating the responses to all regressors in a general linear model, followed by a T-test for $V_1$ or $V_2$ (or an F-test when including derivatives and dispersion of the HRF). We refer the reader to chapters 11 and 12 in (Friston et al. 2007) for details. It is noted in particular that it was unnecessary in this framework to orthogonalize the regressors.

In brief, the set up was in terms of a reduced and full model, with a null hypothesis: that the full model was not better at explaining the data than the reduced model. To test the statistical significance of one Volterra regressor, the regressors of the reduced model consisted of the other kernel, movement parameters (for fMRI), R-R pulse intervals (for fNIRS) and a constant. The full model contained the reduced model and the Volterra kernel of interest. An F-test compared the residual errors of the full and the reduced model. When we considered kernels built out of the canonical HRF only, the F-test simplified to a Student T-test. Therefore, most of the statistical tests shown in this work are Student T-tests for the null hypotheses for the significance of $V_1$ or of $V_2$. For fMRI, a confidence level of 95% after false positive correction was aimed for. This was sometimes too stringent, since clinically relevant information was available just below the threshold. Thus we found it valuable to report results of lesser statistical significance and considered either the significance of $V_1$ or $V_2$ at the 99.9% confidence level without false positives correction, or the significance of the F-test for the combined effect of both $V_1$ and $V_2$. With fNIRS, a methodology for false positives correction is not currently available for F-tests or for the patient level. To target a 95% confidence level after false positive correction, an uncorrected 99% confidence level is likely to be a conservative approximation of the true corrected threshold. This was used for Patients 1 and 2. However, this is insufficient to eliminate false positives originating from surface physiology. Due to such effects, fNIRS suffers from problems of specificity (see discussion). Finally, the group analysis performed at the patient level on the group of sessions was a standard fixed effects analysis, which considered the variability within session, ignoring the variability between the sessions. This analysis was done as an unweighted average of the sessions for fMRI as is standard using SPM8, but with a precision-weighted average of the sessions for fNIRS, as is standard using NIRS_SPM.

### *2.4 Real patient data acquisition and analysis methodology*

Patients with refractory epilepsy were recruited in accordance with University Hospital Centers CHU (Notre-Dame Hospital) and CHUME (Sainte-Justine Hospital) ethics committees' guidelines and signed a written consent. Two weeks prior to imaging, their medication treatment was interrupted. They underwent a thorough

neurological evaluation prior to the imaging procedures which consisted of a high-resolution MRI, long-term scalp video-EEG monitoring, ictal SPECT, PET, fMRI-EEG, fNIRS-EEG, MEG-EEG, and finally intracranial EEG monitoring prior to surgery, as described in detail elsewhere (Gallagher et al. 2008; Nguyen et al. in press).

Table 1. Temporal characteristics of spike interval distributions, for the 3 patients, and mean of 100 simulated random protocols of types 1 and 2. Close match on most metrics between Patient 1 with Protocol 1, and Patients 2 and 3 with Protocol 2. Mismatch between the average number of frequent spikes for Patients 2 and 3 and Protocol 2, which may require a more complex spike generating algorithm to simultaneously fit all shown distributional metrics. Note similarity of spike pattern of Patients 2 and 3. Only Protocol 1 shown in simulation results.

| Spike interval characteristics | | Patient | Protocol | | Patient | Patient | Protocol |
|---|---|---|---|---|---|---|---|
| | | 1 | 1 | | 2 | 3 | 2 |
| mean interval between spikes (s) | | 5.1 | 4.9 | | 2.3 | 2.3 | 2.2 |
| median interval between spikes (s) | | 1.2 | 1.1 | | 1.3 | 1.3 | 1.2 |
| standard deviation in spike interval | | 10.2 | 9.1 | | 3.6 | 5.4 | 4.3 |
| spike intervals less than 1 s (%) | | 46 | 39 | | 32 | 38 | 32 |
| spike intervals between 1 and 5 s | | 32 | 38 | | 59 | 53 | 60 |
| spike intervals greater than 10 s | | 13 | 15 | | 2.9 | 1.8 | 4.6 |
| average number of frequent spikes | | 3.8 | 5 | | 6.6 | 5.8 | 12 |
| average number of infrequent | | 1.6 | 1.6 | | 1.3 | 1.1 | 1.3 |

*2.4.1 fMRI-EEG*

fMRI-EEG was acquired in either 3 sessions of 15 minutes (Patient 1) or in sessions of 6 minutes (Patient 2: 6 sessions, however, the last two sessions were discarded due to movement; Patient 3: 8 sessions). Electrophysiology (EEG, ECG, VOG) were recorded on 64 electrodes according to the 10-10 system at 5 kHz with BrainCap and BrainRecorder (BrainProducts, Germany). T2*-weighted fMRI BOLD was acquired with a Philips 3T Achieva scanner: 47 slices of 80 x 80, 3 x 3 x 3 mm voxels covering the whole head with a slightly varying repetition time of 3.013 ± 0.001 s (this glitch, which complicates artifact removal, was due to a display option on the scanner, resolved for later acquisitions), echo time of 30 ms and flip angle of 90. A T1-weighted anatomical image, 176 slices of 256 x 256 (1 x 0.94 x 0.94 mm voxels) was also obtained.

EEGs were filtered with BrainVision Analyzer 2 software. Briefly, gradient artifacts were subtracted using the method in (PJ Allen, Josephs, and Turner 2000) implemented as Template Drift Detection in Analyzer 2, and the dataset was downsampled to 250 Hz. Cardioballistic artifacts were removed in Analyzer 2, by semi-automatic detection of cardiac pulses (PJ Allen et al. 1998). Notch filtering was performed at the slice repetition frequency of 17 Hz and its harmonics. Data was bandpass filtered between 0.3 Hz and 35 Hz. EEGs were marked by an expert epileptologist (DKN). EEG fragments were ignored where no cardioballistic correction had taken place. EEGs were marked aiming to capture most of the spikes, rather than just the strongest. fMRI BOLD data was batch processed using standard parameters in SPM8 (Friston et al. 2007) according to methodology developed in-house. A set of statistical GLMs were also run including some with non-standard HRF (Jacobs et al. 2009).

*2.4.2 fNIRS-EEG*

For simultaneous fNIRS-EEG recording, we again refer to (Gallagher et al. 2008; Nguyen et al. in press) for details. The night prior to fNIRS imaging, the patients were kept awake to increase the likelihood of seizures, which may have modulated the spiking rate of Patient 2 (see section 3.2.2). However none of the patients experienced seizures in these recordings (nor for fMRI). fNIRS-EEG data was recorded in 15 minutes sessions (5 sessions for Patient 1; 6 sessions for Patient 2, of which only the first 4 were usable; 3 sessions for Patient 3). EEGs were recorded with Neuroscan Synamps 2 system (Compumedics, USA) by means of 19 homemade carbon fiber electrodes placed on the helmet according to the 10-20 system. EEG data, as well as ECG, VOG and EMG, were acquired at 500 Hz and bandpass filtered between 0.1 and 100 Hz with a 60 Hz notch filter. The EEGs were then marked by an epileptologist (DKN) using EEG Focus software (BESA, Germany). fNIRS measurements were acquired at 19.5 Hz with a multi-channel Imagent Tissue Oximeter (ISS, USA) with up to 64 sources and up to 16 detectors. Two wavelengths were recorded, one more sensitive to HbR (690 nm) and one more sensitive to HbO (830 nm).

For fNIRS data analysis, we have developed in Matlab (MathWorks, USA) an SPM compatible toolbox with a Matlabbatch graphical interface for pipeline processing, which is available upon request. This toolbox incorporates several modules from the

NIRS_SPM package (Ye et al. 2009; KE Jang et al. 2009). Minimal processing of fNIRS data was performed. Source detector pairs separated by more than 6 cm were excluded. The helmets were designed so that channels expected to be the most important were 3 cm in length, but a few channels as short as 1.6 cm were present (For Patient 3, it was found that removing short channels clarified the results, see section 3.2.3). Channels with standard deviation greater than 20% of the median signal were also excluded.

The next preprocessing steps were performed identically for the simulation data and for the patient data: fNIRS data in each session was normalized to unit median and optical intensities were converted to HbO and HbR changes. Total hemoglobin, HbT = HbO+HbR, a proxy for cerebral blood volume under the assumption of constant hematocrit, was also produced (but mostly not presented in the results as very similar to HbO). A Butterworth 5$^{rd}$ order infinite response filter at 250 s for Patient 1, 200 s for Patient 2, was applied as high-pass filter, and a Gaussian filter of 1.5 s was applied as a low-pass filter (to remove cardiac artifacts, and crucially to produce precolored data, from which an accurate number of degrees of freedom could be calculated for use in the statistics). GLMs were defined with the marked epileptic events as stimuli; otherwise the design matrix was constructed as for the simulations (See section 2.4), with in addition a regressor for heart rate R-R peaks, of no interest but which helped reduce some of the physiological noise. Precoloring (Ye et al. 2009) was the method used to account for temporal noise correlations. The GLM proceeded by calculating the pseudo-inverse of the design matrix, the estimated response and its covariance, and the residual sum of squares, for each session separately. After the GLM estimations, two-dimensional interpolated statistical maps for chosen contrasts were generated for each projected view (e.g. left) and each session, with or without the tube formula correction against false positives. The maps from different sessions were then combined as fixed effects group analysis, thus producing session precision-weighted patient level results. However the patient level results were not corrected against false positives as the technology to perform this correction is not currently available, and a Bonferroni correction would be overly conservative. Amplitudes and statistics were extracted from specific channels at or close to the maxima of the interpolated maps.

# 3. RESULTS

## 3.1 Simulation Results

### *3.1.1 Estimability of the 1st kernel*

We first considered the estimability of the first Volterra response following (Machado et al. 2010). Results are presented as a warm-up and extension of that previous work, to introduce the 2nd Volterra response later and also because our analysis differed in a few details. Here, 1- We attempted to build more realistic protocols (called Type 1 and 2 earlier) combining frequent and infrequent spikes, calibrated to match in several of their distributional characteristics the spike interval profiles seen on our patients EEG data; 2- We used the NIRS_SPM GLM with precoloring but without WMDL (except for Appendix A.5, Fig. S-8), instead of the two GLM methods studied in (Machado et al. 2010); 3- We specified the simulated signal $\beta_1$ (and later $\beta_2$) amplitude(s) as a percentage of the standard deviation of the filtered data, rather than the SNR, as this allowed more consistent comparison of the simulations. Our protocols consisted of 180 for Protocol 1 (except for Appendix A.2, Fig. S-5, and 400 spikes for Protocol 2), for 10 channels of HbO and HbR each, with data size of 15 minutes acquired at 19.5 Hz. For these simulations, we evaluated 4 estimability measures, as in (Machado et al. 2010): The receiver operating characteristic (ROC) curves, the ratio of the estimated to simulated amplitudes $\mathbf{R} = \frac{\widehat{\beta_1}}{\beta_1}$, the T-statistic $\mathbf{T} = \frac{\widehat{\beta_1}}{\sigma_{\beta_1}}$, and the SNR.

Results on the estimability of the 1st Volterra response are provided in Figs. 4 and S-1. 3 amplitude pairs ($\beta_1$, $\beta_2$) were simulated: (0.25,0), (0.5,0) and (0.75,0), illustrating the improvement on the 4 estimability measures with increasing the amplitude of the 1st Volterra response when no 2nd Volterra is simulated. At an amplitude of 0.25, the 1st Volterra response was not highly estimable (Fig. 4). Beyond that, estimability improves rapidly. Results for protocols of Type 2 of 400 spikes were qualitatively similar and not shown; we note in passing that increasing the number of spikes improves estimability, at constant simulated amplitude (See Appendix A.2). For all the additional figures in the appendix, the box-whisker plots are standard as generated by

Matlab, with the median as the central line, the lower and upper boundaries for the box are 25$^{th}$ and 75$^{th}$ percentiles, and the ends of whiskers are the minimum and maximum of the distribution except for possible outliers indicated by plus signs. For ratios of estimated to simulated amplitudes (Fig. S-1A), the median was close to 1, indicating no bias in the estimation. For that measure, and for the T-statistic (Fig. S-1B), improvement was approximately linear in the amplitude. Finally (Fig. S-1C), the SNR increased by about 6 dB with a doubling in amplitude (as expected since the SNR is defined in terms of the power). In comparison to (Machado et al. 2010, Figs. 2 and 3), using (0.5,0) for example, which corresponds to about their simulations at about -15 dB, our ROC area is comparable, our t-statistics are much lower yet significant, but the variability of our results was considerably less. As mentioned earlier, this was mostly accounted for by specifying simulated amplitudes normalized to the standard deviation of filtered data and measuring the SNR with respect to filtered data and convolved protocol.

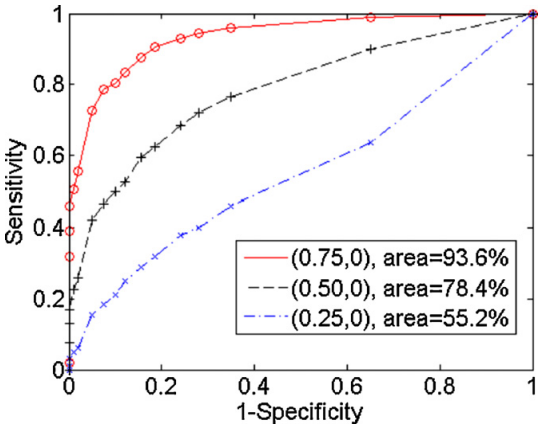


Figure 4. ROC curves for estimability of 1st Volterra response for canonical HRF, in simplified case when no 2nd Volterra was simulated, for 3 amplitude pairs: (0.75, 0), (0.5, 0) and (0.25, 0). On ROC measure, estimability was excellent for amplitude of 0.75 or more (ROC area exceeding 90%), and poor for 0.25 and below (area less than 60%).

### *3.1.2 Estimability of the 2nd kernel*

For the same random protocols, both first and second kernels contributions were added as described in section 2.3 to the fNIRS data. Since in the presence of nonlinearities, estimability is reduced, we increased the simulated amplitudes compared to section 3.1.1: simulations were carried out for amplitude pairs (1,-1), (2,-2) and (3,-3). We noted that estimability of the 2nd Volterra is very similar to the 1st, only slightly lower (Figs. 5, S-2 and S-3). As explained in subsection 2.3.4, for the T-tests on one Volterra regressor or the other, the other Volterra response was treated as a confounding factor of no interest. For Figs. S-2 and S-3, the box plots are laid out as for Fig. S-1, with the exception of Fig. S-3C, which shows the ratio of the estimated 2nd to the estimated 1st Volterra amplitude. Clearly this cancellation effect is due to the strong correlation of the 2 Volterras (between 90% and 97%, depending on the random protocol of spikes). In summary, all results obtained were consistent with a simple message (valid for the simulated number of spikes: 180 for a 15 minutes dataset): $V_1$ and $V_2$ were separately estimable as long as each simulated amplitude was greater than about 1 in absolute value (or 4 times larger than what was required for estimability in the absence of nonlinearities).

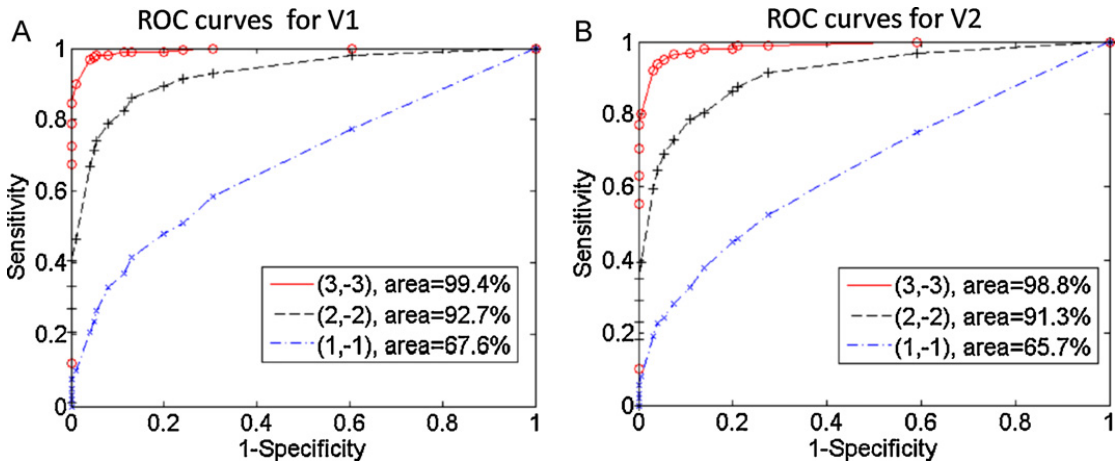


Figure 5. ROC curves for estimability of A. 1st Volterra (V1) and B. 2nd Volterra (V2) response, for 3 amplitude pairs (3, −3), (2, −2) and (1, −1). 2nd Volterra only slightly less estimable than 1st, by about one percent on area measure. Poor estimability of either for amplitudes below (1, −1), but excellent for (2, −2) and above.

## 3.2 Patient results

### *3.2.1 Patient 1*

Patient 1 is a 44 y.o. right-handed man suffering from pharmacoresistant partial epilepsy since age 8 years. Seizures were characterized by right head deviation, elevation of right arm, right facial and arm clonic jerking, altered consciousness and occasionally generalized tonic-clonic movements. Presurgical evaluation revealed left fronto-centro-temporal interictal spikes with or without secondary bilateral synchrony and left hemispheric low voltage fast ictal rhythms during video-scalp EEG monitoring, left frontal hypometabolism on PET, and left parietal activation on ictal SPECT. At the time of EEG-fNIRS and fMRI imaging, medication treatment consisted of levetiracetam (LEV) and carmabazepine (CBZ). An invasive EEG study with extensive left frontal, parietal, temporal subdural strip and grid electrode coverage localized the epileptogenic zone to the left premotor cortex. Left frontal premotor corticectomy led to seizure-freedom (follow-up 17 months).

In Table 1, we show the distributional properties of the more focal spikes (Fig. S-10) without secondary bilateral synchrony. The spikes with bilateral synchrony were fewer in number and often closely associated in time with the more focal ones. Their effects were treated as regressors of no interest. The frequency per minute, and standard deviation over sessions, of focal spikes, in each session, were comparable, at 13.2 ± 2.6 for fMRI and 11.7 ± 3.4 for fNIRS. Spatial coverage with fNIRS is shown in Fig. S-11A and S-11B, with 46 channels remaining on the left projection.

For the focal spikes, we compared statistics of the $V_1$ and $V_2$ Volterra regressors (Fig. 6 and Tables 2a and 2b). There were significant Volterra nonlinearities for all modalities. We also showed that these results were unaffected for fMRI when including the time derivative and dispersion of the HRF as regressors in the 1$^{st}$ and 2$^{nd}$ Volterra kernels (Fig. S-12). This suggested that the HRF for this patient was close to canonical, except for the Volterra nonlinearities. The effect of derivatives was small and had no impact on the presence of nonlinearities, despite the much larger number of regressors (increase from 36 to 102 regressors for the 3 fMRI sessions, without or with derivatives of the HRF). Results of F-tests with false positives correction

including derivatives of the HRF showed the significance separately of the 1st or the 2nd Volterra (Fig. S-12). Thresholded F-maps were very similar to the analysis with T-tests for the significance of the 1st or the 2nd Volterra (Fig. 6), thus Fig. S-12 can be seen as a more detailed view of Fig. 6A for the epileptogenic zone.

Focusing then on the results of GLMs without derivatives (Fig. 6), with BOLD fMRI, $V_1$ was significant at $p<0.05$ with family-wise error (FWE) correction, while $V_2$ was significant at $p<0.001$ without FWE but not with FWE at $p<0.05$. At the epileptic focus (superior frontal gyrus), a positive BOLD signal was seen for $V_1$, accompanied by an inhibitive (opposite sign) effect for $V_2$. One mid-hemisphere sagittal slice was displayed that allowed showing at the same time part of the focus activation and part of the parietal deactivation. With fNIRS, an uncorrected threshold of $p<0.01$ was used (to approximate a tube formula FWE corrected threshold of $p<0.05$ (Ye et al. 2009)). In the focus region, a decrease of both HbR and HbO was seen (and also an increase of HbR). These decreases in $V_1$ amplitude accompanied by increases in $V_2$ for both HbR and HbO were seen in 4 of the 5 sessions at a significant level with the tube formula correction at $p<0.05$ (Table 2a), indicating the robustness of the response at the epileptic focus with fNIRS. The amplitudes observed (Table 2a) for either Volterra were comparable between fMRI and fNIRS, and were in a range where simulations indicated that estimability would be challenging but perhaps attainable (estimated Volterra amplitudes of the order of the standard deviation of the filtered fNIRS data). As noted in the simulation results, the $V_2/V_1$ ratio is expected to show much variability. Despite the session-to-session fluctuations, there was some consistency in the estimated amplitude of the ratio at the patient level: we found a 2nd Volterra response with an amplitude between -40% and -125% of the 1st Volterra. In all sessions with fMRI and fNIRS, this ratio was seen to be negative, corresponding to an inhibition of the hemodynamic response. Inferior to the epileptic zone was a large irritative zone, which was surgically removed along with the focus, for which a standard response (decrease of HbR, increase of HbO) was seen with fNIRS, and with fMRI (at a lower significance level than shown on Fig. 6), all with similar nonlinearities with a negative $V_2/V_1$ ratio. Also prominent in this patient was a large parietal region of inverted response (negative BOLD with fMRI; centered on inferior parietal lobule, sagittal slice shown in Fig. 6 only catching the edge of the response).

We quantified the nonlinearities at the peak of this inverted response (Table 2b) and found also an inhibition of the hemodynamic response, in the range of -45% to -135% for all sessions except session 2 with fNIRS HbO, where amplitudes were close to zero (note that in the case of a weak response, the ratio is meaningless). Interestingly, for this patient, as well as for the upcoming patients, further (de)activations were also seen in other brain areas, especially (de)activations mirror to the epileptic focus, with a varying degree of concordance between fMRI and fNIRS (see (Morrell and deToledo-Morrell 1999) for a review of mirror epileptic foci),. While the focus was clearly localized to the frontal lobe, there remains a limitation of fNIRS to lateralize the focus with complete specificity.

*3.2.2 Patient 2*

This 14-year-old boy had onset of seizures at age 5 years. Spells were characterized by fixed gaze, with or without right and/or left facial jerks and tonic limb extension. His seizure condition progressively worsened over the years with multiple daily seizures (resistant to six antiepileptic drug trials) and epilepsy surgery was considered. The presurgical evaluation included a normal MRI, right inferior frontal hypometabolism on PET and no clear activation on ictal SPECT. Video-EEG monitoring showed very frequent right frontal interictal spikes (Fig. S-13) and diffuse desynchronization followed by non-localizing rhythmic activity during seizures. At imaging, treatment consisted of LEV, CBZ and topiramate. Quantitative analysis of MRI revealed a subtle cortical dysplasia at the bottom of a deep sulcus in the right inferior frontal gyrus confirmed by surgical resection. The patient has remained seizure-free since then (follow-up 13 months). The frequency per minute of focal spikes was 5.2 ± 3.2 for fMRI and 25.7 ± 9.5 for fNIRS. The much higher value for fNIRS may be due in part to forced sleep deprivation prior to fNIRS imaging. Spatial coverage with fNIRS is shown in Fig. S-11C, with 27 channels for the right-side projection.

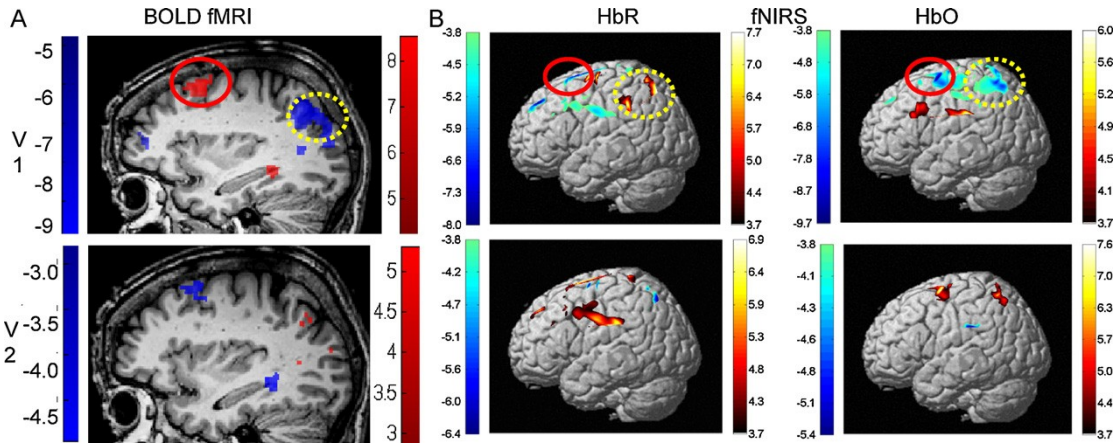


Figure 6. Patient 1: Left-side views of T-statistic maps for 1st (V1, upper row) and 2nd Volterra (V2, lower row) regressors for BOLD fMRI and fNIRS HbR and HbO. The left frontal premotor activation with fMRI was in excellent concordance with clinical results for localization of epileptic focus. At focus, a decrease of HbR (inside solid ellipse), was present, but with an inverted response nearby, both with V2 nonlinearities. For HbO at the focus, the response was inverted, also with V2 nonlinearity. In addition, there were large parietal inverted responses concordant in fMRI and fNIRS, with corresponding nonlinearities. (For interpretation of the references to color in this figure legend, the reader is referred to the web version of the article.)

Table 2a Patient 1, epileptic focus: Comparison between fMRI BOLD and fNIRS HbR T-statistics, amplitudes (normalized with respect to standard deviation of filtered data) at patient level and for each session, for 1st (V1) and 2nd (V2) Volterra responses, and V2/V1 ratio, at epileptic focus (defined as maximum of V1 map for fMRI, and at minimum of fNIRS HbR map in focus area (red ellipse in Fig. 6)). Patient-level T-statistics and amplitudes equally weighted from session data. Patient-level uncertainties computed as SEM from session-level data. Degree of inhibition, as quantified by V2/V1 ratio, found relatively stable. In summary, good concordance between fMRI and fNIRS was found for amplitudes and ratios at epileptic focus.

| **fMRI** | T-stat | All sess. | Sess. 1 | Sess. 2 | Sess. 3 | | |
|---|---|---|---|---|---|---|---|
| V1 amplitude | 8.5 | 1.04 ±0.13 | 0.91 | 1.3 | 0.92 | | |
| V2 amplitude | -4.9 | -0.62±0.14 | -0.36 | -1.0 | -0.50 | | |
| V2/V1 ratio | | **-60** ± 10**%** | -40% | -75% | -55% | | |
| | | | | | | | |
| **fNIRS HbR** | | All sess. | Sess. 1 | Sess. 2 | Sess. 3 | Sess. 4 | Sess. 5 |
| V1 amplitude | -7.0 | -1.4 ± 0.29 | -0.38 | -1.4 | -1.7 | -2.1 | -1.2 |
| V2 amplitude | 5.5 | 1.0 ± 0.25 | 0.57 | 1.4 | 0.96 | 1.7 | 0.56 |
| V2/V1 ratio | | **-76** ± 14% | -123% | -99% | -57% | -83% | -48% |

**Table 2b**. Patient 1, left parietal region with inverted response, same setup as Table 2a. Statistics calculated at minimum of fMRI BOLD V1 map and maximum of HbR V1 map for fNIRS in parietal area (inside dotted yellow ellipse on Fig. 6). Responses inverted in all modalities (except session 3 for HbO), and nonlinearities between fMRI and fNIRS concordant and inhibitive (except HbO session 2), despite variability between sessions.

| **fMRI** | T-stat | All sessions | Sess. 1 | Sess. 2 | Sess. 3 | | |
|---|---|---|---|---|---|---|---|
| BOLD 1 | -9.6 | -0.91 ± 0.11 | -0.86 | -1.04 | -0.83 | | |
| BOLD 2 | 5.2 | 0.63 ± 0.12 | 0.39 | 0.79 | 0.72 | | |
| V2/V1 ratio | | **-69** ± 13% | -45% | -76% | -87% | | |
| | | | | | | | |
| **fNIRS** | | All sessions | Sess. 1 | Sess. 2 | Sess. 3 | Sess. 4 | Sess. 5 |
| HbR 1 | 7.5 | 1.6 ± 0.19 | 1.4 | 1.0 | 2.1 | 1.6 | 1.8 |
| HbR 2 | -6.3 | -1.3 ± 0.41 | -0.77 | -0.52 | -2.8 | -1.1 | -1.4 |
| V2/V1 ratio | | **-86** ± 15% | -57% | -51% | -134% | -73% | -81% |
| HbO 1 | -4.3 | -0.75 ± 0.57 | -1.05 | -0.25 | 1.2 | -1.9 | -1.7 |
| HbO 2 | 3.2 | 0.23 ± 0.49 | 0.52 | -0.32 | -1.4 | 1.2 | 1.2 |
| V2/V1 ratio | | -31 ± 42% | -50% | 130% | -115% | -60% | -68% |

**Table 3**. Patient 2: Concordant fMRI and fNIRS nonlinearities. Same setup as Table 2 (but transposed), at epileptic focus (maximum of V1 map for fMRI, minimum of HbR V1 map for fNIRS).

| Focus | All sess. | | All sess. | | All sess. |
|---|---|---|---|---|---|
| BOLD 1 | 0.85 ± 0.2 | HbR 1 | -0.85 ± 0.15 | HbO 1 | 0.89 ± 0.11 |
| BOLD 2 | -0.63 ± 0.4 | HbR 2 | 0.67 ± 0.12 | HbO 2 | -0.56 ± 0.10 |
| Ratio 2/1 | **-74%** | | **-80%** | | -65% |

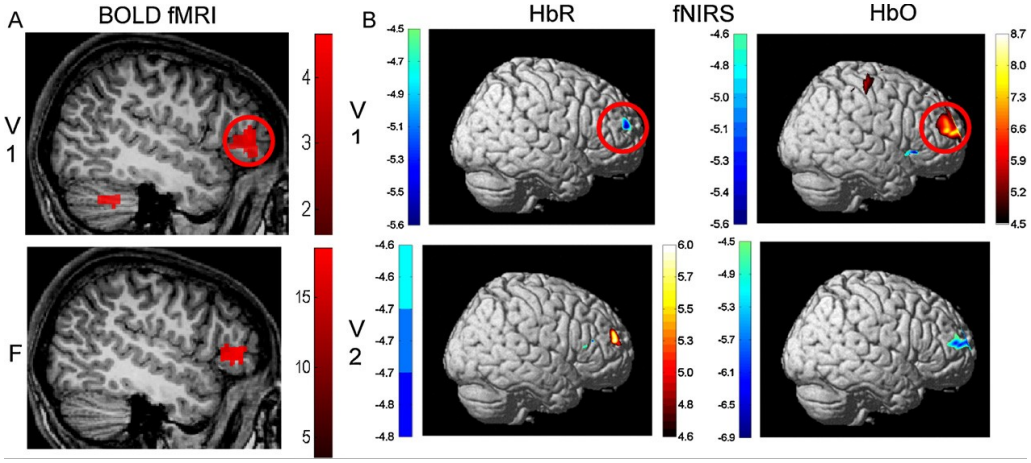


Figure. 7. Patient 2: Right-side views. A. fMRI lateral sagittal slice (first row: T-statistic for V1, second row: F-statistic for combined effect of V1 and V2). B. Topographic reconstructions of HbO and HbR for fNIRS, T-statistics for V1 and V2. The activated areas with fMRI and fNIRS were in excellent concordance with a cortical dysplasia found on anatomical MRI. No negative BOLD, after false positive correction. Significant inhibitive nonlinearities with fNIRS for HbO and HbR, also present but statistically weaker with fMRI.

In Fig. 7 and Table 3, we show our results on nonlinearities for fNIRS and fMRI. The right frontal activated areas seen with all modalities were in excellent concordance with the cortical dysplasia found on anatomical MRI. The focus was clearly localized to the frontal lobes, but mirror (de)activations on the left side were present with fNIRS and also to a weaker degree with fMRI (not shown). Due to epileptic activity with accompanying movement in all but the first two sessions each of the fMRI and fNIRS recordings of this young patient, estimates had large variances except for the first two sessions each, so results are shown at the patient level only. The use of precision-weighting in calculating estimates amounted in effect to almost neglecting those affected sessions. For fMRI, $V_1$ was statistically significant by itself ($p<0.001$, uncorrected), but $V_2$ was not, and an F-test combining $V_1$ and $V_2$ was significant ($p<0.05$, FWE corrected). For fNIRS, $V_1$ and $V_2$ were statistically significant on their own ($p<0.01$, approximating a corrected threshold of $p<0.05$; HbO increase, HbR decrease for $V_1$, with an inhibitive contribution from $V_2$). There was no significant negative BOLD after false positives correction. There was a good agreement on the $V_2/V_1$ ratio at the patient level between fMRI and fNIRS despite the weaker statistical significance of the results compared to Patient 1.

*3.2.3 Patient 3*

This 19-year-old woman with tuberous sclerosis suffered from refractory partial epilepsy since age 14 years. Seizures were characterized by blurred vision with or without altered consciousness. Epilepsy surgery was considered following ten unsuccessful antiepileptic drug trials. At imaging, treatment consisted of LEV, lamotrigine and brivaracetam. Brain MRI disclosed several subependymal nodules, posterior subcortical band heterotopias and several cortical tubers. Video-EEG monitoring showed frequent left posterior quadrant interictal spikes (Fig. S-14) and seizures were associated with left temporo-occipital rhythmic activity. PET showed left posterior quadrant hypometabolism and ictal SPECT showed multiple activation sites including the left inferior temporal region, right temporo-occipital junction, with the maximal hyperperfusion over the left posterior quadrant. To better delineate the epileptogenic zone, an intracranial EEG study was performed which found seizures to originate from the left parieto-occipital area with rapid diffusion to the left inferior occipito-temporal area. Resection of the left superior occipital gyrus (arcus parieto-

occipitalis) and portion of the left posterior parietal gyrus led to seizure-freedom (follow-up 15 months). Pathological analysis of the resected specimen confirmed an underlying cortical dysplasia of Taylor. The frequency per minute of focal spikes was: 17.5 ± 7.3 for fMRI, 25.7 ± 7.7 for fNIRS. After removing channels shorter than 2.8 cm, 23 channels remained on the occipital view for spatial coverage with fNIRS (Fig. S-11D).

Table 4. Patient 3: Larger normalized amplitudes and V2/V1 ratios than previous patients, for V1 and V2 responses at epileptic focus (maximum of V2 map for fMRI, minimum of HbR V2 map for fNIRS). For BOLD, T-tests for V1 or V2 built with canonical HRF were not significant, thus the large error bars; however the F-tests (including HRF derivatives) shown in Fig. 8 were significant.

| Focus | All sess. | | Sess. 1 | | Sess. 1 |
|---|---|---|---|---|---|
| BOLD 1 | 1.6 ± 0.5 | HbR 1 | 2.3 ± 0.34 | HbO 1 | -2.2 ± 0.35 |
| BOLD 2 | -2.8 ± 1.9 | HbR 2 | -2.7 ± 0.25 | HbO 2 | 2.7 ± 0.26 |
| Ratio 2/1 | **-176%** | | **-118%** | | -120% |

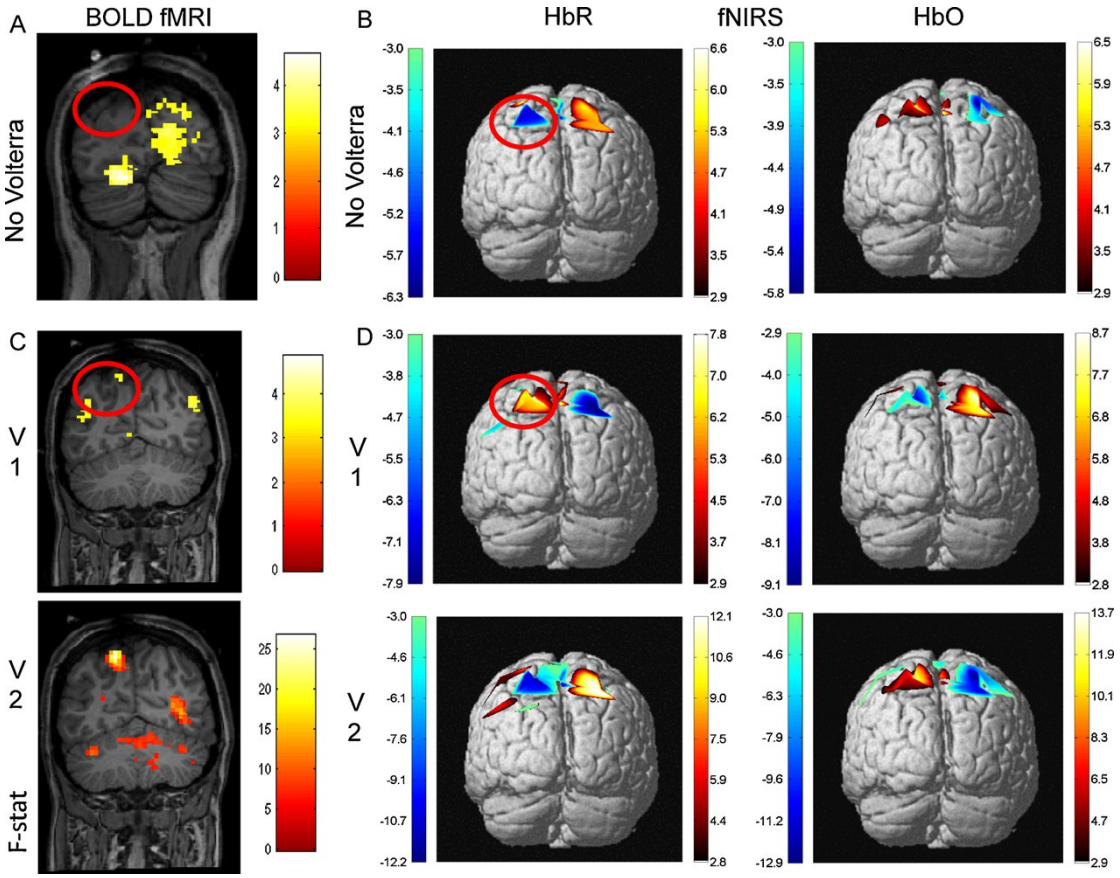


Figure. 8. Patient 3. Analysis with (C and D) and without (A and B) Volterra nonlinearities. With fMRI, no activation was seen at epileptic focus (red ellipses) without including nonlinearities in the GLM (A), but HbR decrease at focus was seen with fNIRS (B). There was no paradox however, since a weak fMRI activation posterior to the focus was present (not shown). Including Volterra nonlinearities, a significant V2 response but weak V1 response were seen at focus with fMRI (C) and fNIRS (D). Including Volterra nonlinearities flipped the sign of the responses for HbR and HbO, indicating the need to include more terms in the Volterra expansion.

Results on nonlinearities from fMRI and fNIRS imaging are presented in Fig. 8 and Table 4. With fMRI, GLM analyses without including Volterra nonlinearities did not localize correctly the epileptic focus (at $p<0.001$, uncorrected), but found other relevant occipital (de)activations (see Fig. 8A, F-statistic for canonical HRF and its derivatives, $p<0.05$, FWE corrected; note that without HRF derivatives, fMRI analyses yielded nothing). With fNIRS, it was found that by excluding short channels, of length less than 2.8 cm, much surface physiological noise correlated with the spikes could be removed, and this simpler analysis was presented (at $p<0.05$, uncorrected; main (de)activations survive at $p<0.01$, but are much reduced in extent). Without including Volterra nonlinearities in the analysis, fNIRS HbR correctly restricted the focus location to the left occipital lobe (a right occipital mirror activation was also seen). Note that there is no paradox between the fNIRS and fMRI results, because an activation posterior to the focus was present with fMRI (not shown), and fNIRS topographic reconstructions cannot discriminate between activations at different depths in the brain. As for the Volterra analysis with fMRI, Fig. 8C showed a T-map for V1 constructed of canonical HRF only, $p<0.001$, uncorrected, and an F-map for V2, constructed from HRF and derivatives, $p<0.05$, FWE corrected. Therefore, with fMRI, the V2 effect was statistically stronger than the V1 effect. A similar observation held with fNIRS. With $2^{nd}$ order Volterra nonlinearities, the fNIRS responses flipped sign. Note that with a correlation of 90 to 95% between the $1^{st}$ and $2^{nd}$ Volterra regressors, a flip of sign of $1^{st}$ Volterra response is automatic if the $2^{nd}$ Volterra amplitude is larger than the $1^{st}$. Thus was an indication that the nonlinearities were very strong, and that more terms could be significant in the Volterra expansion. This was confirmed by a GLM analysis including the $3^{rd}$ Volterra regressor, which was significant (with another overall flip of sign in the responses, restoring the expected pattern of an HbR decrease of $1^{st}$ Volterra at the focus, results not shown). In addition, it was likely that the HRF of this patient was not canonical, due to statistical significance of the derivatives of the HRF in the BOLD analyses. In summary, Volterra nonlinearities were seen with all modalities for this patient. Although the results were not fully understood due to the large amplitudes of nonlinear effects, they were clinically informative.

# 4. DISCUSSION

## 4.1 Summary of results

On general grounds, to understand mechanistically the complex processes of ictogenesis and epileptogenesis, by which inhibitory and excitatory neuronal pathways become destabilized, it is essential to study nonlinear phenomena (See for example chapters 36 and 39 in (Friston et al. 2007)). As a step in that direction, this work aimed to assess whether nonlinearities can be estimated with fNIRS.

The extensive simulations performed here allowed setting boundaries on required signal amplitudes in realistic data when studying nonlinear phenomena. Results showed that second-order kernels can be estimated under appropriate conditions. For realistic amplitudes, when measured as a fraction of the filtered standard deviation present in the signal, we found that there is a narrow window where the estimability issues are not trivial. Without nonlinear responses, for the protocol of spikes studied with 180 spikes in a 15 minutes time period, this window is for amplitudes between 25% and 100% of the standard deviation of the filtered baseline data. With a $2^{nd}$ Volterra response, the window is between 100% and 300%. Beyond these ranges, the response is either obviously present or poorly estimable. In Appendix A.6, Fig. S-9, we also showed in simulations that if nonlinearities were present in the data, it was essential to include the nonlinear regressor in the GLM analysis. Otherwise estimability will be much lower (worse than chance in this simulated case), with a large bias in the estimates.

In a second part of this work, we applied our estimation methodology to patient data. We observed normalized Volterra amplitudes in our three patients that were sufficiently high to enable the nonlinear estimation (namely larger than the standard deviation of the filtered fMRI or fNIRS data). Since these nonlinear contributions were statistically significant and of high enough amplitude, this work suggests taking additional care in the analysis of epileptic data from patients showing frequent spiking activity. This statement was reinforced by the observation that in the third patient, accounting for nonlinearities was an essential step in our fMRI GLM analysis pipeline, since analyses without nonlinearities failed to localize the focus.

We compared fNIRS and fMRI Volterra amplitudes and nonlinear ratios (of the second to first amplitude) and found a general agreement in the size of amplitudes, the sign of the ratios, and in the correspondence of a positive BOLD signal with a decrease of HbR and an increase of HbO. However, a number of differences from these general expectations were noted. In Patient 1, both HbR and HbO decreases were seen at the focus (as well as an increase of HbR very close to the focus). The nonlinear ratio was seen to be an unstable quantity in simulations, and this was reflected in patient data. This ratio showed a large variability between sessions for Patients 2 and 3. However at the patient level, for Patients 1 and 2, the ratio was seen to be stable, with a degree of inhibition approximately in the range of -50% to -100%. The sessions where this ratio was unstable coincided with the sessions where the GLMs were uninformative. As discussed further in section 4.6, this degree of inhibition that was found in patient data was strong, corresponding to a regime where a refractory response (as illustrated in Fig. 3) can be observed to a large number of spikes in close succession. Estimated nonlinearities with fNIRS were larger than with fMRI, though perhaps not significantly different.

**4.2 Focus localization**

Localization of the epileptogenic zone for these patients with fMRI-EEG could be clearly achieved. For Patient 1, it could be considered routine and straightforward, since the focus localizing information was statistically strong for all 3 sessions (Table 2a). For Patient 2, some care was needed in spike marking and focus localizing information came principally from the first of 6 sessions (Table 3), with the other sessions very artefacted by movement. For Patient 3, focus localizing information was absent without Volterra nonlinearities, and resulted from pooling all 8 sessions when including nonlinearities. For fNIRS-EEG, focus localization was less clear due to the presence of several responses in other areas of the brain, mainly mirror sites to the epileptic focus: sensitivity was good but specificity less so. Extracerebral physiological responses correlated with spikes was the main probable cause of this lack in specificity, but more technical issues could not be ruled out: inaccurate interpolation between channels or inaccuracy in setting map thresholds to account for false positives. Three-dimensional tomographic reconstruction might improve upon the two-dimensional topographic reconstructions shown here.

### 4.3 fNIRS preprocessing and filters

Various fNIRS preprocessing steps and filters were tested in turn (results in this section not explicitly shown) and in the light of these tests, results were presented with a minimal set of preprocessing steps and filters that produced the strongest statistical responses and were most concordant with clinical results. fNIRS channels were removed if they exceeded a standard deviation criterion of 20% on the raw time series. Such channels were clearly noisy, and including them lowered the statistical significance of the activations, thus these channels were excluded. Other preprocessing steps were attempted, but also led to less significant responses: Cutting the sessions into segments free of movement ("sub-sessions") and removing (HbO, HbR) channel pairs where heart beats were not detectable on HbO channels. The filters of course played an important role. Simulations seemed to indicate that the Gaussian low-pass filter at 0.67 Hz was close to optimal, but the optimal frequency might depend on the baseline heart rate. Although WMDL may be optimal on cognitive group studies, WMDL for epileptic patient data with frequent spiking in our data led to much reduced responses. A Butterworth high pass filter with a long cutoff was finally chosen as a minimal filter of the drifts in the data. Using no high pass filter also led to much reduced responses. Further work would be required to confirm or enhance the optimality of the processing pipeline.

A more complex issue is the validity of the interpolation to produce maps of T- or F-statistics. When channels are spatially very close (perhaps even on coinciding pixels on the interpolated maps), the two-dimensional interpolation process occasionally generated maps with seemingly absurd (very high) statistical values. This was perhaps due to a breakdown in the Gaussian assumptions required for applicability of inhomogeneous random field theory methods (Ye et al. 2009). We believe that spatial 3-dimensional Gaussian smoothing of the fNIRS data would address this issue, as it does in conventional fMRI analysis, but this has not been done to date. Removal of channels based on a standard deviation criterion (and of short channels for Patient 3) was the strategy used in this article to bypass this interpolation issue.

While the presence of systemic physiology did not impact on the presence of nonlinearities, two techniques may help with getting more specificity for focus

localization, which we plan to use in future acquisitions: recording pulse oximetry and using fNIRS channels separated by very short distances (such as 0.5 cm).

**4.4 Effect of HRF derivatives and non canonical HRFs**

To focus on nonlinearities and simplify the presentation, we did not discuss so far (except for cursory remarks in subsection 3.2.1, Fig. S-12 and subsection 3.2.3, Fig. 8) the role of derivatives of the HRF, or of non-canonical HRFs, which are well-known to be important in epilepsy. It is expected that optimizing the HRF to each patient would improve the statistical significance of the overall response (F-test on all Volterra regressors), both for fMRI and for fNIRS. Perhaps this optimization would also have the effect of increasing the statistical significance of the 1$^{st}$ Volterra (linear) response while reducing the significance of the 2$^{nd}$ Volterra (nonlinear) response. Therefore, it is of importance to estimate the impact of non-canonical HRFs on the results, and find out if some of the nonlinearities could be accounted for by a different shape of the HRF. Since the space of basis functions to describe the hemodynamic response is infinite dimensional, it was not straightforward to test in all generality what impact the precise shape of the HRF would have on the nonlinearities. Several approaches will be discussed in this section.

For completeness for the three patients presented here, detailed calculations were done with fMRI with canonical HRF and derivatives, and with gamma function HRF (results for the remaining of this section not shown). The gamma function HRF performed overall slightly less well than the canonical HRF, with similar activation regions but lower statistical significance, both for the real data and for simulations (recall Fig. S-6). At least for simulations, this lower performance was probably due to the chosen gamma function having less temporal support than the canonical HRF. A gamma function with a larger temporal support may perform better than the canonical HRF in simulations. For the effect of time and dispersion derivatives, we evaluated either F-statistics for the joint effect of canonical HRF and derivatives (masked by positive or negative responses) or T-statistics on the canonical HRF regressor with derivatives treated as confounding regressors. Without entering into details, including derivatives in the GLM usually performed worse or much worse than the canonical HRF alone (with the exception of Patient 3, Fig. 8). In other tests, GLMs were

constructed without nonlinear effects, but with different HRFs, with onsets moved forward or back in time according to the method of (Jacobs et al. 2009). This provided a test that indicated that small or even large time shifts of the HRF were not significant features of these patients' HRFs. Thus the HRF of these patients may be close to canonical on well separated spikes, with the derivatives and dispersion contributing little (except Patient 3). Note that including additional regressors in the GLM weakened the statistics by reducing the number of degrees of freedom and F-statistics are generally weaker (less sensitive) tests than T-statistics. In summary, we did not see that nonlinearities in these patients could be eliminated by using a different HRF.

**4.5 Negative BOLD**

In some animal models (Zhao et al. 2009; Boorman et al. 2010), the negative BOLD signal was suggested to originate from an increase of HbR and a decrease of HbO and HbT. This is what was observed in Patient 1 (parietal region) and Patient 3 (occipital). On the other hand, a decrease of HbR with a decrease of HbO was seen near the focus for Patient 1. Much more work is certainly required before these observations can translated in some generality to humans.

**4.6 Perturbative vs non-perturbative methods**

The Volterra approach taken here was perturbative (a functional Taylor expansion) and may not account for the full nonlinearities present in the signal. In particular, more work is required to account for the non-stationarity of epileptic spike time series: It is well-known that there is a large variability in spike-spike intervals of epileptics. This non-stationarity is likely to be reflected in non-stationary patterns of activation and deactivation, varying from session to session. Such non-stationarity was observed in all 3 patients (mostly not shown, except for Table 2, Patient 1). The sign reversal of the Volterra responses at the epileptic site from one session to the next is one example of this phenomenon.

In addition, we noted some instances of $2^{nd}$ Volterra amplitudes larger than the $1^{st}$ Volterra amplitudes, which was a signal that more terms in the perturbative Volterra expansion could be required. We did not study the estimability of the $3^{rd}$ and higher Volterra kernels, but took a cursory look at the $3^{rd}$ Volterra response for the 3 patients

(results not shown). In some sessions as well as at the patient level, some 3rd kernel responses were significant and of the same sign as the 1st volterra responses. The interpretation of such higher terms is not clear a priori, and perhaps biophysical models (Buxton et al. 2004; Buxton, Wong, and Frank 1998; Zheng et al. 2002; Huppert, MS Allen, et al. 2009) could provide an explanation for their origin, sign and amplitude.

### 4.7 Clinical perspectives

Two of the patients had frontal lobe epilepsy (FLE). FLE is the second most prevalent form of refractory complex partial seizures. Although prognosis of epilepsy surgery for lesional FLE can be good, it remains poor when MRI fails to detect an underlying epileptogenic substrate (Mosewich et al. 2000; Rasmussen 1983). While this work is too preliminary to be of direct clinical relevance, it may be that the study of the nonlinearities and runaway behavior that lead to seizures may improve surgical prognosis by better localizing the epileptic zone, and better understanding the structures and mechanisms of the epileptogenic brain network.

## 5. CONCLUSION

In this work, we showed that 2nd order Volterra nonlinearities are estimable in fNIRS simulated data and are present in real data from 3 epileptic patients with both fMRI and fNIRS. In one patient, inclusion of nonlinearities allowed for correct localization of the epileptic focus with fMRI, which was missed in standard analyses without nonlinearities. The nonlinearities observed in patient data were all inhibitive, and even refractory: Namely at every voxel in fMRI statistical maps and every site on the fNIRS projected maps, when a nonlinearity was significantly present, it had an amplitude of the opposite sign than the linear response (and of a comparable order of magnitude). In future work, we hope to understand the nonlinearities better using a non-perturbative approach.

**Appendix A**: Further results on the simulations

*A.1 Estimability of HbO compared to HbR*

In the next several sections, we present briefly a few results from the simulations (Figures S-4 to S-9 in Supplementary Materials). In (Machado et al. 2010), a difference was noted between HbO and HbR estimability. With the same simulation setup as in subsection 3.1.2, but increasing the sample size to 1000 protocols (only here for this subsection), we considered the difference in estimability between 10 HbO and 10 HbR channels, for amplitude pairs (1,-1), (2,-2) and (3,-3). Note that HbO and HbR were simulated with the same canonical HRF; we did not here attempt to say anything about the complex issues of how real HbO and HbR responses differ in real data; instead, the purpose of the simulation pertained to estimability relative to a noise background constructed of either HbO or HbR measurements. Although there was no significant difference between mean HbO and HbR estimability, we saw more variability in HbR than in HbO estimability (Fig. S-4). This variability disappeared entirely when considering 100 channels each for HbO and HbR (not shown). Thus the difference in HbO and HbR estimability seen in (Machado et al. 2010) may be due to considering too few channels or protocols, or some of the reasons mentioned in subsection 3.1.1.

*A.2 Estimability as a function of the number of epileptic spikes in the protocol*

Again with the set up in subsection 3.1.2, back to 100 protocols for all the remaining subsections, we considered estimability as a function of the number of simulated epileptic spikes, for 360, 180 and 90 spikes, for the amplitude pair (2,-2). The estimability fell rapidly with the number of spikes (Fig. S-5), with the 2$^{nd}$ Volterra estimability falling more rapidly than that of the 1$^{st}$ Volterra. From this result, it follows that patients with the highest spike frequency offer the best chance at detecting nonlinear responses.

*A.3 Estimability variability as a function of the HRF and incorrectly specifying the HRF*

Still within the same framework, for the amplitude pair (2,-2), we considered the effect of simulating spikes with either the canonical (C) HRF or the gamma (G) HRF,

and estimating the response again with either HRF (Fig. S-6). Thus 4 GLMs were run, referred to as CC, GG, CG and GC, with the letters indicating which HRF was used to simulate the spikes and estimate the GLM response, respectively. GLM CC performed better than the others, but GG was very close. GLMs CG and GC explored the effect of incorrectly specifying the HRF: CG performed slightly worse, but GC performed much worse, with a large negative bias in the estimated amplitude. These results illustrated that Volterra nonlinearities would be less estimable if the HRF used in the GLM was not the true HRF.

*A.4 Estimability as a function of the degree of nonlinearity*

Again within the same framework, we considered varying the amplitude of the 2nd Volterra response, with the 1st Volterra response held constant (Fig. S-7). 4 amplitude pairs were generated: (2,-2), (2,-1), (2,1) and (2,2). 1st Volterra estimability was unaffected by the change in 2nd Volterra amplitude. The sign of the 2nd Volterra amplitude, whether negative or positive, had little impact on the ROC curves. However the ratio $V_2/V_1$ was much more volatile for positive $V_2$ amplitude. This was due to the runaway behavior of greater-than-linear responses, with small errors getting magnified. This led to a greater skew in the estimated to simulated $V_2$ amplitude ratio for positive $V_2$ amplitude. On the other hand, the SNR was much higher for positive than negative $V_2$ amplitude, again due to the magnification of the response for positive $V_2$ amplitude, against the inhibition of the response for negative $V_2$ amplitude. Hence, SNR by itself was not a useful measure of estimability.

*A.5 Estimability as a function of the low frequency data filter*

Still in the same framework, we considered the effect of the low frequency, or high-pass, filter on NIRS data (Fig. S-8). For amplitude pair (2,-2), 3 GLMs were run, labeled B, W and B+W, whether a Butterworth order 5 high pass filter with 250 s cutoff (B), the Wavelet Minimum Description Length (WMDL) method (Ye et al. 2009) (W), or both methods (B+W) were used. On this data, B performed slightly better than either W or B+W. We noted that W showed a bias (which disappeared for B+W) in the estimated to simulated $V_1$ and $V_2$ amplitudes, underestimating the amplitude of the response by about 5% for pair (2,-2). This effect was more

significant for larger simulated amplitudes. This result justified focusing on the B filter for presentation of patient results in this work.

*A.6 Estimability in the presence or absence of nonlinear effects*

Finally, still in the same framework, we considered the effect of estimating nonlinearities when there were none, and inversely of ignoring nonlinearities when they were present (Fig. S-9). For amplitude pair (1,-1), 4 GLMs were run, labeled VV, VN, NV and NN, with letters indicating if Volterra nonlinearity was generated (V) or not (N) and was estimated using a GLM regressor (V) or not (N), respectively. Clearly, the estimability was much greater when there were no nonlinearities in the data, and they were not looked for by including $V_2$ in the GLM (NN). Indeed, if there were no nonlinearities, including them in the GLM led to much worse estimability measures, but no worse than if nonlinearities had been present (compare NN to NV, and then to VV). On the other hand, if nonlinearities were present in the data (VN), ignoring them in the GLM led to estimability worse than chance alone (ROC area less than 50%). The $V_1$ estimated amplitude suffered a large bias in this case. From these results, we concluded that if nonlinearities were present in the data, it was important to search for them in the GLM, otherwise estimability will be poor, with a large bias in the estimates. As discussed in more detail in section 3.2.3, the results for patient 3, Fig. 8, probably reflect this observation.

## Appendix B. Supplementary data

Supplementary data associated with this article can be found, in
the online version.

## Acknowledgments

We would like to thank A. Machado for useful conversations, I. Gutberlet from Brain Vision for assistance, two anonymous reviewers for their constructive comments and especially C. Bonnery for developmental work on the fNIRS toolbox. This work was supported in part by the Emerging Team Grant Program of the Canadian Institutes of Health Research, the Discovery Grant Program of the Natural Sciences and Engineering Research Council of Canada, by the Programmes cliniques FRSQ (Fonds de la Recherche en Santé du Québec), by the Canadian Foundation for Innovation and by the Imaginc group at Ecole Polytechnique Montreal.

## REFERENCES

Allen, PJ, O Josephs, and R Turner. 2000. “A method for removing imaging artifact from continuous EEG recorded during functional MRI.” NeuroImage 12 (2): 230-239.

Allen, PJ, G Polizzi, K Krakow, DR Fish, and L Lemieux. 1998. “Identification of EEG events in the MR scanner: the problem of pulse artifact and a method for its subtraction.” NeuroImage 8 (3) (October): 229-239.

Boorman, L, AJ Kennerley, D Johnston, M Jones, Y Zheng, P Redgrave, and J Berwick. 2010. “Negative blood oxygen level dependence in the rat: A model for investigating the role of suppression in neurovascular coupling.” Journal of Neuroscience 30 (12) (March): 4285-4294.

Boynton, GM, SA Engel, GH Glover, and DJ Heeger. 1996. “Linear systems analysis of functional magnetic resonance imaging in human V1.” The Journal of Neuroscience 16 (13) (July 1): 4207-4221.

Buchheim, K, H Obrig, W Pannwitz, A Mueller, H Heekeren, A Villringer, and H Meierkord. 2004. “Decrease in haemoglobin oxygenation during absence seizures in adult humans.” Neuroscience Letters 354 (2) (January): 119-122.

Buxton, RB, K Uludag, DJ Dubowitz, and TT Liu. 2004. “Modeling the hemodynamic response to brain activation.” NeuroImage 23 Suppl 1: S220-233.

Buxton, RB, EC Wong, and LR Frank. 1998. “Dynamics of blood flow and oxygenation changes during brain activation: the balloon model.” Magnetic Resonance in Medicine 39 (6) (June): 855-864.

Delpy, D T, M Cope, P van der Zee, S Arridge, S Wray, and J Wyatt. 1988. “Estimation of optical pathlength through tissue from direct time of flight measurement.” Physics in Medicine and Biology 33 (12) (December): 1433-1442.

Desjardins, M, P Pouliot, and F Lesage. 2010. “Principles and applications of diffuse optical tomography for the brain.” Current Medical Imaging Reviews.

Friston, KJ, J Ashburner, S Kiebel, T Nichols, and W Penny. 2007. Statistical parametric mapping□: the analysis of funtional brain images. 1st ed. Elsevier/Academic Press.

Friston, KJ, O Josephs, G Rees, and R Turner. 1998. “Nonlinear event-related responses in fMRI.” Magnetic Resonance in Medicine 39 (1) (January): 41-52.

Friston, KJ, A Mechelli, R Turner, and CJ Price. 2000. “Nonlinear responses in fMRI: the Balloon model, Volterra kernels, and other hemodynamics.” NeuroImage 12 (4) (October): 466-477.

Gallagher, A, D Bastien, I Pelletier, P Vannasing, AD Legatt, SL Moshé, R Jehle, et al. 2008. “A noninvasive, presurgical expressive and receptive language investigation in a 9-

year-old epileptic boy using near-infrared spectroscopy." Epilepsy & Behavior 12 (2) (February): 340-346.

Glover, GH. 1999. "Deconvolution of impulse response in event-related BOLD fMRI."NeuroImage 9 (4) (April): 416-429.

Grouiller, F, L Vercueil, A Krainik, C Segebarth, P Kahane, and O David. 2009. "Characterization of the hemodynamic modes associated with interictal epileptic activity using a deformable model-based analysis of combined EEG and functional MRI recordings." Human Brain Mapping: NA-NA.

Hamandi, K, HWR Powell, H Laufs, MR Symms, GJ Barker, GJM Parker, and L Lemieux. 2008. "Combined EEG-fMRI and tractography to visualise propagation of epileptic activity." Journal of Neurology, Neurosurgery & Psychiatry 79 (5) (May): 594-597.

Hansen, KA, SV David, and JL Gallant. 2004. "Parametric reverse correlation reveals spatial linearity of retinotopic human V1 BOLD response." NeuroImage 23 (1) (September): 233-241.

Hawco, CS, AP Bagshaw, Y Lu, F Dubeau, and J Gotman. 2007. "BOLD changes occur prior to epileptic spikes seen on scalp EEG." NeuroImage 35 (4) (May): 1450-1458.

Huppert, TJ, MS Allen, SG Diamond, and DA Boas. 2009. "Estimating cerebral oxygen metabolism from fMRI with a dynamic multicompartment Windkessel model." Human Brain Mapping 30 (5) (May): 1548-1567.

Huppert, TJ, SG Diamond, MA Franceschini, and DA Boas. 2009. "HomER: a review of time-series analysis methods for near-infrared spectroscopy of the brain." Applied Optics 48 (10) (April 1): D280-298.

Jacobs, J, C Hawco, E Kobayashi, R Boor, P LeVan, U Stephani, M Siniatchkin, and J Gotman. 2008. "Variability of the hemodynamic response as a function of age and frequency of epileptic discharge in children with epilepsy." NeuroImage 40 (2) (April): 601-614.

Jacobs, J, P LeVan, F Moeller, R Boor, A Stephani, J Gotman, and M Siniatchkin. 2009. "Hemodynamic changes preceding the interictal EEG spike in patients with focal epilepsy investigated using simultaneous EEG-fMRI." NeuroImage 45 (4) (May): 1220-1231.

Jacquez, JA, and P Greif. 1985. "Numerical parameter identifiability and estimability: Integrating identifiability, estimability, and optimal sampling design." Mathematical Biosciences 77 (1-2) (December): 201-227.

Jang, KE, S Tak, J Jung, J Jang, and JC Ye. 2009. "Wavelet minimum description length detrending for near-infrared spectroscopy." Journal of Biomedical Optics 14 (3): 034004.

Kobayashi, E, AP Bagshaw, C Grova, F Dubeau, and J Gotman. 2006. “Negative BOLD responses to epileptic spikes.” Human Brain Mapping 27 (6) (June): 488-497.

Krakow, K, L Lemieux, D Messina, CA Scott, MR Symms, JS Duncan, and DR Fish. 2001. “Spatio-temporal imaging of focal interictal epileptiform activity using EEG-triggered functional MRI.” Epileptic Disorders 3 (2) (June): 67-74.

Laufs, H, and JS Duncan. 2007. “Electroencephalography/functional MRI in human epilepsy: what it currently can and cannot do.” Current Opinion in Neurology 20 (4) (August): 417-423.

LeVan, P, L Tyvaert, F Moeller, and J Gotman. 2010. “Independent component analysis reveals dynamic ictal BOLD responses in EEG-fMRI data from focal epilepsy patients.” NeuroImage 49 (1) (January 1): 366-378.

Machado, A, J-M Lina, J Tremblay, M Lassonde, DK Nguyen, F Lesage, and C Grova. 2010. “Detection of hemodynamic responses to epileptic activity using simultaneous electro-encephalography (EEG)/near infrared spectroscopy (NIRS) acquisitions.” NeuroImage (December).

Morrell, F, and L deToledo-Morrell. 1999. “From mirror focus to secondary epileptogenesis in man: an historical review.” Advances in Neurology 81: 11-23.

Mosewich, RK, EL So, TJ O’Brien, GD Cascino, FW Sharbrough, WR Marsh, FB Meyer, CR Jack, and PC O’Brien. 2000. “Factors predictive of the outcome of frontal lobe epilepsy surgery.” Epilepsia 41 (7) (July): 843-849.

Nguyen, DK, J Tremblay, P Pouliot, P Vannasing, O Florea, L Carmant, F Lepore, M Sawan, F Lesage, and M Lassonde. 2011. “Noninvasive continuous EEG-fNIRS recording of temporal lobe seizure.” Accepted in Epilepsy Research.

Osharina, V, E Ponchel, A Aarabi, R Grebe, and F Wallois. 2010. “Local haemodynamic changes preceding interictal spikes: A simultaneous electrocorticography (ECoG) and near-infrared spectroscopy (NIRS) analysis in rats.” NeuroImage 50 (2) (April): 600-607.

Rasmussen, T. 1983. “Characteristics of a pure culture of frontal lobe epilepsy.” Epilepsia 24 (4) (August): 482-493.

Soltysik, D, K Peck, K White, B Crosson, and R Briggs. 2004. “Comparison of hemodynamic response nonlinearity across primary cortical areas.” NeuroImage 22 (3) (July): 1117-1127.

Toyoda, H, K Kashikura, T Okada, S Nakashita, M Honda, Y Yonekura, H Kawaguchi, A Maki, and N Sadato. 2008. “Source of nonlinearity of the BOLD response revealed by simultaneous fMRI and NIRS.” NeuroImage 39 (3) (February 1): 997-1013.

Vanzetta, Ivo, Corey Flynn, Anton I Ivanov, Christophe Bernard, and Christian G Bénar. 2010. “Investigation of linear coupling between single-event blood flow responses and interictal discharges in a model of experimental epilepsy.” Journal of Neurophysiology 103 (6) (June): 3139-3152. doi:10.1152/jn.01048.2009.

Vaudano, AE, H Laufs, SJ Kiebel, DW Carmichael, K Hamandi, M Guye, R Thornton, et al. 2009. “Causal hierarchy within the thalamo-cortical network in spike and wave discharges.” PLoS ONE 4 (8) (August): e6475.

Ye, JC, S Tak, KE Jang, J Jung, and J Jang. 2009. “NIRS-SPM: Statistical parametric mapping for near-infrared spectroscopy.” NeuroImage 44 (2) (January): 428-447.

Zhao, M, H Ma, M Suh, and TH Schwartz. 2009. “Spatiotemporal dynamics of perfusion and oximetry during ictal discharges in the rat neocortex.” Journal of Neuroscience 29 (9) (March): 2814-2823.

Zheng, Y, J Martindale, D Johnston, M Jones, J Berwick, and J Mayhew. 2002. “A model of the hemodynamic response and oxygen delivery to brain.” NeuroImage 16 (3 Pt 1) (July): 617-637.

Supplementary figure S1

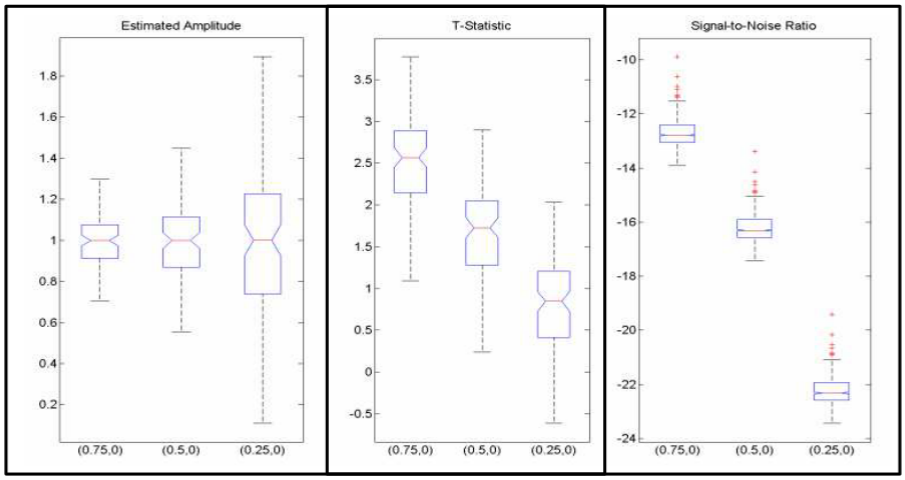


Figure S-1: 3 additional estimability measures for 1st Volterra response with amplitudes 0.75, 0.5 and 0.25, showing decrease in estimability with decreasing amplitude. A. Ratio of estimated to simulated amplitude. Mean close to 1 (no bias). B. Distribution of T-statistics. Amplitude of 0.5 or more required to pass T-test with strong significance (assuming typical threshold of 1.9 for 95% confidence level). C. Distribution of SNR, calculated in decibels from ratio of filtered convolved protocol power to filtered baseline power.

Supplementary figure S2

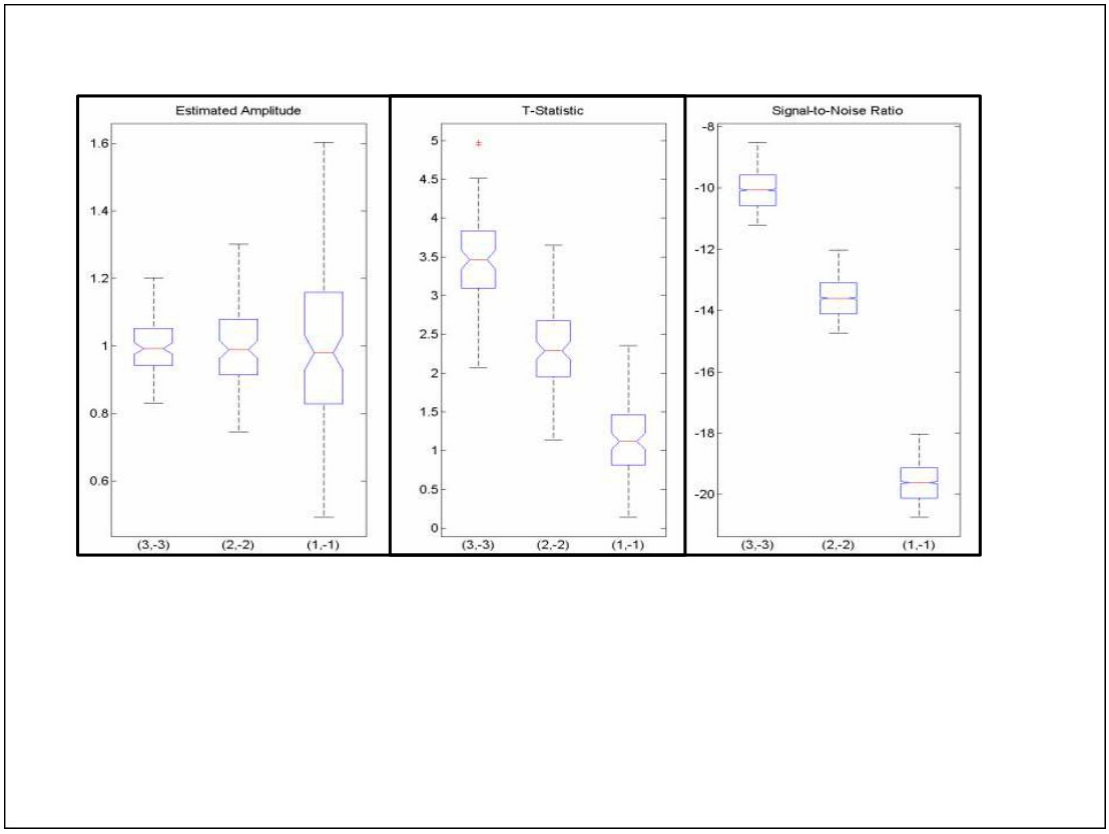


Figure S-2: Additional measures for estimability of 1st Volterra amplitude, for pairs (3,-3), (2,-2) and (1,-1). Same setup as Fig. S-1.

Supplementary figure S3

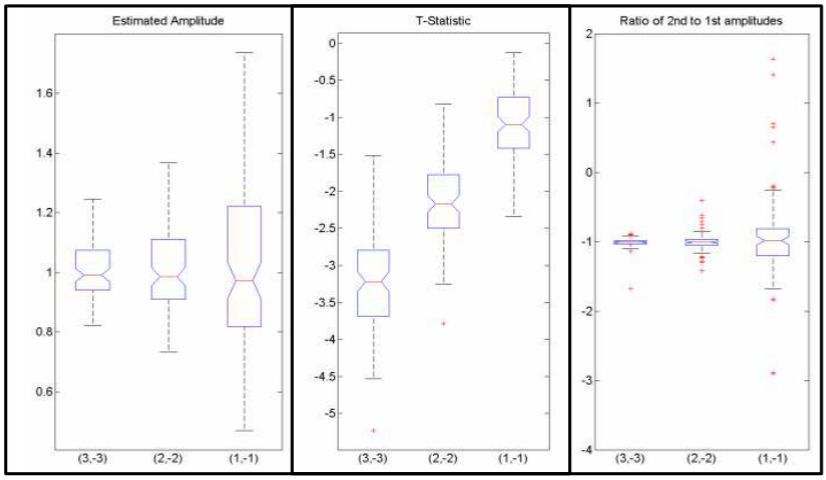


Figure S-3: Additional measures for estimability of 2nd Volterra amplitude, for pairs (3,-3), (2,-2) and (1,-1). A. Ratio of estimated to simulated 2nd Volterra. B. T-statistic distribution. C. Ratio V2/V1 between estimated 2nd and estimated 1st Volterra amplitudes. Ratio seen as very volatile.

Supplementary figure S4

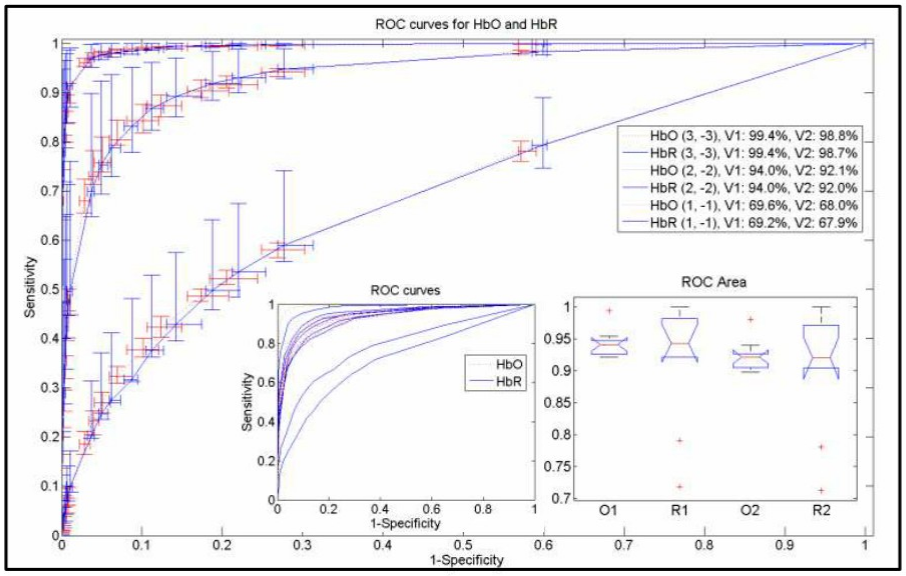


Figure S-4: ROC curves comparison of HbO and HbR for 1000 protocols, mean of 10 channels for each of HbO and HbR, for amplitude pairs (3, -3), (2, -2) and (1, -1), for 1st Volterra response and canonical HRF. ROC areas in legend. No significant difference in mean HbO and HbR estimability. HbR here more volatile than HbO (HbR had 2 channels with ROC area of 100% and 2 much weaker channels), however difference between HbO and HbR volatility disappeared for additional run for pair (2,-2) with 100 channels each (not shown). Horizontal and vertical error bars from 25th to 75th percentile of the distribution over protocols of the sensitivity and specificity mean over channels. Insets: (Left) For pair (2,-2) and V1, HbO and HbR ROC curves for each channel, and (Right) ROC area distributions for V1 and V2. Labels: letter O or R for HbO or HbR and digit 1 or 2 for V1 or V2. Results for V2 very similar to V1, only slightly lower.

Supplementary figure S5

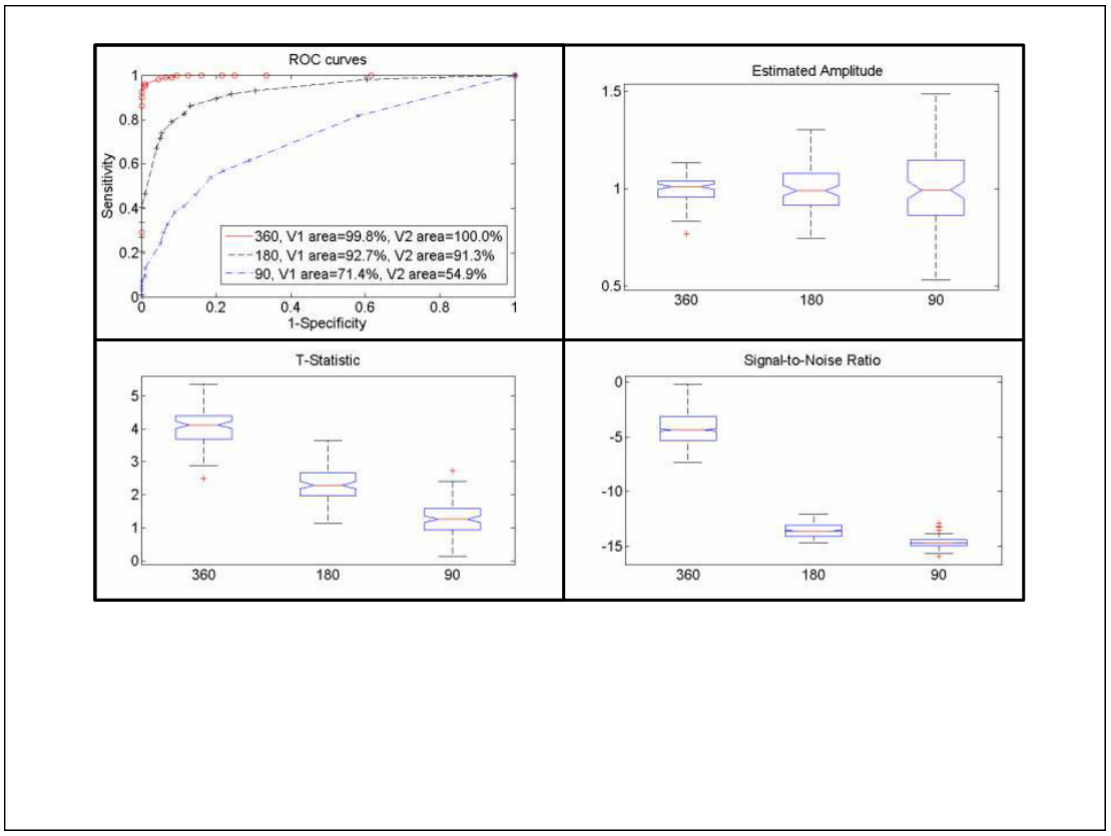


Figure S-5: Estimability of 1st Volterra as function of number of simulated epileptic spikes, for amplitude pair (2, -2) and canonical HRF. Rapid decrease in estimability with decreasing number of spikes. A. ROC curves. Area of 2nd Volterra also specified in legend. V2 performance equally good as V1 for about 180 spikes per 15 minute protocol, but much worse than V1 with half as many spikes (90), and better than V1 with twice more spikes (360), also seen on additional measures for V2 (not shown). B. Ratio of estimated to simulated V1 (no bias). C. T-statistic distribution for V1. D. SNR distribution. SNR comparable for 180 and 90 spikes due to 2nd Volterra cancellation effect for 180 or more spikes, causing reduced amplitudes, an effect weaker for 90 or fewer spikes (as typical interspike intervals become too large). Protocols with indicated number of spikes

Supplementary figure S6

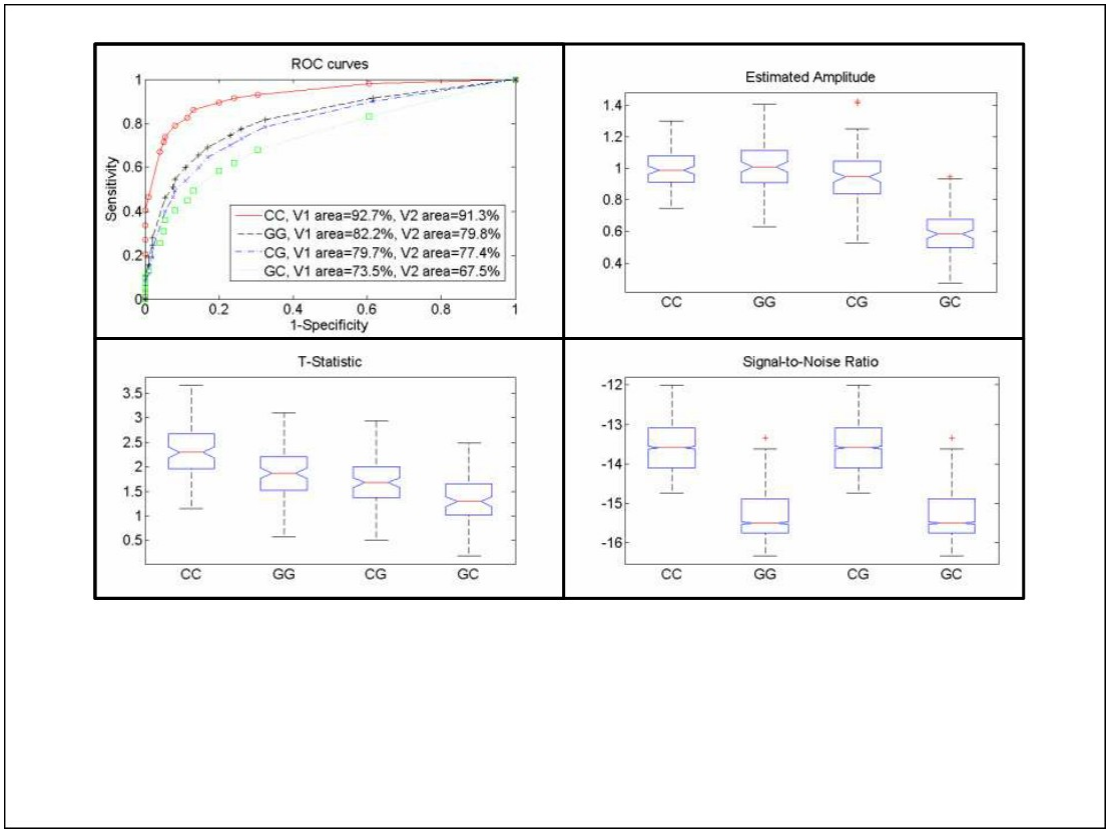


Figure S-6: 1st Volterra, comparison of canonical (C) and gamma (G) HRFs and effect of using suboptimal HRF, for amplitude pair (2, -2). 4 GLMs were run, labeled CC, GG, CG and GC, with first letter indicating HRF used to simulate spikes and second letter indicating HRF used to estimate GLM response. A. ROC curves. CC slightly better than GG. CG and GC worse than either CC or GG. CG much better than GC. V2 areas also shown in legend, slightly smaller than corresponding V1 areas. B. Ratio of estimated to simulated V1. Large bias present for GC. C. T-statistic distribution for V1. D. SNR lower for simulated G than C HRF. Additional 2nd Volterra results not shown, as very similar to 1st Volterra, only slightly lower on all measures.

Supplementary figure S7

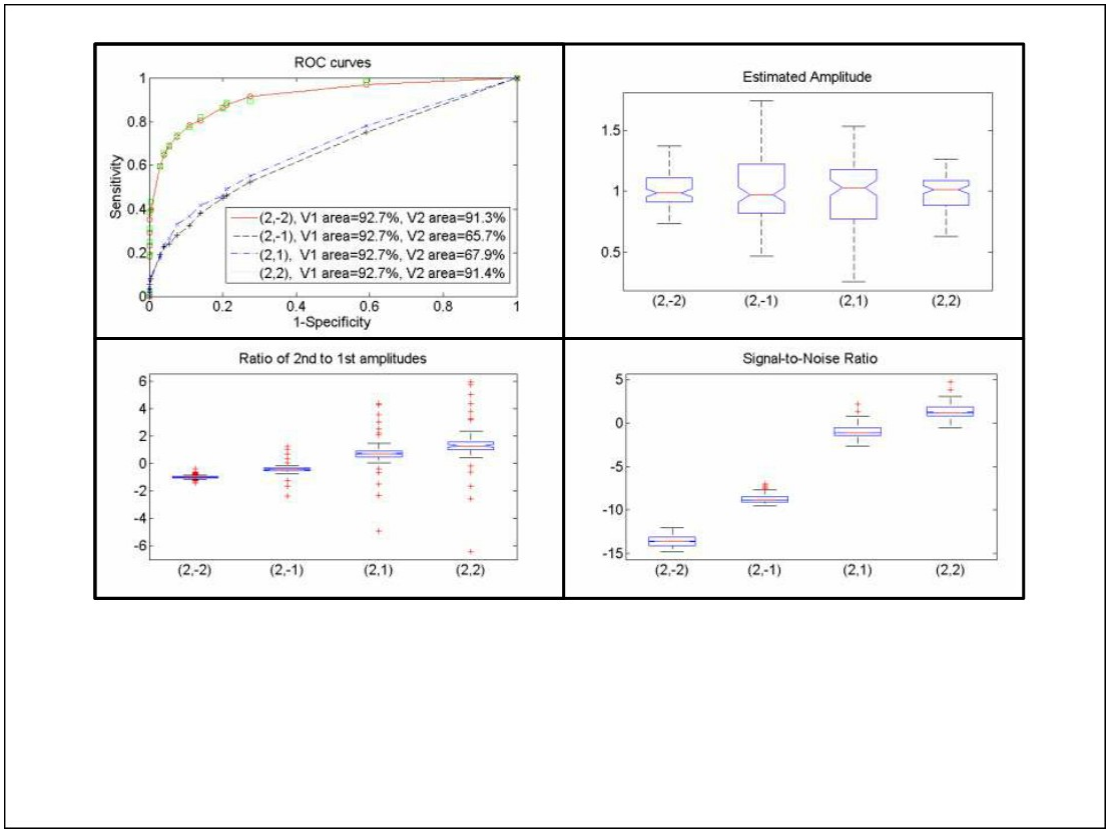


Figure S-7: Effect of varying amplitudes of 2nd Volterra, comparison of amplitude pairs (2, -2), (2,-1), (2,1) and (2,2). No effect on 1st Volterra estimability. A. Negligible impact of sign of 2nd Volterra on ROC curves. B. Small impact on ratio of estimated to simulated amplitude, except for downward skew for positive 2nd Volterra. C. Greater volatility in V2/V1 ratio with increase of V2 amplitude (related to downward skew). D. SNR increase with increase of V2 amplitude, due to signal cancellation for negative V2 and signal build-up for positive V2.

Supplementary figure S8

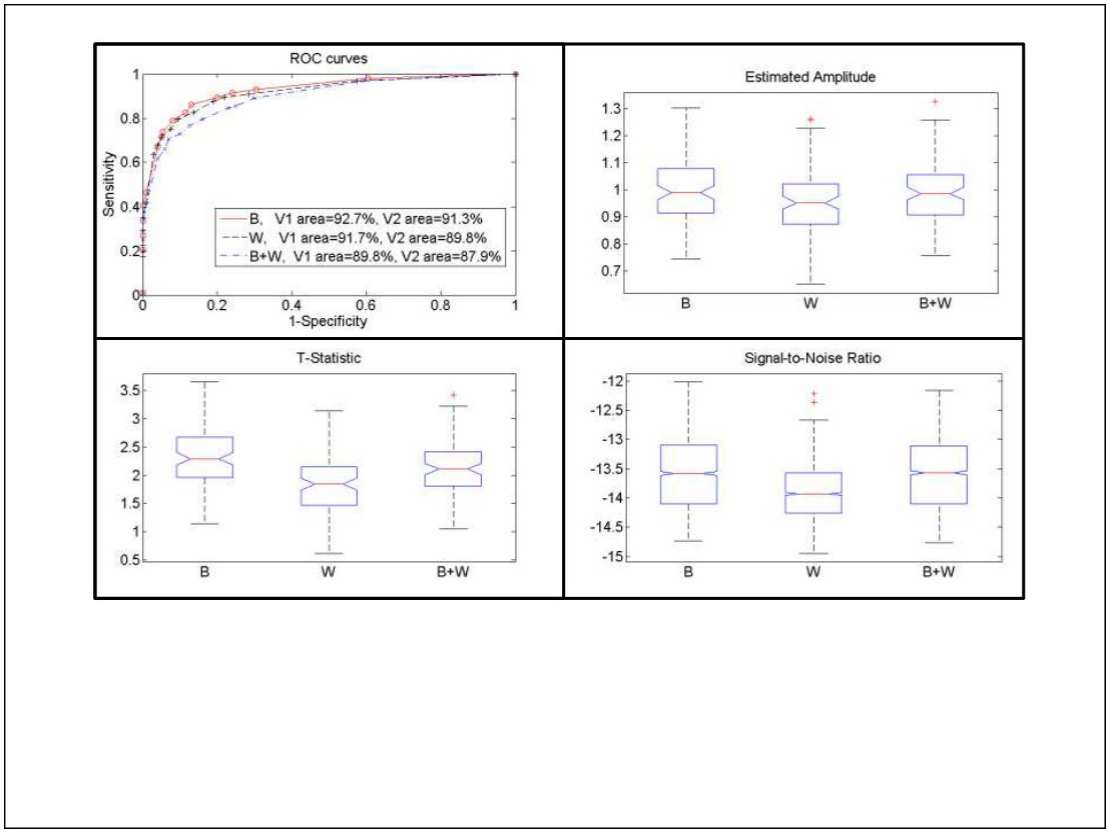


Figure S-8: Effect on 1st Volterra of varying high pass filter (B: Butterworth of order 5, cutoff at 250 s), W: Wavelet method of Ye et al. (2009), B+W: Both filters applied). A. Negligible impact of filter on ROC curves, with B slightly better. B. Bias present for wavelet method on ratio of estimated to simulated amplitude (mean of 0.95, significantly different from 1). Bias absent when wave method combined with Butterworth filter. C. Lower T-statistic and D. lower SNR for wavelet method. For 2nd Volterra (not shown), bias also present and T-statistic worse for wavelet method. Ratio V2/V1 more volatile for B+W method (not shown).

Supplementary figure S9

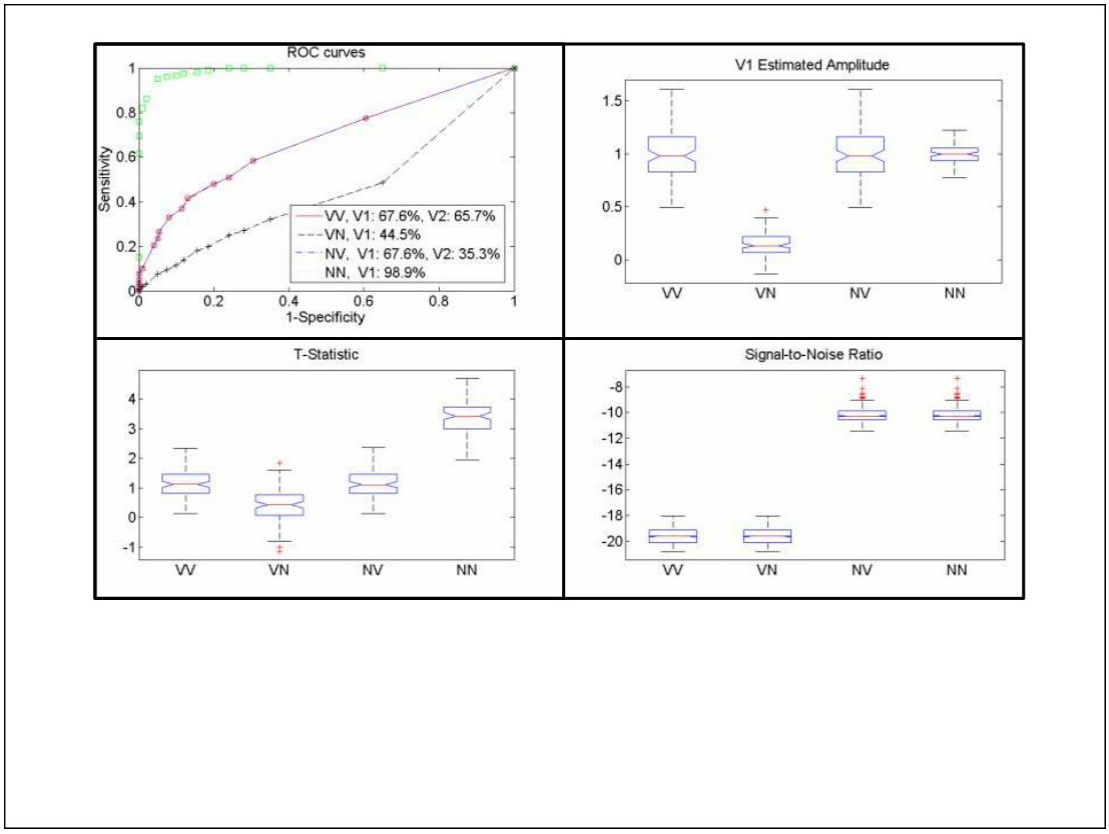


Figure S-9: Estimability of 1st Volterra in presence or absence of 2nd Volterra for pair (1,-1). 4 GLMs were run, labeled VV, VN, NV, NN, with 1st letter indicating 2nd Volterra response added (V) or not included (N) and 2nd letter indicating 2nd Volterra regressor included in GLM (V) or not included (N). A. Estimability much higher when no Volterra effect present in data and not looked for in GLM (NN). Estimability very poor (worse than chance alone) if Volterra present in data but not accounted for in GLM (VN). Estimability of V1 unaffected by whether Volterra effect is present in data for GLM including V2 regressor (VV and NV), but again much lower than NN. No V2 effect found if not there (NV). B. Large bias in V1 estimation if V2 present in data but ignored in GLM (VN). C. T-statistic much higher for NN. D. SNR lower by about 10 dB in presence of V2 effect in data.

Supplementary figure S10

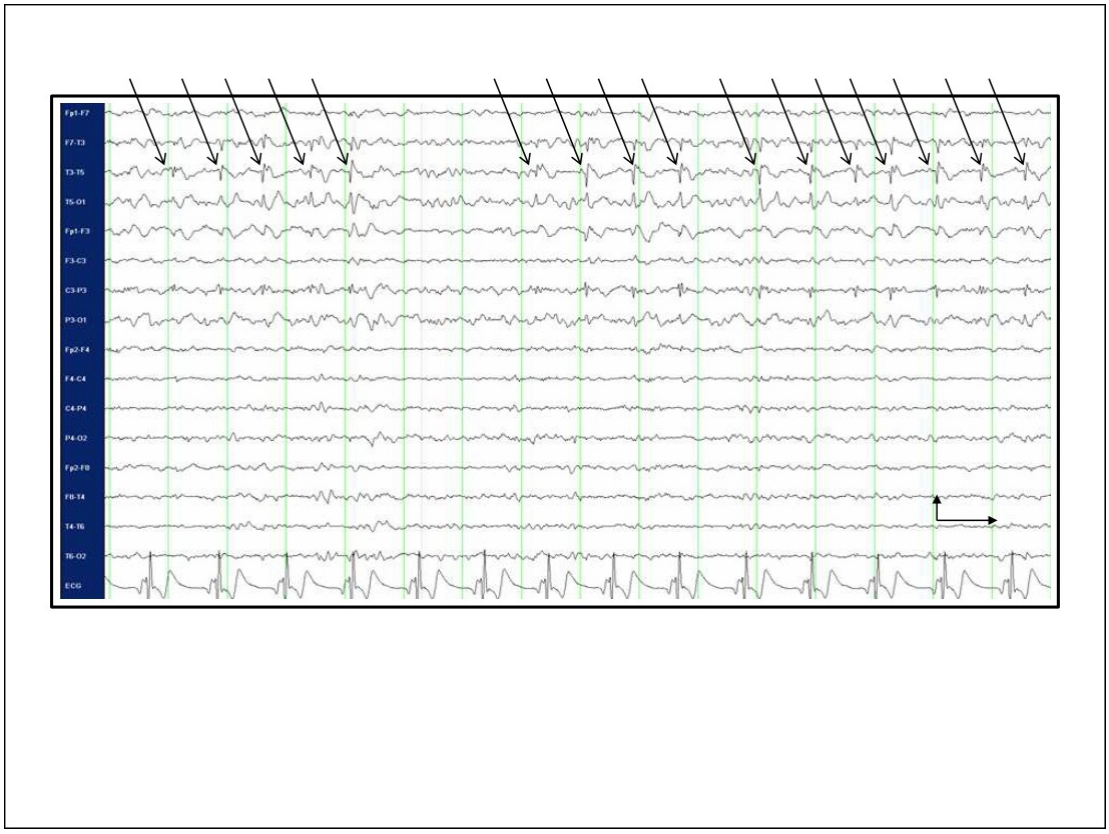


Figure S-10: Patient 1: EEG sample (16 s) with frequent left fronto-centro-temporal focal spikes.

Supplementary figure S11

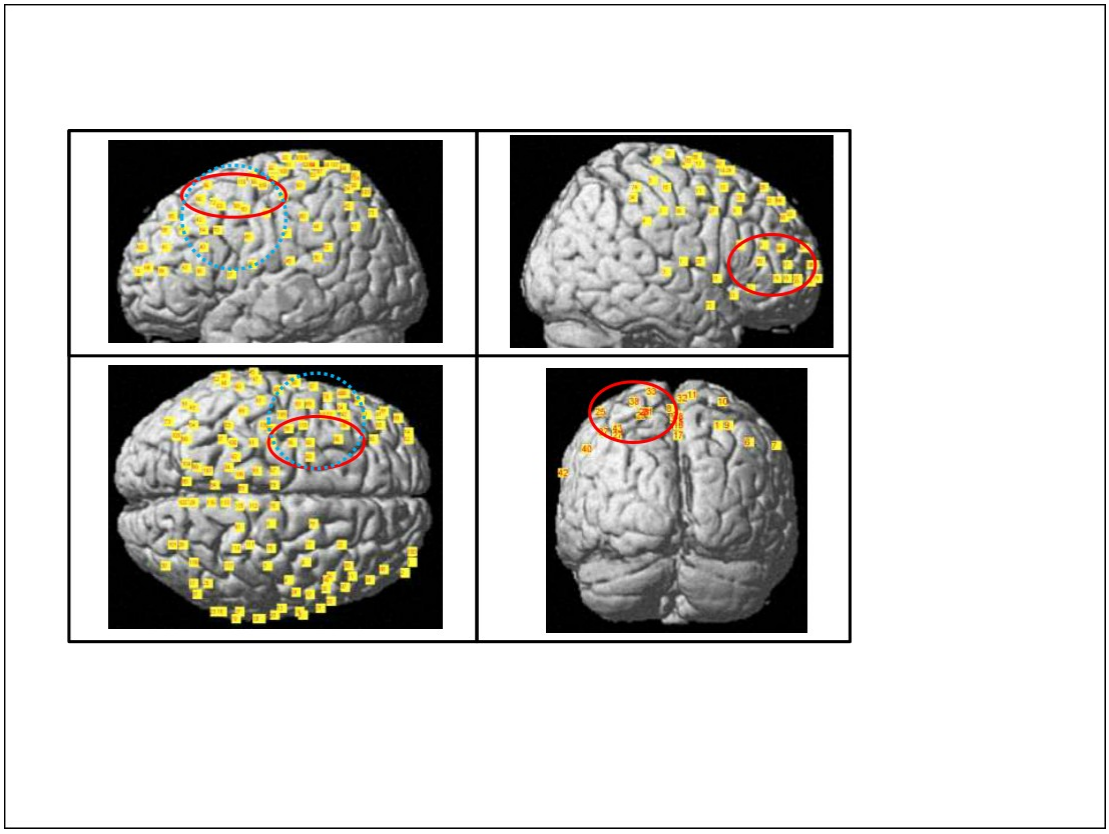

Figure S-11: fNIRS channel coverage. Location of epileptogenic zone indicated with red solid ellipses, irritative zone with blue dotted ellipses. Patient 1: A. Left side view. B. Dorsal. Patient 2: C. Right side view. Patient 3: D. Occipital view.

Supplementary figure S12

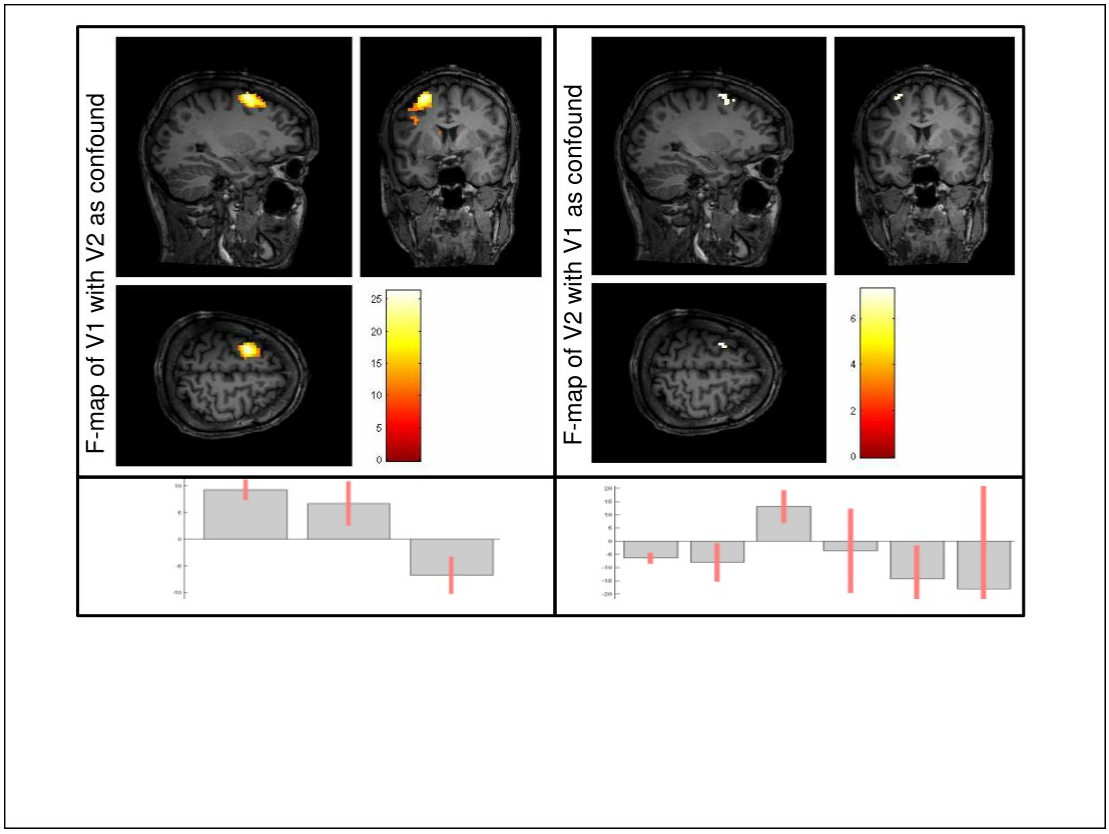


Figure S-12: Effect of including time derivative (t) and dispersion (d) of canonical HRF (c), Patient 1, fMRI analysis. Output from SPM8. F-statistic map (masked for positive1st Volterra BOLD response), with false positives correction, $p< 0.05$ for null hypothesis of significance of reduced model where A. 1st Volterra regressors (c, t and d) excluded, showing they were significant, and B. 2nd Volterra regressors (cc, ct, cd, tt, td and dd) excluded, showing they were also significant. All 1st and 2nd Volterra regressors, spikes with bilateral synchrony (also convolved in a Volterra expansion and including their interaction with focal spikes), movement correction parameters and cosine high pass drifts included in full model. Mean and 90% confidence intervals of V1 regressors (C) and V2 regressors (D), unweighted average over the 3 sessions. Large variance for regressor dd, shown truncated. While t, d and td showed some significance, indicating variability of Patient 1's hemodynamic response compared to canonical HRF, the presence of nonlinearities was unaffected by including many additional regressors in GLM to account for effect of derivatives.

Supplementary figure S13


Figure S-13: Patient 2: EEG sample (15 s) with frequent right frontal focal spikes.

Supplementary figure S14

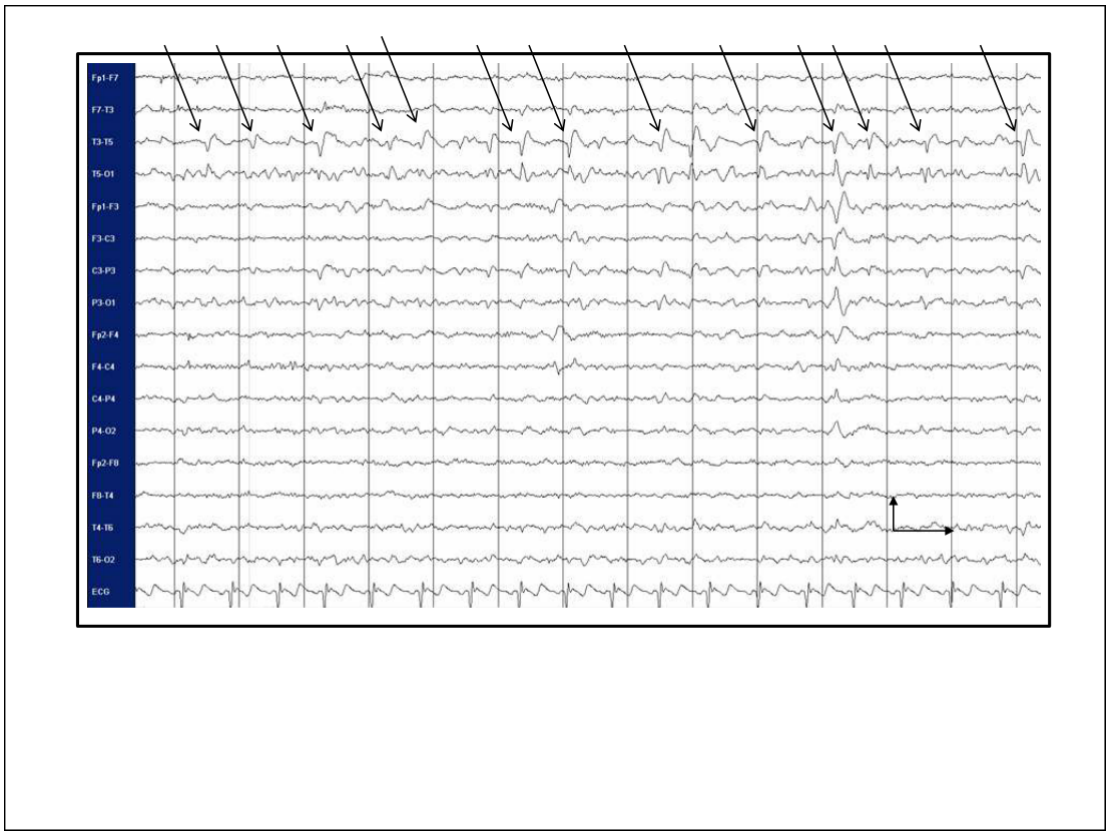


Figure S-14: Patient 3: EEG sample (13 s) with frequent left temporal-occipital focal spikes.

**ANNEXE 5**

***Multichannel wearable system dedicated for simultaneous electroencephalography/near infrared spectroscopy real-time data acquisitions***

**Published by:**
Journal of Biomedical Optics 16(9), 096014 (September 2011)

**Etienne Lareau[a], Frederic Lesage[a], Philippe Pouliot[a], Dang Nguyen[b], Jerome Le Lan[a], and Mohamad Sawan[a]**

[a]*Ecole Polytechnique de Montreal, Department of Electrical Engineering, Montreal, Quebec, H3C-3A7 Canada*
[b]*Centre Hospitalier de l'Universite de Montreal, Montreal, Quebec, H3C-3A7 Canada*

Keywords: near-infrared spectroscopy; electroencephalography; portable instrumentation; continuous monitoring.

**ABSTRACT**

Functional neuroimaging is becoming a valuable tool in cognitive research and clinical applications. The clinical context brings specific constraints that include the requirement of a high channel count to cover the whole head, high sensitivity for single event detection and portability for long-term bedside monitoring. For epilepsy and stroke monitoring, the combination of electroencephalography (EEG) and functional near infrared spectroscopy (fNIRS) is expected to provide useful clinical information and efforts have been deployed to create prototypes able to simultaneously acquire both measurement modalities. However, to the best of our knowledge, existing systems lack NIRS sensitivity and have low channel count or are a combination of two different devices, one for EEG and one for NIRS. We present a battery powered, portable system with up to 32 EEG channels and 128 NIRS channels. Avalanche photodiodes (APD) allow for high NIRS sensitivity and the autonomy of the system is more than 24 hours. The performance of the prototype was tested on phantoms. Further validation was done on 5 healthy adults using a visual stimulation protocol to detect local hemodynamic changes and visually evoked potentials (VEP). Results show good concordance with literature regarding functional activations and suggest sufficient performance for clinical use.

**INTRODUCTION**

The detection of brain activity and diagnostic of brain dysfunctions have been facilitated by the emergence of technologies such as functional magnetic resonance imaging (fMRI) and positron emission tomography (PET). While highly efficient in some applications and giving coverage over the entire brain, these modalities suffer from high cost and the requirement for acquisitions to be performed in a tightly controlled environment. In clinical applications where continuous acquisitions are necessary, such as epilepsy monitoring, cardiac surgery and brain computer interface, these imaging modalities are cumbersome as they are not portable, a limitation that calls for alternatives. Electroencephalography (EEG) and near-infrared spectroscopy (NIRS) are such alternatives, since they can both be made portable and used for long periods of time, even with difficult populations such as children and neurologically impaired subjects.

While EEG has been well established in the clinical practice, NIRS is a relatively new functional imaging modality [17, 73, 74] using near-infrared light propagation (650-900 nm) in biological tissues. Since hemoglobin is the main absorber in this range, NIRS has enabled researchers to image hemodynamics, which represent the variations of concentration of different blood chromophores in this case, *in vivo* through centimeters of biological tissues using non-ionizing, low dose radiation. By acquiring data at two or more wavelengths, it can distinguish and record simultaneous changes in deoxyhemoglobin (HbR) and oxyhemoglobin ($HbO_2$). NIRS has seen growing interest in neuroscience due to the recent widespread availability of commercial instruments and their low cost when compared to alternatives. A non-exhaustive list of applications include functional brain imaging [39, 75], stroke [4, 5], epilepsy [3, 53-55] and neuropsychology [12, 76, 77] studies.

The impetus for this work originated from a clinical need to investigate concurrent EEG-NIRS signal in the context of epilepsy. While benefiting from a vast documentation and being the gold standard for epilepsy diagnostic, EEG has poor spatial resolution when it comes to applications such as epileptogenic foci localization [78] performed prior to surgery. Recent evidence in epilepsy has shown potential benefits in measuring hemodynamics as in some cases it may occur prior to ictal events [7, 57] or be used as a predictor of the spatial location of epileptic foci when using EEG triggered inter-ictal hemodynamic data [79]. While blood oxygen level-dependent (BOLD) fMRI can be used in combination with EEG to measure hemodynamics, continuous monitoring is difficult as patients will not always have (inter)-ictal events in the scanner, and the imaging sequence generates artifacts that even when removed, yields EEG data that is difficult to interpret. Furthermore, movement artifacts recorded in fMRI are hard to remove. Here NIRS has an advantage as it does not interact with EEG and it may be possible to measure optical data continuously with reduced movement artifact sensibility compared to fMRI. It has recently been demonstrated that the combination of EEG and NIRS is valuable [80, 81] but available systems still suffer from several shortcomings.

To be well suited for clinical use, a combined EEG-NIRS system has to be capable of continuous monitoring. As epilepsy patients are usually monitored over days, the

system should generate minimal discomfort to the patient, communicate wirelessly, be battery-operated, cover the whole head with a large number of detection channels and be sensitive enough to get good quality optical and electrical signals despite the presence of scalp hair. Commercial EEG products with acceptable performances are readily available but existing NIRS systems all lack at least one of the criteria mentioned above [64, 82, 83]. Furthermore, the only combined EEG-NIRS systems developed either come from the use of commercial EEG and non-portable NIRS as separate products or research prototypes with few channels [70, 80, 84] for which demonstration was only performed on the forehead as they had low sensitivity for acquisitions over hair-covered scalp. In short, none of these systems answered the clinical need described above.

In this paper, we describe a new portable EEG-NIRS system composed of up to 32 EEG channels, 32 light sources and 32 light detectors that has the potential to cover the whole head for an adult. These light sources and detectors allow to acquire data from up to 128 optical input channels. The prototype realized in a reduced channel count version is battery powered, transmits results in real-time to a computer via a USB cable, has high sensitivity and to the best of our knowledge, is the first system combining all these features.

Characterization of various NIRS parameters was first conducted with phantoms. *In vivo* measures were then acquired using a visual pattern reversal protocol to detect oxygen level changes and visually evoked potentials (VEP). Results demonstrated that the system is capable of reliably detecting local blood oxygenation variations as well as EEG evoked potentials when stimuli are presented. The results were then compared to the literature to test the reproducibility of the protocols with our prototype. The implications of the presented system and its validation are then given and followed by a final conclusion including the next steps of our research.

## Portable EEG-NIRS prototype

### Requirements

Clinical use of EEG and NIRS on adults requires a system design respecting several restrictions. We review in the following section the critical elements that have to be addressed for both EEG and NIRS modalities.

EEG signals emerge from synchronized neuronal activation and are picked up by electrodes attached to the scalp. Since signal amplitude ranges approximately from less than 20 to 150 μV, these oscillations have to be amplified with a gain between 1 000 and 100 000, in order to obtain a signal strength that exceeds the noise floor of the recording device. A band-pass filter is used to keep only the frequencies of interest, typically from 0.25 to 70 Hz. Analog to digital conversion is performed at a rate between 200 and 1 000 samples per second (SPS) depending on the application (research systems may use even higher rates). The contact electrical impedance between the skin and the electrodes can reach several thousand ohms thus the input impedance of the first amplifier stage has to be over 100 MΩ. Other design considerations regarding EEG requirements can be found in [45].

In the case of NIRS, the quality of light detection is critical for the ability to record functional changes in the brain. Optical signals detected have a power that is 7 to 9 orders of magnitude smaller than the light injected for a typical adult head and optodes separation distance of 4 cm [39]. The illumination intensity that reaches the detector depends primarily on the illumination source power and on the distance between the source and the detector. It is also affected by the quality of optical coupling and the color and thickness of hair. Two types of detectors are well suited for portable continuous wave (CW) NIRS: silicon photodiodes (SiPD) and avalanche photodiodes (APD). SiPDs generate a small current when excited by photons and have the advantage of being inexpensive and widely available. However, their sensitivity is limited and their use limits NIRS applications to infants and adult frontal cortex as attenuation is reduced in these cases. APDs are similar to SiPDs but induce an internal gain, hence better sensitivity, when biased with a high voltage, usually over 100 V. Their disadvantages include high cost and temperature sensitivity. Since the transport of signals via optical fiber is not practical for portable systems, detectors have to be placed directly on the scalp and special care has to be taken to insure that the high voltage is safely brought to the head in the case of APDs.

Source-detector distance has a major impact on the strength of signal but is also directly related to the depth from which intensity changes originate. A larger source-

detector distance reduces the raw signal, but enables to reach greater depths thus showing stronger signal during activation [38].

Low channel numbers is typical in current portable NIRS systems and limits the coverage of the brain rendering their use ineffective for applications such as epileptogenic foci localization [64]. Other available systems have a high channel count but low sensitivity due to the use of silicon photodiodes limiting their application to the frontal cortex [68]. Covering the whole head with sufficient sensitivity is thus required to broaden the potential applications of such systems. For the EEG, common practice will use the international 10-20 system for positioning, requiring 22 electrodes from which 19 are used to record signals, one sets a voltage reference and the last two optional electrodes can be used in a right-leg drive type feedback circuit to reduce common mode interference. For NIRS, no international standard exists yet a compromise between optode density on the head, depth of penetration and signal strength is necessary.

Following these considerations, the objectives for the proposed device were set to 32 EEG channels with an acquisition rate of 320 samples per second (SPS) and 20 SPS for each combination of the 32 light sources with the 32 NIRS detectors. The additional EEG electrodes compared to the 10-20 standard can be used to increase resolution in a specific area in the case of source localization [85]. For NIRS, the high number of optodes would allow coverage of the whole head. A much higher number of sources and detectors than proposed here would become problematic as installation of the sensing elements would take significantly longer and the high probe density would be harder to manage, in part because of increased cross-talk between channels.

Portable system design requirements as mentioned above include small size, light weight, wireless communication and low power consumption enabling long term acquisition using battery power. Our goal is to design a system that can operate for 24 hours on a single battery charge without interruption.

Any medical device to be tested on humans has to be designed following strict regulations to ensure subject safety. The IEC601.1 standard sets specific guidelines to follow for this prototype. As electrodes are connected directly to the subject for EEG measurements but not directly to the heart, this instrument falls into the Class II BF category. Protection circuits thus have to be designed accordingly and will be discussed in a later section.

**System design**

Figure 1 shows a prototype of a reduced channel count (8 sources, 8 detectors, 8 EEG channels) of the proposed system used for *in vivo* tests.

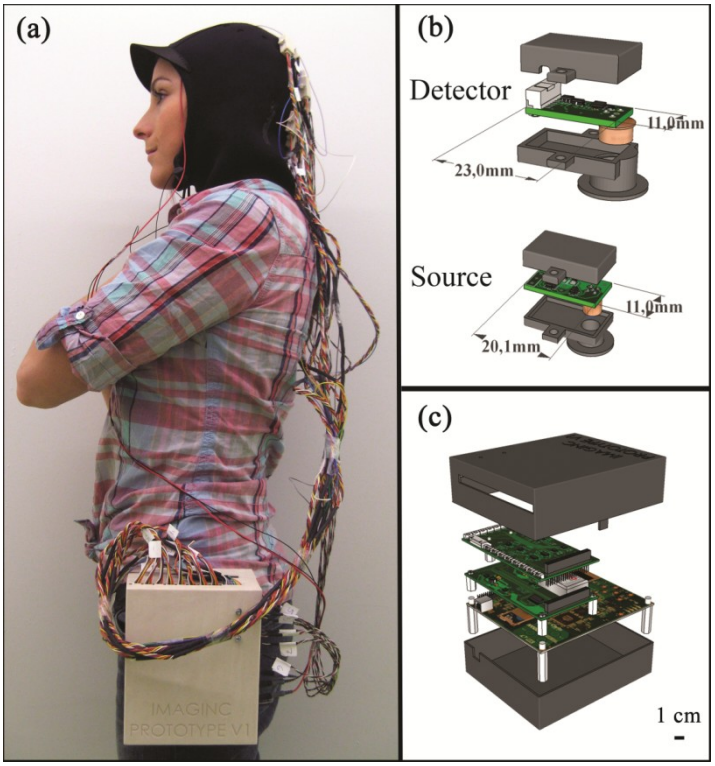


Figure 1. (a) Photograph of the control module and detection helmet, (b) 3D view of NIRS detector and source, EEG electrode on detector not shown, (c) 3D view of control module.

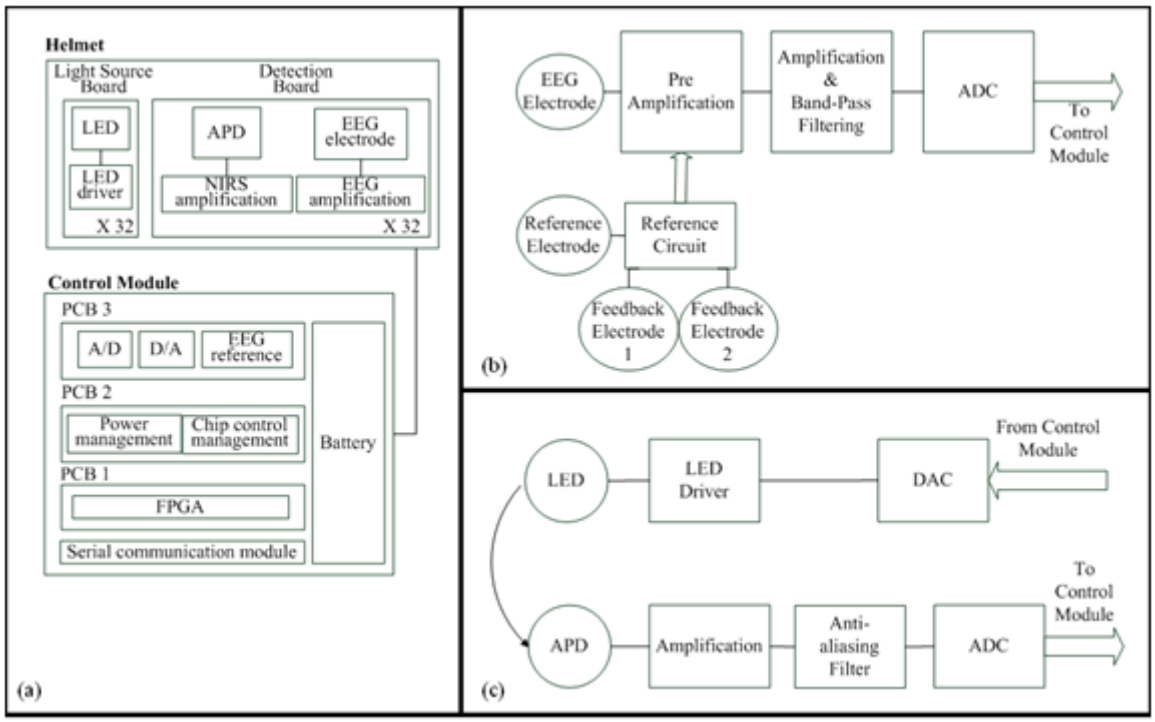


Figure 2. (a) System block diagram, (b) EEG amplification chain for one channel and reference circuit, (c) NIRS illumination and amplification chain for one channel.

The architecture of the system is presented in Fig. 2 (a). We present in the following sections both the EEG and the NIRS acquisition chains. Different architecture and safety aspects will then be analyzed briefly.

*EEG signal chain*

The amplification chain for an EEG channel, shown in Fig. 2 (b), was inspired by a circuit found in [86] to which we added an amplification stage close to the electrode so that the recorded signal is less sensitive to background electrical noise. A circuit dedicated to setting a reference potential on the subject head and located in the control module uses three dedicated electrodes distinct from the signal electrodes. Two feedback electrodes, typically placed on the left and right mastoids, are used to minimize the common mode interference and the reference electrode, typically installed on the forehead, sets the head to a potential of 2.5 V, the mid-point of the amplifier dynamic range. Each signal electrode is connected to an instrumentation amplifier followed by 2 more amplification stages including second order band-pass filters between 0.1 Hz and 100 Hz. The original signal is amplified with a gain of 10 000 before being digitized at 320 SPS by a 16 bits analog to digital converter (ADC),

which is located in the control module. The data is transferred to a FPGA over 3 lines following the SPI protocol.

*NIRS signal chain*

The selection of the light source and detector has a major influence on the performance that can be achieved by NIRS systems. In this design, the illumination sources were light emitting diodes (LED) emitting at 735 nm and 850 nm fitted in a single TO-18 package (Epitex, L2x735/2x850-40B32). This choice was motivated by the small dimensions of the package and safety considerations when compared to laser diodes. Ref. [35] elaborates on the pros and cons of light source types for NIRS. For detection, APDs (Hamamatsu, S2384) were used for their high sensitivity. The high voltage needed to bias the photodiode is generated by a single DC-DC converter (EMCO, CA02-5N) located on the control module. One such supply is sufficient for the 8 detectors and according to the product datasheet, the performance should not change significantly for 32 channels. This last aspect has yet to be validated. The illumination and amplification chain for a NIRS channel is shown in Fig. 3-2 (c). First, a digital-to-analog converter (DAC) generates the drive signal for the light source. This drive signal is then passed on to a voltage-controlled current source that feeds the LEDs. Next, light that has propagated through the brain towards the detector is converted to a small current. This current is amplified by a transimpedance amplifier with a gain of 10 MV/A. An anti-aliasing filter is then applied prior to digitization of the signal at 20 SPS by a 16 bits ADC. The size of each illumination printed circuit board (PCB) is 20.1 mm by 11.0 mm. The detection PCB is 23.0 mm by 11.0 mm.

*System architecture*

The high channel count required the adoption of specific strategies to make it portable. This system was separated in 3 parts: a graphical user interface (GUI) housed in a laptop computer, a control module that is worn by the patient and a detection helmet. The control module and detection helmet were optimized towards low power consumption and small physical footprint.

The GUI is written in Matlab (MathWorks Inc.), allows user control of the acquisition parameters and records the data in real time via a USB cable or a wireless transfer

module. It generates the timing sequences required by the hardware and also has an installation mode that helps clinicians validate signal quality when installing the system on patients.

The helmet is made of flexible neoprene and holds the light sources and the NIRS and EEG detectors. In order to fit 32 elements of each type on the head, NIRS and EEG detection and amplification are integrated on the same PCB. A 3D model of the illumination and detection optodes is shown in Fig. 1 (b).

The control module has 3 different PCBs. The first PCB is an Arrow Low Power Reference Platform, a commercial prototyping platform made for battery powered applications using an Altera Cyclone III field programmable gate array (FPGA). Its role is to synchronize the acquisition process and communicate the data in real time with the computer. The second PCB manages the power supply and the communication with the different chips of the system. Three different voltages are required: 5 V for the analog part, 3.3 V for the digital part and -150 V for APD biasing. Communication with all the chips on the third PCB is made via an SPI bus. In order to decrease the number of FPGA pins necessary for communication, a decoder is used to address the signals. The third PCB has all the ADCs and DACs that connect to the elements on the helmet and comes in 4 copies for the whole system as every board includes 8 EEG channels, 8 light sources and 8 NIRS detection channels. Every PCB is stacked on top of the other with stack-through connectors saving space and allowing for a reduced channel count version. The results presented in this paper were obtained with the 8-channel version of the system. A 3D model of this reduced version of the control module, measuring 16 cm by 13 cm by 8.2 cm, is shown in Fig. 1 (c).

As a single communication bus is used for all the ADCs and DACs, a specific acquisition sequence is generated by the GUI is order to synchronize data retrieval. This sequence ensures correct NIRS and EEG sampling rates and allows setting the minimum light power needed for sufficient signal quality. Furthermore, because light source switching causes a current surge from the power supply and hence a spike on

the EEG signal, it is important to let the power rails come back to steady state before acquiring the next EEG sample when the lighting is changed.

*Power considerations*

Light generation is one of the main power consumption parts of the proposed system. Turning on every LED on the helmet at the same time would require a large transient current and amount to a considerable energy waste. A time multiplexing strategy was thus used. Additionally, every time a light source is turned on, every detector coupled to it records a sample reducing the illumination time and saving energy.

Wireless communication being power hungry, the data rates transferred were minimized by using data averaging on the NIRS data, but not on EEG data, before sending it to the computer. This strategy reduced the number of NIRS samples sent by a factor of 8 without a significant complexity increase.

*Safety considerations*

Isolation from the power supplies was achieved by powering the system with a battery. When communicating with a USB cable, an optical isolation circuit protects the patient against computer malfunction. In wireless mode, optical isolation is not necessary. The trigger signal used for EEG experiments was also electrically isolated from the computer by optical means.

The use of high voltage to bias the APDs on the head needed special care to ensure safe operation of the device. First, each detection board, containing an APD, was encapsulated in a custom-made non-conductive mold providing an electrical barrier and preventing any physical contact with the APD pins or high voltage traces. This electrical isolation also has a functional use for the system because as the APD body is grounded, applying it directly to the head would force a 0 V potential at the same time as the 2.5 V reference supplied by the EEG electrode thus unbalancing the DC potential mapping and generating unwanted currents from the reference to the photodiode case. Furthermore, additional protection in case of high voltage wire rupture was provided with the use of current-limiting resistors placed directly at the output of the high voltage regulator. Finally, a high-voltage regulation capacitor was used with the APD. In case of sudden system failure, accumulated charge could

possibly hurt the subject. The allowed accumulated energy by the IEC601.1 standard is 2 mJ and the capacitor was chosen accordingly.

The EEG electrodes which are attached on the head with conductive paste create a low impedance contact to the device. Current-limiting resistors were added to comply with the IEC601.1 regulation regarding leakage currents from parts in contact with the patient.

Even if LEDs do not represent a direct danger for the eye as lasers do, tissue damage can happen when high illumination power is used. Semiconductor heating seems to be the predominant hazard in this application and is discussed in [35, 42]. Time multiplexing the LEDs helps to maintain tissue heating at a safe level. As the LEDs used in our system are from the same company and product series as in [42], we used these results to evaluate the heating effects of this prototype. Since the mean irradiance generated with maximum illumination power was 14.8 $mW/cm^2$ for our system and [42] evaluates the heating effect between 12 and 25 $mW/cm^2$, we expect an absolute maximum temperature increase of less than 4 °C *in vivo*.

## METHODS

### EEG Phantom

The EEG amplification chain was tested using a resistive phantom similar to those described in [87]. Square pulses with amplitude of 40 µV peak-to-peak and frequency ranging from 1 to 8 Hz were injected to validate proper signal representation. The input referred noise was also measured.

### NIRS Phantom

The NIRS signal chain was tested with an optical phantom made of polyester resin, to which India ink was added as an attenuation agent and $TiO_2$ as a diffusive agent. The phantom's absorption coefficient at 758 nm was measured to be 0.017 $mm^{-1}$ and its diffusion coefficient 0.7 $mm^{-1}$, similar to results published in [88] for the human forehead. A single detector was coupled to a single light source, separated by a distance of 4 cm.

First, different light intensities and avalanche gains were applied to study the influence of these factors on baseline value and noise amplitude to DC level ratio (NDCR). The NDCR is meaningful because the signals of interest for this application typically have peak-to-peak amplitude of 1% of the DC value. To ensure good data quality, the NDCR should be well under 1%. Then a 1 Hz sinusoidal light signal similar to *in vivo* signals was injected in the phantom to compute the signal-to-noise ratio (SNR) with various avalanche gains. Finally, baseline signals were acquired *in vivo* on the frontal and visual cortices of two adult subjects with the same source-detector separation distance and light intensity with different avalanche gains to compare to the previous findings with phantoms.

**Combined EEG-NIRS visual task**

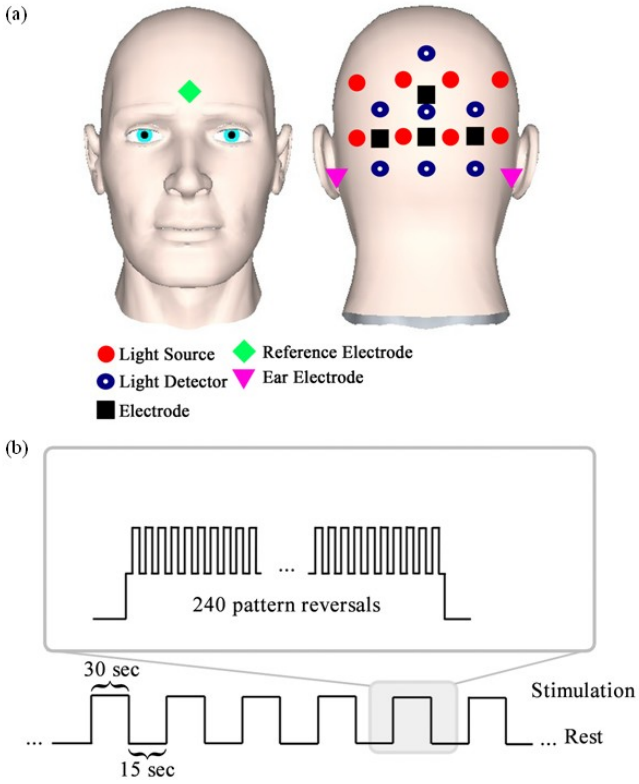


Figure 3. In vivo measurements (a) Placement of electrodes and optodes on subject, where electrodes are placed at standard positions O1, O2, Oz and POz; (b) Procedure for pattern reversal task. Subjects were asked to gaze at a screen in front on them. Each stimulation period of 30 seconds was followed by a rest period of 15 seconds. Pattern reversals occurred at a rate of 8 Hz for a total of approximately 240 pattern reversals per stimulation period. Each recording time consisted of 10 stimulation and 10 rest periods.

Validation of the whole system was made using an 8-channel version of the prototype with 5 healthy adult subjects and was approved by the Ecole Polytechnique de Montreal's Ethic Committee. *In vivo* signals were recorded on the primary visual cortex using 4 EEG electrodes, 7 NIRS detectors and 8 light sources for a total of 20 NIRS channels. Electrodes were positioned on standard 10-20 and 10-10 locations O1, O2, Oz and POz. NIRS optodes were placed as illustrated in Fig. 3 (a) with an average source-detector distance of 3.1 cm. This shorter distance compared to *in vitro* tests was used in order to get good amplitude signal even with dark or long haired subjects. The 8$^{th}$ detection channel was used to record the trigger signal to synchronize evoked potentials with visual stimuli.

A visual pattern reversal task was performed by subjects 3 to 5 to generate EEG and NIRS activations simultaneously. The subjects were sitting in front of a computer screen, at a distance of 55 cm, in a dimly lit room and a baseline was recorded during 30 seconds. A black and white checkerboard, with every square spanning 3° to 4° in the field of view, was then displayed with pattern reversal happening at a frequency of 8 Hz for 30 seconds. A rest period of 15 seconds followed and this pattern reversal-rest routine was repeated 10 times to allow averaging. VEPs for EEG were obtained by averaging all the moments where pattern reversal happened, which is approximately 480 times per stimulation period. Considering the first checkerboard used as a contrast of 100%, as defined in [70], another acquisition was made using pattern reversal at 8 Hz and a contrast of 10%. In order to verify if contrast effects could be detected at other stimulation frequencies, subject 4 was stimulated at 4 Hz.

A second protocol was used on all subjects using a windmill pattern, as described in [70, 89], spanning 70° on the screen. Pattern reversal at 4 Hz was applied with the same timing parameters as the first protocol. This protocol was repeated 4 times by rotating the pattern by 90° so the 4 quadrants of the screen were covered (lower left, lower right, upper left, upper right).

These parameters were varied in order to verify the repeatability of experimental protocols used in the literature [70, 89, 90] with this portable system. The correlation between the VEPs amplitude and NIRS response amplitude was also computed [91].

he power consumption of the system was measured during acquisition at maximum illumination power. Communication of data in real time was done using a USB cable.

## RESULTS

*EEG Phantom*

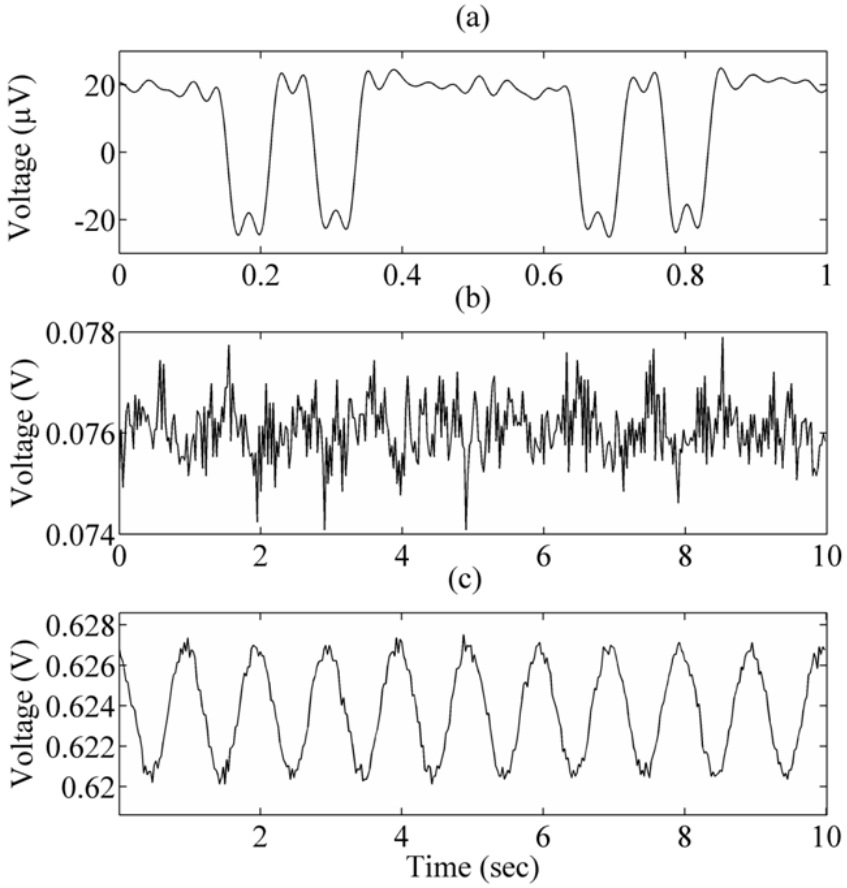


Figure 4. (a) Typical results for resistive phantom measurements, referred to the input. Low-pass filtering was applied at 35 Hz in order to remove the strong 60 Hz artifact. Typical results for NIRS phantom measurements for sinusoidal physiology-like stimulation (b) with no avalanche gain. The signal is distorted and has a SNR of -4.6 dB. (c) with avalanche gain of 19. The signal has a SNR of 18.9 dB.

The curves obtained for the square pulses, as shown in Fig. 4 (a), injected in the resistive phantom show an amplitude of approximately 40 μV peak-to-peak and the correct expected shape. Strong digital finite impulse response filtering at 35 Hz had to be applied because a high amplitude 60 Hz component and its harmonics were present. The input referred noise was measured to be 0.36 $\mu V_{rms}$ once the 35 Hz filter was applied.

*NIRS Phantom*

Table 1. NIRS phantom results with pulsed light

| **Optical power (mW)** | **Avalanche gain** | **DC level (mV)** | **Noise amplitude ($mV_{rms}$)** | **NDCR (%)** |
|---|---|---|---|---|
| 3 | 0 | 4.64 | 0.55 | 11.885 |
| 14 | 0 | 84.17 | 6.42 | 7.627 |
| 28 | 0 | 177.55 | 0.68 | 0.385 |
| 45 | 0 | 273.27 | 0.44 | 0.162 |
| 3 | 19 | 137.3 | 0.18 | 0.132 |
| 14 | 19 | 698.3 | 0.23 | 0.033 |
| 28 | 19 | 1 448 | 0.37 | 0.026 |
| 45 | 19 | 2 328 | 0.34 | 0.015 |
| 3 | 31 | 204.3 | 0.23 | 0.111 |
| 14 | 31 | 1 034 | 0.43 | 0.041 |
| 28 | 31 | 2 154 | 0.60 | 0.028 |
| 45 | 31 | 5 000 | - | - |
| 3 | 39 | 261.7 | 0.27 | 0.104 |
| 14 | 39 | 1 321 | 0.63 | 0.048 |
| 28 | 39 | 5 000 | - | - |
| 45 | 39 | 5 000 | - | - |

Table 1 shows results for the NIRS phantom used with the standard illumination strategy at different intensities and avalanche gain. The DC voltage and noise values at the ADC are followed by the NDCR ratio. For a fixed avalanche gain, higher illumination power yields stronger DC output and better NDCR ratio. For constant light intensity, higher avalanche gain results in stronger DC level. The absolute noise level and NDCR ratio in function of avalanche gain seem to respond in a non linear fashion and optimal results are found with an avalanche gain of 19 and a lighting power of 45 mW.

Table 2. NIRS phantom results with physiology-like stimulation

| Avalanche gain | Averaging | DC level (mV) | SNR (dB) |
|---|---|---|---|
| 0 | no | 76 | -8.6 |
| 19 | no | 626 | 14.4 |
| 31 | no | 916 | 13.7 |
| 39 | no | 1 161 | 13.5 |
| 0 | yes | 76 | -4.6 |
| 19 | yes | 624 | 18.9 |
| 31 | yes | 913 | 19.0 |
| 39 | yes | 1 156 | 18.5 |

Table 2 shows the phantom results obtained with physiology-like light injection (1 Hz sine wave, amplitude at 1% of the DC level) and different avalanche gains. This stimulation was used because it is very similar to the heart beat which is the predominant feature of the NIRS signal. The DC level of the signal increases with avalanche gain as shown in Table 3.1. SNR was computed by isolating the 1 Hz sine wave with a digital filter and considering the remaining oscillations as noise. The use of avalanche gain significantly increases the SNR. Fig. 3-4 (b) and (c) shows typical curves obtained in linear and avalanche mode. The effect of the averaging function of the system is measured to increase SNR by 4.7 dB by taking 4 NIRS samples per channel and averaging them every time a light source is activated instead of one. Fig. 3-5 (a) shows how the averaging function works.

Fig. 5 (b) and (c) compare phantom results with *in vivo* measures on the frontal and occipital cortex for a shaved subject (subject 3) and for a subject with short but dense red hair (subject 4). These subjects were chosen to show the high inter-subject variability of signal attenuation depending on the hair factor. Fig. 5 (b) shows the DC levels for phantom and *in vivo* data, which informs on light absorption of the medium crossed by light. Intra-subject variations of up to two orders of magnitude were found between the frontal and occipital cortices. Inter-subject variations were found to be over one order of magnitude. The phantom had similar optical properties to the *in vivo* frontal cortex. Fig. 5 (c) uses the signal of interest's amplitude over DC level

(SADC) ratio, which gives an indication of the validity of the protocol used to find the SNR of the system when comparing phantom to *in vivo* curves. For the phantom, the amplitude of the signal of interest was found by applying a 1 Hz notch filter and then computing the amplitude. For *in vivo* results, that value was found by applying a 0.8 Hz high-pass filter in order to keep only the heart-beat signal and the high frequency noise. The amplitude was then computed. SADC ratios found are close to 1%, as stated in literature [92] for the adult human brain.

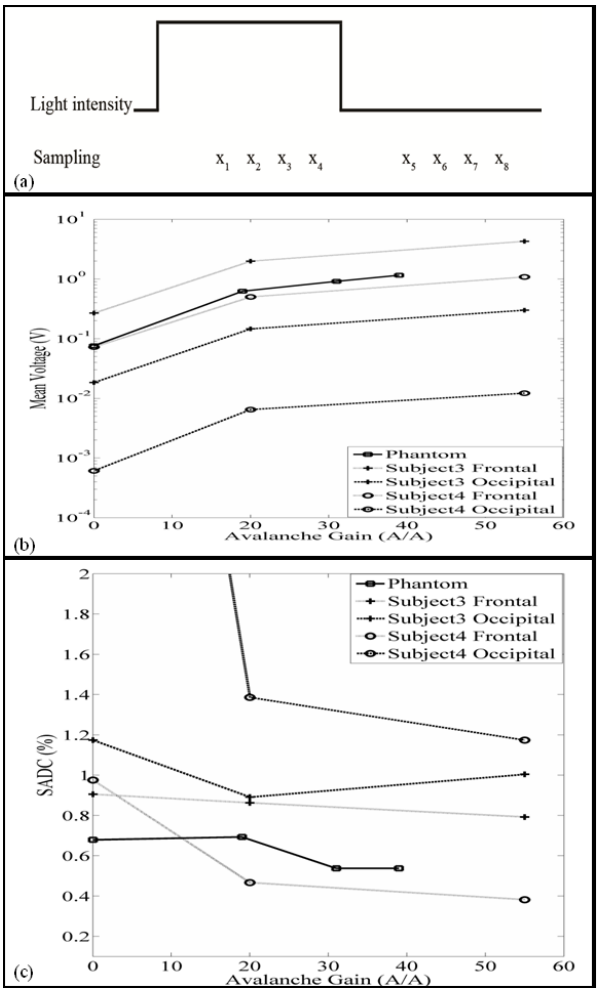


Figure 5. (a) Schematic illustration of time multiplexed illumination and detection for one NIRS channel. When averaging is activated, samples $x_1$ to $x_4$ are averaged by the FPGA and only one sample is sent to the computer. When averaging is turned off, only sample $x_4$ is used. Samples $x_5$ to $x_8$ are used to further reduce the contribution of ambient light to the signal. This was not used for the results presented in this paper. (b) DC level of phantom results compared to in vivo baseline levels at the same illumination power and source-detector distance. (c) SADC ratio for phantom and in vivo results.

*Combined EEG-NIRS visual task*

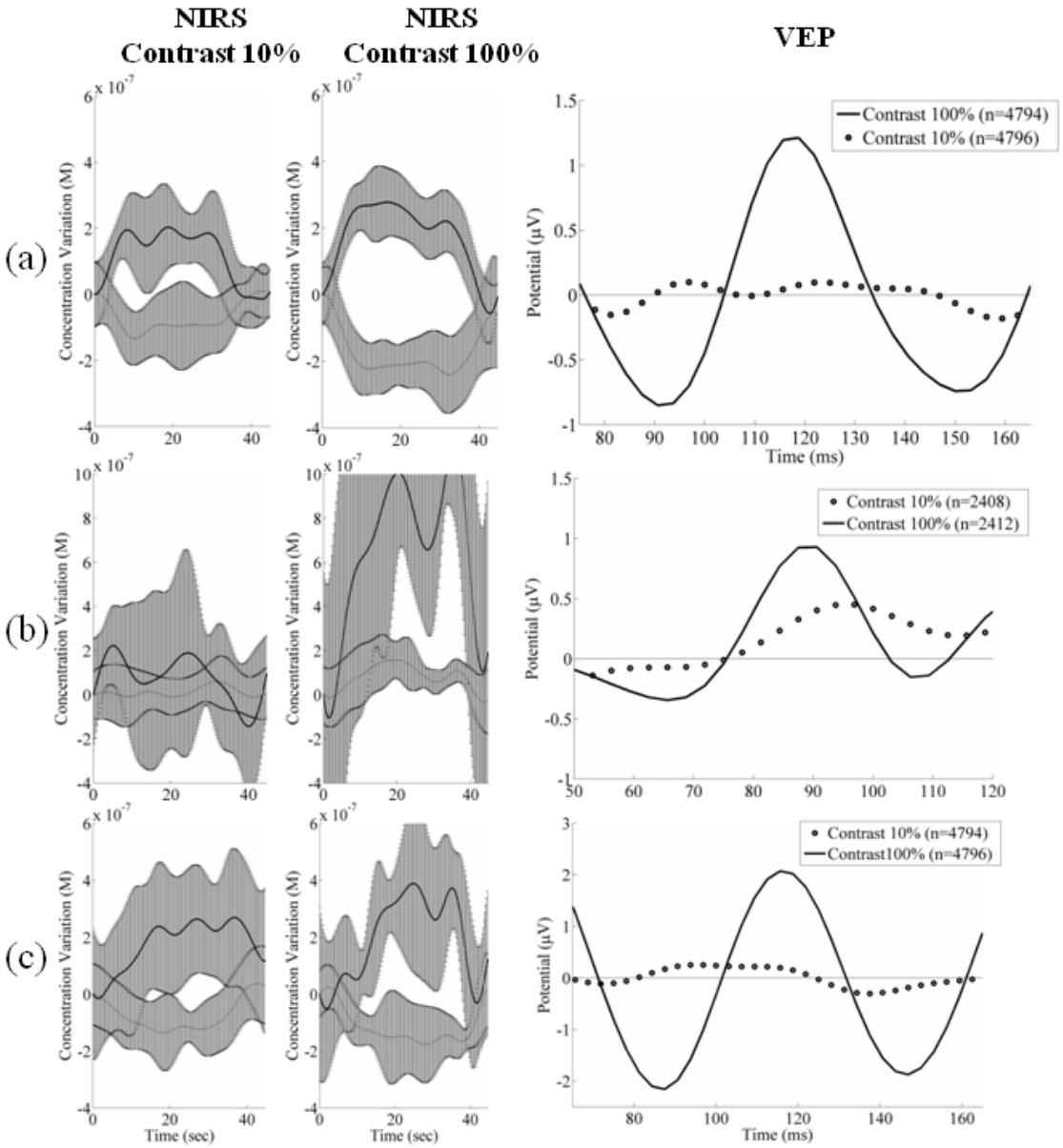


Figure 6. Effect of contrast on neuronal response measured by NIRS and EEG with contrasts of 10% and 100% for subjects 3 to 5 (a to c respectively). In NIRS figures, bold lines represent $HbO_2$ and dashed lines represent HbR. Error bars show the standard deviation for the variations throughout the 10 averaged stimulation blocks. In EEG figures, timing was adjusted to show the main peak of the VEP, between 90 and 120 ms.

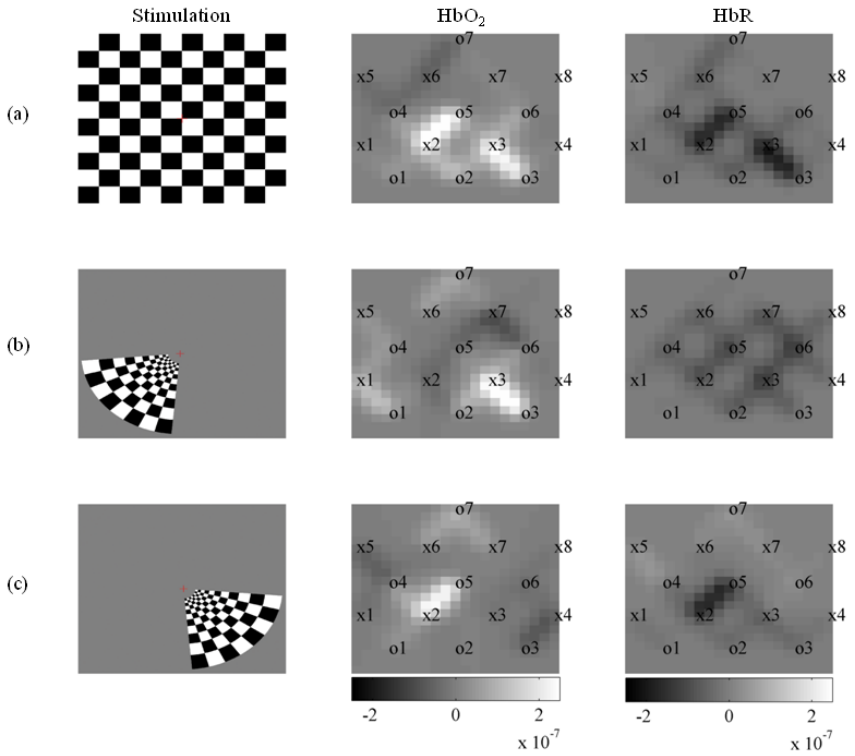


Figure 7. NIRS topographic reconstruction for subject 3 showing block averaged $HbO_2$ and HbR concentration variations (units in M). The x and o elements in the $HbO_2$ and HbR columns represent the position of NIRS light sources and detectors respectively. (a) Checkerboard protocol with 100% contrast. (b) Windmill pattern protocol for lower left visual field. (c) Windmill pattern protocol for lower right visual field.

The raw data for EEG was treated with EEGLAB [93], an open source toolbox for Matlab. Every channel was band-pass filtered between 1 and 40 Hz and each event was averaged for each subject. Fig. 6. shows averaged VEPs for subjects 3 to 5 using the flashing checkerboard protocol reversing at 8 Hz for subjects 3 and 5 and 4 Hz for subject 4 for contrasts of 10% and 100% at electrode POz. Error bars are not shown but the standard deviation found between trials is similar for all subjects, ranging from 9.3 to 10.6 μV. The standard error being greater than the signal of interest explains why so many trials are necessary to obtain good results.

The raw data for NIRS was processed with HOMER [18], an open source toolbox for Matlab. Every channel was band-pass filtered between 0.005 Hz and 0.1 Hz and with a principal component analysis (PCA) filter, removing the first eigenvector component, helping to reduce the effect of motion artifacts and other inter-channel covariant data. A differential pathlength factor (DPF) correction was also applied to generate concentration values. Averaging was applied to each stimulation block. Fig.

7 shows the averaged hemodynamic response for $HbO_2$ and HbR for subjects 3 to 5 for the low and high contrast checkerboard protocol.

The values of VEPs and NIRS averaged responses were computed for subjects 3 to 5 and are shown in Table 3. For VEPs, the RMS value for the curve showed in Fig. 6 was used and for NIRS, the mean concentration variation for the 0 to 45 seconds period was used.

Table3. Value of VEPs and NIRS response to contrast variations

| **Subject** | **Contrast 10%** | | | **Contrast 100%** | | | **Variation (in %)** | | |
|---|---|---|---|---|---|---|---|---|---|
| | **VEP (µV)** | **$HbO_2$ (µM)** | **HbR (µM)** | **VEP (µV)** | **$HbO_2$ (µM)** | **HbR (µM)** | **VEP** | **$HbO_2$** | **HbR** |
| 3 | 0.091 | 0.117 | -0.068 | 0.672 | 0.173 | -0.171 | 638 | 48 | 151 |
| 4 | 0.209 | 0.076 | 0.012 | 0.417 | 0.640 | 0.078 | 100 | 742 | 550 |
| 5 | 0.183 | 0.177 | -0.073 | 1.386 | 0.192 | -0.112 | 657 | 8 | 53 |

To confirm spatial localization of the activations, topographic reconstruction using a back-projection algorithm provided in HOMER was done for $HbO_2$ and HbR for all 5 subjects. Fig. 7 shows results from subject 3 for the checkerboard high contrast protocol compared with lower visual field protocols. Activation in both hemispheres was observed for the checkerboard protocol as well as lateralized activations for the lower field protocol. Lateralized activations respectively correspond spatially with those generated by the checkerboard stimuli. Upper visual field results are not shown as significant activation was difficult to reproduce between subjects.

During acquisitions, power consumption was measured to be 1.86 W when using maximum illumination power. Consumption of the FPGA prototyping platform was 0.44 W while light sources consumed 0.93 W and the rest of the system, 0.49 W. With a Li-Ion battery of 10 Ah this leads to an autonomy of 32 hours for this channel count. The use of a high density battery allows relatively small physical footprint of 7.6 cm by 8.0 cm by 4.0 cm and weight of 404 g.

## DISCUSSION

### EEG Phantom

The results for the EEG amplification chain corresponded well to what was expected from the device. However, the high level of electromagnetic noise in the measurement environment introduced wide amplitude 60 Hz oscillations that had to be filtered digitally. As was seen in ulterior testing (*in vivo* data for subject 1), acquiring data was a lot easier when a Faraday cage setup was available. It should be kept in mind that clinical settings do not always allow optimal measuring conditions possible and thus, optimization of the power supply rejection ratio and cable shielding should be evaluated in order to get better performance.

The input referred noise is sufficiently low to provide good quality measurements when an EEG bandwidth up to 35 Hz is sufficient, which is the case in most clinical situations. As stated above, the 60 Hz interferences, with harmonics at 120 Hz, strongly affect the quality of measurements in noisy environments.

### NIRS Phantom

Data found in Table 1 suggests that an increase in illumination power or avalanche gain produces a better NDCR leading to better SNR. As illumination accounts for up to 50% of the power consumption of the system in this context and a higher avalanche gain produces marginal consumption increase, using high avalanche gain and the lowest possible light power was best suited for this application.

Table 2 shows significant SNR improvement when using an avalanche gain instead of using the APD in linear mode. However, the SNR only slightly changed when going from an avalanche gain of 19 to 40. This is a known effect and is explained by the increase of dark current noise when increasing bias voltage.

Comparison of phantom results with in-vivo baseline DC signals suggests that the phantom used provides a reasonably good model for NIRS applied to adult subjects in the frontal area. However, it represents an optimistic solution when the device should be sensitive enough for hair-covered areas as the visual cortex. A higher absorption

coefficient might help to reflect that factor. The high intra-subject and inter-subject variability found in DC levels also confirms the need for a wide dynamic range and calls for flexibility in terms of illumination power and avalanche gain.

Concerning the SADC ratio, results found for the phantom are similar to the frontal *in-vivo* data. This suggests that injecting a sinusoidal signal of 1% the DC level in the phantom reflects reasonably well in-vivo results and can be used as a simple tool to evaluate the sensitivity of the detectors and amplification chain in CW NIRS systems. It should be noted that it does not take into account the effects of light source multiplexing and modulation as the illumination signal used is continuous.

For the phantom and both subjects, the SADC ratio had a tendency to decrease as avalanche gain was increased, probably because SNR increases, minimizing the contribution of noise to the ratio. That tendency was most noticeable with the red haired subject, where signals had a higher noise level, mostly when no avalanche gain was used, due to higher light absorption and lower detected intensity.

**Combined EEG-NIRS visual task**

The checkerboard pattern reversal protocol was used to evaluate the effect of contrast on the strength of response in EEG and NIRS.

In the case of VEPs, the higher peak amplitudes found for higher contrast in all 3 subjects is in agreement with [70, 94]. Results found for subjects 3 and 5 are similar in timing and the amplitude difference might be caused by inter-subject variability and electrode placement bias. For these subjects, the N75, P100 and N145 peaks, as described in [95], can be observed in Fig. 6. VEPs for subject 4 showed similar response intensity and shape but the timing is slightly different. Timing and amplitude variation between subjects and compared to other results found in literature could be caused by experimental protocol variations such as check size [95], stimulation frequency [96] and intensity [97] but also by attention level variability [98].

NIRS results also show concordance with published studies. Increasing contrast generated an increase in $HbO_2$ and decrease in HbR, as expected in [70, 94]. It should be noted that no partial volume correction was applied to data and according to [99], this fact might explain an underestimation of more than 50% of the concentration variations reported here. Subject 4 showed high variability and poor HbR response in his results that could have been caused by variations in the experimental setup, which included higher level of ambient light and more sources of distraction in the surroundings. On the other hand, subjects 3 and 5 show similar responses in timing and intensity for both $HbO_2$ and HbR and are in agreement with the results of [70].

Topographic reconstructions for localization of activated areas showed good correlation between the activation of the whole visual field and the lower left or right fields. The lower left and right stimulation results corresponded well with [89] with respect to the localization of activation for 4 out of 5 subjects. Subject 4 showed poor result quality for the same reasons mentioned above. Upper field activations were less reproducible between subjects. The possible cause might be that the activation zone is smaller in that case, generating a smaller signal that might not be strong enough to measure considering the relatively small number of stimulation blocks used. Furthermore, considering the lower spatial resolution of this experiment, the lack of reproducibility might also be caused by not covering adequately the activated area in some subjects.

The repeatability of VEPs and NIRS activations between subjects varied depending on the protocol. VEPs obtained for the contrast study showed good correlation with literature in shape and timing. Occipital cortex activation was observed in EEG and NIRS for all subjects, but the amplitude of response varied significantly, mostly in NIRS. That variability seems to be frequent with this modality and can be partly explained in this case by a relatively low SNR, inter-subject physiological variability and spatial variations in optode locations, as stated in [90]. NIRS topography could be repeated with success on 80% of our subjects, even if subjects 1 and 2 were stimulated with different reversal frequencies (respectively 1 and 2 Hz). A quiet and dimly lit experimental environment with a low level of electromagnetic interference

was not always available and will be used for further experiments in order to increase the significance of our results.

With a 10 Ah high density Li-Ion battery supplying 7.4 V, the autonomy of the prototype that was built can be estimated at almost 40 hours when using full power illumination. For the same acquisition parameters, the consumption of the 32 channel version of the device can be approximated at 3 W for an autonomy of slightly over 24 hours. Thus, the maximum acquisition time that can be reached with a single charge should be enough for clinical applications. Considering that at maximum illumination intensity, 50% of the power is used for light generation, it should be mentioned that longer activity periods can be reached with lower light levels. However, this is not always an option as dark or dense haired subjects typically need high light power in order to get quality optical signals.

**CONCLUSION**

In order to meet the requirements of a portable functional brain imaging system capable of simultaneous EEG and NIRS measurements, a system designed to acquire up to 32 EEG electrodes, 32 light sources and 32 detectors for NIRS was proposed. We confirmed that this novel portable device was capable of high sensibility, complete head coverage and sufficient autonomy for clinical applications. The results obtained on a reduced channel count prototype show good concordance with existing literature and suggest satisfactory performance for clinical applications.

Future efforts will concentrate on improving the performances of the device for the clinical environment. First, EEG and NIRS sensibility will be optimized with a focus on electronics but also by designing a new helmet which will enable better electrical and optical coupling. Various techniques will then be applied to reduce the power consumption of the system and PCB physical footprint. Once this is done, the battery size can be reduced and system packaging adapted.

**Acknowledgments**

Authors acknowledge support from the Fonds Quebecois de Recherche sur la Nature et les Technologies (FQRNT), the Canadian Institutes of Health Research (CIHR), the Institute of Circulatory and Respiratory Health (ICRH), and the Heart and Stroke Foundation of Canada (HSFC).

## REFERENCES


[1] H. Shibasaki, "Human brain mapping: hemodynamic response and electrophysiology," *Clinical neurophysiology*, vol. 119, no. 4, pp. 731-43, 2008.

[2] M. Wolf, M. Ferrari, et V. Quaresima, "Progress of near-infrared spectroscopy and topography for brain and muscle clinical applications," *Journal of Biomedical Optics*, vol. 12, no. 6, 2007.

[3] E. Watanabe, Y. Nagahori, et Y. Mayanagi, "Focus diagnosis of epilepsy using near-infrared spectroscopy," *Epilepsia*, vol. 43, pp. 50-5, 2002.

[4] G. Strangman, R. Goldstein, S. L. Rauch, et J. Stein, "Near-Infrared Spectroscopy and Imaging for Investigating Stroke Rehabilitation: Test-Retest Reliability and Review of the Literature," *Archives of physical medicine and rehabilitation.*, vol. 87, no. 12, pp. 12, 2006.

[5] C. Terborg, S. Bramer, S. Harscher, M. Simon, et O. W. Witte, "Bedside assessment of cerebral perfusion reductions in patients with acute ischaemic stroke by near-infrared spectroscopy and indocyanine green," *Journal of neurology, neurosurgery, and psychiatry*, vol. 75, no. 1, pp. 38-42, 2004.

[6] J. Furusho, A. Suzuki, Y. Takakusa, F. Kawaguchi, N. Ichikawa, et T. Kato, "Simultaneous study of interictal EEG and near-infrared spectroscopy in a boy with epilepsy," *International congress series.*, vol. 1232, pp. 673-676, 2002.

[7] V. Osharina, E. Ponchel, A. Aarabi, R. Grebe, et F. Wallois, "Local haemodynamic changes preceding interictal spikes: A simultaneous electrocorticography and near-infrared spectroscopy analysis in rats," *NeuroImage*, vol. 50, no. 2, pp. 600-607, 2010.

[8] H. F. Achigui, "Conception d'amplificateurs opérationnels à basse tension pour des systèmes de dépistage de crises épileptiques," Mémoire de Maîtrise, Polytechnique de Montréal, Canada, 2007.

[9] F. Normandin, "Conception d'un circuit intégré dédié à la réception des signaux optiques dans un système d'imagerie basé sur la spectroréflectométrie infrarouge," Mémoire de Maîtrise, École Polytechnique de Montréal, 2007.

[10] F. Chénier, "Mise en oeuvre d'un système d'imagerie cérébrale fonctionnelle basé sur la spectrométrie infrarouge," Mémoire de Maîtrise, École Polytechnique de Montréal, 2008.

[11] V. C. Scanlon et T. Sanders, "Chapter 11: Blood," in *Essentials of anatomy and physiology*, Philadelphia: F.A. Davis Co., 2007.

[12] M. Izzetoglu, S. C. Bunce, K. Izzetoglu, B. Onaral, et K. Pourrezaei, "Functional Brain Imaging Using Near-Infrared Technology," *IEEE Engineering in Medicine and Biology magazine*, vol. 26, no. 4, pp. 38-46, 2007.

[13] Alzheimer'sAssociation, "Brain Tour : Supply Lines," pp., 2010. Disponible: http://www.alz.org/brain/02.asp. [Consulté le 28 novembre 2010].

[14] Drugs.com, "Subdural Hematoma," pp., 2010. Disponible: http://www.drugs.com/cg/subdural-hematoma-aftercare-instructions.html. [Consulté le 28 novembre 2010].

[15] H. Owen-Reece, C. E. Elwell, J. S. Wyatt, et D. T. Delpy, "The effect of scalp ischaemia on measurement of cerebral blood volume by near-infrared spectroscopy," *Physiological measurement.*, vol. 17, no. 4, pp. 279, 1996.

[16] R. Saager et A. Berger, "Measurement of layer-like hemodynamic trends in scalp and cortex: implications for physiological baseline suppression in functional near-infrared spectroscopy," *Journal of Biomedical Optics*, vol. 13, no. 3, 2008.

[17] F. F. Jöbsis, "Noninvasive, infrared monitoring of cerebral and myocardial oxygen sufficiency and circulatory parameters," *Science*, vol. 198, no. 4323, pp. 1264-7, 1977.

[18] T. J. Huppert, S. G. Diamond, M. A. Franceschini, et D. A. Boas, "HomER: A review of time-series analysis methods for near-infrared spectroscopy of the brain," *Applied Optics*, vol. 48, no. 10, pp. D280-D298, 2009.

[19] A. Duncan, J. H. Meek, M. Clemence, C. E. Elwell, P. Fallon, L. Tyszczuk, M. Cope, et D. T. Delpy, "Measurement of Cranial Optical Path Length as a Function of Age Using Phase Resolved Near Infrared Spectroscopy," *Pediatric research.*, vol. 39, no. 5, pp. 889, 1996.

[20] M. Hiraoka, M. Firbank, M. Essenpreis, M. Cope, S. R. Arridge, P. van der Zee, et D. T. Delpy, "A Monte Carlo investigation of optical pathlength in inhomogeneous tissue and its application to near-infrared spectroscopy," *Physics in medicine and biology*, vol. 38, no. 12, pp. 1859-76, 1993.

[21] M. Kohl, C. Nolte, H. R. Heekeren, et S. Horst, "Determination of the wavelength dependence of the differential pathlength factor from near-infrared pulse signals," *Physics in medicine and biology.*, vol. 43, no. 6, pp. 1771, 1998.

[22] D. T. Delpy, M. Cope, P. van der Zee, S. Arridge, S. Wray, et J. Wyatt, "Estimation of optical pathlength through tissue from direct time of flight measurement," *Physics in medicine and biology*, vol. 33, no. 12, pp. 1433-42, 1988.

[23] B. Chance, J. S. Leigh, H. Miyake, D. S. Smith, S. Nioka, R. Greenfeld, M. Finander, K. Kaufmann, W. Levy, M. Young, P. Cohen, H. Yoshioka, et R. Boretsky, "Comparison of Time-Resolved and -Unresolved Measurements of Deoxyhemoglobin in Brain," *Proceedings of the National Academy of Sciences of the United States of America*, vol. 85, no. 14, pp. 4971-4975, 1988.

[24] D. Contini, A. Torricelli, A. Pifferi, L. Spinelli, F. Paglia, et R. Cubeddu, "Multi-channel time-resolved system for functional near infrared spectroscopy," *Optics Express*, vol. 14, no. 12, pp. 5418-32, 2006.

[25] C. D. Kurth et W. S. Thayer, "A multiwavelength frequency-domain near-infrared cerebral oximeter," *Physics in medicine and biology.*, vol. 44, no. 3, pp. 727, 1999.

[26] G. Strangman, M. A. Franceschini, et D. A. Boas, "Factors affecting the accuracy of near-infrared spectroscopy concentration calculations for focal changes in oxygenation parameters," *NeuroImage*, vol. 18, pp. 865-879, 2003.

[27] L. Kocsis, P. Herman, et A. Eke, "The modified Beer-Lambert law revisited," *Physics in medicine and biology.*, vol. 51, no. 5, pp. N91-N98, 2006.

[28] D. A. Boas, A. M. Dale, et M. A. Franceschini, "Diffuse optical imaging of brain activation: approaches to optimizing image sensitivity, resolution, and accuracy," *NeuroImage*, vol. 23, pp. 275-88, 2004.

[29] H. Sato, N. Tanaka, M. Uchida, Y. Hirabayashi, M. Kanai, T. Ashida, I. Konishi, et A. Maki, "Wavelet analysis for detecting body-movement artifacts in optical topography signals," *Neuroimage*, vol. 33, no. 2, pp. 580-587, 2006.

[30] M. Izzetoglu, A. Devaraj, S. Bunce, et B. Onaral, "Motion artifact cancellation in NIR spectroscopy using Wiener filtering," *Ieee Transactions on Biomedical Engineering*, vol. 52, no. 5, pp. 934-938, 2005.

[31] S. Perrey, "Non-invasive NIR spectroscopy of human brain function during exercise," *Methods*, vol. 45, no. 4, pp. 289-99, 2008.

[32] A. M. Dale, "Optimal experimental design for event-related fMRI," *Human brain mapping*, vol. 8, no. 2-3, pp. 2-3, 1999.

[33] M. A. Franceschini, D. K. Joseph, T. J. Huppert, S. G. Diamond, et D. A. Boas, "Diffuse optical imaging of the whole head," *Journal of Biomedical Optics*, vol. 11, no. 5, 2006.

[34] A. P. Gibson, J. C. Hebden, et S. R. Arridge, "Recent advances in diffuse optical imaging," *Physics in medicine & biology.*, vol. 50, no. 4, pp. R1-R43, 2005.

[35] C. Soraghan, "Development of A Versatile Multichannel CWNIRS Instrument for Optical Brain-Computer Interface Applications," PhD thesis, National University of Ireland, Maynooth, 2010.

[36] K. Uludag, J. Steinbrink, A. Villringer, et H. Obrig, "Separability and cross talk: optimizing dual wavelength combinations for near-infrared spectroscopy of the adult head," *NeuroImage*, vol. 22, no. 2, pp. 583-589, 2004.

[37] N. Okui et E. Okada, "Wavelength dependence of crosstalk in dual-wavelength measurement of oxy- and deoxy-hemoglobin," *Journal of Biomedical Optics*, vol. 10, no. 1, 2005.

[38] H. Sato, M. Kiguchi, et A. Maki, "Wavelength Dependence of Effective Pathlength Factor in Noninvasive Optical Measurements of Human Brain Functions," *Japanese Journal of Applied Physics Part 2 Letters*, vol. 45, no. 12/16, pp. L361-L449, 2006.

[39] G. Strangman, D. A. Boas, et J. P. Sutton, "Non-invasive neuroimaging using near-infrared light," *Biological psychiatry*, vol. 52, no. 7, pp. 679-93, 2002.

[40] J. M. Masciotti, J. M. Lasker, et A. H. Hielscher, "Digital Lock-In Detection for Discriminating Multiple Modulation Frequencies With High Accuracy and Computational Efficiency," *IEEE transactions on instrumentation and measurement.*, vol. 57, no. 1, pp. 182, 2008.

[41] C. J. Soraghan, T. E. Ward, F. Matthews, et C. Markham, "Optical safety assessment of a near-infrared brain-computer interface," *Signals and Systems Conference*, no. 539, pp. 174-179, 2008.

[42] A. Bozkurt et B. Onaral, "Safety assessment of near infrared light emitting diodes for diffuse optical measurements," *Biomedical engineering online*, vol. 3, no. 1, 2004.

[43] J. Pernier, *Electro et magnétoencéphalographie : biophysique, techniques et méthodes*, Paris: Lavoisier, 2007.

[44] E. Niedermeyer, "Ultrafast EEG activities and their significance," *Clinical EEG and neuroscience*, vol. 36, no. 4, pp. 257-62, 2005.

[45] A. J. Casson, D. C. Yates, S. J. M. Smith, J. S. Duncan, et E. Rodriguez-Villegas, "Wearable Electroencephalography," *IEEE Engineering in Medicine and Biology Magazine*, vol. 29, no. 3, pp. 44, 2010.

[46] M. J. Herrmann, T. Huter, M. M. Plichta, A. C. Ehlis, G. W. Alpers, A. Mühlberger, et A. J. Fallgatter, "Enhancement of activity of the primary visual cortex during processing of emotional stimuli as measured with event-related functional near-infrared spectroscopy and event-related potentials," *Human brain mapping*, vol. 29, no. 1, pp. 28-35, 2008.

[47] R. Kennan, S. Horovitz, A. Maki, Y. Yamashita, H. Koizumi, et J. Gore, "Simultaneous Recording of Event-Related Auditory Oddball Response Using Transcranial Near Infrared Optical Topography and Surface EEG," *NeuroImage*, vol. 16, no. 3a, pp. 587-592, 2002.

[48] R. J. Cooper, N. L. Everdell, L. C. Enfield, A. P. Gibson, A. Worley, et J. C. Hebden, "Design and evaluation of a probe for simultaneous EEG and near-infrared imaging of cortical activation," *Physics in medicine and biology.*, vol. 54, no. 7, pp. 2093-2102, 2009.

[49] R. P. Kennan, D. Kim, A. Maki, H. Koizumi, et R. T. Constable, "Non-invasive assessment of language lateralization by transcranial near infrared optical topography and functional MRI," *Human brain mapping*, vol. 16, no. 3, pp. 183-9, 2002.

[50] S. Zechner, "Functional imaging with near-infrared spectroscopy: correlation between brain response, ApoE genotype, and neuropsychological test performance," Thèse de Doctorat, University of Basel, Basel, 2005.

[51] C. Hock, K. Villringer, F. Müller-Spahn, R. Wenzel, H. Heekeren, S. Schuh-Hofer, M. Hofmann, S. Minoshima, M. Schwaiger, U. Dirnagl, et A. Villringer, "Decrease in parietal cerebral hemoglobin oxygenation during performance of a verbal fluency task in patients with Alzheimer's disease monitored by means of near-infrared spectroscopy -- correlation with simultaneous rCBF-PET measurements," *Brain research*, vol. 755, no. 2, pp. 293-303, 1997.

[52] s. Institut canadien d'information sur la, B. Canadian, C. Nerve Health, et C. Fédération des sciences neurologiques du, "Le fardeau des maladies, troubles et traumatismes neurologiques au Canada," pp., 2007. Disponible: http://epe.lac-bac.gc.ca/100/200/301/cihi-icis/burden-f/H118-42-2007F.pdf.

[53] E. Watanabe, A. Maki, F. Kawaguchi, Y. Yamashita, H. Koizumi, et Y. Mayanagi, "Noninvasive Cerebral Blood Volume Measurement During Seizures Using Multichannel Near Infrared Spectroscopic Topography," *Journal of Epilepsy*, vol. 11, no. 6, pp. 335-340, 1998.

[54] K. Haginoya, M. Munakata, R. Kato, H. Yokoyama, M. Ishizuka, et K. Iinuma, "Ictal cerebral haemodynamics of childhood epilepsy measured with near-infrared spectrophotometry," *Brain*, vol. 125, pp. 1960-1971, 2002.

[55] D. K. Sokol, O. N. Markand, E. C. Daly, T. G. Luerssen, et M. D. Malkoff, "Near infrared spectroscopy distinguishes seizure types," *Seizure*, vol. 9, no. 5, pp. 323-7, 2000.

[56] P. D. Adelson, E. Nemoto, M. Scheuer, M. Painter, J. Morgan, et H. Yonas, "Noninvasive Continuous Monitoring of Cerebral Oxygenation Periictally Using Near-infrared Spectroscopy: A Preliminary Report," *Epilepsia*, vol. 40, no. 11, pp. 1484, 1999.

[57] T. H. Schwartz, "Neurovascular coupling and epilepsy: hemodynamic markers for localizing and predicting seizure onset," *Epilepsy currents*, vol. 7, no. 4, pp. 91-94, 2007.

[58] H. Kato, M. Izumiyama, H. Koizumi, A. Takahashi, et Y. Itoyama, "Near-Infrared Spectroscopic Topography as a Tool to Monitor Motor Reorganization After Hemiparetic Stroke: A Comparison With Functional MRI," *Stroke*, vol. 33, no. 8, pp. 2032, 2002.

[59] H. Saitou, H. Yanagi, S. Hara, S. Tsuchiya, et S. Tomura, "Cerebral blood volume and oxygenation among poststroke hemiplegic patients: Effects of 13 rehabilitation tasks measured by near-infrared spectroscopy," *Archives of Physical Medicine and Rehabilitation*, vol. 81, no. 10, pp. 1348-1356, 2000.

[60] K. G. Jordan, "Emergency EEG and Continuous EEG Monitoring in Acute Ischemic Stroke," *Journal of clinical neurophysiology*, vol. 21, no. 5, pp. 341, 2004.

[61] P. K. Myint, E. F. Staufenberg, et K. Sabanathan, "Post-stroke seizure and post-stroke epilepsy," *Postgraduate medical journal*, vol. 82, no. 971, pp. 568-72, 2006.

[62] L. Rumbach, "AVC : 1ère cause d'épilepsie vasculaire ", 2006. Disponible: http://www.santea.com/gp/santea/pro/specialites/neurologie/etudes_et_congres/avc_1ere_cause_d_epilepsie_vasculaire. [Consulté le 13 décembre 2010].

[63] T. Vaithianathan, I. D. C. Tullis, N. Everdell, T. Leung, A. Gibson, J. Meek, et D. T. Delpy, "Design of a portable near infrared system for topographic imaging of the brain in babies," *Review of scientific instruments.*, vol. 75, no. 10, pp. 3276, 2004.

[64] A. Bozkurt, A. Rosen, H. Rosen, et B. Onaral, "A portable near infrared spectroscopy system for bedside monitoring of newborn brain," *Biomedical engineering online*, vol. 4, no. 1, 2005.

[65] D. Haensse, P. Szabo, D. Brown, J. C. Fauchère, P. Niederer, H. U. Bucher, et M. Wolf, "A new multichannel near infrared spectrophotometry system for functional studies of the brain in adults and neonates," *Optics Express*, vol. 13, no. 12, pp. 4525-38, 2005.

[66] M. A. Franceschini et D. A. Boas, "Noninvasive measurement of neuronal activity with near-infrared optical imaging," *NeuroImage*, vol. 21, no. 1, pp. 372-386, 2004.

[67] B. Onaral et K. Pourrezaei, "Functional optical brain imaging sensor," 2004. Disponible: http://www.biomed.drexel.edu/ResearchPort/Contents/Biomedical_Optics/Overview/default.cfm?SLD=2. [Consulté le 27 décembre 2010].

[68] H. Atsumori, M. Kiguchi, A. Obata, H. Sato, T. Katura, T. Funane, et A. Maki, "Development of wearable optical topography system for mapping the prefrontal cortex activation," *Review of Scientific Instruments*, vol. 80, no. 4, 2009.

[69] L. Rovati, S. Fonda, L. Bulf, R. Ferrari, G. Biral, G. Salvatori, A. Bandera, et M. Corradini, "Functional cerebral activation detected by an integrated system combining CW-NIR spectroscopy and EEG [5326-31]," *Proceedings - SPIE*, vol. 5326, pp. 118-125, 2004.

[70] L. Rovati, G. Salvatori, L. Bulf, et S. Fonda, "Optical and electrical recording of neural activity evoked by graded contrast visual stimulus," *Biomedical engineering online*, vol. 6, 2007.

[71] C. C. Fu, C. K. Chen, S. Y. Tseng, S. Kang, E. Chua, et W. C. Fang, "Portable Brain-Heart Monitoring System," in *Database Theory and Application, Bio-Science and Bio-Technology*, Berlin: Springer, 2010, pp. 241-250.

[72] C. T. Lin, L. W. Ko, M. H. Chang, J. R. Duann, J. Y. Chen, T. P. Su, et T. P. Jung, "Review of wireless and wearable electroencephalogram systems and brain-computer interfaces--a mini-review," *Gerontology*, vol. 56, no. 1, pp. 112-9, 2010.

[73] A. Yodh et B. Chance, "Spectroscopy and Imaging with Diffusing Light," *Physics today.*, vol. 48, no. 3, pp. 34, 1995.

[74] A. Maki, Y. Yamashita, Y. Ito, E. Watanabe, Y. Mayanagi, et H. Koizumi, "Spatial and temporal analysis of human motor activity using noninvasive NIR topography," *Medical physics*, vol. 22, no. 12, pp. 1997-2005, 1995.

[75] A. Villringer et B. Chance, "Non-invasive optical spectroscopy and imaging of human brain function," *Trends in neurosciences.*, vol. 20, no. 10, pp. 435, 1997.

[76] T. Hoshino, K. Sakatani, Y. Katayama, N. Fujiwara, Y. Murata, K. Kobayashi, C. Fukaya, et T. Yamamoto, "Application of multichannel near-infrared spectroscopic topography to physiological monitoring of the cortex during cortical mapping: technical case report," *Surgical neurology*, vol. 64, no. 3, pp. 272-5, 2005.

[77] S. Sumitani, T. Tanaka, S. Tayoshi, K. Ota, N. Kameoka, M. Morimune, S. Shibuya-Tayoshi, S. Kinouchi, S. Ueno, et T. Ohmori, "Hemodynamic changes in the prefrontal cortex during mental works as measured by multi channel near-infrared spectroscopy," *The journal of medical investigation*, vol. 52, pp. 302-3, 2005.

[78] L. F. Quesney, "Extratemporal epilepsy: clinical presentation, pre-operative EEG localization and surgical outcome," *Acta neurologica Scandinavica. Supplementum*, vol. 140, pp. 81-94, 1992.

[79] J. Furusho, A. Suzuki, Y. Takakusa, F. Kawaguchi, N. Ichikawa, et T. Kato, "Simultaneous study of interictal EEG and near-infrared spectroscopy in a boy with epilepsy," *International Congress Series*, vol. 1232, pp. 673-676, 2002.

[80] A. Gallagher, M. Lassonde, D. Bastien, P. Vannasing, F. Lesage, C. Grova, A. Bouthillier, L. Carmant, F. Lepore, R. Béland, et D. K. Nguyen, "Non-invasive pre-surgical investigation of a 10 year-old epileptic boy using simultaneous EEG-NIRS," *Seizure*, vol. 17, no. 6, pp. 576-82, 2008.

[81] N. Roche-Labarbe, B. Zaaimi, P. Berquin, A. Nehlig, R. Grebe, et F. Wallois, "NIRS-measured oxy- and deoxyhemoglobin changes associated with EEG spike-and-wave discharges in children," *Epilepsia*, vol. 49, no. 11, pp. 1871-80, 2008.

[82] M. Giardini et S. Trevisan, "Portable High-End Instrument for In-Vivo Infrared Spectroscopy Using Spread Spectrum Modulation," *IEEE Instrumentation and Measurement Technology Conference Proceedings*, vol. 2, pp. 860-863, 2004.

[83] H. Atsumori, M. Kiguchi, A. Obata, H. Sato, T. Katura, K. Utsugi, T. Funane, et A. Maki, "Development of a multi-channel, portable optical topography system," in *29th*

*Annual International Conference of Engineering in Medicine and Biology Society*, *Lyon, France*, 2007, pp. 3362-3364.

[84] M. Moosmann, P. Ritter, I. Krastel, A. Brink, S. Thees, F. Blankenburg, B. Taskin, H. Obrig, et A. Villringer, "Correlates of alpha rhythm in functional magnetic resonance imaging and near infrared spectroscopy," *NeuroImage*, vol. 20, no. 1, pp. 145-158, 2003.

[85] R. Oostenveld et P. Praamstra, "The five percent electrode system for high-resolution EEG and ERP measurements," *Clinical Neurophysiology*, vol. 112, no. 4, pp. 713-719, 2001.

[86] TexasInstrumentsIncorporated, "Medical Applications Guide," pp. 20, 2007. Disponible: http://www.mouser.com/catalog/specsheets/TIsMedicalAppsGuide.pdf. [Consulté le 5 janvier 2011].

[87] H. Gagnon, M. Cousineau, A. Adler, et A. E. Hartinger, "A Resistive Mesh Phantom for Assessing the Performance of EIT Systems," *IEEE Transactions on Biomedical Engineering*, vol. 57, no. 9, pp. 2257-2266, 2010.

[88] E. Gratton, S. Fantini, M. A. Franceschini, G. Gratton, et M. Fabiani, "Measurements of scattering and absorption changes in muscle and brain," *Philosophical transactions of the Royal Society of London. Series B, Biological sciences*, vol. 352, no. 1354, pp. 727-35, 1997.

[89] B. W. Zeff, B. R. White, H. Dehghani, B. L. Schlaggar, et J. P. Culver, "Retinotopic mapping of adult human visual cortex with high-density diffuse optical tomography," *Proceedings of the National Academy of Sciences of the United States of America.*, vol. 104, no. 29, pp. 12169, 2007.

[90] V. Y. Toronov, X. Zhang, et A. G. Webb, "A spatial and temporal comparison of hemodynamic signals measured using optical and functional magnetic resonance imaging during activation in the human primary visual cortex," *NeuroImage*, vol. 34, no. 3, pp. 1136-1148, 2007.

[91] H. Obrig, H. Israel, M. Kohl-Bareis, K. Uludag, R. Wenzel, B. Müller, G. Arnold, et A. Villringer, "Habituation of the Visually Evoked Potential and Its Vascular Response: Implications for Neurovascular Coupling in the Healthy Adult," *NeuroImage*, vol. 17, no. 1, pp. 1-18, 2002.

[92] S. Coyle, T. Ward, et C. Markham, "Physiological noise in near-infrared spectroscopy: implications for optical brain computer interfacing," *Annual*

*International Conference of the IEEE Engineering in Medicine and Biology Society*, vol. 6, pp. 4540-3, 2004.

[93] A. Delorme et S. Makeig, "EEGLAB: an open source toolbox for analysis of single-trial EEG dynamics including independent component analysis," *Journal of Neuroscience Methods*, vol. 134, no. 1, pp. 9-21, 2004.

[94] M. Zaletel, M. Strucl, T. Pogacnik, et B. Zvan, "Effects of visual contrast on visual evoked potentials and Doppler signal," *The European journal of neuroscience*, no. 19, pp. 3353-3358, 2004.

[95] S. Kurita-Tashima, S. Tobimatsu, M. Nakayama-Hiromatsu, et M. Kato, "Effect of check size on the pattern reversal visual evoked potential," *Electroencephalography and clinical neurophysiology*, vol. 80, no. 3, pp. 161-166, 1991.

[96] C. S. Herrmann, "Human EEG responses to 1-100 Hz flicker: resonance phenomena in visual cortex and their potential correlation to cognitive phenomena," *Experimental brain research*, vol. 137, no. 3-4, pp. 3-4, 2001.

[97] C. R. Lines, M. D. Rugg, et A. D. Milner, "The effect of stimulus intensity on visual evoked potential estimates of interhemispheric transmission time," *Experimental brain research*, vol. 57, no. 1, pp. 89-98, 1984.

[98] K. S. Rauss, G. Pourtois, P. Vuilleumier, et S. Schwartz, "Attentional load modifies early activity in human primary visual cortex," *Human brain mapping*, vol. 30, no. 5, pp. 1723-33, 2009.

[99] T. Durduran, G. Yu, M. G. Burnett, J. A. Detre, J. H. Greenberg, J. Wang, C. Zhou, et A. G. Yodh, "Medical Optics and Biotechnology - Diffuse optical measurement of blood flow, blood oxygenation, and metabolism in a human brain during sensorimotor cortex activation," *Optics letters.*, vol. 29, no. 15, pp. 1766, 2004.

[100] Texas Instruments Incorporated, "Designing photodiode amplifier circuits with OPA128," pp. 4, 2000. Disponible: http://focus.ti.com/lit/an/sboa061/sboa061.pdf. [Consulté le 28 décembre 2010].

[101] M. Pachchigar, "Design Considerations for a Transimpedance Amplifier," pp. 4, 2008. Disponible: http://www.national.com/an/AN/AN-1803.pdf. [Consulté le 28 décembre 2010].

[102] S. G. Diamond, T. J. Huppert, V. Kolehmainen, M. A. Franceschini, J. P. Kaipio, S. R. Arridge, et D. A. Boas, "Physiological System Identification with the Kalman

Filter in Diffuse Optical Tomography," *Lecture notes in computer science.*, no. 3750, pp. 649-656, 2005.

[103] S. Prince, V. Kolehmainen, J. P. Kaipio, M. A. Franceschini, D. Boas, et S. R. Arridge, "Time-series estimation of biological factors in optical diffusion tomography," *Physics in medicine & biology.*, vol. 48, pp. 1491-1504, 2003.

**ANNEXE 6**

***Optical imaging of acute epileptic networks in mice***

Published by:
Journal of Biomedical Optics,

**Edgar Guevara[1, 2], Philippe Pouliot[1, 2], Dang Khoa Nguyen[3], Frédéric Lesage[1, 2]**

*[1]Department of Electrical Engineering, École Polytechnique de Montréal, Canada*
*[2]Montreal Heart Institute, Montréal, Canada*
*[3]Department of Medicine, Université de Montréal, Montréal, Canada*

Keywords: Functional connectivity, resting state, intrinsic signals, laser speckle, 4-aminopyridine, animal models of epilepsy.

**SUMMARY**

*Purpose:* To investigate the potential of intrinsic optical imaging and resting state analysis as a tool to study brain networks associated with epileptic seizures.

*Methods:* Using an acute model of epileptiform activity, the 4-AP model in live mice, we observe changes in resting state networks with the onset of seizure activity and in conditions of low level spiking activity.

*Key findings:* Resting state networks identified before and after the onset of epileptiform activity show both decreased and increased homologous correlations, with a small dependence on seizure intensity.

*Significance:* The observed changes were not uniform across the different hemodynamic parameters, suggesting a potential decoupling between blood flow and metabolism in the low frequency networks. This study supports the need for a more extensive investigation of epileptic networks including more than one hemodynamic measurement.

*Key Words:* Functional connectivity, Resting state, intrinsic signals, 4-Aminopyridine, Animal models of epilepsy.

## INTRODUCTION

Epilepsy is a group of neurological disorders where the abnormal synchrony of discharge in large ensembles of neurons results in an epileptic seizure (ictus), which over time may have serious consequences (Kandel et al., 1991). After cerebrovascular disorders, epilepsy is the most common chronic neurological condition, affecting 0.5 to 1% of the population. The current method to visualize abnormal epileptiform discharges in patients with epilepsy is to perform an electroencephalogram (EEG), a technique which uses electrodes to record the spontaneous electrical activity of the brain (Gibbs et al., 1937). Epileptiform abnormalities are usually divided into a) 'interictal' discharges which are brief (milliseconds) asymptomatic paroxysmal EEG transients clearly distinguished from background; and b) 'ictal' discharges which are sudden focal rhythmic activity with characteristic pattern of evolution (with respect to amplitude, frequency and spatial distribution) lasting at least several seconds. These ictal discharges are generally associated with clinical seizure manifestations.

Functional imaging based on cerebral perfusion such as combined functional MRI - electroencephalography (fMRI-EEG) and functional near-infrared spectroscopy (fNIRS –EEG) (Gallagher et al., 2008) have recently been explored for their potential at identifying the epileptic focus as well as study the coupling between brain regions involved in the epileptic network. While hemodynamic changes triggered by epileptic events have potential for localization, neuroimaging observations in patients remain confounded in several ways. An overarching reason is that the hemodynamic response is often not restricted to the epileptogenic focus but spreads across a distributed network of brain structures, with complicated dynamics (Nguyen et al., 2012; Zhao et al., 2007). For example, the presence of mirror activation (Morrell & deToledo-Morrell, 1999) sometimes makes lateralization difficult. Even when there is a clear localized focus, the temporal aspects between oxyhemoglobin ($HbO_2$), deoxyhemoglobin (HbR), cerebral blood flow (CBF), volume, and oxygen metabolism are still very intricate. Interictal discharges, and even more so seizures, are large neuronal discharges requiring high metabolic consumption and thus accompanied by a large increase of perfusion, rendering the interpretation of fMRI and fNIRS data difficult, given the complicated relationship between the various quantities of interest.

The term functional connectivity is applied to a variety of studies that examine coherent inter-regional correlations of neuronal activity during both cognitive tasks and rest (Fox & Raichle, 2007). It is a technique sensitive to spatial and temporal synchronicity of fluctuations in neural activity (Waites et al., 2006). The application of functional connectivity to epilepsy is motivated both by observations of a distributed network of activations during epileptic events and by recent studies with resting-state functional magnetic resonance imaging (rs-fMRI) (Luo et al., 2012; Mankinen et al., 2012; Waites et al., 2006; Wang et al., 2011), that have documented an altered functional connectivity in several functional networks in epileptic patients. In the first of these studies, investigations of functional connectivity in patients with left temporal lobe epilepsy has reported a significant decrease of connectivity in language-related areas during resting-state when compared to controls (Waites et al., 2006). Separate studies of epileptic networks documented a decrease of functional connectivity in the self-referential, somatosensory, visual, and auditory networks (Wang et al., 2011), as well as in the default mode network (Frings et al., 2009; Liao et al., 2011; Luo et al., 2012) and in the dorsal attention network (Zhang et al., 2009). The distributed nature of activation during epileptic seizures, the heterogeneity within the patient population and non-linear coupling (Voges et al., 2012) between vascular components during large neuronal discharges support investigating these phenomena in controlled animal models to better characterize network changes with epileptic events.

We adapted in this work a recently developed technique that combines functional connectivity mapping with optical intrinsic signal imaging (fcOIS) (Bero et al., 2012; White et al., 2011). This allowed measuring the magnitude of bilateral functional connectivity after the induction of focal seizures in the somatosensory cortex, using a seed region-based cross-correlation analysis. In addition to the oxyhemoglobin contrast previously used in (Bero et al., 2012; White et al., 2011), we examined deoxyhemoglobin and also blood flow measured simultaneously with laser speckle imaging to provide an extended set of parameters characterizing hemodynamic changes during large neuronal discharges. This multimodal approach with optical and electrical recordings provides a comprehensive depiction of the resting-state activity, before and after the injection of the neurotoxin. Optical imaging based on intrinsic

signals (OIS) and laser speckle blood flow imaging map hemodynamic variables all over the convexity of the cortex and electrophysiology recordings give a precise measurement of local field potential (LFP) in the area surrounding the epileptic focus. Injection of the neurotoxin 4-Aminopyridine (4-AP) in the left somatosensory cortex was used to produce seizure-like epileptiform discharges (later simply referred to as seizures) resulting from neuronal hyperactivity in cortical neurons (Fabene et al., 2006; Zhao et al., 2009; Zhao et al., 2011). This model offers the possibility to make a comparison of the healthy cortex and the epileptic cortex on the same experimental animal. Motivations for the current study are two-fold: (1) understanding the modulation of brain networks at an early stage in ictogenesis is important to gain a better understanding of the pathophysiology of the disease (Bettus et al., 2011; Luo et al., 2012; Mankinen et al., 2012) and may help uncover the mechanisms by which these brain networks are altered. (2) A long-term motivation is to evaluate the usefulness of resting state analyses to support epileptic focus localization. Our aim in this work was to provide a proof-of-principle study using intrinsic optical imaging on acute epileptiform events, with a perspective of translating these techniques to a more chronic animal model of epilepsy.

## METHODS

### Animal preparation

All surgical procedures, performed according to the recommendations of the Canadian Council on Animal Care, were approved by the Animal Research Ethics Committee of the Montreal Heart Institute. Nine male C57BL/6 mice (8.9 ± 0.2 weeks old, 23.3 ± 2.3 g weight, Charles River, Wilmington, MA) were anesthetized via intraperitoneal injections of urethane (2mg/g body weight) in a 10% (wt/vol) saline solution. Body temperature was maintained at 37°C with a feedback controlled heating blanket (MouseSTAT, Kent Scientific, Torrington, CT).

A tracheotomy was done in order to avoid respiratory distress (Moldestad et al., 2009). Scalp was carefully removed and a stereotaxically guided burr-hole was made over the left somatosensory cortex (coordinates 1 mm lateral to midline, 1mm caudal to bregma Figure 1B) for injection of 4-AP and electrophysiological monitoring, using a #22 gauge needle.

Mice were placed on a stereotaxic apparatus and subcutaneous electrocardiogram was recorded with a single lead ECG amplifier (amp-b01, emka TECHNOLOGIES, Paris). The amplified (1000× gain) and filtered signal (0.2-500 Hz) was sampled at 1 kHz. All vital signals were digitized by a data acquisition card (NI-USB 6353, National Instruments, Austin, TX) controlled by a custom made graphical user interface developed in LabView (National Instruments), which also controlled the image acquisition. To prevent drying of the exposed skull a custom chamber made of bone wax was adhered to the skull with ultrasound gel and filled with mineral oil, after positioning the microelectrode.

**Epilepsy model and electrophysiology**

Epileptiform activity was achieved according to the procedures described by Zhao et al. (Zhao et al., 2009; Zhao et al., 2011), briefly described below. Focal seizures were induced by injection of 500nL of the K+ channel antagonist 4-AP (A78403, Sigma-Aldrich, St. Louis, MO) solution at 15mM, through a glass micropipette with a micro-syringe pump controller (uMC4, World Precision Instruments, Sarasota FL). The volume was injected at a rate of 50nL/min. The borosilicate glass pipette (1mm outer diameter, 0.7mm inner diameter, 75mm long, World Precision Instruments, New Haven, CT) was horizontally pulled on a programmable pipette puller (P-2000, Sutter Instruments, Novato, CA) using program #65.

The glass pipette was removed and then a tungsten microelectrode (0.5 to 2MΩ) was placed at a depth of ~500 μm into the cortex, in order to record extracellular LFP at the injection site. The signal was filtered between 10-5000 Hz, amplified 1000 times with a microelectrode AC amplifier (model 1800, A-M systems, Sequim, WA), then digitized at 10 kHz. LFP data was further filtered between 0.2 and 130 Hz using an order 4 Butterworth digital filter in post-processing. An example of typical epileptiform activity is shown in Figure 1C).

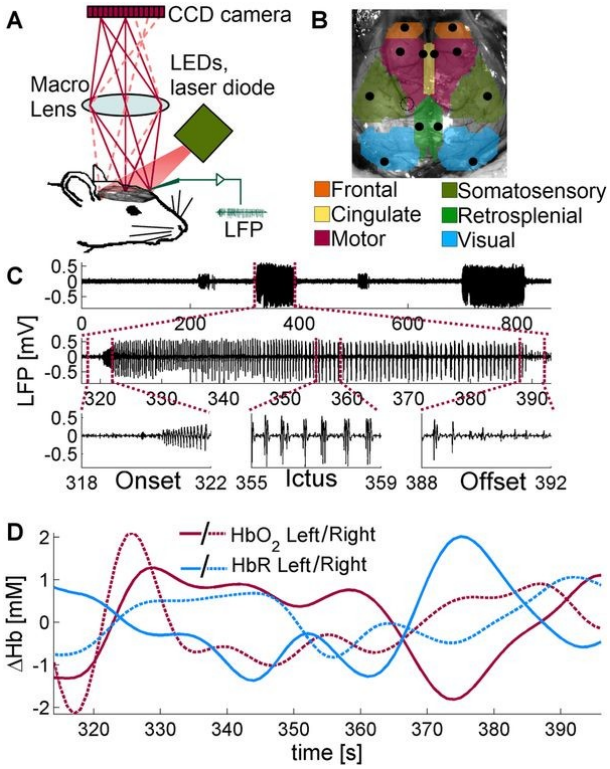


Figure 1. (A) Overview of the intrinsic signal optical imaging system. LEDs and laser diode are timemultiplexed and synchronized to the acquisition system. A tungsten electrode is used to record LFP on the left somatosensory cortex. (B) Functional regions on the mouse cortex and seed placement and size, manually constructed from the work of Bero et al. Dotted circle shows the placement of the LFP electrode. (C) Electrophysiology of 4-AP induced seizure. Top: Example showing some ictal discharges after an injection. 4-AP injection was finished at time 0. Middle: Zoom on a single ictal discharge. Bottom: Expanded view showing the onset of the discharge, the intermediate phase and the offset. (D) Filtered time traces of HBO2 and HbR at the epileptic focus (dotted circle in B), during the seizure. 152x193mm (300 x 300 DPI).

## Optical recording system

Optical images based on intrinsic signals (OIS) were acquired with a 12-bit CCD camera (Pantera 1M60, DS-21-01M60-12E, Teledyne Dalsa, Waterloo, ON) with a pixel size of 12μm and full resolution of 1024×1024 pixels. The setup used in this work is depicted in Figure 1A).

A custom-made interface controls the camera, records images and vital signs, while synchronizing acquisition and illumination. A Macro Lens (105mm f/2.8max, Sigma Corp., Ronkonkoma, NY) with small focal depth (350 μm) was used. Reflectance images of the brain cortex were recorded with time-multiplexed illumination (525, 590, 625 nm) produced by 10W LEDs (LZ4-00MA00, Led Engin, San Diego, CA). Illumination for speckle imaging was provided by 90 mW, 785 nm laser diode

(L785P090, Thorlabs, Newton, NJ) and aperture was adjusted to f/8, so that the pixel size and speckle size were matched. The four temporally multiplexed wavelengths led to a full-frame rate of 5 Hz. A 2×2 binning on camera was performed to allow continuous data streaming to hard drive. Illumination was further adjusted so that no part of the brain was under- or over-saturated by any of the wavelengths. The exposure time of the camera was set to 10 msec. The setup was mounted on an optic table with tuned damping (RS 2000, Newport, Irvine, CA) to avoid spurious signals from vibrations.

**Optical imaging of intrinsic signals (OIS)**

The analysis of spectroscopic images was based on previously published work (Dubeau et al., 2011; Dunn et al., 2003). In short, reflectance images from each LED wavelength were recorded with the CCD camera and interpreted as changes in attenuation (optical density) $\Delta \mathbf{OD} = \mathbf{log}\left(\mathbf{I_0}/\mathbf{I}\right)$, where I is the reflected light intensity and $I_0$ the incident light intensity. Relative changes in oxy- ($HbO_2$) and deoxyhemoglobin (HbR) were found using the modified Beer-Lambert law (Delpy et al., 1988) and a Moore-Penrose pseudoinverse:

$$\Delta OD(\lambda, t) = \sum_i \epsilon_i(\lambda) C_{\mathbf{A}}$$

The differential path length factor, D(λ), was taken from (Dunn et al., 2005) and values out of the 560-610 nm range were extrapolated from (Kohl et al., 2000). Total hemoglobin baseline concentration of 100 μM with 60% oxygen saturation was assumed (Dunn et al., 2005) for the spectroscopic analysis. The hemoglobin extinction coefficients were obtained from (Prahl, 1999) and the reflectance values were corrected for the spectral response of the CCD camera and convolved with the LEDs spectral power distribution (Brieu et al., 2010).

Images of each chromophore ($HbO_2$, HbR) were spatially smoothed with a Gaussian kernel of 11×11 pixels with a 5 pixel standard deviation. An anatomical image was recorded with illumination at 525 nm, and then the region corresponding to brain was manually selected using a closed spline curve to create a brain mask. All further processing was performed only on those pixels belonging to the brain mask.

**Speckle contrast imaging**

In addition to imaging changes in hemoglobin concentrations, changes in cerebral blood flow (CBF) were also computed by laser speckle contrast imaging. Speckle originates from the random interference of multiple backscattered coherent light. In the presence of moving scatterers the interference field fluctuates, creating intensity variations, known as speckle patterns (Boas & Dunn, 2010; Dunn et al., 2001; Dunn et al., 2005). When integrated over the exposure time of the camera, the speckle pattern becomes blurred in areas of increased blood flow. Images of blood flow were obtained by measuring the spatial contrast of the speckle C, defined as the ratio of the standard deviation to the average intensity $\frac{\sigma}{\langle I \rangle}$. The contrast is a function of the CCD camera exposure time T and it is related to the correlation time $\tau_C$ of the speckle, which is assumed to be inversely proportional to the speed of the scattering particles (Briers, 2001). A window of 5×5 pixels was used to compute the speckle contrast images and the relative changes in blood flow were obtained with the following formula:

$$C = \frac{\sigma}{\langle I \rangle}, - \frac{2\Delta C}{C_0} = \frac{\Delta V}{V_0} \mathbf{A}$$

Since $\frac{\Delta v}{v_0}$ laser speckle imaging underestimates CBF by less than 5% (Luckl et al., 2010), in this work both quantities were assumed to be equal. Flow images then underwent the same spatial filtering as the hemoglobin images, and images from all three different contrasts were further resized to ¼ of the original size due to memory constraints.

**Cerebral metabolic rate of oxygen**

Changes in the cerebral metabolic rate of oxygen consumption ($CMRO_2$) were calculated from the images of changes in CBF, total hemoglobin (HbT) and HbR using the steady state relationship (Jones et al., 2001; Mayhew et al., 2000):

$$\frac{\Delta CMRO_2}{CMRO_{2,0}} = \frac{\left(1 + \frac{\Delta CBF}{CBF_0}\right)\left(1 + \gamma_R \frac{\Delta HBR}{HBR_0}\right)}{\left(1 + \gamma_T \frac{\Delta HBT}{HBT_0}\right)} - 1 \qquad (3)$$

A central hypothesis of this relation is the absence of transients with decoupled hemodynamic components. Here, since resting state networks were identified from data filtered between 0.009-0.08 Hz (see below), we hypothesized that for these networks, the relationship was maintained. The constants $\gamma_R$ and $\gamma_T$ where both assumed to be 1, which is within a physiologically plausible range (0.75–1.25) (Jones et al., 2001).

**Functional connectivity**

Multimodal recording sessions (optical and electrical) of 15 minutes were carried out in resting-state conditions, both before the injection of 4-AP and ~5 minutes after the release of the epileptogenic compound in the somatosensory cortex. Time courses of every pixel were temporally band-pass filtered (zero phase-shift fourth-order Butterworth IIR filter) at 0.009-0.08 Hz, according to previous functional connectivity studies (Bero et al., 2012; White et al., 2011). After temporal filtering, each pixel time trace was downsampled from 5 Hz to 1 Hz.

A global brain signal was created from the average of all the pixels time traces. In order to account for coherent variability common to all pixels, this global brain signal was regressed from every pixel's time course, using a General Linear Model (GLM) from the package Statistical Parametrical Mapping (Friston et al., 2006) (SPM8, www.fil.ion.ucl.ac.uk/spm) running on a MATLAB (The MathWorks, Natick, MA) platform.

All seeds were manually placed a priori using the coordinates corresponding to left and right frontal, cingulate, motor, somatosensory, cingulate and visual cortices (White et al., 2011), as shown on Figure 1B). Seed time courses were computed as the mean time course of the pixels within a 3.5 pixel radius from the seed locus. An example of seeds time-traces during seizure are illustrated in Figure 1D).

The metric used to evaluate functional connectivity was a regional bilateral functional correlation, defined as the correlation between each seed time course and its contralateral homologue, yielding six values for each mouse. The Pearson's coefficient r values were converted to Fisher Z measures using $Z(r) = \frac{1}{2}\ln\left[{}^{(1+r)}/_{(1-r)}\right]$ before performing the random effect rank sum tests. Since the assumptions for normal distributions might not hold in this study, significance was determined by the Wilcoxon rank sum test. Values were considered significant at $p<0.05$.

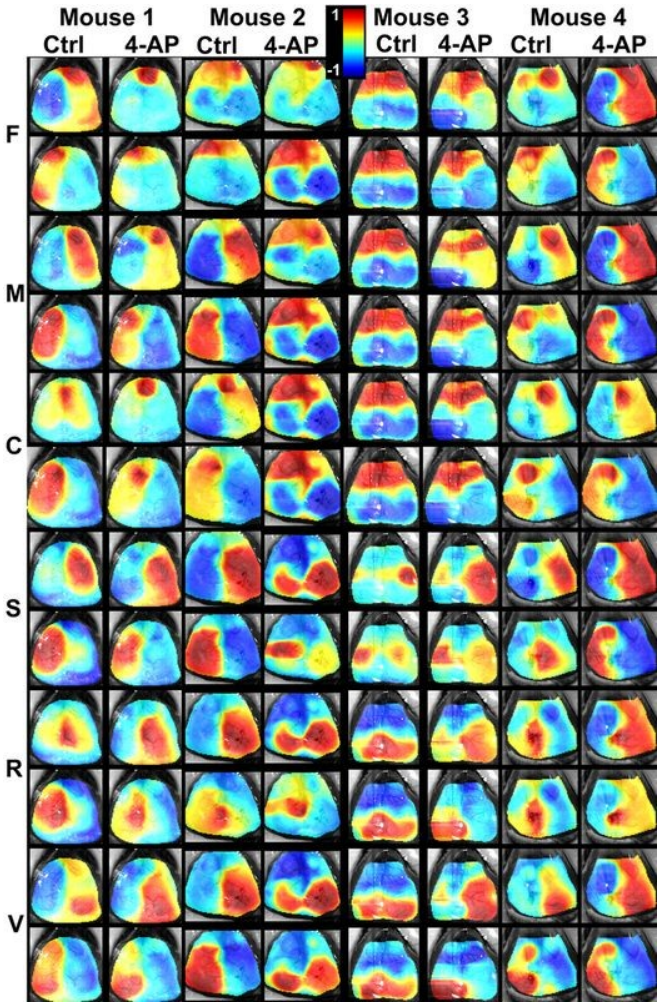


Figure 2. Seed-based HbO2 correlation maps for four mice. One control session and one post-4-AP injection session are displayed for each mouse. (F: frontal cortex, M:motor cortex, C: cingulate cortex, S: somatosensory cortex R: retrosplenial cortex, V: visual cortex). The scale for all correlation maps is from r = -1 to 1. Maps are shown overlaid on the anatomical image of the brain, acquired with green light. 124x191mm (300 x 300 DPI).

## RESULTS

### Identification of functional networks

Functional networks were identified prior to 4-AP injection and in agreement with previous literature (White et al., 2011) across mice for $HbO_2$ (see Figure 2) albeit with a stronger lateralization of some networks.

With multispectral acquisition, the same procedure was also performed for HbR and CBF estimated from speckle imaging, no significant change in spatial network organization was observed (Figure S1 and Figure S2). In one experiment we performed the network analysis using a higher frame rate and compared with a similar analysis performed by dropping camera frame to investigate the effect of acquisition frame rate. No significant difference was observed confirming that the chosen 5Hz acquisition rate was adequate (data not shown).

### Changes in functional connectivity after injection of 4-AP

Out of 9 mice, 5 showed clear seizure-like activity (see Table 1 below) while 4 showed lower intensity spiking activity. All mice were combined in the analysis of this section. To assess the impact of acute seizures and epileptiform activity on resting state networks, resting state sessions acquired following injection of 4-AP were analyzed following the same methodology as above.

Table 1 Seizure data

| **Subject ID** | **Seizure duration (s)** | | **Percentage duration in seizure state (%)** | | **Average seizure duration (s)** |
|---|---|---|---|---|---|
| | ***Session 1*** | ***Session 2*** | ***Session 1*** | ***Session 2*** | ***Both sessions*** |
| **1** | 45, 43, 33, 32 | 35, 32, 27 | 5.2, 4.9, 3.8, 3.7 | 4, 3.7, 3.1 | 35.28 |
| **3** | 27, 33, 34 | - | 2.8, 3.4, 3.5 | - | 31.33 |
| **4** | 114 | 71, 112 | 13.2 | 8.2, 12.9 | 99 |
| **7** | 38, 30, 30 | 33, 32 | 4.4, 3.4, 3.4 | 3.8, 3.7 | 32.6 |
| **9** | 130 | 161 | 15 | 18.6 | 145.5 |

Correlations between homologous seeds were investigated and compared before and after injection of the neurotoxin. Data extracted from the $HbO_2$ time course showed a significant difference in somatosensory and retrosplenial seeds (Figure 3A). For HbR contrast there was no significant difference in any paired seeds time trace (Figure 3B), although a decrease in functional connectivity was seen on the somatosensory region, a trend also seen in flow and $CMRO_2$ data. Seeds of the cingulate, somatosensory and retrosplenial cortex saw significant changes when analyzed with CBF contrast (Figure 3C): a decreased functional connectivity was observed in the somatosensory seeds while increased connectivity was seen in the cingulate and retrosplenial regions.

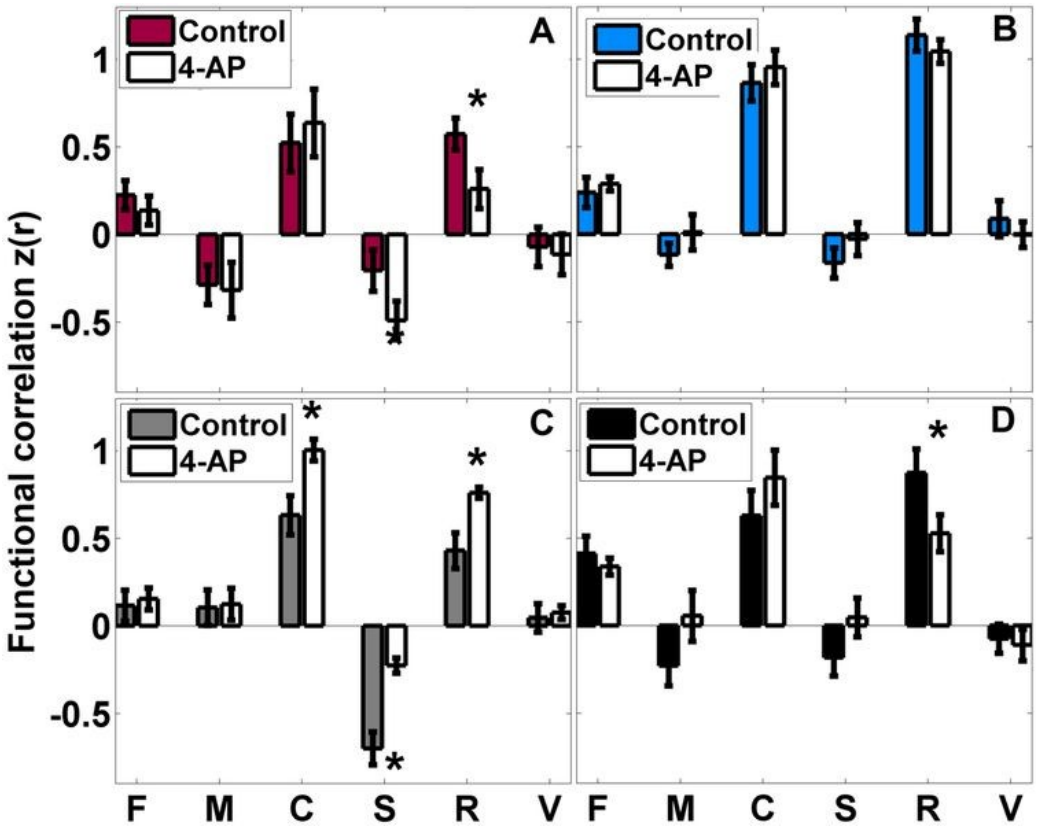


Figure 3. Regional bilateral functional connectivity before and after the 4-AP injection, analysis done for every seed time-trace and its contralateral part. Contrasts shown: (A) HbO2, (B) HbR (C) CBF and (D) CMRO2. * $p<0.05$. Standard error bars shown ($\sigma/\sqrt{N}$), with N=9. Standard error bars shown ($\sigma/\sqrt{N}$), with N=9. 150x119mm (300 x 300 DPI).

To assess whether these hemodynamic changes were associated with metabolic consumption patterns, we computed $CMRO_2$ using steady state formulas given the low frequency fluctuations frequently documented in functional connectivity studies (Biswal et al., 1995; Biswal et al., 2010; Fox & Raichle, 2007; Greicius et al., 2003). Data shows that the only seed pairs showing a significant difference was retrosplenial (Figure 3D). However there was a decrease in functional connectivity in the somatosensory cortex, albeit not significant. All results were evaluated with a Wilcoxon rank sum test.

Functional networks were derived from low frequency filtered imaging data. We were also interested to measure correlation between raw signals, before and after seizures, to observe the degree of disruption in the whole signal prior to regression by the common signal (Figure S3). Data show that all seeds are positively correlated, indicating the presence of a common signal to all the pixels time course, hence the need to regress a global brain signal, obtained from the average time trace of all the pixels marked as belonging to the brain.

**Correlation between seizure duration and functional connectivity**

Restricting the analysis to the mice showing clear seizure activity, we aimed to investigate whether seizure duration impacted network corrections. To calculate changes of bilateral correlation we subtracted the bilateral correlation during control sessions $z_0(r)$ from the bilateral correlation during the post 4-AP injection sessions $z_{4AP}(r)$ and plotted this change versus the average seizure duration of the 4-AP sessions, as illustrated on Figure 4. Overall correlations between seizure duration and changes in bilateral correlations were moderate. For the somatosensory cortex, where the toxin was injected, there was a positive correlation between the duration of the seizure and the changes in bilateral correlation. This same positive correlation was observed from the data extracted from the frontal cortex seeds. For other cortical regions, i.e. motor, cingulate, retrosplenial and visual a reverse effect was observed: the changes are negatively correlated with the seizure duration. For CBF contrast the correlation showed to be strong in the cingulate ($r^2$=0.46), somatosensory ($r^2$=0.67) and retrosplenial ($r^2$=0.77) regions. HbR contrast proved to have a somewhat strong correlation for retrosplenial seeds ($r^2$=0.50), while $HbO_2$ displayed a relatively strong

correlation for the motor seeds ($r^2$=0.41). The average length of seizures was 73.6 ± 51 s. All recording sessions were 863 seconds long. Table 1 provides the duration of seizure-like activity for every recording session, the percentage of the recording session that belongs to seizure-like activity and the average duration of seizures per subject.

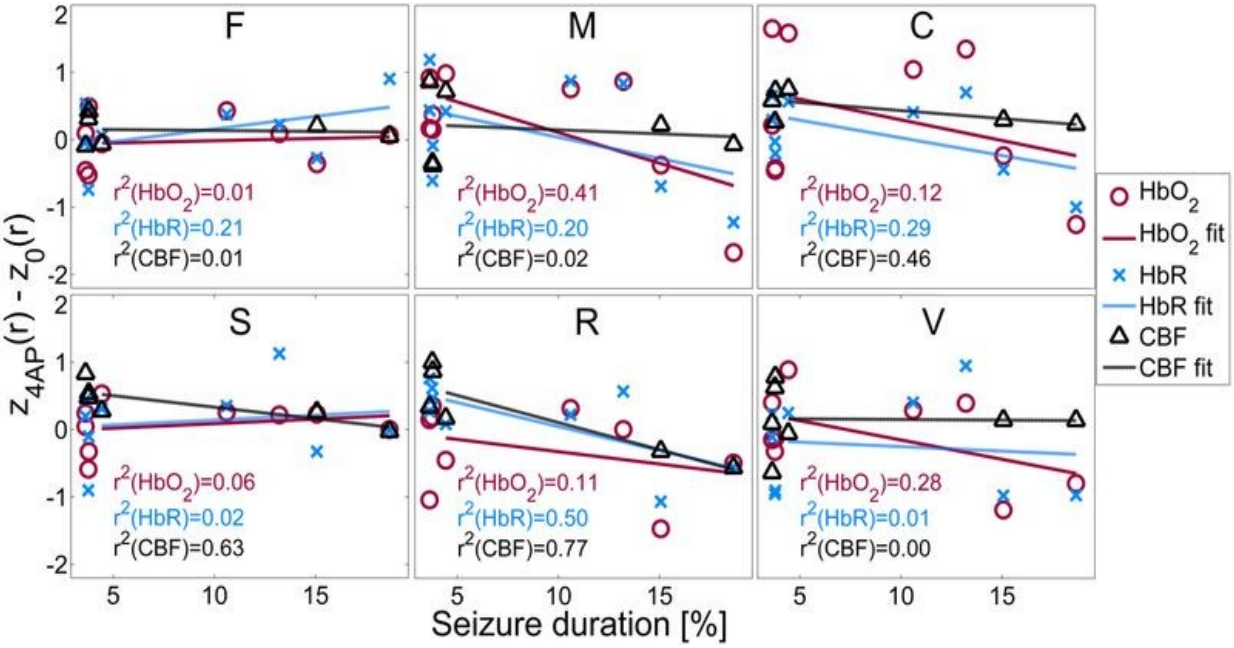


Figure 4. Changes in bilateral functional correlation plotted vs. seizure duration (expressed as a percentage of the recording session) for different cortical regions and different contrasts. (Contrasts: HbO2 oxygenated hemoglobin HbR deoxygenated hemoglobin and CBF cerebral blood flow; cortical regions: F: frontal cortex, M: motor cortex, C: cingulate cortex, S: somatosensory cortex R: retrosplenial cortex, V: visual cortex).

**DISCUSSION**

In this work we investigated regional bilateral functional connectivity using a seed-based correlation analysis; functional connectivity was evaluated before and after the injection of epileptogenic 4-AP in the somatosensory cortex.

Using oxyhemoglobin contrast ($HbO_2$), significant differences were found in the somatosensory and in the retrosplenial cortex. With deoxyhemoglobin (HbR) contrast, no seeds showed a statistically significant difference though most correlations decreased. In the case of relative blood flow contrast a significant difference was observed in the cingulate, somatosensory and retrosplenial regions. The only paired seeds to show a significant decrease of functional connectivity were in the somatosensory cortex, while the retrosplenial and cingulate exhibited an increase in functional correlation. For the estimated $CMRO_2$, a significant decrease in functional connectivity was found in the retrosplenial cortex.

Due to the proximity of cingulate and retrosplenial seeds to the site of 4-AP injection, the significant changes in the bilateral functional connectivity of these regions could be attributed to the proximity to the injection site, suggesting that the neurotoxin 4-AP might have propagated to these regions. However, at the site of injection, homologous connectivity decreased suggesting a decoupling of hemispheric connections linking the somatosensory areas while at the cingulate and retrosplenial sites, connectivity increased. An explanation might be a potential compensatory role for nearby regions (increasing their connectivity) to compensate for a reduction in the somatosensory homologous synchronization. A similar phenomenon was observed in (Brown et al., 2009), where following stroke in the sensory cortex in mice, a functional reorganization in nearby areas was observed but after much longer periods (8 weeks). Another hypothesis is that hemodynamic changes observed here may reflect a local redistribution of blood flow associated with the high metabolic activity at the seizure location.

**Acute seizure activity leads to decrease but also increase in functional connectivity**

In the case of $HbO_2$ both decrease (in somatosensory cortex) and increase (in retrosplenial cortex) of functional connectivity were observed. For HbR networks, there was also a decrease in bilateral connectivity of retrosplenial seeds, an increase in the somatosensory seeds; however the difference between control and post-4-AP injection were not significant in either case. In blood flow contrast an increase of functional connectivity was observed in both cingulate and retrosplenial paired seeds, and there was a decrease for somatosensory cortex. Retrosplenial seeds also showed a decrease in the estimated $CMRO_2$.

Previous literature using fMRI (Liao et al., 2011; Luo et al., 2012; Mankinen et al., 2012; Waites et al., 2006), mostly documented reduced functional connectivity in several functional networks in epileptic patients measured at rest. While a clear distinction is required with current experiments which focused on resting state networks during acute epileptiform events, the picture emerging from this work indicates a complex interplay between the different components of the hemodynamic response leading to both increases and decreases in connectivity in our mouse model. While HbR, which closely correlates to BOLD-fMRI, saw a non-significant decrease in connectivity in most seeds (4/5), $HbO_2$ and CBF saw their bilateral correlations move in opposite directions in seeds closest to the injection site (somatosensory and retrosplenial, for which changes were significant). Hemodynamic component dependent correlation changes indicate a potential uncoupling of flow and metabolism, even in low frequency networks.

These observations suggest that using a single modality, e.g. fMRI BOLD, to investigate resting state network in epilepsy may remain limited without controlling for flow or oxygenation. Whether the observed changes are due to changes in physiology (however no significant change was observed on our ECG), high metabolic demand at the seizure location or neural activity remains to be investigated. Further work with a chronic model investigating networks outside of epileptic periods may help reveal more coherent changes across hemodynamic components.

**Correlation between electrophysiological activity and resting state correlations**

Since electrophysiology was measured simultaneously, we could investigate the effect of seizure duration on pair wise network correlations. Our results show a dependence of the changes in bilateral functional correlations on seizure duration but remain mitigated due the low values of $r^2$ obtained in this analysis. Whether these changes are also present in sub-acute conditions, during simple spiking events, and the cause for network changes observed in patients remain to be studied. Our results are further limited by the fact that electrophysiology was measured in the somatosensory; it may be that similar activity measured at other seeds may lead to a different outcome.

**Metabolic consumption reflect hemodynamic changes**

$CMRO_2$ is potentially the closest marker to neuronal activity. Here we hypothesized that the steady-state relation between hemodynamic signals to estimate $CMRO_2$ held for the resting state networks due to their low frequency support. Assuming this hypothesis to be valid and comparing network correlation changes obtained by $CMRO_2$, our analysis displayed changes that followed similar trends as changes in HbR, except for the visual and frontal seeds where small differences were observed. This observation may in turn support HbR weighted fMRI-BOLD as a proxy for resting state network in epilepsy despite the known physiological confounds and hemodynamic network uncoupling displayed here.

**CONCLUSION**

Our original aim was to investigate the potential of OIS to study epileptic networks. Combining OIS with laser speckle imaging allows for simultaneous imaging of changes in $HbO_2$, HbR, CBF and potentially $CMRO_2$, providing a good set of hemodynamic data for functional connectivity studies during acute seizures. In our work, following 4-AP injection in the somatosensory cortex of mice, we observed significant changes in networks derived from spatial seeds near the injection site. Changes were not uniform across hemodynamic components signaling a complex picture with a potential decoupling of flow and metabolism within the low frequency networks. This study thus supports the need for a more extensive investigation and

characterization of epileptic networks encompassing more than one hemodynamic measurement.

There are several limitations to be mentioned; first and foremost our results were obtained during acute epileptiform events. They cannot therefore be directly compared with connectivity studies in humans typically obtained during rest periods devoid of acute epileptic events. Thus care must be taken when interpreting the current results since several physiological factors may be confounding the observed neuronal activity. Further work will aim to investigate chronic animal models of epilepsy in conditions that are closer to ongoing human resting state studies.

**Acknowledgments**

This research was supported by NSERC Discovery grant to F. Lesage. E. Guevara acknowledges financial support from Mexican National Science and Technology Council (CONACYT) through scholarship No. 304501. The authors wish to thank Tri Truong Van for his assistance in animal preparation and Mingrui Zhao for advice with 4-AP injections.

**Appendix A. Supplementary data** Supplementary data associated with this article can be found, in the online version.

## REFERENCES

Bero AW, Bauer AQ, Stewart FR, White BR, Cirrito JR, Raichle ME, Culver JP, Holtzman DM. (2012) Bidirectional Relationship between Functional Connectivity and Amyloid-β Deposition in Mouse Brain. *J Neurosci.* 32:4334-4340.

Bettus G, Ranjeva J-P, Wendling F, Bénar CG, Confort-Gouny S, Régis J, Chauvel P, Cozzone PJ, Lemieux L, Bartolomei F, Guye M. (2011) Interictal Functional Connectivity of Human Epileptic Networks Assessed by Intracerebral EEG and BOLD Signal Fluctuations. *PLoS One* 6:e20071.

Biswal B, Yetkin FZ, Haughton VM, Hyde JS. (1995) Functional connectivity in the motor cortex of resting human brain using echo-planar MRI. *Magn Reson Med* 34:537-541.

Biswal BB, Mennes M, Zuo X-N, Gohel S, Kelly C, Smith SM, Beckmann CF, Adelstein JS, Buckner RL, Colcombe S, Dogonowski A-M, Ernst M, Fair D, Hampson M, Hoptman MJ, Hyde JS, Kiviniemi VJ, Kötter R, Li S-J, Lin C-P, Lowe MJ, Mackay C, Madden DJ, Madsen KH, Margulies DS, Mayberg HS, McMahon K, Monk CS, Mostofsky SH, Nagel BJ, Pekar JJ, Peltier SJ, Petersen SE, Riedl V, Rombouts SARB, Rypma B, Schlaggar BL, Schmidt S, Seidler RD, Siegle GJ, Sorg C, Teng G-J, Veijola J, Villringer A, Walter M, Wang L, Weng X-C, Whitfield-Gabrieli S, Williamson P, Windischberger C, Zang Y-F, Zhang H-Y, Castellanos FX, Milham MP. (2010) Toward discovery science of human brain function. *Proc Natl Acad Sci U S A* 107:4734-4739.

Boas DA, Dunn AK. (2010) Laser speckle contrast imaging in biomedical optics. *J Biomed Opt* 15:011109.

Briers JD. (2001) Laser Doppler, speckle and related techniques for blood perfusion mapping and imaging. *Physiol Meas* 22:R35-R66.

Brieu N, Beaumont E, Dubeau S, Cohen-Adad J, Lesage F. (2010) Characterization of the hemodynamic response in the rat lumbar spinal cord using intrinsic optical imaging and laser speckle. *J Neurosci Methods* 191:151-157.

Brown CE, Aminoltejari K, Erb H, Winship IR, Murphy TH. (2009) In Vivo Voltage-Sensitive Dye Imaging in Adult Mice Reveals That Somatosensory Maps Lost to Stroke Are Replaced over Weeks by New Structural and Functional Circuits with Prolonged Modes of Activation within Both the Peri-Infarct Zone and Distant Sites. *J Neurosci* 29:1719-1734.

Delpy DT, Cope M, Zee Pvd, Arridge S, Wray S, Wyatt J. (1988) Estimation of optical pathlength through tissue from direct time of flight measurement. *Phys Med Biol* 33:1433-1442.

Dubeau S, Ferland G, Gaudreau P, Beaumont E, Lesage F. (2011) Cerebrovascular hemodynamic correlates of aging in the Lou/c rat: A model of healthy aging. *NeuroImage* 56:1892-1901.

Dunn AK, Bolay H, Moskowitz MA, Boas DA. (2001) Dynamic Imaging of Cerebral Blood Flow Using Laser Speckle. *J Cereb Blood Flow Metab* 21:195-201.

Dunn AK, Devor A, Bolay H, Andermann ML, Moskowitz MA, Dale AM, Boas DA. (2003) Simultaneous imaging of total cerebral hemoglobin concentration, oxygenation, and blood flow during functional activation. *Opt Lett* 28:28-30.

Dunn AK, Devor A, Dale AM, Boas DA. (2005) Spatial extent of oxygen metabolism and hemodynamic changes during functional activation of the rat somatosensory cortex. *NeuroImage* 27:279-290.

Fabene PF, Weiczner R, Marzola P, Nicolato E, Calderan L, Andrioli A, Farkas E, Süle Z, Mihaly A, Sbarbati A. (2006) Structural and functional MRI following 4-aminopyridine-induced seizures: a comparative imaging and anatomical study. *Neurobiol Dis* 21:80-89.

Fox MD, Raichle ME. (2007) Spontaneous fluctuations in brain activity observed with functional magnetic resonance imaging. *Nat Rev Neurosci* 8:700-711.

Frings L, Schulze-Bonhage A, Spreer J, Wagner K. (2009) Remote effects of hippocampal damage on default network connectivity in the human brain. *J Neurol* 256:2021-2029.

Friston KJ, Ashburner JT, Kiebel SJ, Nichols TE, Penny WD. (2006) *Statistical Parametric Mapping: The Analysis of Functional Brain Images*. Academic Press, Great Britain.

Gallagher A, Lassonde M, Bastien D, Vannasing P, Lesage F, Grova C, Bouthillier A, Carmant L, Lepore F, Béland R, Nguyen DK. (2008) Non-invasive pre-surgical investigation of a 10 year-old epileptic boy using simultaneous EEG-NIRS. *Seizure* 17:576-582.

Gibbs FA, Gibbs EL, Lennox WG. (1937) Epilepsy: A Paroxysmal Cerebral Dysrhythmia. *Brain* 60:377-388.

Greicius MD, Krasnow B, Reiss AL, Menon V. (2003) Functional connectivity in the resting brain: a network analysis of the default mode hypothesis. *Proc Natl Acad Sci U S A* 100:253-258.

Jones M, Berwick J, Johnston D, Mayhew J. (2001) Concurrent optical imaging spectroscopy and laser-Doppler flowmetry: the relationship between blood flow, oxygenation, and volume in rodent barrel cortex. *NeuroImage* 13:1002-1015.

Kandel ER, Schwartz JH, Jessell TM. (1991) *Principles of neural science*. Elsevier, New York.

Kohl M, Lindauer U, Royl G, Kuhl M, Gold L, Villringer A, Dirnagl U. (2000) Physical model for the spectroscopic analysis of cortical intrinsic optical signals. *Phys Med Biol* 45:3749-3764.

Liao W, Zhang Z, Pan Z, Mantini D, Ding J, Duan X, Luo C, Wang Z, Tan Q, Lu G, Chen H. (2011) Default mode network abnormalities in mesial temporal lobe epilepsy: a study combining fMRI and DTI. *Hum Brain Mapp* 32:883-895.

Luckl J, Baker W, Sun Z-H, Durduran T, Yodh AG, Greenberg JH. (2010) The biological effect of contralateral forepaw stimulation in rat focal cerebral ischemia: a multispectral optical imaging study. *Front Neuroenergetics* 2:pii: 19.

Luo C, Qiu C, Guo Z, Fang J, Li Q, Lei X, Xia Y, Lai Y, Gong Q, Zhou D, Yao D. (2012) Disrupted Functional Brain Connectivity in Partial Epilepsy: A Resting-State fMRI Study. *PLoS One* 7:e28196.

Mankinen K, Jalovaara P, Paakki J-J, Harila M, Rytky S, Tervonen O, Nikkinen J, Starck T, Remes J, Rantala H, Kiviniemi V. (2012) Connectivity disruptions in resting-state functional brain networks in children with temporal lobe epilepsy. *Epilepsy Res* 100:168-178.

Mayhew J, Johnston D, Berwick J, Jones M, Coffey P, Zheng Y. (2000) Spectroscopic Analysis of Neural Activity in Brain: Increased Oxygen Consumption Following Activation of Barrel Cortex. *NeuroImage* 12:664-675.

Moldestad O, Karlsen P, Molden S, Storm JF. (2009) Tracheotomy improves experiment success rate in mice during urethane anesthesia and stereotaxic surgery. *J Neurosci Methods* 176:57-62.

Morrell F, deToledo-Morrell L. (1999) From mirror focus to secondary epileptogenesis in man: an historical review. *Adv Neurol* 81:11-23.

Nguyen DK, Tremblay J, Pouliot P, Vannasing P, Florea O, Carmant L, Lepore F, Sawan M, Lesage F, Lassonde M. (2012) Non-invasive continuous EEG-fNIRS recording of temporal lobe seizures. *Epilepsy Res* 99:112-126.

Prahl S. (1999) Optical Absorption of Hemoglobin.

Voges N, Blanchard S, Wendling F, David O, Benali H, Papadopoulo T, Clerc M, Bénar C. (2012) Modeling of the neurovascular coupling in epileptic discharges. *Brain Topogr* 25:136-156.

Waites AB, Briellmann RS, Saling MM, Abbott DF, Jackson GD. (2006) Functional connectivity networks are disrupted in left temporal lobe epilepsy. *Annals of neurology* 59:335-343.

Wang Z, Lu G, Zhang Z, Zhong Y, Jiao Q, Zhang Z, Tan Q, Tian L, Chen G, Liao W, Li K, Liu Y. (2011) Altered resting state networks in epileptic patients with generalized tonic-clonic seizures. *Brain Res* 1374:134-141.

White BR, Bauer AQ, Snyder AZ, Schlaggar BL, Lee J-M, Culver JP. (2011) Imaging of functional connectivity in the mouse brain. *PLoS One* 6:e16322.

Zhang Z, Lu G, Zhong Y, Tan Q, Yang Z, Liao W, Chen Z, Shi J, Liu Y. (2009) Impaired attention network in temporal lobe epilepsy: a resting FMRI study. *Neurosci Lett* 458:97-101.

Zhao M, Ma H, Suh M, Schwartz TH. (2009) Spatiotemporal Dynamics of Perfusion and Oximetry during Ictal Discharges in the Rat Neocortex. *J Neurosci* 29:2814-2823.

Zhao M, Nguyen J, Ma H, Nishimura N, Schaffer CB, Schwartz TH. (2011) Preictal and ictal neurovascular and metabolic coupling surrounding a seizure focus. *J Neurosci* 31:13292-13300.

Zhao M, Suh M, Ma H, Perry C, Geneslaw A, Schwartz TH. (2007) Focal increases in perfusion and decreases in hemoglobin oxygenation precede seizure onset in spontaneous human epilepsy. *Epilepsia* 48:2059-2067.

Allen, PJ, O Josephs, and R Turner. 2000. “A method for removing imaging artifact from continuous EEG recorded during functional MRI.” NeuroImage 12 (2): 230-239.

Allen, PJ, G Polizzi, K Krakow, DR Fish, and L Lemieux. 1998. “Identification of EEG events in the MR scanner: the problem of pulse artifact and a method for its subtraction.” NeuroImage 8 (3) (October): 229-239.

Boorman, L, AJ Kennerley, D Johnston, M Jones, Y Zheng, P Redgrave, and J Berwick. 2010. “Negative blood oxygen level dependence in the rat: A model for investigating the role of suppression in neurovascular coupling.” Journal of Neuroscience 30 (12) (March): 4285-4294.

Boynton, GM, SA Engel, GH Glover, and DJ Heeger. 1996. “Linear systems analysis of functional magnetic resonance imaging in human V1.” The Journal of Neuroscience 16 (13) (July 1): 4207-4221.

Buchheim, K, H Obrig, W Pannwitz, A Mueller, H Heekeren, A Villringer, and H Meierkord. 2004. “Decrease in haemoglobin oxygenation during absence seizures in adult humans.” Neuroscience Letters 354 (2) (January): 119-122.

Buxton, RB, K Uludag, DJ Dubowitz, and TT Liu. 2004. “Modeling the hemodynamic response to brain activation.” NeuroImage 23 Suppl 1: S220-233.

Buxton, RB, EC Wong, and LR Frank. 1998. “Dynamics of blood flow and oxygenation changes during brain activation: the balloon model.” Magnetic Resonance in Medicine 39 (6) (June): 855-864.

Delpy, D T, M Cope, P van der Zee, S Arridge, S Wray, and J Wyatt. 1988. “Estimation of optical pathlength through tissue from direct time of flight measurement.” Physics in Medicine and Biology 33 (12) (December): 1433-1442.

Desjardins, M, P Pouliot, and F Lesage. 2010. “Principles and applications of diffuse optical tomography for the brain.” Current Medical Imaging Reviews.

Friston, KJ, J Ashburner, S Kiebel, T Nichols, and W Penny. 2007. Statistical parametric mapping : the analysis of funtional brain images. 1st ed. Elsevier/Academic Press.

Friston, KJ, O Josephs, G Rees, and R Turner. 1998. “Nonlinear event-related responses in fMRI.” Magnetic Resonance in Medicine 39 (1) (January): 41-52.

Friston, KJ, A Mechelli, R Turner, and CJ Price. 2000. “Nonlinear responses in fMRI: the Balloon model, Volterra kernels, and other hemodynamics.” NeuroImage 12 (4) (October): 466-477.

Gallagher, A, D Bastien, I Pelletier, P Vannasing, AD Legatt, SL Moshé, R Jehle, et al. 2008. “A noninvasive, presurgical expressive and receptive language investigation in a 9-year-old epileptic boy using near-infrared spectroscopy.” Epilepsy & Behavior 12 (2) (February): 340-346.

Glover, GH. 1999. “Deconvolution of impulse response in event-related BOLD fMRI.”NeuroImage 9 (4) (April): 416-429.

Grouiller, F, L Vercueil, A Krainik, C Segebarth, P Kahane, and O David. 2009. “Characterization of the hemodynamic modes associated with interictal epileptic activity using a deformable model-based analysis of combined EEG and functional MRI recordings.” Human Brain Mapping: NA-NA.

Hamandi, K, HWR Powell, H Laufs, MR Symms, GJ Barker, GJM Parker, and L Lemieux. 2008. “Combined EEG-fMRI and tractography to visualise propagation of epileptic activity.” Journal of Neurology, Neurosurgery & Psychiatry 79 (5) (May): 594-597.

Hansen, KA, SV David, and JL Gallant. 2004. “Parametric reverse correlation reveals spatial linearity of retinotopic human V1 BOLD response.” NeuroImage 23 (1) (September): 233-241.

Hawco, CS, AP Bagshaw, Y Lu, F Dubeau, and J Gotman. 2007. “BOLD changes occur prior to epileptic spikes seen on scalp EEG.” NeuroImage 35 (4) (May): 1450-1458.

Huppert, TJ, MS Allen, SG Diamond, and DA Boas. 2009. “Estimating cerebral oxygen metabolism from fMRI with a dynamic multicompartment Windkessel model.” Human Brain Mapping 30 (5) (May): 1548-1567.

Huppert, TJ, SG Diamond, MA Franceschini, and DA Boas. 2009. “HomER: a review of time-series analysis methods for near-infrared spectroscopy of the brain.” Applied Optics 48 (10) (April 1): D280-298.

Jacobs, J, C Hawco, E Kobayashi, R Boor, P LeVan, U Stephani, M Siniatchkin, and J Gotman. 2008. “Variability of the hemodynamic response as a function of age and frequency of epileptic discharge in children with epilepsy.” NeuroImage 40 (2) (April): 601-614.

Jacobs, J, P LeVan, F Moeller, R Boor, A Stephani, J Gotman, and M Siniatchkin. 2009. “Hemodynamic changes preceding the interictal EEG spike in patients with focal epilepsy investigated using simultaneous EEG-fMRI.” NeuroImage 45 (4) (May): 1220-1231.

Jacquez, JA, and P Greif. 1985. “Numerical parameter identifiability and estimability: Integrating identifiability, estimability, and optimal sampling design.” Mathematical Biosciences 77 (1-2) (December): 201-227.

Jang, KE, S Tak, J Jung, J Jang, and JC Ye. 2009. “Wavelet minimum description length detrending for near-infrared spectroscopy.” Journal of Biomedical Optics 14 (3): 034004.

Kobayashi, E, AP Bagshaw, C Grova, F Dubeau, and J Gotman. 2006. “Negative BOLD responses to epileptic spikes.” Human Brain Mapping 27 (6) (June): 488-497.

Krakow, K, L Lemieux, D Messina, CA Scott, MR Symms, JS Duncan, and DR Fish. 2001. "Spatio-temporal imaging of focal interictal epileptiform activity using EEG-triggered functional MRI." Epileptic Disorders 3 (2) (June): 67-74.

Laufs, H, and JS Duncan. 2007. "Electroencephalography/functional MRI in human epilepsy: what it currently can and cannot do." Current Opinion in Neurology 20 (4) (August): 417-423.

LeVan, P, L Tyvaert, F Moeller, and J Gotman. 2010. "Independent component analysis reveals dynamic ictal BOLD responses in EEG-fMRI data from focal epilepsy patients." NeuroImage 49 (1) (January 1): 366-378.

Machado, A, J-M Lina, J Tremblay, M Lassonde, DK Nguyen, F Lesage, and C Grova. 2010. "Detection of hemodynamic responses to epileptic activity using simultaneous electro-encephalography (EEG)/near infrared spectroscopy (NIRS) acquisitions." NeuroImage (December).

Morrell, F, and L deToledo-Morrell. 1999. "From mirror focus to secondary epileptogenesis in man: an historical review." Advances in Neurology 81: 11-23.

Mosewich, RK, EL So, TJ O'Brien, GD Cascino, FW Sharbrough, WR Marsh, FB Meyer, CR Jack, and PC O'Brien. 2000. "Factors predictive of the outcome of frontal lobe epilepsy surgery." Epilepsia 41 (7) (July): 843-849.

Nguyen, DK, J Tremblay, P Pouliot, P Vannasing, O Florea, L Carmant, F Lepore, M Sawan, F Lesage, and M Lassonde. 2011. "Noninvasive continuous EEG-fNIRS recording of temporal lobe seizure." Accepted in Epilepsy Research.

Osharina, V, E Ponchel, A Aarabi, R Grebe, and F Wallois. 2010. "Local haemodynamic changes preceding interictal spikes: A simultaneous electrocorticography (ECoG) and near-infrared spectroscopy (NIRS) analysis in rats." NeuroImage 50 (2) (April): 600-607.

Rasmussen, T. 1983. "Characteristics of a pure culture of frontal lobe epilepsy." Epilepsia 24 (4) (August): 482-493.

Soltysik, D, K Peck, K White, B Crosson, and R Briggs. 2004. "Comparison of hemodynamic response nonlinearity across primary cortical areas." NeuroImage 22 (3) (July): 1117-1127.

Toyoda, H, K Kashikura, T Okada, S Nakashita, M Honda, Y Yonekura, H Kawaguchi, A Maki, and N Sadato. 2008. "Source of nonlinearity of the BOLD response revealed by simultaneous fMRI and NIRS." NeuroImage 39 (3) (February 1): 997-1013.

Vanzetta, Ivo, Corey Flynn, Anton I Ivanov, Christophe Bernard, and Christian G Bénar. 2010. "Investigation of linear coupling between single-event blood flow responses

and interictal discharges in a model of experimental epilepsy." Journal of Neurophysiology 103 (6) (June): 3139-3152. doi:10.1152/jn.01048.2009.

Vaudano, AE, H Laufs, SJ Kiebel, DW Carmichael, K Hamandi, M Guye, R Thornton, et al. 2009. "Causal hierarchy within the thalamo-cortical network in spike and wave discharges." PLoS ONE 4 (8) (August): e6475.

Ye, JC, S Tak, KE Jang, J Jung, and J Jang. 2009. "NIRS-SPM: Statistical parametric mapping for near-infrared spectroscopy." NeuroImage 44 (2) (January): 428-447.

Zhao, M, H Ma, M Suh, and TH Schwartz. 2009. "Spatiotemporal dynamics of perfusion and oximetry during ictal discharges in the rat neocortex." Journal of Neuroscience 29 (9) (March): 2814-2823.

Zheng, Y, J Martindale, D Johnston, M Jones, J Berwick, and J Mayhew. 2002. "A model of the hemodynamic response and oxygen delivery to brain." NeuroImage 16 (3 Pt 1) (July): 617-637.

Supplementary figure S1

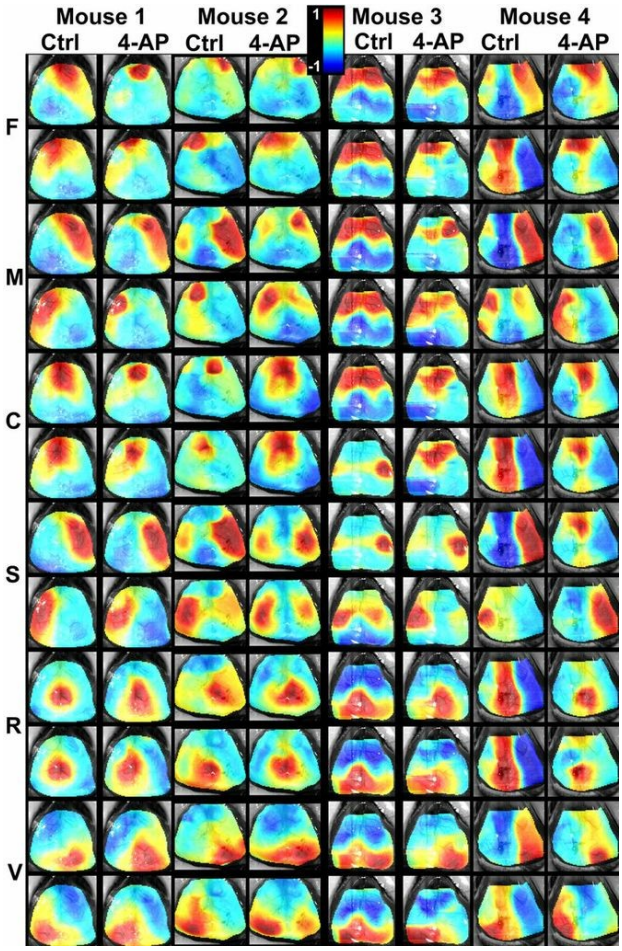


Figure S1. Seed-based HbR correlation maps for four mice. One control session and one post-4-AP injection session are displayed for each mouse. (F: frontal cortex, M:motor cortex, C: cingulate cortex, S: somatosensory cortex R: retrosplenial cortex, V: visual cortex). The scale for all correlation maps is from r = -1 to 1. Maps are shown overlaid on the anatomical image of the brain, acquired with green light.

Supplementary figure S2

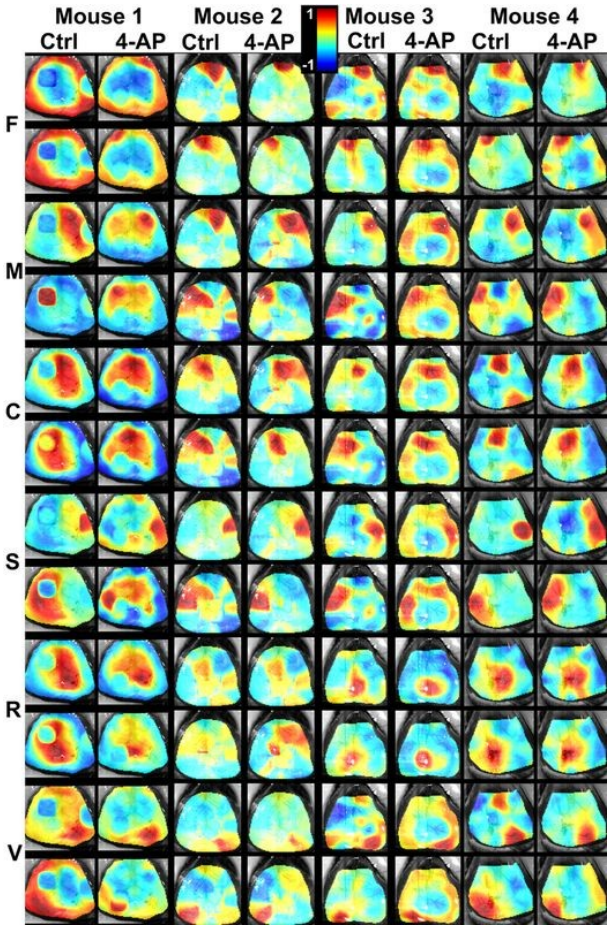


Figure S2. Seed-based CBF correlation maps for four mice. One control session and one post-4-AP injection session are displayed for each mouse. (F: frontal cortex, M:motor cortex, C: cingulate cortex, S: somatosensory cortex R: retrosplenial cortex, V: visual cortex). The scale for all correlation maps is from r = -1 to 1. Maps are shown overlaid on the anatomical image of the brain, acquired with green light.

Supplementary figure S3

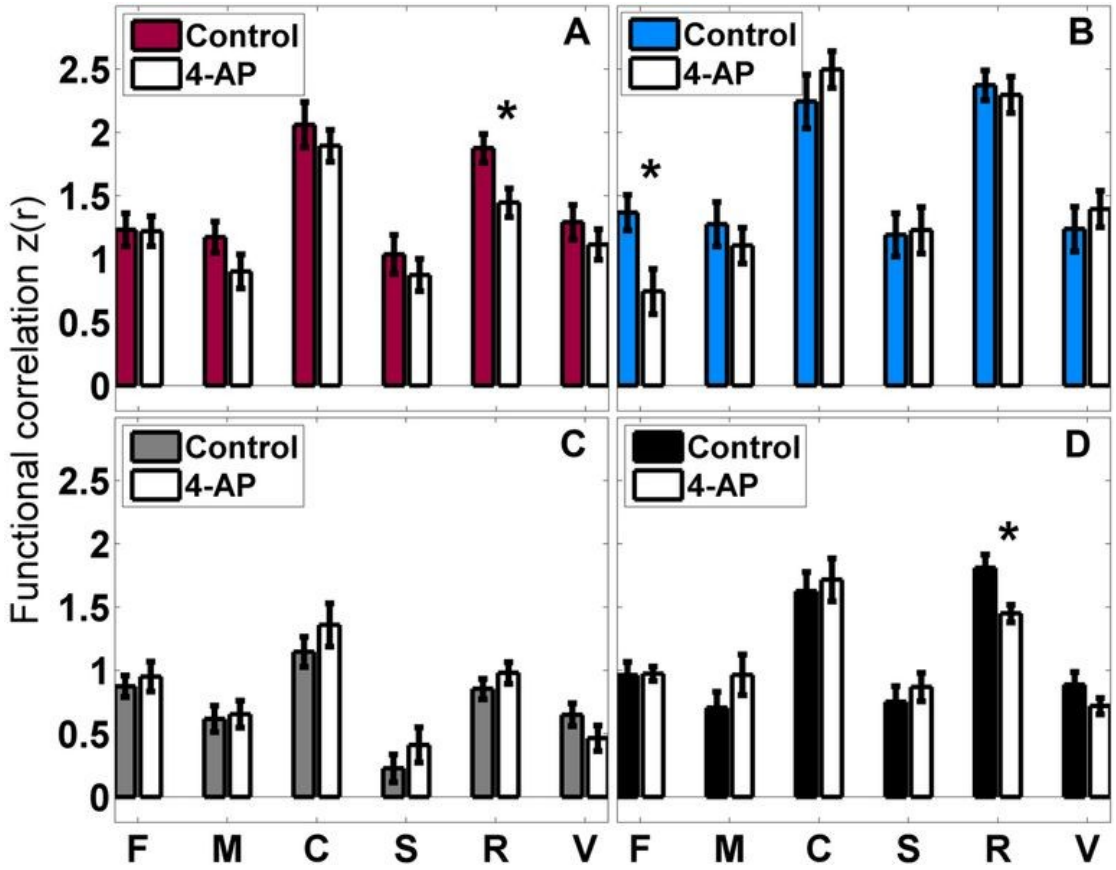


Figure S3. Regional bilateral functional connectivity before and after the 4-AP injection, analysis done for every seed time-trace and its contralateral part, using raw signals. Contrasts shown: A) $HbO_2$, B) HbR C) CBF and D) $CMRO_2$. All measures are based on seed raw time traces, before filtering and regression. * $p<0.05$. Standard error bars shown ($\sigma/\sqrt{N}$), with N=9. (F: frontal cortex, M:motor cortex, C: cingulate cortex, S: somatosensory cortex R: retrosplenial cortex, V: visual cortex).